VOLUME 118 NUMBER 2

THE ASTROPHYSICAL JOURNAL

AN INTERNATIONAL REVIEW OF SPECTROSCOPY AND ASTRONOMICAL PHYSICS

SEPTEMBER 1953

SOLAR FLARES AND ASSOCIATED 200 MC/SEC RADIATION
Helen W. Dodson, E. Ruth Hedeman, and Leif Owren 169
STELLAR ABSORPTION LINES IN NIGHT-SKY SPECTRA
Joseph W. Chamberlain and Norman J. Oliver 197
ORIGIN OF THE CONTINUUM IN THE NIGHT-SKY SPECTRUM . . *A. B. Meinel* 200
LABORATORY IONIC-IMPACT EMISSION SPECTRA . . *C. Y. Fan and A. B. Meinel* 205
VIBRATION-ROTATION BANDS OF *OH* . . . *Robert C. Herman and George A. Hornbeck* 214
VIBRATIONAL TRANSITION PROBABILITIES OF DIATOMIC MOLECULES: COLLECTED RESULTS N_2, N_2^+, *NO*, O_2^+ . . *W. R. Jarmain, P. A. Fraser, and R. W. Nicholls* 228
ETA CARINAE. II. THE SPECTRUM . . . . . *E. Gaviola* 234
THE BALMER DECREMENT IN SOME Be STARS *G. R. Burbidge and E. Margaret Burbidge* 252
SPECTROGRAPHIC OBSERVATIONS OF SV CAMELOPARDALIS . . *W. A. Hiltner* 262
HD 50169, A SPECTRUM VARIABLE WITH EMISSION AT $H\alpha$ . . *Kenneth R. W. Brewer* 265
VARIATION IN LIGHT OF THE SPECTRUM VARIABLE 56 ARIETIS *Sanford S. Previn* 281
A STATISTICAL STUDY OF THE ROTATION OF THE STARS . . . *Su-Shu Huang* 285
A RADIO MODEL OF THE GALAXY . . . . . *Stanley P. Wyatt, Jr.* 304
PHOTOELECTRIC MAGNITUDE SEQUENCES FOR THE MAGELLANIC CLOUDS
Arthur N. Cox and Kenneth L. Hallam 314
STUDIES IN GALACTIC STRUCTURE. I. A PRELIMINARY DETERMINATION OF THE SPACE DISTRIBUTION OF THE BLUE GIANTS
W. W. Morgan, A. E. Whitford, and A. D. Code 318
BLUE GIANTS IN THE NEIGHBORHOOD OF NGC 6231
W. W. Morgan, Graciela González, and Guillermina González 323
INHOMOGENEOUS STELLAR MODELS. III. MODELS WITH PARTIALLY DEGENERATE ISOTHERMAL CORES . . . . *M. Schwarzschild, I. Rabinowitz, and R. Härm* 326
ASPHERIC FIELD CORRECTORS FOR LARGE TELESCOPES . . . . *A. B. Meinel* 335

NOTES

BLUE GIANTS IN THE DIRECTION OF THE GALACTIC CENTER
W. W. Morgan, Guillermina González, and Graciela González 345
NOTE ON THE CEPHEID VARIABLE ZETA GEMINORUM . . . . . *D. L. Harris* 346
EM CYG, A POSSIBLE EX-NOVA . . . . . *E. Margaret Burbidge and G. R. Burbidge* 349
ROTATIONAL TEMPERATURES OF AURORAL N_2^+ BANDS
A. Vallance Jones, D. M. Hunten, and G. G. Shepherd 350
NOTE ON THE PAPER "STUDIES OF VARIABLES IN THE MAGELLANIC CLOUDS. I. TWENTY NEW FAINT VARIABLES IN A REGION IN THE SMALL CLOUD"
Martin Dartayet and Jorge Landi Dessy 351

THE UNIVERSITY OF CHICAGO PRESS
CHICAGO, ILLINOIS, U.S.A.

September 1953 Vol. 118, No. 2

THE ASTROPHYSICAL JOURNAL

AN INTERNATIONAL REVIEW OF SPECTROSCOPY AND ASTRONOMICAL PHYSICS

Published in Collaboration with the American Astronomical Society

S. CHANDRASEKHAR
Managing Editor

GERARD P. KUIPER
Associate Editor

Yerkes Observatory of the University of Chicago

EDITORIAL BOARD

H. W. BABCOCK (1953-57)
Mount Wilson Observatory of the Carnegie Institution of Washington

G. HERZBERG (1952-56)
National Research Council, Ottawa

FRED L. WHIPPLE (1952-54)
Harvard College Observatory

C. D. SHANE (1952-55)
Lick Observatory, University of California

LYMAN SPITZER, JR. (1952-53)
Princeton University Observatory

The Astrophysical Journal is published bimonthly by the University of Chicago at the University of Chicago Press, 5750 Ellis Avenue, Chicago 37, Illinois, during January, March, May, July, September, and November. ¶Two volumes are published per year, one beginning with the January issue and the other beginning with the July issue. The subscription price is $6.00 per volume or $12.00 per year; the price of single copies is $3.00. (Orders for service of less than a volume will be charged at the single copy rate.) ¶Postage is prepaid by the publishers on all orders from the United States and its possessions. No extra charge is made for postage to countries in the Pan American Postal Union. ¶Postage is charged extra as follows: for Canada, 20 cents per volume, 40 cents per year (total $6.20 per volume, $12.40 per year); on single copies 5 cents (total $3.05); for all other countries in the Postal Union, 40 cents per volume, 75 cents per year (total $6.40 per volume, $12.75 per year), on single copies 10 cents (total $3.10). ¶Subscriptions are payable in advance. Please make all remittances payable to The University of Chicago Press, in United States currency or its equivalent by postal or express money orders or bank drafts.

The following is an authorized agent:

For the British Empire, except North America and Australasia: The Cambridge University Press, Bentley House, 200 Euston Road, London, N.W. 1, England. Prices of yearly subscriptions and of single copies may be had on application.

Claims for missing numbers should be made within the month following the regular month of publication. The publishers expect to supply missing numbers free only when losses have been sustained in transit, and when the reserve stock will permit.

Business correspondence should be addressed to The University of Chicago Press, Chicago 37, Illinois.

Communications for the editors and manuscripts should be addressed to: S. Chandrasekhar, Editor of THE ASTROPHYSICAL JOURNAL, Yerkes Observatory, Williams Bay, Wisconsin.

Line drawings and photographs should be made by the author, and all marginal notes such as co-ordinates, wave lengths, etc., should be included in the cuts. It will not be possible to set up such material in type.

One copy of the corrected galley proof should be returned as soon as possible to the editor, Yerkes Observatory, Williams Bay, Wisconsin. Authors should take notice that the manuscript will not be sent to them with the proof.

The cable address is "Observatory, Williamsbay, Wisconsin."

The articles in this journal are indexed in the *International Index to Periodicals*, New York, N.Y.

Applications for permission to quote from this journal should be addressed to The University of Chicago Press, and will be freely granted.

Microfilms of complete journal volumes are available to regular subscribers only and may be obtained at the end of the year. Orders and inquiries should be addressed to University Microfilms, 313 North First Street, Ann Arbor, Michigan.

Notice to subscribers: If you change your address, please notify us and your local postmaster immediately.

Entered as second-class matter, July 31, 1940, at the Post-Office at Chicago, Ill., under the Act of March 3, 1879.
Acceptance for mailing at special rate of postage provided for in United States Postal Act of October 3, 1917, Section 1103, amended February 28, 1925.
Copyright 1953 by the University of Chicago.

[PRINTED IN U.S.A.]

THE ASTROPHYSICAL JOURNAL

AN INTERNATIONAL REVIEW OF SPECTROSCOPY AND ASTRONOMICAL PHYSICS

VOLUME 118 SEPTEMBER 1953 NUMBER 2

SOLAR FLARES AND ASSOCIATED 200 MC/SEC RADIATION*

HELEN W. DODSON, E. RUTH HEDEMAN, AND LEIF OWREN†

McMath-Hulbert Observatory, University of Michigan, and School of Electrical Engineering, Cornell University

Received February 20, 1953

ABSTRACT

Study of 200 Mc/sec solar radiation for the times of 194 flares indicates distinctive radio events associated with 78 per cent of the flares. The flare-associated distinctive events can be divided into ten descriptive types or categories: major burst, major burst with second part, minor burst, minor burst with second part, micro burst, group of bursts, series of bursts, noise storm in progress, onset of noise storm, and rise in base level. In addition, there is the designation "null," or no distinctive event. Consideration of the time relationships between flares and 200 Mc/sec events suggests that two quite different types of phenomena may be represented in the flare-associated 200 Mc/sec radiation. The first or "early" phenomenon includes very sudden, relatively isolated, burstlike features which occur close to the time of start of the flare. The second or "late" phenomenon includes the more gradual rises in base level and onsets of noise storms. These usually start at or after the time of flare maximum. The "early" and "late" phenomena can occur in conjunction with each other, or either of the two can occur separately. The importance of the flare, position on the solar disk, and accompanying ionospheric disturbances are considered with respect to the form and energy excess of the flare-associated 200 Mc/sec events. The various aspects of the complex flare phenomenon, as observed photographically and visually, are discussed. An association is suggested between the high-velocity ejections observed at the *onset* of certain flares and the occurrence of a major burst at 200 Mc/sec. From the point of view of the parameters considered in this paper, the flares for which there were no distinctive events on the 200 Mc/sec records constitute a random sample from the entire set of 194 flares.

INTRODUCTION

During the last two years the School of Electrical Engineering of Cornell University and the McMath-Hulbert Observatory of the University of Michigan have been conducting a co-operative program in which records of 200 Mc/sec radiation from the sun have been compared in detail with solar activity observed photographically and visually. Although this work has indicated that a number of different solar phenomena apparently influence the 200 Mc/sec records, the relationships between solar flares and the radio data are the most clear cut.

A number of investigators have reported coincidences of certain solar flares and sudden ionospheric disturbances with bursts of solar radio emission at different frequencies. The more extensive studies dealing with a systematic comparison of solar flares and solar radio-frequency emissions include one by Allen[1] in 1947, in which he brought together

* This paper is supported in part by contracts with the Office of Naval Research.

† On leave of absence from the Institute of Theoretical Astrophysics, University of Oslo, Oslo, Norway.

[1] *M.N.*, **107**, 386, 1947.

200 Mc/sec observations and solar features observed visually with spectrohelioscope and spectroscope. He found occasional time coincidences between the onset of solar flares and 200 Mc/sec outbursts. Hey, Parsons, and Phillips[2] investigated the relation of solar radio bursts at 4.1 meters (73 Mc/sec) to solar flares, radio fadeouts, and magnetic crochets. This study states that the chance of observing a burst during the occurrence of a flare increases with the "importance" of the flare and that there is an "apparent tendency for coincidences between flares and bursts to be greater on the eastern half than on the western half of the sun's disk."[2] Studies by Payne-Scott and Little,[3] Hatanaka and Moriyama,[4] and S. E. Williams[5] have further amplified the association between certain solar flares and emission at radio frequencies.

The present paper covers the period between July 23, 1948, when observations of 200 Mc/sec radiation from the sun were started at Cornell University, and December 31, 1950. It has as its goal the detailed description of 200 Mc/sec data at the time of solar flares and comparison of this radio radiation with certain aspects of the *Hα* phenomena. The study includes all flares in this period for which the authors have clear-cut *Hα* data and for which the Cornell records are available. The initial investigation was based on those flares for which photometric light-curves or photographic records had been secured at the McMath-Hulbert Observatory. In order to provide a larger number of cases, the study was extended to include all flares completely reported by the International Astronomical Union, the Fraunhofer Institute, or the Central Radio Propagation Laboratory of the National Bureau of Standards and which fell within the period of the Cornell records. A total of 194 flares met these requirements.

The "association" here reported between a flare and a distinctive event on the 200 Mc/sec records is a time association. In the initial phase of the investigation, with photometric light-curves or complete photographic data available for the flares, close time coincidence was deemed necessary for an implied association. The pattern that emerged from this study of the best data indicated that certain types of distinctive events at 200 Mc/sec start very late in the course of the flare. Extension of the study to include the inherently less exact data of flares observed visually necessitated greater tolerance in assigning association between flare and radio event. Nevertheless, only 9 of the distinctive events in this study began more than *10 minutes* before the reported starting time of the flare, and only 4 began after the reported end of the flare. The designation "null" indicates that there was no distinctive event during the flare or within ½ hour of the reported times of start and end of the *Hα* brightening.

THE RADIO DATA

The records of 200 Mc/sec solar radiation were secured at Cornell University on a regular daily schedule. Two different antenna systems were used for the observation of solar radio-frequency radiation in the period 1948–1950. The earliest observations were made with a 6×8 dipole array, with the dipoles spaced ½ wave length to either side. The array was backed by a reflecting screen and placed on an alt-azimuth mount. The antenna array had to be moved manually, and observations were made for only 2 hours near noon each day, the antenna being reset every 10 minutes. After October 14, 1949, the solar observations were made with an equatorially mounted parabolic reflector, 17 feet in diameter. At the focus of the parabola there is a half-wave dipole antenna with a half-wave parasitic reflector. This antenna tracks the sun automatically and makes possible daily observations of the sun for 8 hours or more.

The receivers used for the radio-frequency observations were designed and constructed at Cornell University especially for solar and galactic observations at 200 Mc/sec. The receivers were of the superheterodyne type with a cascode radio-frequency amplifier, frequency converter, intermediate frequency amplifier, and a linear detector. The recording system consisted of a direct-current amplifier and a 0–5 milliampere Esterline Angus

[2] *M.N.*, **108**, 354, 1948.

[3] *Australian J. Sci. Res., A*, **5**, 32, 1952.

[4] *Report of Ionosphere Research in Japan*, **6**, 99, 1952.

[5] *J. R. Soc. Western Australia*, **34**, 17, 1948.

recording milliammeter. The center frequencies of the receivers were 205 ± 1 Mc/sec during the period July 23, 1948—April 6, 1950 and 200 ± 1 Mc/sec during the period April 11, 1950—December 31, 1950. For each receiver the over-all band width was about 5 Mc/sec, the average noise figure about 9. The noise figure tells by which factor the noise-power output of the actual receiver exceeds the noise-power output of a similar, ideal (noise-free) receiver, in terms of the noise power from a reference resistor at room temperature. The recorder time constant was 0.5 seconds. The receiver gain could be adjusted by insertion or removal of attenuation in the intermediate frequency-amplifier section.

The receiver input could be connected either to the antenna feed cable or to a reference resistor, at ambient temperature, by means of a coaxial switch. When the receiver input was connected to the reference resistor, the total noise output from the detector was reduced to a predetermined value of 2.0 volts by means of the attenuators inserted between the intermediate frequency-amplifier stages. This reduced detector output was then balanced out by applying an equivalent back-bias potential from a temperature-controlled battery. When the receiver input was connected to the antenna, the difference between the detector output voltage and the back-bias potential was amplified and recorded.

On each day of observation, an antenna sweep was made along the parallel of declination +28°, which passes through the region of minimum radiation near the north galactic pole. During each observing period the receiver input was also automatically connected every ½ hour to the reference resistor for a 2-minute interval. The combination of the north galactic pole observation and the half-hourly calibration mark provided a reference level from which the solar radiation could be measured. For part of the reported period daily measurements were made of the receiver-noise figure, the detector-output voltage with the receiver connected to the reference resistor, and the center frequency of the receiving system. During the same period the scale of the recording milliammeter was calibrated at regular intervals in terms of the power input to the receiver by means of a temperature-limited diode noise generator connected in shunt with the reference resistor.

The normal operating sensitivity of the recording system was such that full-scale deflection of the milliammeter corresponded to a power input to the receiver of about ten times that observed for the quiet sun. The flux density of the radiation from the quiet sun at 200 Mc/sec is approximately 8×10^{-22} watts/m^2/c/s. The sensitivity could be increased or decreased to follow variations in solar radiation. On the least sensitive scale used, full-scale deflection corresponded to five times the power input required for full-scale deflection on the sensitivity ordinarily used. A recording chart speed of 12 inches per hour was used for all observations. Supplementary survey records were taken at a speed of 3 inches per hour. The solar observations were corrected for background radiation due to the Milky Way.

THE PHOTOGRAPHIC AND VISUAL DATA

The extensive collection of *Hα* spectroheliograms of the solar disk photographed in the 50-foot solar tower of the McMath-Hulbert Observatory shows the outbreak and development of many flares. In general, the spectroheliograms were photographed at intervals of 30 seconds with a telescope of 20-foot focal length and through a spectrograph slit transmitting 0.4 A. The optics and techniques used in this solar tower are fully described in the literature.[6] The films are standardized for photometric work and permit studies of the intensity of the flares as well as their extent, position, and time relationships. Through the use of a densitometer designed and constructed at the McMath-Hulbert Observatory especially for photometric measurement of 35-mm film it is possible to determine the intensity of any point in the flare in units of the neighboring, undisturbed *Hα* disk. Variations with time in the intensity of *Hα* can be shown for any desired point in the flare by a so-called "light-curve."

Observation has shown that the bright flare is just one aspect of a *complex* solar phenomenon. The most familiar feature of this complex phenomenon is the flare itself—the

[6] R. R. McMath, *Pub. Obs. U. Michigan*, **7**, 1, 1939.

relatively sudden increase in intensity of $H\alpha$ and other monochromatic radiations for time intervals that range usually from tens of minutes to several hours. The flare brightenings generally take place in *plage* areas near sunspots, and the region on the sun involved in the brightening may be large or small, a single bright region, or many small patches. In area, most flares cover only several ten-thousandths of the solar hemisphere. No flare as large as one-half of 1 per cent of the solar hemisphere has been observed. Some flares spread with time to parts of the *plage* quite distant from the initial brightening. In certain of these cases, the distant parts brighten but do not attain "flare intensity."

Evidence for the complexity of what is here termed the "flare phenomenon" comes from a number of different sources and types of observation. First "active dark flocculi" are commonly observed in the neighborhood of flares. These dark absorption features usually appear after the onset of the brightening and are observed first to the short- and then to the long-wave-length side of $H\alpha$. These absorption features, often with large radial velocities, can be followed photographically on the Lake Angelus spectroheliograph, since the effective wave length of the spectroheliograms can be changed at will. Changes in the direction of the Doppler shifts and in the form of these "active dark flocculi" are consistent with their interpretation as surge-type prominences observed in projection on the disk.[7]

Second, a large number of flares are accompanied by a concurrent and sudden disturbance of the earth's ionosphere, herein referred to as an "S.I.D." This includes among a number of other effects[8] a fadeout of radio transmission at 5–20 Mc/sec. These ionospheric disturbances, associated particularly with the D-layer, imply a burst of intense ultraviolet radiation at the time of the $H\alpha$ flare.

In addition, certain flares are apparently accompanied by the actual ejection from the sun of material particles which, hours or days later, may impinge upon the earth's atmosphere and cause a geomagnetic storm and an aurora. At the McMath-Hulbert Observatory, high-velocity ejections have been observed at the time of *onset* of certain flares near the solar limb.[9] The velocity of these ejections is much greater than that observed for the "active dark flocculi" and surge-type prominences.

Finally, the growing body of observations of solar radiation at radio frequencies indicates still another form of solar activity at the time of $H\alpha$ flares. The present study shows that 200 Mc/sec radiation at the time of flares exhibits a wide range both in the magnitude of the energy excess and in the kind of distinctive event recorded.

PRESENTATION OF OBSERVATIONS

The basic observational data for this study are summarized in Table 1. For the $H\alpha$ flares, the dates, times, importance, and heliographic co-ordinates are given. If starting or stopping times are underscored, the times refer to the beginning or ending of the flare

NOTES TO TABLE 1 ON $H\alpha$ AND 200 MC/SEC DATA FOR 194 FLARES BETWEEN JULY 23, 1948, AND DECEMBER 31, 1950

Sources of flare data.—(*a*) McMath-Hulbert Observatory; (*b*) *Quarterly Bulletin* of IAU; (*c*) Central Radio Propagation Laboratory, National Bureau of Standards, F Series; (*d*) *Sonnen Zircular*, Fraunhofer Institut.

* Photometric light-curve for flare is available.

( ) With flare importance, indicates value was assigned by authors.

(U) Classified as outburst at Cornell.

† Time classification, "Late." Radio record starts after start of flare, preventing detection of possible early component.

⊕ Time classification uncertain because of incomplete flare data.

Energy excess values.—> Record goes off scale. . . Too small or otherwise impossible to measure.

[7] H. W. Newton, *M.N.*, **102**, 2, 1942; M. A. Ellison, *M.N.*, **102**, 11, 1942; R. R. McMath and Orren Mohler, *Observatory*, **68**, 110, 1948.

[8] M. A. Ellison, *Pub. R. Obs. Edinburgh*, **1**, 53, 1950.

[9] H. W. Dodson, E. R. Hedeman, and J. Chamberlain, *Ap. J.*, **117**, 66, 1953.

TABLE 1

NO.	DATE	SOURCE	Hα FLARE OBSERVED (UT)	Hα FLARE MAX. (UT)	Hα FLARE IMP.	Hα FLARE POSITION	SID TIME (UT)
	1948						
1	Aug. 17	b	1726		2	13N 09E	no
2	Aug. 30	b	1650 - 1705		1	25N 54W	WWV fade
3	Oct. 11	b	1210 - 1455	1240	2	15N 78E	1220 - 1345
4	Oct. 21	b	1705 - 1711		1	11S 32W	no
5	Oct. 22	b	1139 - 1210	1142	1+	11S 43W	no
6	Oct. 27	a	1700 - 1750		2	05S 50W	no
7	Nov. 10	b	1322 - 1435		2	11S 04W	no
8	Nov. 10	b	1600 - 1620		1	11S 06W	no
9	Nov. 13	b	1645 - 1652		2	08S 63E	1649 - 1715
10	Nov. 22	b	1312 - 1415		2	12S 60W	1353 - 1445
11	Dec. 3	b	1345 - 1349		1	11N 22W	1345 - 1420
12	Dec. 10	b	1758 - 1808		2	09S 49E	no
13	Dec. 24	b	1704 - 1719		1	15S 10W	1634 - 1805
	1949						
14	Feb. 9	b	1706 - 1719		2	09S 58W	1651 - 1810
15	Feb. 17	b	1707 - 1717		1	11S 13W	1704 - 1730
16	Mar. 11	b	1302 - 1311		1	09S 53E	no
17	Apr. 13	b	1130 - 1315	1210	3	22N 48E	1157 - 1212
18	Apr. 25	b	1056 - 1107		1	16N 12E	no
19	Apr. 25	b	1132 - 1150		1	15N 10E	no
20	Apr. 27	a	1750		2	10S 30W	1755 - 1805
21	Apr. 28*	a,b	1745 - 1810	1752	2	10S 44W	1753 - 1810
22	Apr. 29	a	1636 - 1700	1641	1	10N 90W	1640 - 1800
23	Apr. 29	a	1713 - 1730		1	10S 50W	no
24	May 8	a,b	1528 - 1720	1531	2+	20S 37E	1529 - 1900
25	June 1	a	1755		1	05N 10W	no
26	June 2	a,b	1539 - 1625	1550	1+	05N 25W	no
27	June 4*	a,b	1605 - 1730	1621,1635	2	04N 51W	1613 - 1920
28	June 22*	a,b	1703 - 1900	1714	2	09N 55E	1705 - 1925
29	June 27	a,b	1553 - 1627	1605	1+	16N 45W	no
30	June 28	b	1628 - 1636		1	06S 05E	no
31	June 28	b	1734 - 1745		1	17N 50W	no
32	July 15	b	1729 - 1815	1733	1	19N 04W	WWV fade
33	July 17	b	1725 - 1736	1729	1	19N 34W	no
34	July 28	a,b	1743 - 1755	1747	1	12S 28E	no
35	July 31	a,b	1411 - 1610	1430,1513	2	21S 06E	1420 - 1600
36	Aug. 7	a	1653		1-	19S 85W	WWV fade
37	Aug. 16*	a,b	1700 - 1830	1748	2	13N 22E	1745 - 1820
38	Sept. 12	b	1520 - 1548		2	16S 45W	1522 - 1600
39	Sept. 17	a,b	1716 - 2051	1719	3	15S 10W	1717 - 2040
40	Sept. 24	b	1721 - 1736	1726	1	08S 22E	no
41	Sept. 24	b	1946 - 2024	2008	2	16S 16W	1944 - ---
42	Sept. 24	b	2005 - 2019	2011	1	08S 20E	2000 - 2045
43	Oct. 1	b	1705 - 1723	1710	1	08N 76E	1710 - 1750
44	Oct. 3	b	1609 - 1614		1	08N 47E	no
45	Oct. 4	b	1610 - 1637	1623	2	14N 30E	1620 - 1640
46	Oct. 11	b	1514 - 1654	1523	2	19N 22E	1517 - 1740
47	Oct. 15	b	1630 - 1700	1638	2	20N 31W	1635 - 1800
48	Oct. 22	b	1352 - 1515	1356	2	05S 50W	1355 - 1440
49	Oct. 29*	a,b	1525 - 1550	1540	3	24N 72E	1531 - 1605
50	Nov. 1*	a,b	1637 - 1705	1639	1+	25N 32E	1642 - 1720
51	Nov. 1	b	1822 - 1852	1836	1	08S 90E	1824 - 1945
52	Nov. 1*	a,b	1954 - 2050	1957	2	25N 37E	no
53	Nov. 5	b	1827 - 1907	1829	1	26N 01E	1830 - 1905
54	Nov. 11	b	1512 - 1532	1527	3	10N 35E	1520 - 1600
55	Nov. 29	a,b	1927 - 2016	1938	1+	20N 37W	1939 - 2150
56	Dec. 1	b	2057 - 2114	2058	2	18N 64W	no
	1950						
57	Jan. 22	b	1501 - 1518		1+	20N 60E	1455 - 1525
58	Jan. 24	b	1500 - 1540	1509	2	12S 40W	WWV fade
59	Jan. 30	b	1420 - 1430		1	23N 59W	no
60	Jan. 30	d	1451 - 1502		1-	18N 45W	no
61	Feb. 18	a,b	1506 - 1536	1511	1	12N 10E	1513 - 1540
62	Feb. 20	b	1618 - 1630		1	11N 16W	1522 - 1620
63	Feb. 23	b	1550 - 1605		1	12N 75W	no
64	Mar. 5	b	1608 - 1628	1621	1	03S 09E	1612 - 1655
65	Mar. 7	b	1430 - 1455	1441	1	27N 03E	no

TABLE 1 (Continued)

NO.	TYPE	200 MC/S RADIO EVENT TIME (UT)		TIME CLASS.	EN.EXC.	REMARKS
1	Minor+	1720 - 1723	1723 - 1745	Double	18.5	
2	Group	1644 - 1654	---	Early	0.70	
3	Major+	1216½- 1219	1219 - 1345	Double	>320.0	
4	Minor	1700 - 1701½	---	Early	1.58	
5	Minor+	1140 - 1141	1141½- 1214	Double	27.75	
6	RBL	---	1725 - 1750	Late	43.8	
7	Minor	1319½- 1320	---	Early	>2.62	
8	Minor	---	1621 - 1622	Late	0.76	
9	Major+(U)	1644½- 1650	1652 - 1709	Double	>23.2	Bursts 2800 Mc/s
10	Major+(U)	1305½- 1307	1326 - 1424	Double	>455.9	
11	Null			Null		
12	Minor	1749 - 1750½	---	Early	>6.15	
13	Minor+	1636 - 1638	1720 - 1805	Double	49.8	
14	Minor	1649½- 1650½	---	Early	>1.54	
15	Onset	---	1738 - 1759	Late	>31.5	
16	Minor	1301 - 1303	---	Early	2.80	
17	Major+	1152½- 1204	1211 ->1230	Double	>62.4	
18	Minor	1057	---	Early	0.52	
19	Micro	---	1142 - 1151	Late	-----	
20	Major+	1724½- 1729	1749 ->1800	Double	>9.72	
21	Series	1751 ->1800		Concurrent	5.20	Precursor 1714-1750 UT
22	Minor	1632 - 1634	---	Early	2.09	
23	Null			Null		
24	RBL	---	<1600 - 1700	Late†	>111.6	
25	Series	1735 - 1756		----0	5.88	
26	Onset	---	1700 ->1800	Late†	>79.1	
27	Major+(U)	1606 - 1614	1614 - 1630	Double	>80.8	Bursts 2800 Mc/s
28	RBL	---	1715 - 1730	Late	12.9	Flare spreads with time
29	Series	---	1620 - 1712	Late†	16.7	
30	Null			Null		
31	Minor	1738½- 1740	---	Early	0.27	
32	Major+(U)	1731½- 1734	1738 ->1800	Double	>23.8	Bursts 2800 Mc/s
33	Null			Null		
34	Minor	1735	---	Early	3.75	
35	RBL	---	<1522 - 1600	Late†	>171.0	
36	Micro	1653 - 1656	---	Early	0.58	
37	Null			Null		Flare has two maxima
38	RBL	---	<1600 - 1635	Late†	>94.5	
39	Null			Null		
40	Major	1722½- 1725½	---	Early	>23.1	
41	Null			Null		No event prior to 2006 UT
42	Major (U)	2006 - 2014	---	Early	>21.8	Bursts 2800, 480, 51 Mc/s
43	Onset	---	1705 - 1810	Late	55.3	
44	Major+	1607½- 1612½	1620 - 1649	Double	7.60	
45	Null			Null		
46	RBL	---	<1605 - 1645	Late†	>16.0	
47	Minor+	1635 - 1637½	1641 - 1700	Double	3.25	Precursor 1625½-1626 UT
48	Major+	1354 - 1401	1358 - 1415	Double	16.4	
49	Null			Null		
50	Micro	---	1644 - 1646	Late	0.092	
51	Micro	1814 - 1856		Concurrent	0.769	Three isolated bursts between 2002 and 2015 UT
52	Onset	---	2035 ->2130	Late	>198.0	
53	Major+	1827½- 1831	1859 - 2010	Double	>266.4	
54	Minor+	1507	1528 - 1610	Double	29.95	
55	Major+	1930 - 1937	2007 - 2029	Double	81.2	
56	Minor	2058 - 2101	---	Early	>9.0	
57	Major	1454½- 1501	---	Early	41.1	
58	Major+	1500 - 1507	1508 - 1550	Double	239.0	
59	Minor	1423 - 1423½	---	Early	0.294	
60	Minor	1444	---	Early	0.318	
61	Major (U)	1500½- 1518	---	Early	350.0	Burst 2800 Mc/s
62	Onset	---	1530 ->1900	Late	>141.0	
63	Series	---	1610 - 1627	Late	5.78	
64	Onset	---	1700 - 1800	Late	18.2	
65	Null			Null		

TABLE 1 (Continued)

NO.	DATE	SOURCE	Hα FLARE OBSERVED (UT)	MAX. (UT)	IMP.	POSITION	SID TIME (UT)
	1950						
66	Mar. 11	b	1522 - 1530	1524	1	28N 48W	no
67	Mar. 28	c	1525 - 1558	1540	(1)	18S 40W	no
68	Apr. 1	c	<1548 - 1616	1600	(1)	14N 36E	1539 - 1615
69	Apr. 5	c	1700 - 1739	1710	(2)	24N 22W	1701 - 1725
70	Apr. 11	b	2005 - 2100	2014	2	14N 24E	1959 - 2130
71	Apr. 12	b	1848 - 2212	1911	2	14N 10E	1839 - 2120
72	Apr. 13	c	1724 - 1804		(1-)	13N 05E	1722 - 1800
73	Apr. 13	c	1850 - 1912	1856	(1-)	13N 05E	no
74	Apr. 13	b	2029 - 2037	2030	1	14N 05W	2025 - 2040
75	Apr. 14	c	1605 - 1620	1609	(1-)	17N 15W	no
76	Apr. 14	c	1649 - 1720	1652	(1)	12N 11W	1649 - 1720
77	Apr. 14	c	1756 - 1811	1800	(1-)	10N 12W	1755 - 1810
78	Apr. 15	b	1521 - 1540		1	14N 26W	1511 - 1530
79	Apr. 18	b	1905 - 1917	1909	1	14N 09E	1903 - 1920
80	Apr. 26	b	1632 - 1640	1635	1	11S 14E	no
81	Apr. 26	b	1747 - 1758	1752	1	13S 12E	1751 - 1805
82	Apr. 28	d	1434 - 1441		1-	21S 33W	no
83	Apr. 28	d	1503 - 1505		1-	21S 33W	no
84	May 3	b	1644 - 1750	1716	1	15N 02E	1710 - 1730
85	May 5	c	1720 - 1815	1746	(1)	18N 27W	1722 - 1845
86	May 5	b	1935 - 2016	1951	1	14N 35W	1937 - 2045
87	May 6	b	1220 - 1248		2	04N 79E	no
88	May 6	a,b	1330 - 1437	1344	2	14N 40W	1330 - 1455
89	May 8	b	2033 - 2111	2041	1	06N 47E	2035 - 2120
90	May 16	c	1950 - 2020	2002	(1-)	03S 65W	no
91	May 20	a,c	1348 - 1440	1352	1	10N 75E	1345 - 1420
92	May 20	a	1618 - 1630	1621	1-	10N 85E	no
93	May 20*	a,b	1806 - 1825	<1815	1	17S 26E	1805 - ---
94	May 20*	a,b	1830 - 1948	1840	2	17S 26E	1830 - 2000
95	May 22	b	2041 - 2102	2044	1	09N 49E	2040 - 2110
96	May 23	b	1230 - 1236	1233	1+	08N 44E	1228 - 1250
97	May 23	b	1352 - 1409	1357	1	08N 44E	1359 - 1435
98	May 31	c	1805 - 2345	1846	(1)	04N 13E	no
99	June 1	a	<1504		1	13N 34W	no
100	June 1*	a	1615 - 1720	1647	1+	05N 03E	1636 - 1700
101	June 1	a,b	1720 - 1750		1	05N 03E	1737 - 1755
102	June 1*	a,b	<1811 - 1859	1816	2	05N 03E	1803 - 1830
103	June 2	b	1752 - 1832	1804	1	05N 15W	no
104	June 6	a,b	1230 - 1244	1239	1	05N 70W	no
105	June 6	a,b	1713 - 1740		1-	04N 70W	no
106	June 8	b	<1159 - 1207		1	16N 34W	1155 - 1210
107	June 9	b	2003 - 2046	2016	1	18S 62E	2003 - 2030
108	June 13	b	1904 - 1945	1906	1	19S 10E	1913 - 1930
109	June 20	a,b	<1230 - 1316	1238	1	10N 23E	1225 - 1315
110	June 20	c	1859 - 2103	1951	(2+)	22N 15E	no
111	June 20	a,c	2024 - 2145	2028	1	10N 20E	WWV fade
112	June 24	c	1750 - 1820	1800	(1)	08N 01E	no
113	June 24	c	1820 - 1850	1840	(1-)	08N 01E	no
114	June 25	c	1610 - 1645	1621	(1)	10N 12W	no
115	June 25	c	1910 - 2000	1919	(1)	12N 03W	no
116	June 26	b	1920 - 2005	1934	1	12N 19W	no
117	June 29	c	1425 - 1500	1444	(1-)	18S 17W	no
118	June 29	b	1714 - 1736		1+	26S 75W	no
119	June 29	b	1736 - 1838	1747	1	09N 63W	no
120	July 1	a,b	1615 - 1626	1616	1-	15S 46W	no
121	July 2	b	1854 - 2059	1913?	1	15S 63W	WWV fade
122	July 4	b	1528 - 1535		1	13S 90W	no
123	July 6	a,b	<1437 - 1512		1-	16N 44W	no
124	July 6	a	1614 - 1650		1-	16N 44W	no
125	July 6	a,c	1850 - 2055	1934	1	16N 12W	no
126	July 7	a	1308 - 1335		1-	19N 59W	no
127	July 7	a	<1800 - 1802		1-	19N 60W	no
128	July 8*	a	1845 - 1958	1850	1	16N 30W	no
129	July 10	a	1310		1-	12N 24W	no
130	July 15*	a,b	1826 - 1925	1837	2	20N 15E	1829 - 1905

TABLE 1 (Continued)

NO.	TYPE	200 MC/S RADIO EVENT TIME (UT)	TIME CLASS.	EN.EXC.	REMARKS
66	Null		Null		
67	Null		Null		
68	Series	--- ; 1638 ->1700	Late	>1.03	
69	Onset	--- ; 1705 ->1715	Late	>28.0	
70	Null		Null		
71	Onset	--- ; 1907 - 1942	Late	36.2	
72	Null		Null		
73	Series	--- ; 1856 - 1905	Late	2.94	
74	Null		Null		
75	Group	1602½ - 1616	Concurrent	6.89	
76	Series	1634 - 1739	Concurrent	3.06	
77	Series	1757 ->1830	Concurrent	>0.594	
78	Null		Null		
79	Series	1905 - 1919	Concurrent	2.03	
80	Minor	1631½- 1632½; ---	Early	9.25	
81	Major+(U)	1748½- 1756 ; 1756 - 1823	Double	>116.3	Bursts 2800 and 73 Mc/s
82	Minor	1429½- 1430 ; ---	Early	-----	
83	Major+(U)	1458 - 1502½; 1511 - 1530	Double	30.0	
84	Null		Null		
85	Series	1700 - 1745 ; 1830 ->2005	Double	2.61	
86	Noise	1830 ->2005	In progress	-----	
87	Onset	--- ; 1230 - 1340	Late	112.0	
88	Onset	--- ; 1400 - 1450	Late	35.7	Isolated burst 1345-46 UT
89	Major	2033 - 2042 ; ---	Early	4.60	
90	Minor	--- ; 2005 - 2010	Late	>4.13	
91	Null		Null		
92	Null		Null		
93	Minor	1810 ; ---	Early	0.094	Light curve decline only
94	Major+(U)	1830 - 1907½; 1907½- 2100	Double	>689.9	Flare spreads
95	Minor+	2040 - 2043 ; 2051 ->2100	Double	>8.0	
96	Onset	--- ; 1250 - 1515	Late	25.3	
97	Noise	1250 - 1515	In progress	-----	
98	Noise	1620 ->2050	In progress	-----	
99	Minor	1450½- 1452½; ---	Early	0.625	
100	Series	1640 - 1720	---- *	6.05	Light curve for decline
101	Series	--- ; 1743 - 1752	Late	3.27	
102	Onset	--- ; 1807 - 2015	Late	152.0	Light curve for decline
103	Noise	1638 ->2100	In progress	-----	
104	Minor	1233 - 1236 ; ---	Early	0.813	
105	Null		Null		
106	Minor	1153 - 1159 ; ---	Early	0.498	
107	Null		Null		
108	Major (U)	1903½- 1912½; ---	Early	106.0	Bursts 2800 and 73 Mc/s
109	Major+(U)	1220 - 1235 ; 1310 - 1440	Double	37.2	Burst 73 Mc/s
110	Null		Null		
111	Minor	2021 - 2023 ; ---	Early	8.4	
112	Noise	{1630 ->1945}	In progress	-----	
113	Noise		In progress	-----	
114	Noise	{1400 ->2100}	In progress	-----	
115	Noise		In progress	-----	
116	Group	1909 - 1922 ; ---	Early	9.38	
117	Series	1417 - 1500	Concurrent	4.07	
118	Series	1635 - 1713 ; ---	Early	3.16	
119	Series	1728 - 1805	Concurrent	6.18	
120	Minor	--- ; 1619½- 1621½	Late	0.25	
121	Series	1825 - 1955	Concurrent	6.75	
122	Micro	1515 - 1518 ; ---	Early	0.42	
123	Series	1430 - 1530	Concurrent	2.32	
124	Series	1610 - 1700	Concurrent	0.76	
125	Null		Null		
126	Minor	--- ; 1317 - 1318	Late	1.86	
127	Minor	1752 - 1753 ; ---	Early	0.36	
128	Null		Null		
129	Micro	1250 - 1309 ; ---	Early	0.36	Flare has small initial brightening at 1820 UT
130	Null		Null		

TABLE 1 (Continued)

NO.	DATE	SOURCE	Hα FLARE OBSERVED (UT)	Hα FLARE MAX. (UT)	Hα FLARE IMP.	Hα FLARE POSITION	SID TIME (UT)
	1950						
131	July 17	b	1339 - 1406		1+	10N 36E	1335 - 1400
132	July 18	a,b	<1316 - 1440		2-	20N 30W	1312 - 1340
133	July 19	a,b	1500 - 1547	1504	1	20N 48W	no
134	July 20	c	<1939 - 1955	1942	(1)	07N 13E	no
135	July 21*	a,b	1311 - 1344	1318	2+	10N 10E	1315 - 1340
136	July 21*	a,b	1342 - 1400	1345	2	18N 70W	no
137	July 22*	a,c	<1525 - 1540		1-	10N 07W	WWV fade
138	July 22*	a,b	1549 - 1625	1552	1+	10N 07W	1548 - 1605
139	Aug. 1	b	1325 - 1350	1328	2	10S 40E	no
140	Aug. 1	b	1635 - 1710	1646	1+	10S 40E	WWV fade
141	Aug. 1	b	1725 - 1900	1820	1	10S 40E	no
142	Aug. 1	b	1935 - 2015	1948	1	10S 40E	no
143	Aug. 1	c	2054 - 2115	2100	1	10S 40E	no
144	Aug. 2*	a	1518 - 1525	1521	1-	10S 25E	no
145	Aug. 2*	a,b	1547 - 1615	1554	2	10S 25E	1547 - 1610
146	Aug. 7	a	1305		1+	08S 35W	no
147	Aug. 7	a,c	1650 - 1716	1705	1-	07S 45W	no
148	Aug. 10*	a,c	1754 - 1815	1758	1-	15N 17E	no
149	Aug. 13	b	1449 - 1522		1	21S 78W	no
150	Aug. 15	b	1748 - 1851	1804	1	15N 04E	1752 - 1818
151	Aug. 16	b	1335 - 1343		1	03N 00E	no
152	Aug. 17*	a,c	1415 - 1452	1440	1	13N 08W	no
153	Aug. 19	a,b	1549 - 1611	1552	1	13N 40W	WWV fade
154	Aug. 22	c	1725 - 1915	1743	1	12N 14W	WWV fade
155	Aug. 22	c	2035 - 2120	2043	1	12N 14W	no
156	Aug. 23*	a,b	1332 - 1430	1336	1	12S 27W	no
157	Aug. 23	c	1700 - 1711	1704	(1-)	13S 26W	no
158	Aug. 24	b	1400 - 1410		1	18S 31W	no
159	Aug. 24*	a	1832 - 1855	1838	1-	13S 33W	no
160	Aug. 24*	a	1909 - 1940	1920	1-	13S 33W	no
161	Aug. 24*	a	2023 - 2100	2030	1	18S 50W	no
162	Aug. 26	b	1500 - 1515		1	13S 75W	no
163	Aug. 28	b	1339 - 1440		1	15N 80E	no
164	Aug. 29	a,b	1455 - 1520		1	13N 64E	no
165	Aug. 29	c	1810 - 1845	1826	(1)	14N 69E	1816 - 1850
166	Aug. 30	b	1450 - 1515	1459	1	14N 58E	no
167	Aug. 30	c	1734 - 1750	1738	(1-)	16N 55E	no
168	Aug. 30	b	1819 - 1846	1834	1	15N 55E	1827 - 1840
169	Sept. 7	a	1800 - 1812		1-	02S 74E	no
170	Sept. 7	a,c	1844 - 1857	1849	1	02S 74E	no
171	Sept. 8	b	1952 - 2023	1959	1	04S 54E	no
172	Sept. 26*	a	1800 - 1925	1820	1	15N 12E	no
173	Oct. 2	c	1718 - 1730	1721	(1-)	07S 28E	no
174	Oct. 9	b	1622 - 1638	1628	1	14S 67E	no
175	Oct. 14	b	1803 - 1822	1805	2	14S 06E	no
176	Oct. 16*	a	1757 - 1807	1800	1-	12S 28W	no
177	Oct. 16*	a	1810 - 1835	1815	1-	12S 28W	no
178	Oct. 16*	a	1846 - 1905	1850	1-	12S 28W	no
179	Oct. 17*	a	1435 - 1500	1437	1-	12S 40W	no
180	Oct. 17*	a	1525 - 1545		1-	12S 40W	no
181	Oct. 17*	a	1740 - 1800	1750	1-	12S 40W	no
182	Oct. 17*	a	1806 - 1850	1821	1	12S 40W	no
183	Oct. 18*	a	1756 - 1840	1758, 1830	1-	12S 50W	no
184	Oct. 18*	a	1935 - 2010	1944, 1956	1-	12S 50W	WWV fade
185	Oct. 18*	a,b	2023 - 2052	2038	1	12S 50W	no
186	Oct. 22	c	1657 - 1720	1701	(1)	28N 08W	no
187	Oct. 31	a,c	1805 - 1835	1809	1-	14N 44E	no
188	Nov. 9	b	1601 - 1652	1612	1	15S 07E	no
189	Nov. 12	c	1545 - 1700	1619	(1)	15N 42E	no
190	Nov. 13	c	1905 - 1930	1915	(1)	17N 26E	no
191	Dec. 5	c	1925 - 1950	1930	(1-)	19N 37W	no
192	Dec. 6	c	2005 - 2018	2010	(1-)	14S 48E	no
193	Dec. 13	b	1434 - 1450	1436	1	15N 00E	no
194	Dec. 14	c	1740 - 1800	1747	(1)	16N 24W	no

TABLE 1 (Continued)

NO.	TYPE	200 MC/S RADIO EVENT TIME (UT)	TIME CLASS.	EN.EXC.	REMARKS
131	Null		Null		
132	Null		Null		
133	Series	1452 - 1537	Concurrent	4.66	
134	Major	1937 - 1942 ; ---	Early	9.50	Light curve for max. and decline; bursts 2800, 545, 255, 80 and 73 Mc/s
135	Major+(U)	1310½- 1322 ; 1325 - 1400	Double	>66.2	
136	Null		Null		Light curve decline only
137	Minor+	1522 - 1524 ; 1534 - 1538	Double	1.95	Light curve decline only
138	Major+	1549 - 1555 ;<1602 - 1622	Double	>42.9	
139	Series	--- ; 1358 - 1435	Late	36.6	
140	Noise		In progress	-----	
141	Noise	1628 ->2100	In progress	-----	
142	Noise		In progress	-----	
143	Noise		In progress	-----	
144	Minor	1518 - 1519½; ---	Early	4.50	
145	Major+(U)	1547 - 1557 ; 1600 - 1640	Double	>61.1	Bursts 545, 255, 73 Mc/s
146	Minor	1302½- 1303 ; ---	Early	0.312	
147	Group	1650 - 1655 ; ---	Early	5.80	Precursor 1632-1633 UT
148	Micro	1750 - 1752 ; ---	Early	0.30	
149	Noise	1430 ->2000	In progress	-----	
150	Major+(U)	1751½- 1756 ; 1800 - 2100	Double	>392.4	Bursts 2800 Mc/s
151	Minor	1329 ; ---	Early	0.017	
152	Group	1417 - 1435 ; ---	Early	2.40	Flare brightens gradually
153	Series	1534 - 1547 ; ---	Early	2.40	
154	Null		Null		
155	Null		Null		
156	Null		Null		
157	Null		Null		
158	Null		Null		
159	Series	--- ; 1837 - 1850	Late	0.783	
160	Micro	1912 - 1930	Concurrent	0.277	
161	Series	--- ; 2032 - 2100	Late	1.97	
162	Onset	--- ; 1530 - 1915	Late	>349.0	
163	Series	1404 - 1530	Concurrent	27.5	
164	Series	1508 - 1517	Concurrent	2.25	
165	Series	1808 - 1854	Concurrent	0.30	
166	Null		Null		
167	Series	1720 - 1730 ; ---	Early	0.046	
168	Series	1819 - 1900	Concurrent	1.89	
169	Series	1803 - 1810	Concurrent	1.50	
170	Null		Null		
171	Null		Null		
172	Null		Null		Flare brightens gradually
173	Micro	1719½ ; ---	Early	-----	
174	Minor	1621 - 1625 ; ---	Early	0.56	
175	Null		Null		
176	Series	1758 - 1920	Concurrent	0.998	Three small but definite brightenings
177	Series		Concurrent		
178	Series		Concurrent		
179	Micro	1434½ ; ---	Early	0.035	
180	Null		Null		Light curve decline only
181	Null		Null		
182	Minor	1806 - 1807 ; ---	Early	0.382	
183	Null		Null		
184	Micro	1934 - 1935 ; ---	Early	0.09	
185	Series	2014 - 2056	Concurrent	2.87	
186	Null		Null		
187	Minor	1759½- 1800 ; ---	Early	1.51	
188	Noise	<1330 - 1715	In progress	-----	
189	Series	1532 - 1607 ; ---	Early	4.20	
190	Onset	--- ; 1907 - 2030	Late	159.0	
191	Null		Null		
192	Major	2003½- 2009½; ---	Early	2.16	See text, Figure 10; burst 2800 Mc/s
193	RBL(U)	--- ; 1433½- 1515	Late	>175.7	
194	Major	1736½- 1742½; ---	Early	16.4	

itself. If the times are not underscored, they refer to the period during which the flare was observed to be in progress. The importance of the flare is an estimate based on an evaluation of both intensity and area. It is designated on a scale of 1–3, 3 referring to an exceptionally large and bright flare. When several observers reported the same flare to the *Quarterly Bulletin on Solar Activity*, but with slightly different times, positions, or even importance, the differences have been resolved as equitably as possible within the judgment of the writers, on the basis of all reported data for the flare in question and all photographic records available at the McMath-Hulbert Observatory. For 36 flares in this study, photometric light-curves are available. These flares are indicated by an asterisk in column 2 of Table 1. The times given for the accompanying S.I.D.'s are usually those for the sudden ionospheric disturbances observed at the National Bureau of Standards, Washington, D.C. Otherwise they refer to the earliest starting time and the latest stopping time reported by the many stations observing the event. The meaning of the quantities entered for the radio data are explained later in the text.

DESCRIPTIVE CLASSIFICATION OF FLARE-ASSOCIATED EVENTS ON 200 MC/SEC RECORDS

Examination of the 200 Mc/sec records shows that the *distinctive events* at the times of the 194 flares included in this study can be divided into ten descriptive categories or types. In addition, there are null cases. For the principal types, a representative radio event and light-curve (when available) of the associated flare are shown in Figures 1 and 2. The ten qualitative, descriptive types are as follows:

1. *Major burst.*—Outbursts[10] and other bursts of large amplitude and more than average duration. The bursts are usually of the complex type, with duration of the order of 1–10 minutes

2. *Major burst and second part.*—A double rise in flux. This type is regarded as the prototype of a flare event at 200 Mc/sec. In the most clear-cut cases there are two distinct increases in the radiation, called the "early rise" and the "late rise," respectively. The early rise, or first part, is a major burst. The late rise, or second part, increases more slowly than the major burst, lasts for 20 minutes or longer, and may consist of a rise in base level, a group or series of bursts, or the onset of a noise storm.

3. *Minor burst.*—A burst of moderate or small amplitude, and duration of the order of 1–2 minutes.

4. *Minor burst and second part.*—A double rise in flux in which the early rise is a minor burst.

5. *Micro burst.*—A just detectable burst of small amplitude, and duration of the order of seconds. Discernible only in quiet periods and assigned as a distinctive event only when the remainder of the record is practically featureless.

6. *Group of bursts.*—A cluster of bursts. Duration of the order of minutes.

7. *Series of bursts.*—Bursts or groups of bursts, occurring intermittently over an interval of time of the order of minutes or hours. Such series of bursts are assigned as distinctive events only when they occur on a smooth record or show as a distinct change in the activity.

8. *Noise storm in progress.*—A temporary increase in radiation is already in progress at the time of the outbreak of the flare, and no other distinctive event is recorded. The noise storm is characterized by numerous, closely spaced bursts, by an increase in the continuum, or by both. Duration is of the order of hours or days.

9. *Onset of noise storm.*—The commencement of a noise storm.

10. *Rise in base level.*—A temporary increase in the continuum with duration of the order of tens of minutes to an hour.

Null cases.—No distinctive event. In a quiet period this means that no detectable event appears on the record. In periods of slight activity it means that there is no event that differs from the general activity.

[10] *Radio Astronomy Status Report No. 15* (School of Electrical Engineering, Cornell University, 1951), p. 7.

Distribution of the 194 flares by type of 200 Mc/sec event and importance of the *Hα* brightening shows that for 151, or 78 per cent of the flares, there were distinctive events on the radio records (see Table 2). Of the 43 flares for which there were no distinctive events on the 200 Mc/sec records, 32 were relatively unimportant flares, but in at least 11 cases the *Hα* phenomena were of major proportions.

TIME RELATIONSHIPS

A comparison of the starting times of the radio events with the *starting* times of the associated flares is shown in Figure 3 and Table 3. The starting times of major, minor, micro, and groups of bursts cluster about the time of commencement of the *Hα* flare.

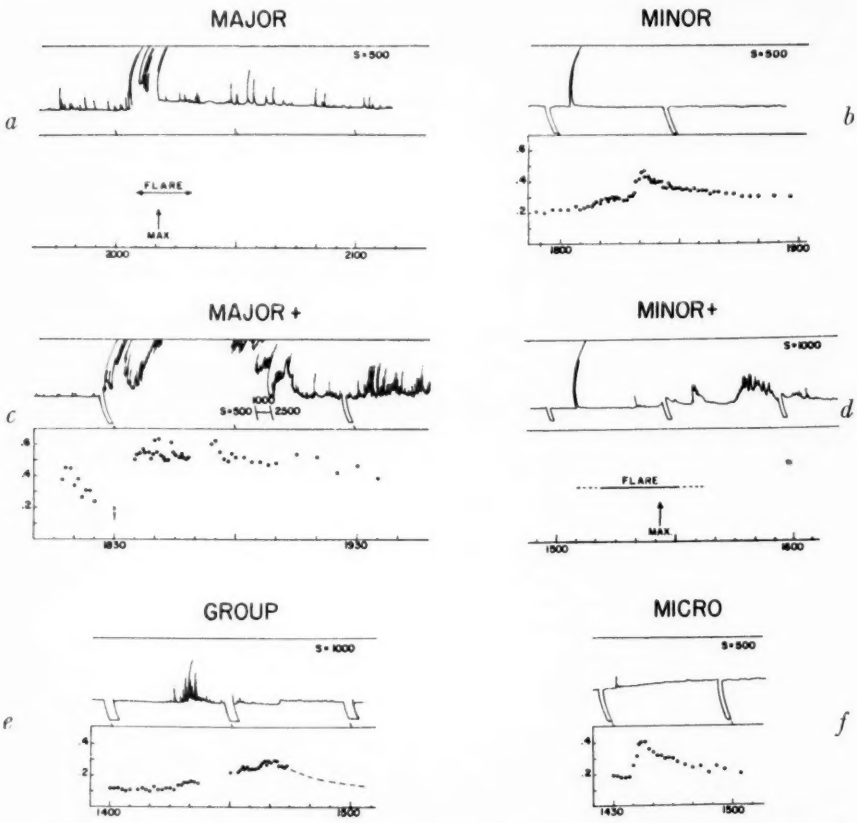

FIGS. 1 and 2.—Examples of types of distinctive events on 200 Mc/sec records at the times of solar flares. The terms "major +" and "minor +" stand for major and minor bursts *with second parts*. *S* gives the value in millivolts of total deflection on the 200 Mc/sec records. The half-hourly reference marks on the radio records correspond approximately to the power received when the antenna is pointed toward the region near the North Galactic Pole.

Photometric light-curves (when available) are given for the associated flares. Ordinates for the light-

For 10 of these flares the starting times are known with great exactness from photometric light-curves. In 8 of these cases the times of commencement for the *Hα* and 200 Mc/sec events agree within 1 minute; for the other 2 cases, the differences are 2 and 4 minutes, respectively.

Onsets of noise storms and rises in base level, although showing a wide scatter, all started *after* the commencement of the flare in *Hα*. The "second parts" of major and minor events show a time distribution similar to that for the onsets of noise storms.

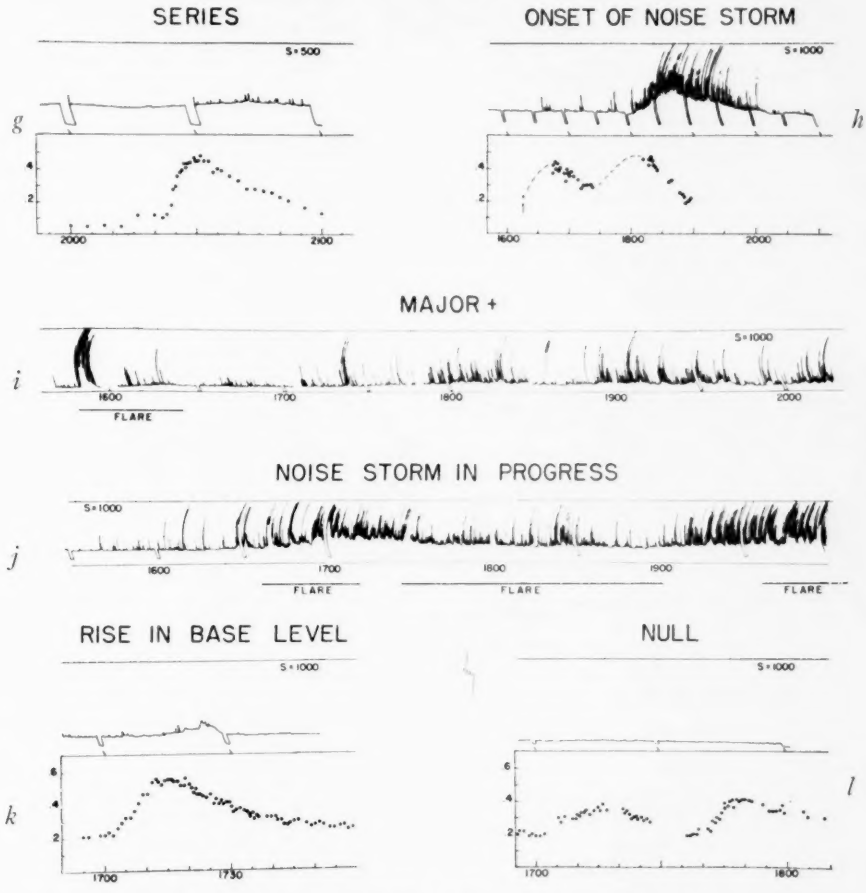

curves are log I/I_0, where I is the intensity of the flare and I_0 is the intensity of the neighboring undisturbed *Hα* disk. All times are U.T.

Dates of flares and corresponding number in Table 1 are as follows: (*a*) September 24, 1949 (42); (*b*) October 17, 1950 (182); (*c*) May 20, 1950 (94); (*d*) November 11, 1949 (54); (*e*) August 17, 1950 (152); (*f*) October 17, 1950 (179); (*g*) August 24, 1950 (161); (*h*) June 1, 1950 (102); (*i*) July 22, 1950 (138) (the second part is onset of a noise storm); (*j*) August 1, 1950 (140), (141), (142); (*k*) June 22, 1949 (28); (*l*) August 16, 1949 (37).

TABLE 2

DISTRIBUTION OF 194 FLARES BY DESCRIPTIVE TYPE OF 200 MC/SEC EVENT AND IMPORTANCE OF FLARE

TYPE OF RADIO EVENT	IMPORTANCE						TOTAL
	1−	1	1+	2	2+	3	
Bursts: Major +	1	6	2	9	1	1	20
Major	1	7	1	...	...	...	9
Minor +	1	1	2	2	...	1	7
Minor	8	17	1	4	...	...	30
Micro	7	3	1	...	...	...	11
Group	2	3	...	...	...	...	5
Series	11	18	3	2	...	...	34
Onset of noise storm	...	6	2	6	...	...	14
Storm in progress	1	12	1	...	...	...	14
Base-level rise	...	1	...	5	1	...	7
No distinctive event	8	23	1	8	1	2	43
Total	40	97	14	36	3	4	194
Percentage with distinctive event	80	76	93	78	67	50	78

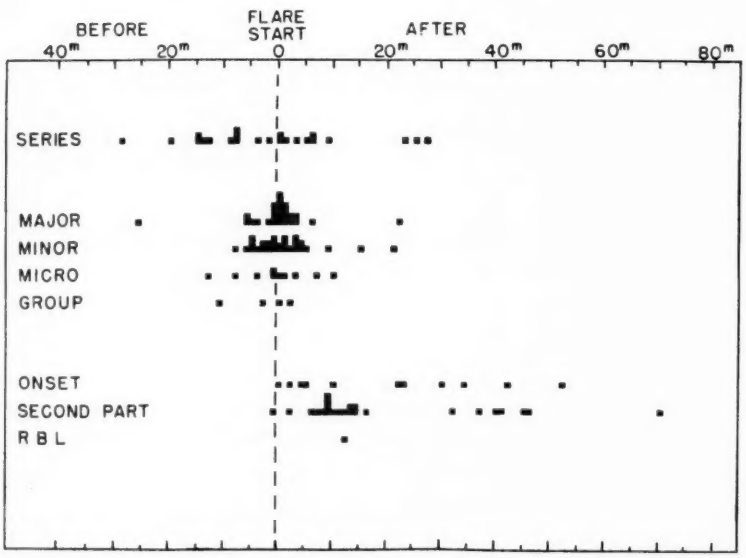

FIG. 3.—Comparison of time of *start* of flare with time of *start* of 200 Mc/sec event. The dashed vertical line represents the starting time of flare. Each square represents the start of a radio event. If it is plotted to the left of the dashed line, the radio event began before the start of the flare.

For the events classified as "series of intermittent bursts" there is a wide scatter and no clear-cut pattern. This category is probably not a homogeneous group.

A comparison of the starting times of the radio events with the times of *maxima* of the associated flares is shown in Figure 4 and Table 3. Practically all the burst-type events were in progress well before the *Hα* maximum of the flare had been attained. The radio events classified as onsets of noise storms, rises in base level, and "second parts" of major and minor events started near *Hα* maximum or even later in the course of the flare. These delayed events on the radio record tend to increase in intensity as the flare fades and often attain their greatest intensity just as the *Hα* flare has faded completely.

CLASSIFICATION OF 200 MC/SEC FLARE-ASSOCIATED EVENTS ON BASIS OF TIME RELATIONSHIPS

The above considerations suggest a separation of the flare-associated 200 Mc/sec "distinctive events" into categories determined by their time relationship to the *Hα* flare.

TABLE 3

COMPARISON OF STARTING TIME OF 200 MC/SEC EVENT WITH START AND MAXIMUM OF *Hα* FLARE

	START OF FLARE* (MIN.)		MAXIMUM OF FLARE* (MIN.)	
	Mean Difference	S.E. of Mean	Mean Difference	S.E. of Mean
Major bursts	− 0.2	±1.4	− 8.3	±1.2
Minor bursts	+ 1.6	±1.2	− 6.0	±1.8
Micro bursts	− 0.4	±2.0	− 6.8	±3.1
Group of bursts	− 2.8	±2.8	−18	±3.9
Onsets and R.B.L.	+20	±4.6	+13	±6.3
Second parts	+18	±3.1	+ 6.8	±3.1

* Negative sign indicates that radio event preceded the *Hα* phenomenon.

1. *Double event.*—This class includes all cases for which there is one distinctive event starting and ending very early in the course of the flare, followed by a second event, which is generally postmaximum in both start and duration.

2. *Early event.*—The distinctive event starts either before or close to the starting time of the *Hα* flare and is concluded long before the end of the flare.

3. *Late event.*—The distinctive event either starts or has its maximum late in the course of the flare. All distinctive events for which the starting time is later than that of the reported flare maximum are here included.

4. *Concurrent event.*—The distinctive event starts approximately with the flare and continues until approximately the end of the flare.

5. *Event in progress.*—This term is used to designate those cases in which a flare occurs in the midst of a noise storm and for which there is no other distinctive event.

The above classification according to time relationships shows that for 28 flares in this study, the 200 Mc/sec events were double. For 50 flares only an early component was present, and for 35 only a late. Furthermore, the early events include principally the relatively isolated burst-type features, while the late events are predominantly rises in base level and the onsets of noise storms. The wide distribution of time relationships repre-

sented in the group of distinctive events described as series of bursts seems to indicate that this type is less homogeneous than the other descriptive classifications (see Table 4).

These studies suggest that two quite different types of phenomena may be represented in the 200 Mc/sec radiation associated with solar flares, one occurring very early in the course of the flare and the other generally taking place at or after flare maximum. This suggestion is strengthened when duration as well as starting time is considered. Figure 5 shows schematically the start and duration of 102 flare-associated distinctive events with

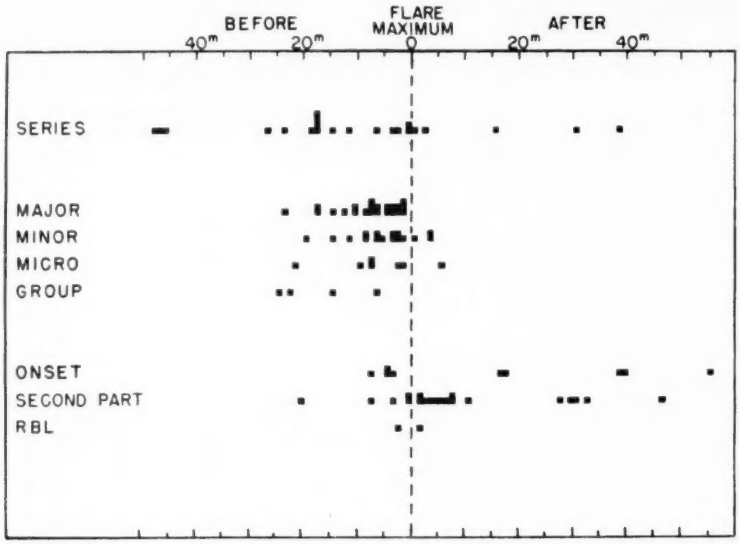

FIG. 4.—Comparison of time of *maximum* of flare with time of *start* of 200 Mc/sec event. The dashed vertical line represents time of maximum of flare. Each square represents the start of a radio event. If it is plotted to the left of the dashed line, the radio event began before the maximum of the flare.

TABLE 4

TIME CLASSIFICATION OF 194 FLARE-ASSOCIATED 200 MC/SEC EVENTS

	Double	Early	Late	Concurrent	In Progress	No Distinctive Event	Incomplete Data	Total
Major burst	20	9						29
Minor burst	7	26	4					37
Micro burst		7	2	2				11
Group of bursts		4		1				5
Series of bursts	1	4	9	19			1	34
Onset of noise storm			13				1	14
Storm in progress					14			14
Base-level rise			7					7
No distinctive event						43		43
Total	28	50	35	22	14	43	2	194

respect to the starting time of the flare. Data for flares which took place while a noise storm was in progress or for which certain time measurements were unknown are omitted from this diagram. From the material here considered, it would seem that the early and late 200 Mc/sec phenomena can occur in conjunction with each other or that either of the two can occur separately.

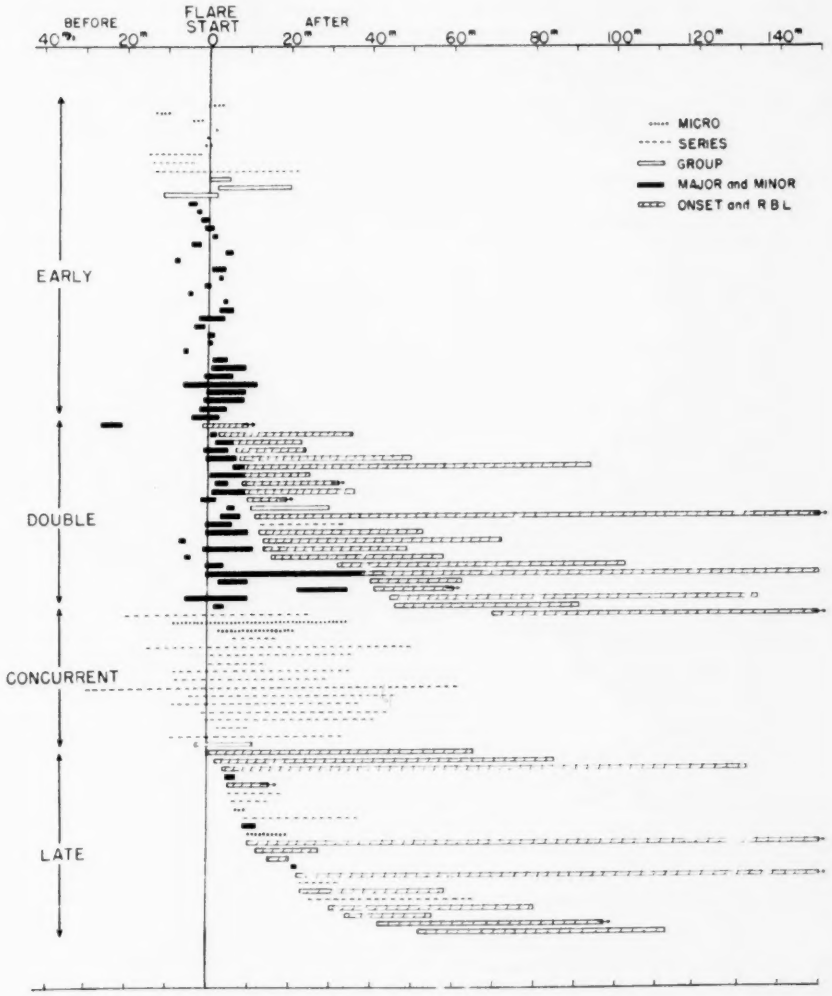

FIG. 5.—Diagram comparing start and duration of 200 Mc/sec event with starting time of flare. The full vertical line represents starting time of flare. Each entry represents a flare-associated radio event. Descriptive type or form of the 200 Mc/sec event is indicated by the drawing code in upper right. Classification, based on time relationships, is shown at the left. Data for flares during a noise storm or for which certain time measurements are unknown are omitted from this diagram, which includes 102 flares.

ENERGY EXCESS OF FLARE-ASSOCIATED DISTINCTIVE EVENTS

In order to put the data on as nearly quantitative a basis as possible, the energy excess of each flare-associated distinctive event has been determined. The energy excess of a distinctive event is defined as the energy content of that part of the received radio-frequency radiation which exceeds the mean flux of solar radiation recorded before the occurrence of the distinctive event. The energy excess is expressed in units of the energy received from the quiet sun in 1 minute and in each instance has been evaluated by graphical integration of the area representing the excess energy for the duration of the

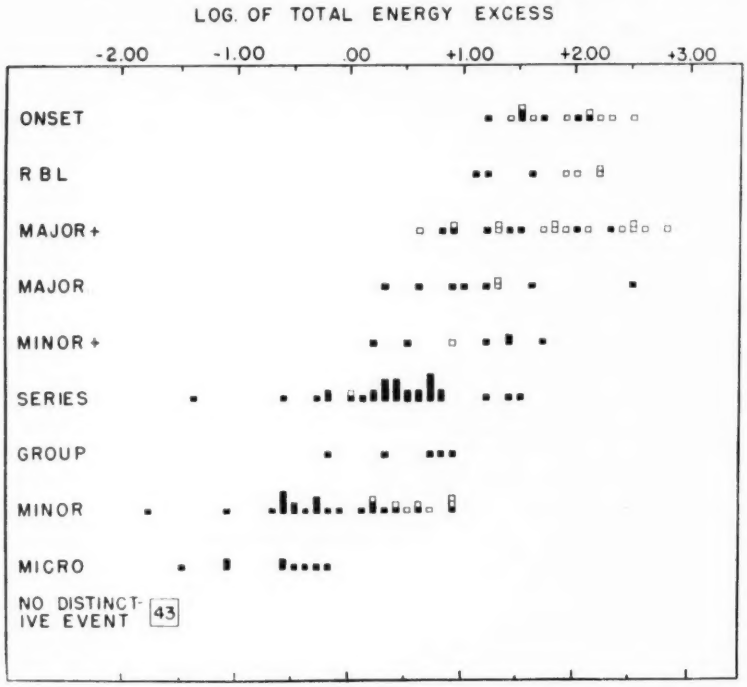

FIG. 6.—Log total energy excess for flare-associated 200 Mc/sec distinctive events separated into descriptive types or classes. Open square indicates lower limit of energy excess; record off scale.

distinctive event on the 200 Mc/sec record. Energy excesses have been obtained for 134 flares. For the 43 null cases and for the 14 flares occurring while a noise storm was in progress, no such measures could be obtained. In the remaining 3 cases the distinctive events were too small to lead to significant values.

For each distinctive event the logarithm of the energy excess in units of the energy from the quiet sun during 1 minute is shown in Figure 6, where the data are distributed according to the descriptive classification of the flare-associated events. Onsets of noise storms, rises in base level, and major bursts with second parts are the types with the greatest energy excess. The other descriptive classes grade down to the very small micro events for which the energy excesses are only about one-thousandth that of the major events.

DISCUSSION OF OBSERVATIONS

IMPORTANCE OF FLARE

A study that attempts to bring together observations of solar flares and concomitant 200 Mc/sec radiation should attempt to answer certain questions that immediately present themselves, once the observations are available. First, it is of interest to know how the greatness of the *Hα* flare compares with that of the associated 200 Mc/sec distinctive event. In order to approach this question, it is necessary to adopt certain quantities as indices of the magnitudes of the two phenomena. For the 200 Mc/sec event, the most obvious measure to choose is energy excess, even though in 26 per cent of the cases in this study the tracings were off scale and only lower limits to the values are available. The only index for all the *Hα* flares is the subjectively assigned quantity "importance." It must be borne in mind that observers at different stations may use different scales in assigning importance. Until measured quantities can replace this qualitative estimate of the greatness of a flare, it will be necessary to guard against overanalysis of the data.

From the information presented in Tables 2 and 5 it can be seen that, for the flares

TABLE 5

PERCENTAGE OF FLARES WITH DISTINCTIVE EVENT AT 200 MC/SEC

Importance of Flare	Total No.	Percentage with Distinctive Event at 200 Mc/Sec
1	151	79
2	39	77
3	4	50
	194	78

TABLE 6

RELATION BETWEEN ENERGY EXCESS OF 200 MC/SEC EVENT AND IMPORTANCE OF ASSOCIATED FLARE

Log Energy Excess	No. of Flares	Percentage of Flares of Importance 2 and 3
≤0.00	36	0
0.01–1.00	49	14
1.01–2.00	34	47
2.01–3.00	18	50

in this study, the proportion of flares accompanied by some form of distinctive event on 200 Mc/sec records does not increase with the importance of the flare. Any direct relationship between the greatness of the flare and that of the 200 Mc/sec event is far from clear, even when consideration is given to the magnitude of the energy excess of the distinctive event. Figure 7 shows a comparative plot of the two quantities—importance of the flare and energy excess of the associated 200 Mc/sec event. The scatter of points is very great. It can be said, however, that the average energy excess of distinctive events associated with flares of importance 2 is greater than that associated with flares of importance 1. Even this most general relationship appears to break down for flares of importance 3. Only 4 flares of importance 3 are included in this study. For 2 of these major flares there was no distinctive event at 200 Mc/sec. For the other 2 the distinctive events, though definite and clear cut, were far from being the greatest of the 200 Mc/sec events considered in this study. See Figure 1, *d*, for an example of the 200 Mc/sec record of a flare of importance 3.

In Table 6 the flares have been grouped according to the magnitude of the energy excess. As the energy excess increases, there is an increasing percentage of flares of importance 2 and 3 in each group. Nevertheless, 50 per cent of the 200 Mc/sec events with highest energy excess occurred at times of flares of importance 1.

The 43 flares for which there were no distinctive events on the 200 Mc/sec records are excluded from Table 6 and from the above discussion. They constitute a group of flares associated with essentially zero energy excess on the 200 Mc/sec records. On the basis

of the figures in Table 6, they might be expected to include only unimportant flares. This is not the case; 11 flares, or 26 per cent of the group, were of importance 2 and 3 (see Table 2). The proportion of flares of importance 1, 2, and 3 for the null cases is very similar to that for the total set of 194 flares. Of the eleven descriptive categories into which the flares have been divided, the null group is the only one for which this is the case (see Fig. 8).

The data have been examined for indications of a possible relationship between the form or type of the distinctive event and the importance of the *Hα* flare. The results are presented in Figure 8. There appears to be a much higher percentage of flares of importance 2 and 3 associated with the major and minor bursts *with second parts* than with the major and minor bursts alone. The high percentage of flares of importance 2 with cases of

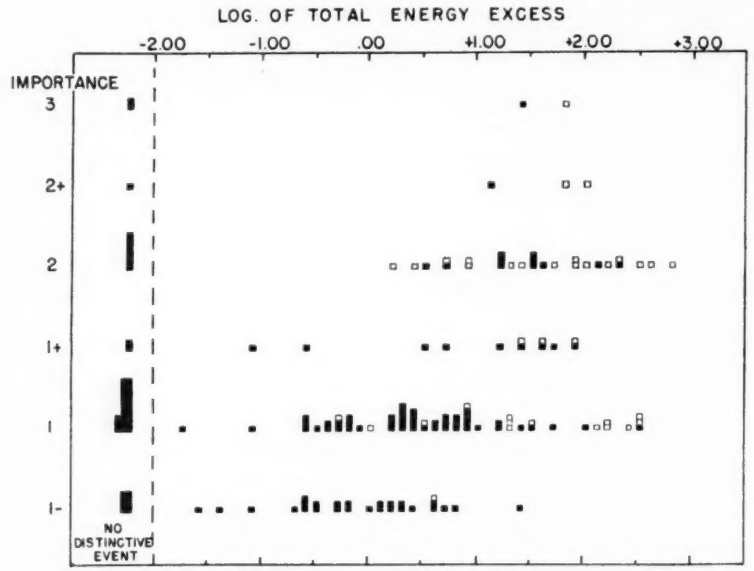

FIG. 7.—Log total energy excess of flare-associated distinctive events separated into groups according to the importance of the associated flare. Open square indicates lower limit of energy excess; record off scale.

onsets of noise storms and rises in base level, both "late" phenomena, further stresses this apparent association between important flares and the occurrence of the postmaximum or "late" event on the 200 Mc/sec records. Of the 32 distinctive events associated with flares of importance 2 and 3, 26, or 81 per cent, were 200 Mc/sec events with a late component (see Tables 2 and 4). It would therefore appear that if an important flare has an associated 200 Mc/sec event, it is likely to be of either the double or the late type.

SUDDEN IONOSPHERIC DISTURBANCES (S.I.D.)

Thirty-eight per cent of all the flares in this study were associated with sudden disturbances of the earth's ionosphere. Separation of the flares into two groups according to the presence or absence of an associated distinctive event at 200 Mc/sec does not affect this percentage. Ionospheric disturbances occurred with 38 per cent of the flares having distinctive 200 Mc/sec events and with 37 per cent of the null cases (see Tables 7 and 8).

The occurrence of a 200 Mc/sec distinctive event does not, in itself, seem to change the probability of an S.I.D. accompanying a flare. Nevertheless, consideration of the magnitude of the flare-associated 200 Mc/sec events permits separation of the flares into groups in which the frequency of S.I.D.'s is significantly different from the average (see Table 7). Ionospheric disturbances accompanied 67 per cent of all flares in this study for which the log of the energy excess of the associated 200 Mc/sec event was >1.0. Such disturbances occurred with only 17 per cent of the flares for which the log of the energy excess at 200 Mc/sec was zero or negative.

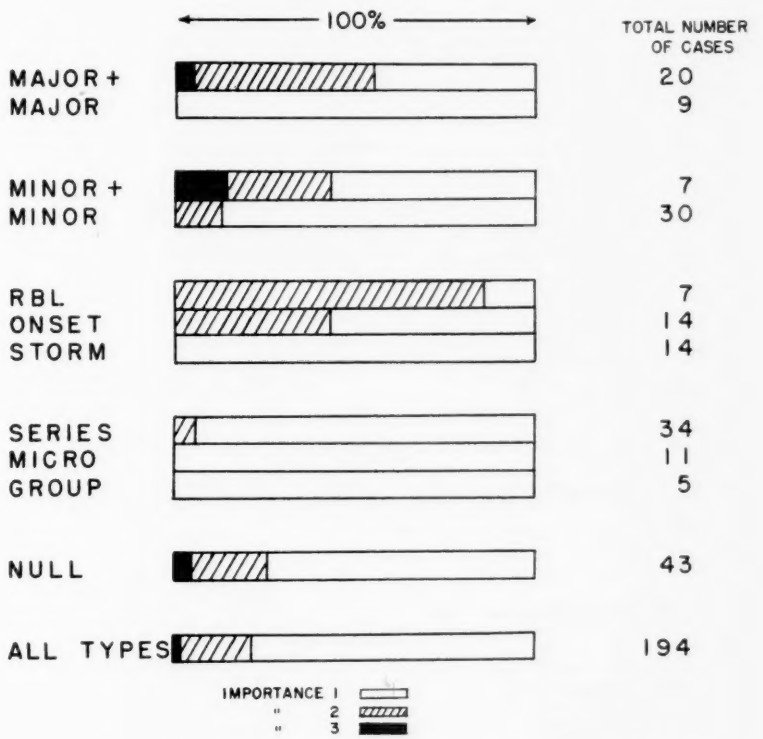

FIG. 8.—Percentage of flares of importance 1, 2, and 3 for each descriptive type of flare-associated 200 Mc/sec distinctive event.

A much higher percentage of S.I.D.'s occurred with flares for which the 200 Mc/sec distinctive events were classified as major bursts, major or minor bursts with second parts, rises in base level, and onsets of noise storms than with the flares in the five other descriptive classifications (see Table 8). The types of 200 Mc/sec events here shown to have a high percentage of associated S.I.D.'s are also the types with large average values of the energy excess.

The flares in this study exhibit the well-known fact the S.I.D.'s occur more frequently with flares of importance 2 and 3 than with flares of importance 1 (see Table 9).

POSITION OF FLARE ON DISK

The data have been examined for a possible relationship between the various aspects of the flare and its position on the solar disk. No clear dependence on position has been found. The average central meridian distance is 35°.0 for all flares in the study—34°.9 for flares of importance 1; 35°.0 for flares of importance 2; and 41°.2 for the 4 flares of importance 3. For flares with associated ionospheric disturbances the average distance from the central meridian was 31°.9, and for those without S.I.D.'s, 36°.9. The averages for both these groups thus lie within 3° of the average for all cases.

TABLE 7

RELATION BETWEEN ENERGY EXCESS OF FLARE-ASSOCIATED 200 MC/SEC EVENT AND OCCURRENCE OF S.I.D.

LOG ENERGY EXCESS	TOTAL NO. OF FLARES	FLARES WITH ASSOCIATED S.I.D.'S	
		No.	Per Cent
2.01–3.00	18	12	67
1.01–2.00	34	23	68
0.01–1.00	49	14	29
≤0.0	36	6	17
Noise storm in progress	14	2	14
No distinctive event	43	16	37
All cases	194	73	38

TABLE 8

RELATION BETWEEN TYPE OF FLARE-ASSOCIATED 200 MC/SEC EVENT AND OCCURRENCE OF S.I.D.

TYPE OF 200 MC/SEC EVENT	TOTAL NO. OF FLARES	FLARES WITH ASSOCIATED S.I.D.'S		LOG AVERAGE ENERGY EXCESS
		No.	Per Cent	
Major burst and second part	20	16	80	>2.18
Rise in base level	7	5	72	>1.95
Onset of noise storm	14	9	64	>2.00
Minor burst and second part	7	4	57	>1.30
Major burst	9	5	56	>1.80
Series of bursts	34	10	29	0.71
Micro burst	11	2	18	−0.49
Storm in progress	14	2	14	(?)
Minor burst	30	4	13	0.35
Group of bursts	5	..	0	0.70
Total of all flares with distinctive events	151	57	38	.....
Null	43	16	37	.....
Total	194	73	38	.....

There is some slight indication that the energy excess of the flare-associated distinctive events is greatest for flares near the central meridian of the sun (see Table 10).

The same trend appears from measures of the average meridian distance of the flares associated with each of the types of 200 Mc/sec distinctive events, ranked according to the average energy excess of each type (Table 11). The five types of 200 Mc/sec events with greatest energy excess were associated with flares which were, on the average, closer to the central meridian than were the flares associated with the principal types having lower energy excess. Individual cases showed wide departures from the trend suggested by the average values.

TABLE 9

RELATION BETWEEN IMPORTANCE OF FLARE AND OCCURRENCE OF S.I.D.

IMPORTANCE	TOTAL NO. OF FLARES	FLARES WITH ASSOCIATED S.I.D.'s	
		No.	Per Cent
3	4	4	100
2	39	27	69
1	151	42	28
Total	194	73	38

TABLE 10

AVERAGE ENERGY EXCESS OF 200 MC/S FLARE-ASSOCIATED EVENTS FOR FLARES DISTRIBUTED ACCORDING TO POSITION ON SOLAR DISK

Central Meridian Distance of Flare	Log Average Energy Excess	No. of Cases
0°–15°	1.80	33
16°–30°	1.72	25
31°–45°	1.47	32
46°–60°	1.47	26
61°–75°	1.50	13
76°–90°	1.81	8

TABLE 11

AVERAGE MERIDIAN DISTANCE OF FLARES ASSOCIATED WITH DIFFERENT TYPES OF 200 MC/SEC DISTINCTIVE EVENTS

Type	Log Average Energy Excess	Average Meridian Distance of Observed Flares	No. of Cases
Major +	>2.18	32°.4	20
Onset	>2.00	34.0	14
RBL	>1.95	30.7	7
Major	>1.80	28.2	9
Minor +	>1.30	26.2	7
Series	0.71	40.3	34
Group	0.70	28.2	5
Minor	0.35	40.8	30
Micro	−0.49	45.4	11
Noise	Not measured	26.3	14
Null		32.7	43
All cases		35.0	194

Of the flares in this study, 92 occurred in the eastern and 102 in the western half of the solar disk. Twenty-seven per cent of the eastern flares and 18 per cent of the western flares were of importance greater than 1. Furthermore, 49 per cent of the eastern flares and only 27 per cent of the western flares were accompanied by S.I.D.'s. These figures indicate that in this study the eastern flares include a higher proportion of large, intense flares than do the western cases. In spite of this preponderance of important flares in the group to the east of the central meridian, there is no marked difference in the proportion associated with distinctive events at 200 Mc/sec. Seventy-nine per cent of the eastern flares and 76 per cent of the western flares were associated with a 200 Mc/sec event.

EXTENT OF FLARE-ASSOCIATED ACTIVITY ON 200 MC/SEC RECORDS

The data included in this study do not lend themselves readily to an evaluation of the extent to which flares can be associated with the many enhancements observed on records of 200 Mc/sec solar radiation. Nevertheless, it can be said that (1) on many days when no flares were observed, the 200 Mc/sec records were smooth; (2) the 200 Mc/sec records

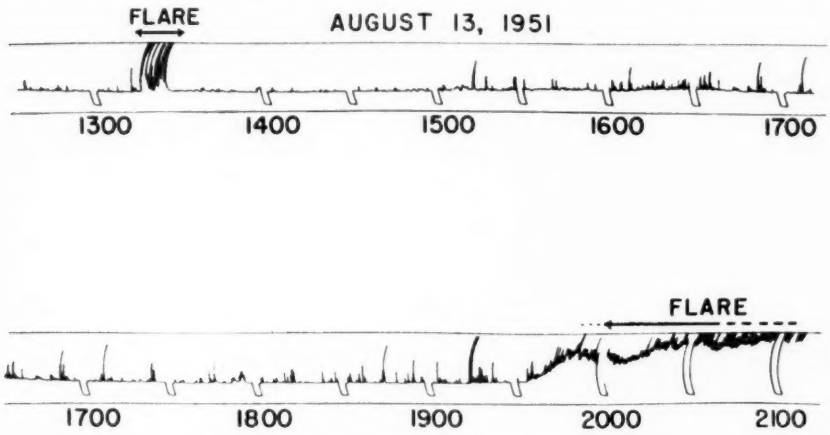

FIG. 9.—Record of 200 Mc/sec solar radiation, August 13, 1951

often showed marked activity when no flare was in progress; (3) on some of the disturbed days, flares can be associated with all the principal enhancements (see Fig. 9).

An association between flares and outbursts has been pointed out by many observers. The material in this study can serve to show the closeness of the correlation between these two phenomena. Twenty-two events on the 200 Mc/sec records between July 23, 1948, and December 31, 1950, were classified as "outbursts" by the Cornell group. According to the Cornell definition, an outburst is "a sudden increase of very large amplitude of the order of twenty times the basic thermal radiation with duration of the order of minutes."[11] If, with the normal recorder sensitivity, a burst was off scale for more than 1 minute, it has been classified at Cornell as an outburst. In those research centers where the dynamic spectra of radio bursts can be determined, "outbursts" are identified by their occurrence over a wide range of frequencies, a slow drift with time to lower frequencies, and duration of the order of minutes.[12] Data published by the IAU and by Coving-

[11] *Ibid.*

[12] J. P. Wild and L. L. McCready, *Australian J. Sci. Res.*, **3**, 387, 1950.

ton[13] in Ottawa provide evidence of outstanding events on radio frequencies other than 200 Mc/sec for 15 of the 22 "outbursts" reported by Cornell.

Eighteen of the 22 distinctive events classified as "outbursts" took place at the time of known flares or S.I.D.'s. No solar observations were being made at the McMath-Hulbert Observatory at the times of the remaining 4 cases (see Table 12).

The starting times of the outbursts and the observed flares agreed closely. For 6 cases the differences were 1 minute or less. For only 1 of the 15 flares here associated with "outbursts" did the starting time differ by more than 5 minutes from that of the outburst.

The latter case was that of December 13, 1950, for which the outburst occurred at 15^h05^m U.T., but the flare was observed as early as 14^h34^m U.T. Examination of the 200 Mc/sec record for this date shows that a small rise in flux began at 14^h33^m U.T. and increased greatly at 15^h05^m U.T., the reported time of the outburst. Comparison with other records brings out the fact that the rate of increase at 15^h05^m U.T., though very great, was more gradual than was the case for other outbursts (see Fig. 10). Covington[13] reports

TABLE 12

ASSOCIATION BETWEEN 22 "OUTBURSTS" AND OBSERVED FLARES AND S.I.D.'S

	No. of Cases	
Flare and S.I.D.	12	
Flare only	3	
S.I.D. only	3	No solar observations were being made at the McMath-Hulbert Observatory at the time of these 7 outbursts
Neither flare nor S.I.D.	4	

an outstanding event of 27 minutes duration starting at 15^h07^m on the 2800 Mc/sec records for this same date. Even though this burst on December 13, 1950, was of great amplitude, lasted for minutes, and occurred on at least two frequencies, its more gradual rise and the fact that it was a "late" phenomenon with respect to the flare suggest that it may be more closely associated with 200 Mc/sec events here classified as rises in base level than with those classified as major bursts. All other outbursts were "early" phenomena. These considerations emphasize the difficulty of identifying homogeneous phenomena from the extensive lists of solar activity at radio frequencies.

It would be valuable to be able to make a study similar to the above for all onsets of noise storms recorded on the Cornell records. However, a complete list of events of this type is not at present available.

ASSOCIATION OF 200 MC/SEC EVENTS WITH SPECIFIC ASPECTS OF COMPLEX FLARE PHENOMENON

Comparison of the photometric light-curves of the *Hα* flare and the 200 Mc/sec records shown in Figures 1 and 2 make it clear that the major, minor, and micro bursts have lifetimes which constitute only small fractional parts of the period of brightening in *Hα*. Furthermore, these bursts are essentially premaximum events and therefore do not seem linked with the "active dark flocculi" or surges which usually occur after *Hα* maximum has been attained. There is limited observational evidence for the ejection of material particles from the sun with very high velocities at the *start* of solar flares.[9] For five flares near the solar limb, such ejections are shown on spectroheliograms and spectra secured with the Stone spectroheliograph of the McMath-Hulbert Observatory. These high-velocity ejections of both hydrogen and ionized calcium atoms were of short duration and

[13] *Reports of Solar Radiation at 2800 Mc/s Recorded at the National Research Council, Ottawa, Canada* (1950).

occurred at the time of the *onset* of the flares. For the times of 4 of the 5 flares, radio observations of the sun are available. They indicate bursts or outbursts of solar radiation at the times of the start of these flares and ejections. Since such bursts do not occur with all flares, the observations suggest that the "early" burst-type events on 200 Mc/sec records may be associated with high-velocity ejections. This interpretation is consistent with the results of interferometric measures made in Australia on 97 Mc/sec which indicate that the sources of certain outbursts at radio frequencies are in rapid motion.[3]

The fact that the "second parts" of 200 Mc/sec events, the rises in base level, and the onsets of noise storms are all primarily postmaximum phenomena suggests a possible association with solar events other than the primary brightening in *Hα*. For some of the

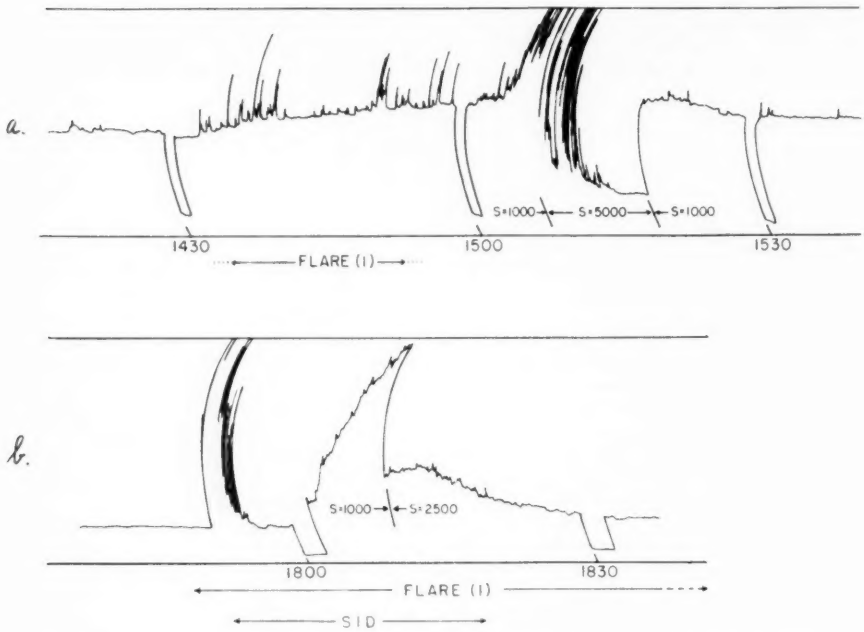

FIG. 10.—*a*, 200 Mc/sec record for December 13, 1950; *b*, 200 Mc/sec record for August 15, 1950

flares with extensive "late" components, there was a significant spreading of the *Hα* flare to adjacent regions after the maximum intensity of *Hα* had been passed. In other cases, but not all, extensive "active dark flocculi" were observed during the course of the postmaximum 200 Mc/sec events. It should be pointed out that "active dark flocculi" were often present with flares for which there was no "late" component and even with the null cases. No definite relationship between these phenomena has been established.

THE NULL CASES

Finally, an attempt should be made to identify possible characteristic features of the group of flares for which there were no distinctive events on the 200 Mc/sec records. From the point of view of the parameters considered in this paper, the null group is not

unique in any way. The proportion of flares of importance 1, 2, and 3 for these null cases is very similar to that for the total set of 194 flares (see Fig. 8). The null group includes 11 flares of importance 2 and 3. The 43 flares with no distinctive event on the 200 Mc/sec records occurred near the center of the solar disk as well as near the limb and in the east as well as in the west. They had the same percentage of accompanying S.I.D.'s as did the flares with distinctive events at 200 Mc/sec. From the above considerations, the 43 null flares appear to be merely a random sample from the entire set of 194 flares. For 7 of the 43 cases there are reports of outstanding events at other radio frequencies; for still other cases the photometric light-curves are atypical. More information for other frequencies and more photometric light-curves may make it possible in the future to arrive at a clearer interpretation of this interesting group of flares.

CONCLUSIONS

1. Although 151, or 78 per cent of the 194 flares included in this study, were found to have accompanying events at 200 Mc/sec, 43 flares, including 11 major *IIa* phenomena, did not. The flares for which no distinctive event took place at this radio frequency represent a random sample of the entire set of 194 flares.

2. A characteristic flare event at 200 Mc/sec exhibits a double rise in flux. The first part of this increase consists in a sudden major burst of complex shape. The second part is an enhancement in the 200 Mc/sec radiation which starts more gradually. When the second part is fully developed, it is identical with the feature known as a "noise storm." The first of the components occurs at the time of the commencement of the flare. The second component starts after the beginning of the flare, usually after the time of flare maximum and as the flare is fading. Not all flare events show the complete double pattern. In this study, 28 flare events were found to be double, in 50 cases only the early component appeared, and for 35 flare-associated events only the late component was present. There were 22 flare events at 200 Mc/sec that conformed neither to the complete nor to the truncated characteristic pattern but had to be described in terms of series or groups of bursts occurring concomitantly with the flare.

3. Relationships were sought between the 200 Mc/sec flare-associated events and the following parameters of the flare phenomenon: (*a*) the importance of the flare, (*b*) the position of the flare on the sun's disk, and (*c*) the occurrence or nonoccurrence of an S.I.D.

a) For the flares in this study, the percentage accompanied by an associated event at 200 Mc/sec does not increase with the importance of the flare. However, the energy excess of distinctive events associated with flares of importance 2 tends to be greater than that associated with flares of importance 1. For flares of importance 3, the number of cases is too small to permit definite statements, but it is significant that flares of importance 3 can occur which are not accompanied by a distinctive event at 200 Mc/sec. When a major flare has an associated event at 200 Mc/sec, it is likely to be of either the double or the late type.

b) There is no marked relationship between the position of a flare on the solar disk and the associated 200 Mc/sec radiation. There is some indication that the average energy excess of flare-associated distinctive events is greatest for flares occurring nearest the central meridian of the sun. No preference for either the eastern or the western half of the sun's disk was shown by the flares which were associated with 200 Mc/sec events.

c) Whether or not a 200 Mc/sec event accompanies a flare appears to have no direct bearing on whether or not an S.I.D. occurs in conjunction with the flare. When a flare was accompanied by both a radio event and an S.I.D., the radio event usually was of a type having a large energy excess. Ionospheric disturbances accompanied 67 per cent of the flares for which the log of the energy excess was >1.0.

4. The close association of outbursts with flares already noted by other observers is borne out by this study.

5. It is suggested that the "early" burst-type events on 200 Mc/sec may be associated with high-velocity ejections of material particles. Five flares have been observed near the solar limb for which ejection of material particles at the *start* of the flare is known to have taken place. For 4 of the 5 cases, reports of solar radiation at radio frequencies are available and indicate the occurrence of bursts or outbursts at the start of the flare and ejection.

The writers wish to express their appreciation to Dr. Robert R. McMath, director of the McMath-Hulbert Observatory, and to Dr. Charles R. Burrows, director of the School of Electrical Engineering, Cornell University, for their constant support and guidance in this joint program. Long series of observations are possible only through the co-operation of many persons. The writers are grateful to their colleagues who have shared in this investigation and especially to Mr. C. L. Seeger and Mr. S. M. Colbert, who secured many of the 200 Mc/sec records; to Mrs. Helen M. Tryon and Mrs. Cecelia Reineke, who assisted in their reduction; and to Mr. Willard Olson and Mr. Clifford Bennett, who took part in both the photography of solar activity and the presentation of the data in this paper. They also wish to express their gratitude to Dr. Ralph Williamson for his interest in the work and his reading of the manuscript.

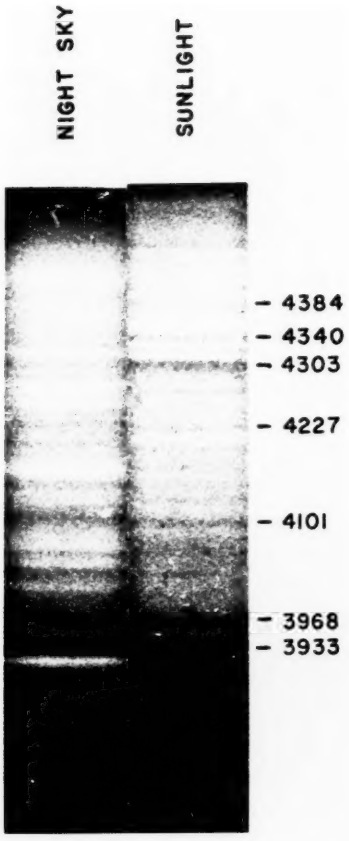

FIG. 1.—A comparison of spectra of the night-sky light and scattered sunlight in the blue region

STELLAR ABSORPTION LINES IN NIGHT-SKY SPECTRA

JOSEPH W. CHAMBERLAIN AND NORMAN J. OLIVER
Geophysics Research Directorate, Air Force Cambridge Research Center,
Air Research and Development Command
Received April 16, 1953

ABSTRACT

Evidence is presented that the blue and violet regions of the light of the night sky are primarily composed of starlight rather than airglow emission. Most of the features heretofore believed to be emission bands are probably unreal, the deceptive appearance being produced by surrounding absorption lines. This interpretation not only explains numerous previously unidentified features but also may reconcile the observed intensities of true emissions with their theoretical transition probabilities. Moreover, the night-sky continuum, so predominant in the blue, is attributed to stellar, not to airglow, radiation.

Spectra of the night sky in the blue and violet contain a large number of features that have not yet received satisfactory identifications. We have noticed on spectra of these regions recently secured in Massachusetts; Thule, Greenland; and Point Barrow, Alaska, that many of the most pronounced "depressions" between "emissions" coincide with some of the strong absorption lines in the solar spectrum. Subsequently, several plates of scattered sunlight have been obtained with the airglow spectrograph (65 A/mm in the second order of the grating) for comparison purposes. Since the same optical arrangement and slit width were used, the daytime-sky exposures were less than 10^{-6} the duration of those on the night sky to produce spectra of comparable density.

A comparison of spectra and microphotometer tracings of the night sky and scattered sunlight, as shown in Figures 1 and 2, strongly suggests that the blue region of the night-sky light contains a large amount of stellar, as well as some airglow,[1] radiation. An examination of spectra and tables of measured wave lengths published by various other observers indicates that this absorption spectrum appears on all plates obtained in the blue region, in spite of the usual precautions to exclude the zodiacal light and starlight from the Milky Way. Our plates covering the spectrum shortward of 5000 A show many absorption lines, but there is some evidence that airglow emission may be relatively more important in the green than in the blue region. Longward of 5500 A the "infrared" *OH* bands are quite prominent, and the stellar continuum is consequently not so conspicuous. Similarly, the region shortward of 3800A is probably not greatly affected by the stellar light. Whereas sunlight scattered into the earth's atmosphere by interplanetary dust could conceivably produce the observed effect, it is more likely that light from naked-eye and unresolved stars and to some extent the diffuse illumination in the galaxy[2] are responsible.

Observations on the light of the Milky Way[3] show that the spectral composition of the galactic light is similar to, although by no means identical with, that of a solar-type star. There is a large number of important differences, as well as similarities, between the solar and night-sky spectra, and many of these discrepancies are attributable to the differences in spectral characteristics between the galactic light and a star of spectral type G0. Original spectral plates of galactic clusters or unresolved Milky Way stars, obtained with an astronomical telescope and a dispersion and resolving power comparable

[1] The term "airglow" is defined as that part of the light of the night sky emitted by the earth's upper atmosphere.

[2] Henyey and Greenstein, *Ap. J.*, **93**, 70, 1941.

[3] E. A. Fath, *Ap. J.*, **36**, 362, 1912. Clusters and extragalactic nebulae give similar spectra; see Fath, *ibid.*, **37**, 198, 1913.

to that commonly used in airglow work, would be valuable in deciphering the airglow spectrum. Also, a comparison of night-sky spectra made on a bright part of the Milky Way at small zenith distances and on a dark region near the horizon should show enhancements of the airglow radiation in the latter spectrum. At present it is difficult to list with certainty very many emissions from the airglow in the region below 5500 A because of the uncertainty in the characteristics of the background radiation.

The feature at 3914 A is definitely an emission and was considerably stronger in Greenland and Alaska than in Massachusetts. However, it is probable that there is considerable fluctuation of λ 3914 at any particular site, and no definite statements can now be made regarding a latitude effect. The most likely identifications for this emission are O_2 Schumann-Runge (1–18) and N_2^+ First Negative (0–0). Our plates give no *definite* evidence of enhancements, in the high-latitude spectra, of other Schumann-Runge bands, whereas our spectrum showing the strongest λ 3914 also gives a slight enhancement at 4278 A, the wave length of First Negative (0–1). In Figure 2 the absorption at 4272 A is shifted slightly to the violet in the night-sky spectrum, which may indicate the pres-

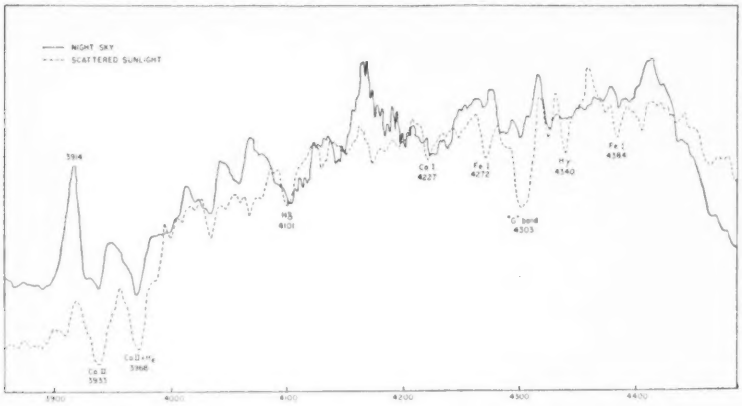

FIG. 2.—Microphotometer tracings of the spectra shown in Fig. 1

ence of emission at 4278 A. The data available at present, however, are not sufficient for a conclusive identification.

To summarize, the following considerations arise from the above interpretation of night-sky spectra.

1. *Identifications.*—Many of the "emissions" heretofore unidentified may be ascribed solely to an illusion, as it were, produced by the absorption lines. On the other hand, many true emissions are probably obscured by the absorption spectrum; for example, $H\gamma$ gives the appearance of being "filled in" by emission, since the $H\beta$ and $H\delta$ absorptions are quite strong in the night sky. A comparison of the solar and night-sky spectra should not be carried too far, however, because numerous false identifications would undoubtedly result. It is quite likely, for instance, judging from Fath's[3] description of the Milky Way spectrum, that the broad, conspicuous brightening on the night-sky spectrum around 4165 A is due to the stellar continuum and that the neighboring continuum is lowered by numerous close absorption lines.[4] It must be emphasized that all identifi-

[4] A quantitative discussion of this effect in a K0 dwarf star has been given by Lewis and Liller, *Ap. J.*, **116**, 428, 1952.

cations shortward of 5500 A should be re-examined when accurate quantitative information on the starlight spectrum becomes available.

2. *Intensities.*—The relative intensities of the Vegard-Kaplan and other bands in the green, blue, and ultraviolet will be affected considerably by the irregular underlying continuum. Herein may lie the explanation of why the Vegard-Kaplan bands in the airglow (if, indeed, they are present at all) give a very poor correlation with the theoretical relative transition probabilities, although eye estimates of the auroral-band intensities correlate very nicely.[5] Although the stellar spectrum is certainly not so relatively important in the red and near infrared, it may produce a number of intensity and identification anomalies that will be more apparent as our dispersion and resolving power are increased.

3. *Continuum.*—The well-known "airglow continuum" lying redward of 3900 A is probably, in fact, a stellar continuum. The appearance of a discontinuity around 3900 A is due in part to absorption lines; however, the night-sky spectrum in the blue region has an intensity distribution with wave length that is very similar to that of a blue, sunlit sky, which, in turn, should have an energy-curve not greatly different from that of the galactic light. Thus it seems likely that no ionospheric reaction need be invoked to explain the continuous spectrum.

[5] Chamberlain and Oliver, *J. Geophys. Res.*, in press.

ORIGIN OF THE CONTINUUM IN THE NIGHT-SKY SPECTRUM*

A. B. MEINEL
Yerkes Observatory
Received April 15, 1953

ABSTRACT

A re-examination of the continuum of the airglow spectrum in the region 3700–4800 A has shown that the continuum may be more completely due to starlight than has been supposed. The H and K lines of calcium and $H\delta$ are found to be prominent on all airglow spectra. The spectral class is definitely earlier than solar (G2), being F8 at $H\gamma$ and F0 at H and K. The emission at 3914 A in the airglow is identified as N_2^+ (0, 0) and represents a true permanent aurora due to the excitation by cosmic-ray particles.

The spectrum of the light of the night sky appears to be dominated in the blue and violet by a strong continuum upon which a few emissions are superimposed. This continuum becomes apparent just below 3900 A and extends without limit to the red. Actual spectra show a dip in the continuum in the green; however, this is only a consequence of the generally lower green sensitivity of the photographic emulsion.

The analysis of this continuum has always presented difficulty. Barbier[1] assigned the continuum (80 per cent) to overlapping molecular airglow bands (53 per cent), to zodiacal light (15 per cent), and to unresolved stars (12 per cent). Recent spectra obtained by Barbier, when combined with extensive nebular spectra obtained at Yerkes and McDonald Observatories, indicate that a re-examination of the continuum is required.

A recent spectrum obtained by Barbier with a one-prism quartz spectrograph and kindly loaned to the author is reproduced in part in Figure 1. This spectrogram of superior resolution shows that the gaps between the "emissions" at 3911, 3947, and 4011 A are considerably deeper than the normal continuum level. This fact and the exact correspondence with the wave lengths of the H and K lines of *Ca* II raises the suspicion that the "continuum" may be more completely due to starlight than has been supposed.

Older reviews of this subject always mentioned the H and K lines as being prominent, notably on spectra taken by Rayleigh.[2] Later studies with higher dispersion, which gave sharper emission features, usually did not show the H and K lines so conspicuously. In fact, some recent reviews have even failed to mention their appearance.

When the spectrum by Barbier (Fig. 1) is carefully examined, one finds that certain other features currently listed as "emissions" are, in fact, gaps between absorption features in a stellar-type continuum. For instance, to the red of 3900 A one readily recognizes the prominent stellar-absorption features shown in the accompanying tabulation.

λ 3888.....	*H*9, *CN* (0, 0)	λ 4144....	*Fe* I
3933 7...	K band, *Ca* II	4215....	*CN* (0, 1)
3968 5...	H band, *Ca* II and *He*	4303....	G band
4101.....	$H\delta$	4344....	$H\gamma$

The reality of these absorption features has been checked by studying the large series of nebular spectrograms taken by Struve and Elvey with a two-prism quartz *F*/1 spec-

* The research in this paper was sponsored by the Geophysics Research Directorate, Air Force Cambridge Research Center, Air Research and Development Command, under Contract AF 19(122)-480.

[1] *Ann. d'ap.*, **10**, 141, 1947.

[2] *Nature*, **106**, 8, 1920.

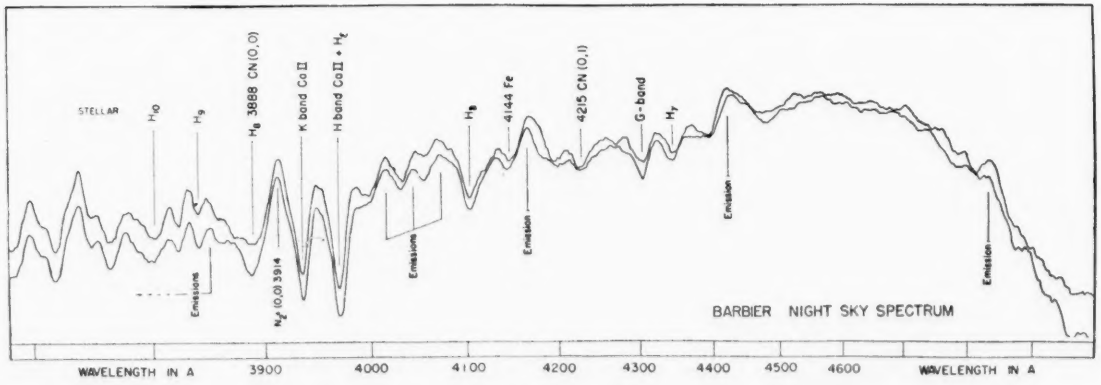

FIG. 1.—Microphotometer tracing of night-sky spectrum (Barbier) between 3700 and 4900 A

trograph. These spectra were taken with the instrument guided on a definite region of the sky. A series of these spectra is shown in Figure 2. The lowest spectrum of the series is by Barbier and has a slightly different dispersion and a higher resolution. The nebular spectra are roughly graded from late-type regions in the lower tracings to early-type regions in the upper. The progressive deepening of the H-line with the growth of the hydrogen Balmer series is apparent.

If one examines the relative appearance of the G band and $H\gamma$, the spectral class would seem to be about F8, while the relative depths of H and K indicate a much earlier class—say, F0. It is apparent, however, that this "continuum" is not solar in origin because of the spectral class, which is definitely earlier than G2. Moreover, the progressive change in class along the spectrum shows that it is a composite spectrum, probably representing the average of the unresolved stars within the visible part of the galaxy, along with scattered sunlight from the zodiacal light. Interstellar scattering of starlight would be added to the direct light of the stars themselves.

The interpretation advanced here—namely, that the continuum seen on airglow spectra has a larger fraction of starlight than hitherto believed—can be checked from the depth of the H and K lines. The depth appearing on the tracings depends on the resolution of the spectrograph and the plate characteristics, so that only an estimate is possible; however, the great depth of these features in the spectrum by Barbier relative to the "stellar" continuum near 4300 A indicates that *there is no discernible airglow continuum*.

This conclusion is verified in a striking manner when certain older problems are reconsidered. Cabannas, Dufay, and Gauzit[3] observed that the strong emissions attributed to the Vegard-Kaplan bands varied from the zenith to the horizon, whereas the group of "lines" near 4300 A did not. They assumed that these lines were due to interstellar or interplanetary emission from *CH*. Elvey, Swings, and Linke[4] concluded that the implied interstellar origin could not be correct, since, if it were, only the first rotational lines should appear in emission. They concluded that interplanetary emission was more likely. The explanation that the features are merely regions between absorptions in stellar spectra provides a simple answer.

The question arises: Which are emissions and which are gaps between absorption features? By comparing the sequence of spectra shown in Figure 2, we arrive at the conclusion that the only features that are real airglow emissions are those shown in the accompanying tabulation.

λ 3911.....	N_2^+ (0, 0)	λ 4175...	VK (3, 14), *OII* (8, 0)
4011.....	?	4416...	VK (2, 14), *OII* (9, 1)
4045.....	H (1, 8)	4535...	VK (3, 15)
4070.....	VK (2, 13)	4837...	VK (2, 15)

The rise of the λ 3911 feature above the continuum level at H and K shows that there must be an emission at this point. Contrary to the previous assignment of this emission to the *V* bands, it is most likely that this emission is the N_2^+ (0, 0) band superimposed on the stellar continuum to the violet of the K line. There are two possible explanations for this line: (*a*) that it is due to the twilight airglow and (*b*) that it represents a true permanent "aurora" due to optical excitations of the air by the flux of cosmic rays. Since this band appears as the strongest emission in spectra excited by high-energy particles in the laboratory (Fan and Meinel),[5] there should be a rather uniform low flux of 3914 A quanta.

[3] *Nature*, **142**, 718, 1938.

[4] *Ap. J.*, **93**, 337, 1941.

[5] *Ap. J.*, **118**, 205, 1953.

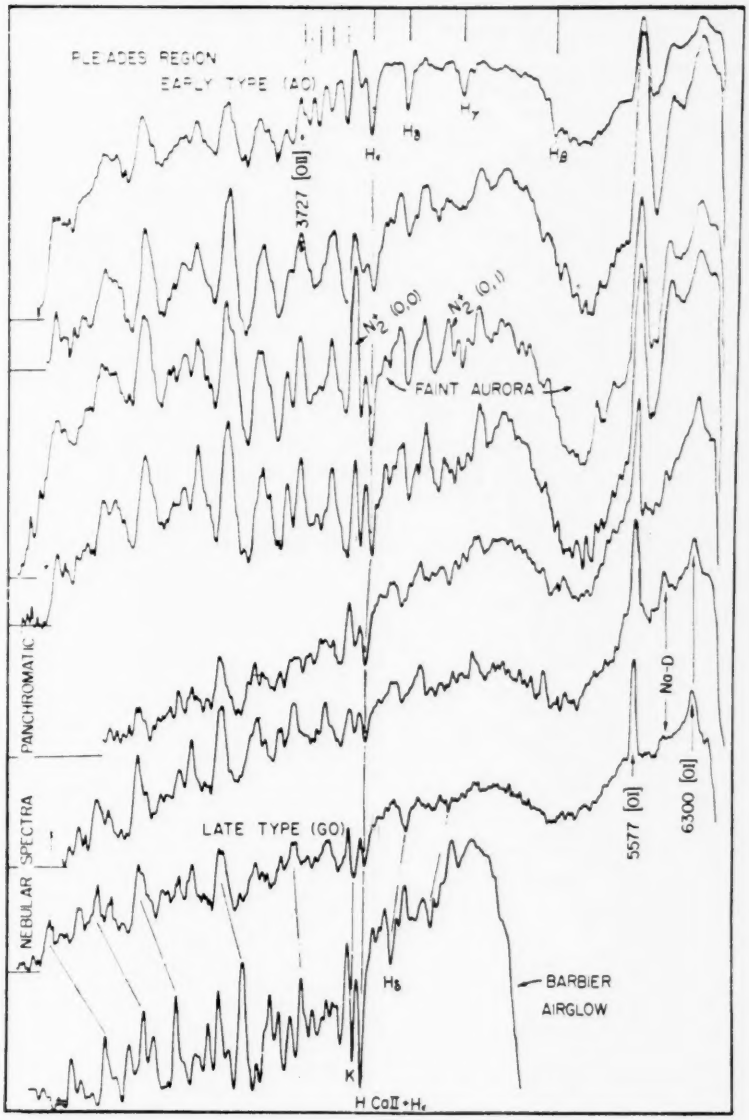

FIG. 2.—Comparison of night-sky spectra from regions of stellar background from A0 to G0, showing variation of H and K contour with spectral class.

We can make a rough estimate of the intensity of the 3914 A (0, 0) band due to the cosmic-ray flux. If the ionization loss in traversing the atmosphere is 10^8 electron volts per particle and an optical excitation is obtained for each 10^2-ev ionization loss, then we get about 10^6 quanta per incident particle, or about 10^6 quanta/cm^2/sec of N_2^+ (0, 0). This is about $\frac{1}{10}$ the normal nightglow flux of the sodium D lines and is compatible with the observed intensity of 3914 A.

The elimination of the "continuum" in the airglow at the same time eliminates the awkward interpretations that have been required for it. It now appears that the objections by Bates and Massey[6] and by Swings[7] to the proposal by Kastler[8] that the continuum would be produced by the formation of O^- atoms are sustained. The writer proposed at the Denver 1952 Upper Atmospheric Symposium of the American Physical Society that a continuum could arise from the quasi-molecule O_2-OH in the excitation of the OH bands; however, Bates[9] believed that the emission rate would be too small for this mechanism to produce a significant continuum.

It will be interesting, however, to see if it is possible to set an upper limit to the intensity that could be ascribed to airglow continuum. This will be a very difficult task because of the uncertainty in evaluating the large contributions from unresolved stars and even from remote nebulae.

The author wishes to express his appreciation to Dr. D. Barbier for his interest in this problem and for the use of one of his best airglow spectra for this study.

[6] *The Emission Spectra of the Night Sky and Aurora* ("Gassiot Comm. Rept." [1940]), p. 48.

[7] See Kuiper, *The Atmospheres of the Earth and Planets* (Chicago: University of Chicago Press, 1949), p. 159.

[8] *Ann. Geophys.*, **2**, 315, 1946.

[9] Private communication.

LABORATORY IONIC-IMPACT EMISSION SPECTRA

C. Y. Fan and A. B. Meinel
Yerkes Observatory, Williams Bay, Wisconsin
Received March 18, 1953; revised May 18, 1953

ABSTRACT

A spectrographic study has been made of the optical emissions from a rarefied air sample under the bombardment of protons (40–230 kev), deuterons (75–320 kev), He^+ ions (150–450 kev), and Ne^+ ions (400 kev). It was found that the ratio of intensity between the N II and N_2^+ emissions is approximately independent of the energies of the bombarding particles but strongly dependent upon the species of particle. As a consequence it is found to be possible to distinguish between protons and heavy ions by the spectrum produced, even when emissions from the exciting particle are absent. This discovery has made it possible to estimate the ratio of protons to heavies in the primary particle beam producing the aurora borealis.

I. INTRODUCTION

It has long been accepted that the aurora borealis is most likely to be excited by the penetration of energetic charged particles into the upper atmosphere. For many years it was thought that these particles were electrons. Numerous problems arose as a consequence of this assumption with respect to the dynamics of these particles in the geomagnetic field. Furthermore, laboratory experiments to reproduce the excitation conditions exhibited by the auroral emission by electronic excitation failed to give convincing confirmation of that hypothesis.

The detection of the elusive hydrogen emissions in 1939 by Störmer and Vegard has given a clue to the excitation mechanism. The subsequent observation by Meinel[1] of a violet Doppler wing on $H\alpha$ extending to an energy greater than 57 kev demonstrated conclusively that energetic protons are impinging upon the atmosphere.

A preliminary experiment by Meinel and Fan,[2] using protons accelerated by the Kevatron of the Institute for Nuclear Studies interacting with a rarefied air sample, showed a striking similarity between the laboratory spectrum and the aurora. Subsequently, a series of experiments was performed with a variety of positive ions over a range of energies and pressures. The most interesting result of these experiments is that it is possible to distinguish between protons and heavy ions by the spectrum produced, even when emissions from the exciting particles are absent. While proton-induced spectra often show Doppler-shifted Balmer emissions, no evidence has been found for the occurrence of emissions from helium and neon ions within the spectral region of the experiment. The significance of this finding, as related to the problem of the origin of auroral emissions, is discussed in the last section.

II. EXPERIMENTAL PROCEDURE

The experimental arrangement is indicated in Figure 1. The absorption chamber, 36 inches in length and 4 inches in diameter, was attached to the Kevatron of the Institute for Nuclear Studies, University of Chicago, and the high-energy particles were permitted to enter the chamber through a $\frac{1}{16}$-inch-diameter thin SiO window, on which a very thin layer of aluminum was sputtered to prevent damage to the window from the heating and electrostatic charge induced by the bombardment of the energetic particles. The energy absorption by the window amounted to 10 kev for 50-kev protons. The beam of the

[1] *Ap. J.*, **113**, 50, 1951.

[2] *Ap. J.*, **115**, 330, 1952.

charged particles was defined by an entrance slit whose size was slightly smaller than that of the window, so that all the particles which could pass through the slit would go into the absorption chamber. A diaphragm with a $\frac{1}{4}$-inch hole at the center was introduced between the entrance slit and the window; when biased with -90 volts with respect to ground, it would prevent both backward ejection of the secondary electrons from the window and forward ejection from the entrance slit. The absorption chamber itself was then regarded as a Faraday cup, and the beam current could thus be measured. A beam current of the order of 0.5 microampere was used for the experiment.

The air pressure of the absorption chamber was measured by a butyl-phthalate manometer. No attempt was made to modify the composition of the room air except to introduce a liquid air trap to condense vapors of water and organic compounds. The chamber was generally maintained at a pressure of 0.3 mm *Hg*.

The spectra of the laboratory emission were obtained with the McDonald Observatory nebular-grating spectrograph. The spectrograph was mounted parallel to the absorption

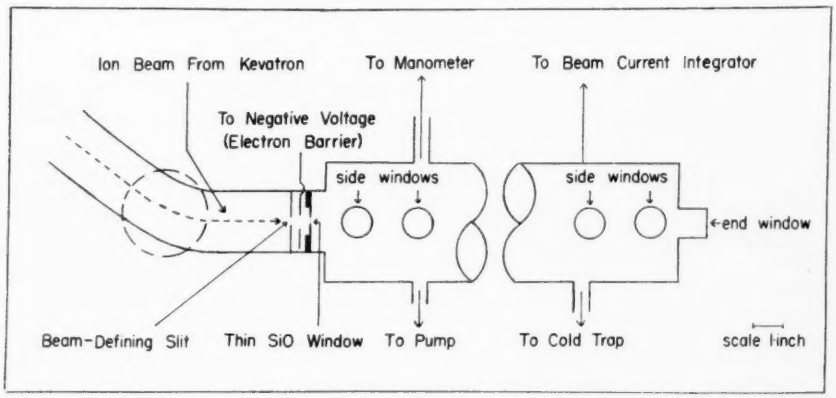

FIG. 1.—Schematic diagram of the apparatus

tube viewing the length of the tube through the end window, so that Doppler-shifted lines, if any, could be detected. The spectrograph provided a dispersion of 400 A/mm at $H\gamma$, 385 A/mm at $H\beta$, and 335 A/mm at $H\alpha$, as used in the first order. Since the spectrograph has a solid-glass Schmidt camera, the ultraviolet spectrum beyond 3700 A was heavily absorbed. The spectrographic film Eastman 103*a*-F(3) was used for all the work; it is sensitive to the spectral region from the ultraviolet to 6800 A.

Calibration of line intensities was accomplished by using a step-slit spectrophotometer with adjacent pieces of a 103*a*-F(3) film. Because no particular precaution had been taken for the selection of films and the controlling conditions of developing, any apparent relative spectral variations within 20 per cent would have little significance.

III. EXPERIMENTAL RESULTS

a) PROTON EXCITATION

The emission spectrum excited by protons has been examined in the range from 40 to 230 kev. Figure 2, *a*, shows examples of spectra for 46-, 178-, and 205-kev protons. The band systems that appear in the spectra are the first positive system (1PG) ($B^3\Pi_g \rightarrow A^3\Sigma_u^+$) and the second positive system (2PG) ($C^3\Pi_u \rightarrow B^3\Pi_g$) of N_2, negative system

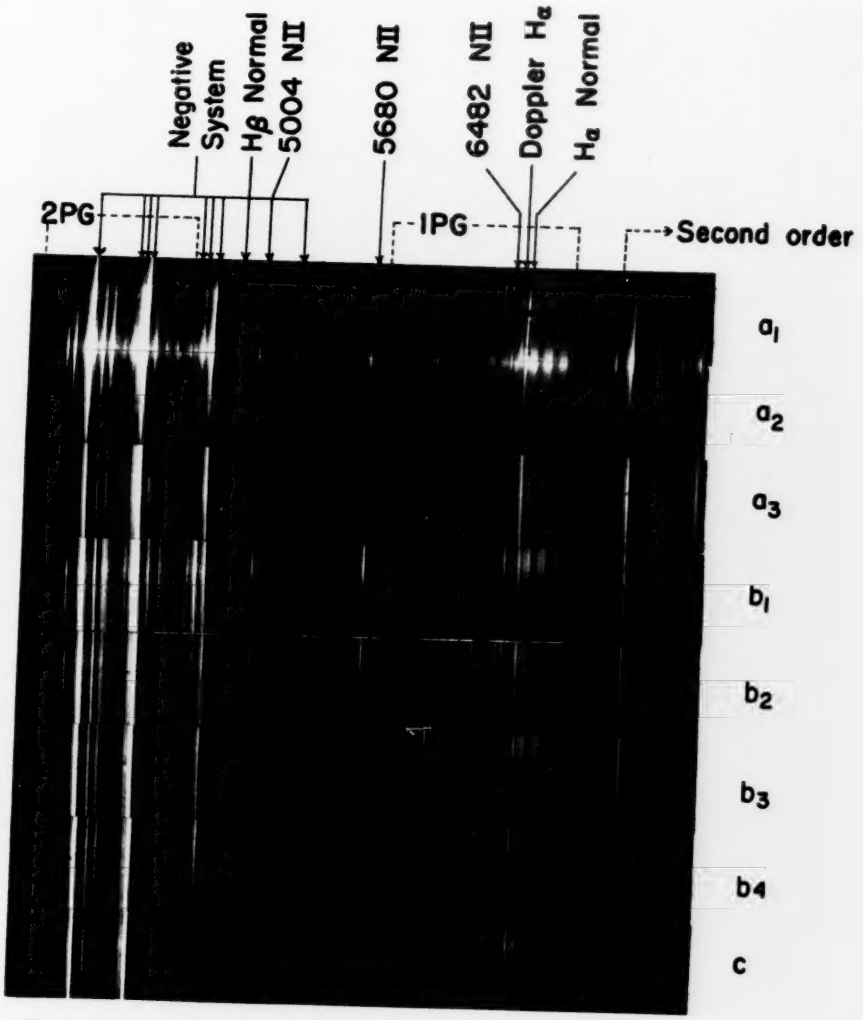

FIG. 2.—a (proton): (a_1) 46 Kev; (a_2) 178 Kev; (a_3) 205 Kev. b (He^+ ion): (b_1) 150 Kev; (b_2) 200 Kev; (b_3) 300 Kev; (b_4) 450 Kev. c (Ne^+ ion): (c) 400 Kev.

($B^2\Sigma_u^+ \rightarrow X\Sigma_g^+$) of N_2^+. There may be traces of other band systems present with very low relative intensities. *Hα*, *Hβ*, and several atomic lines of *N* II are readily identifiable; however, all the forbidden lines of *O* I and *N* I and the Vegard-Kaplan bands are absent, presumably because the molecular density in the absorption chamber was too high to allow their emission.

A spectral comparison showed that the relative intensities of all the bands and lines are fairly insensitive to changes in the proton-beam energy within the experimental range, except for the Doppler-shifted *Hα* line. Since the spectra were taken along the direction of the incident beam, energy-dependent phenomena would be integrated along the path of the decelerating particle beam; however, several spectra obtained at 90° to the beam do not show significant differences in the emission spectrum. There is some indication that the relative intensities of some bands in the second positive system of N_2 and the negative system of N_2^+ change slowly with a change in energy of the incident beam. This feature is more pronounced for the case of He^+ bombardment and will be discussed in the next section.

The intensity of the Doppler-shifted *Hα* line depends very sensitively upon the proton energy. At high energies the Doppler-shifted *Hα* wing could not be observed. The intensity of the wing showed a very sharp increase as the energy was lowered. At 40 kev the Doppler *Hα* line was one of the most prominent features of the spectrum.

The study of the Doppler *Hα* line is rendered rather difficult, since it blends with the strong 6545 A band (7, 4) of the first positive system of N_2. In order to estimate the in-

TABLE 1

Proton Energy (Kev)	I_α/I_{6545}
40	2.3
46	2.5
69	0.9

tensity of the Doppler-shifted line, the profile of the 6545 A band and its intensity relative to its neighboring 6624 A band were first obtained from the spectra excited by high-energy protons or by He^+ beam, in which case no Doppler-shifted line is present. The line intensities estimated in this manner are shown in Table 1. The first column denotes the initial energy of the proton beam, and the second column denotes the ratio of the intensity of the Doppler-shifted *Hα* and the 6545 A band as determined by microphotometer tracings of the spectra. It is to be noted that the first column does not give the energy of the proton which emits a photon of the *Hα* line, but rather the energy of the incident proton beam. The peak of the *Hα* line has a shift which corresponds to an energy only of the order of 15 kev.

b) He^+ EXCITATION

Figure 2, *b*, shows the spectra excited by He^+ ions at different energies. The spectra differ from those of proton excitation in the following features.

In contrast to the case of proton excitation, the relative intensities of the bands in the second positive system of N_2 and the negative system of N_2^+ show variations when the energy of the He^+ beam is low. This is shown in Figure 3, where the relative intensities of the bands of 4709 A (0, 2), 4652 A (1, 3), 4600 A (2, 4), 4554 A (3, 5), and 4516 A (4, 6) of the negative system of N_2^+ for different energies are plotted with the intensity of the 4709 A band taken as unity.

The relative intensities of the *N* II lines are much stronger than when excited by proton bombardment. The ratios of the first two *N* II lines of the 5228 A (0, 3) band are given in Table 2. For convenience of comparison, the same ratios for the case of proton, deuteron, helium, and neon excitations are all given in the same table.

The weak and unidentified band system in the spectra of the proton excitation at 4174 A, 4372 A, 4535 A, etc., appears distinctly in the spectra excited by He^+ ions.

No *He* lines have been identified, even in cases when the bands like 6469 A and 6545 A were heavily overexposed. The important *He* lines in the spectral region are *He* I 3964 A (2^1S-4^1P), *He* I 5015 A (2^1S-3^1P), *He* I 3889 A (2^3S-3^3P), *He* I 5876 A (2^3P-3^3D), and *He* II 4686 A (3^2D-4^2F). If any of these lines were present, they were more than 100 times weaker than the λ 6545 A band. The absence of these lines is found to be important

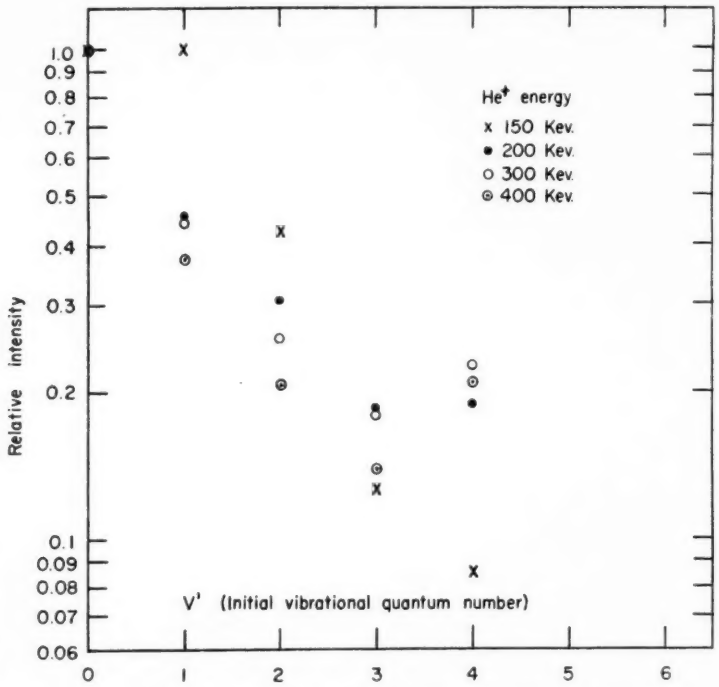

FIG. 3.—Relative intensities of the bands 4709 (0, 2), 4652 (1, 3), 4600 (2, 4), 4554 (3, 5), and 4516 (4, 6) of the negative system of N_2^+.

TABLE 2

	Energy of Proton Beam (Kev)			Energy of Deuteron Beam (Kev)			Energy of He^+ Ion Beam (Kev)			Energy of Ne^+ Ion Beam (Kev)
	40	69	150	75	150	320	150	300	450	400
I_{5004}/I_{5228}	1.4	1.3	1.2	1.2	1.7	1.7	11.6	11.2	7.1	11.7
I_{5680}/I_{5228}	1.9	1.4	1.6	1.8	2.0	2.0	11.9	10.6	6.7	11.3

for the understanding of the excitation mechanism by energetic charged particles, as is discussed in Section IV.

c) EXCITATION BY DEUTERONS AND NEON

The excitation effect of high-energy deuterons was obtained within an energy range of 75–320 kev. Within the experimental uncertainty, the spectra were found to be identical with those produced by proton impact. Doppler-shifted $D\alpha$ lines were also obtained for low-energy deuteron beams.

A spectrum of the emission produced by 400-kev Ne^+ ions is shown in Figure 2, *c*. The spectral feature resembles that produced by the He^+ beam. The intensities of two N II lines relative to the 5228 A band are given in Table 2.

IV. DISCUSSION

a) DOPPLER-SHIFTED $H\alpha$ LINE

The Doppler-shifted hydrogen line could be produced in two ways: (*a*) The moving proton captures an electron directly into an excited state, from which the emission occurs:

$$H^+ + e \rightarrow H^* \rightarrow H + h\nu ,$$

or (*b*) the moving proton captures an electron in the ground state but is excited by a subsequent collision with air molecules into an excited state, leading to the emission:

$$H^+ + e \rightarrow H;\ H + M + E \rightarrow H^* + M;\ H^* \rightarrow H + h\nu .$$

Examination of the results obtained from the He^+ ion-beam experiment permits one to ignore mechanism *b*. Table 3 gives the equilibrium distribution of the fractions of He^0,

TABLE 3

Energy (Kev)	Fraction of He^{++}	Fraction of He^+	Fraction of He^0
150	0.02	0.63	0.35
200	.03	.71	.26
300	.10	.75	.15
450	0.25	0.68	0.07

He^+, and He^{++} for a helium beam in dry air as measured by Snitzer.[3] The absence of *He* lines indicates that the probability of the electron's being captured into the excited states is much lower than that of being captured into the ground state and that the emission due to the excitation of He^+ and He^0 by collisions with air molecules is negligible compared with the emission of other band systems. Since the excitation cross-sections of $H\alpha$, $H\beta$, and *He* I 3889 A, *He* I 5015 A, and *He* I 4472 A by high-energy ionic impact are likely to be of the same order of magnitude (10^{-19} cm^2–10^{-18} cm^2).[4,5,6] One would conclude that the Doppler-shifted $H\alpha$ line is probably produced by the process of electron capture into the excited state rather than by the excitation due to collisions. Furthermore, electron capture by transfer of a bound electron in N_2 must be predominant, the cross-section of the radiative capture being too small (10^{-19} cm^2) to be taken into account.[7]

[3] *Phys. Rev.*, **89**, 1237, 1953.

[4] Döpel, *Ann. Phys.*, **16**, 1, 1933.

[5] Neumann, *Ann. Phys.*, **34**, 603, 1939.

[6] Massey and Burhop, *The Electronic and Ionic Impact Phenomena* (London: Oxford University Press, 1952), pp. 137–143.

[7] Bates, Buckingham, Massey, and Unwin, *Proc. R. Soc. London, A*, **170**, 322, 1939.

The magnitude of the capture cross-section, σ_c^* (the symbol * denoting capture into excited state), can be easily estimated if one assumes that the intensity of the 6545 A band for an He^+ beam of unit flux is the same as for a proton beam of unit flux. Taking the excitation cross-section for *He* I 5015 A as 10^{-19} cm^2, one gets 10^9 photons/cm^3/sec emitted for an He^+ beam of 0.5 μamp/cm^2, at an air pressure of 0.3 mm *Hg*. Since the 6545 A band is at least 100 times stronger than the *He* I lines but is comparable with the intensity of the Doppler-shifted *Hα* line, it follows that $\sigma_c^* \geq \sim 10^{-17}$ cm^2 for a proton of energy ~15 kev.

b) 1PG AND 2PG OF N_2

The excitation of the first and the second positive system of N_2 from the ground state involves a change of multiplicity. Thus the emissions can be produced only by either an N_2 molecule excited through the process of electron exchange or an N_2^+ ion through the process of electron capture, assuming that the contributions of processes such as the recombination of N^+ and N^-, photo-excitation, etc., are negligible.

The process of exchange of bound electrons and the process of capture of a bound electron from one of the impinging particles are perhaps not important, because the intensities of these two systems do not show any sensitive dependence upon the energy of the impinging particles, as does the Dopper-shifted *Hα* line. Therefore, the band intensities of the first and the second positive systems are mainly determined by the number and the energy spectrum of the secondary electrons produced by the ionization effect of the impinging ions.

The ionization effect of a positive ion in passing through a gas is due to two mechanisms:

a) Direct ionization, i.e., an electron is "knocked off" directly from its parent-molecule. The cross-section of the direct ionization, σ_i', depends on the energy of the impinging ion. As the energy E increases, σ_i' increases from zero to a maximum and then drops gradually as $(1/E) \log E$.[6]

b) Electron capture and loss. The positive ion captures an electron from one of the target molecules and subsequently it loses the electron by collision. Let σ_c and σ_l be the cross-sections of the electron capture and the electron loss, respectively; then the cross-section of the ionization effect is $\sigma_i'' = \sigma_c\sigma_l/(\sigma_c + \sigma_l)$. The process of the electron loss is essentially an ionization of the impinging particle by the gas molecule. The energy dependence of σ_c, however, is much more sensitive than that of σ_i'.[8,9] For low-energy particles, such as protons of energy below 50 kev and He^+ ions of energy below 500 kev, σ_i' and σ_i'' are equally important. When the energy gets higher, σ_c drops rapidly, and thus σ_i'' becomes gradually far below σ_i'.

The total ionization cross-section in air, σ_i $(=\sigma_i' + \sigma_i'')$, can be calculated as follows: Let dE be the energy loss of the ion in traversing a distance dx in the air of N molecules per cubic centimeter. Then σ_i is given by

$$\sigma_i = \frac{1}{w}\left(\frac{1}{N}\frac{dE}{dx}\right),$$

where $([1/N]\,[dE/dx])$ is called the "molecular stopping cross-section" and w is the energy loss per ion pair. It was found that in argon, and probably in all noble gases, the value of w is independent of the energy and the type of the impinging particles.[10] In air, however, w is not a constant. Jesse and Sadauskis[11] have measured, for different energies, the

[8] F. L. Ribe, *Phys. Rev.*, **83**, 1217, 1951.

[9] H. Kanner, *Phys. Rev.*, **84**, 1211, 1951.

[10] L. H. Gray, *Proc. Cambridge Phil. Soc.*, **40**, 95, 1944.

[11] *Phys. Rev.*, **75**, 1110, 1949, and especially **78**, 1, 1950.

ratio of the number of ion pairs produced by α-particles in argon to that in air. From these results one can obtain a curve relating the number of ion pairs, n, to the energy of an α-particle, E, in air. The slope of the curve at a particular point E is then the value of $1/w$ at E. It is found that w is equal to 40 e.v. within the experimental energy range. By assuming the same value of w for both the cases of proton and He^+ excitation, one obtains the results shown in Table 4. The values of the molecular stopping cross-section are taken from the measurements of P. K. Weyl.[12]

The number of secondary electrons/cm³/sec produced by a flux F is $FN\sigma_i$, when the ionization effect of the secondary electrons is neglected. When N is taken to be 10^{16} particles/cm³ and σ_i is taken to be 10^{-15} cm², the number of recombinations is 3×10^{13} cm³/sec for a uniform flux 0.5 μamp/cm². If one-fifth of the number of the recombinations is taken as the probability for the electron in the transfer process going to the second and the third excited state of the N_2 molecule, then the total emission in the first and the second positive band systems would be $\sim 6 \times 10^{12}$ photons/cm³/sec.

TABLE 4

	Energy of Proton Beam (Kev)					Energy of He^+ Beam (Kev)				Energy of Ne^+ Beam (Kev)
	30	40	100	150	200	150	200	300	450	400
$(1/N)(dE/dx) \times 10^{15}$ (e.v./mol^{-1} cm²)	30.4	33.0	34.6	31.0	27.0	61.2	67.4	77.0	84.6	116
$\sigma i \times 10^{16}$ (cm²)	7.6	8.2	8.6	7.8	6.8	15.2	16.8	19.2	21.2	33.0

The number of ion pairs per cubic centimeter, n, is given by

$$FN\sigma_i - n^2 \int Q f(v)\, dv = 0\,,$$

where $nf(v)dv$ is the density of electrons with velocities lying between v and $v + dv$ and Q is the cross-section of the recombination. If the energy of the electrons, ϵ, is expressed in units of electron volts, the value of ϵQ for an oxygen ion O^+ is 0.5×10^{-20} e.v./cm².[7] This does not vary appreciably with ϵ and the singly charged ion under consideration. Assuming the same value of ϵQ for N_2^+ and taking the average velocity of the electrons as 2×10^7 cm/sec, one obtains $n \sim 5 \times 10^{12}$/cm³.

The energy distribution of the secondary electrons is not known. However, it is known that the average energy loss of a particle for the production of an ion pair in air is 40 e.v., which is much higher than the ionization potential of O_2 (12.5 e.v.) or that of N_2 (15.7 e.v.). This fact seems to indicate that the percentage of the secondary electrons of energy higher than 7.35 e.v., the excitation energy for the $B^3\Pi_g$ state of N_2, could be high.[13] If the cross-section for the production of high-energy electrons were of the order of 10^{-16} cm², the emission of the 1PG and 2PG bands of N_2 resulting from the excitation effect

[12] *Phys. Rev.* *91*, 289 (1953).

[13] An example would be the case of the ionization of H_2. The average energy loss for an ion pair is 36.0 e.v., and the ionization potential of H_2 is 15.6 e.v. The energy distribution of the secondary electrons produced by electronic impact has been calculated and qualitatively verified experimentally (Mott and Massey, *The Theory of Atomic Collisions* [London: Oxford University Press, 1949], p. 236).

of these high-energy electrons would be 10^{-12} photons/cm^3/sec for $F = 0.5$ μamp/cm^2 and $N = 10^{16}$ particles/cm^3.

c) NEGATIVE SYSTEM OF N_2^+ AND THE N II LINES

The number of positive ions has been estimated to be of the order of 5×10^{12}/cm^3, which is a very small fraction of the density of N_2 molecules (10^{16} particles/cm^3) in the experiments. As a consequence, the emission of N_2^+ bands resulting directly from the excitation of the equilibrium concentration of N_2^+ ions by electronic and ionic impact can be neglected, since the difference in excitation cross-sections can hardly overcome the difference in numbers. The two most likely mechanisms for the production of the negative system of N_2^+ are:

$$N_2 + A^+ \rightarrow (N_2^+)^* + A \text{ (by electron transfer)}, \quad (N_2^+)^* \rightarrow N_2^+ + h\nu , \tag{1}$$

and

$$N_2 + A^+ \text{ (or } A) \rightarrow (N_2^+)^* + A^+ \text{ (or } A) + e \text{ (by direct ionization)}, \quad (N_2^+)^* \rightarrow N_2^+ + h\nu . \tag{2}$$

These appear to be the only processes that can give a reasonable explanation of the total observed emission intensity.

A similar argument can be applied for the case of the intense N II lines. The following reactions, since they involve the un-ionized N_2 molecules, do not require a high dissociation rate for the production of a sufficiently large N^+ population.

$$N_2 + A^+ \rightarrow N + (N^+)^* + A \text{ (by electron transfer)}, \tag{1}$$

and

$$N_2 + A^+ \text{ (or } A) \rightarrow N + (N^+)^* + A^+ \text{ (or } A) + e \text{ (by direct ionization)} \quad (N^+)^* \rightarrow N^+ + h\nu . \tag{2}$$

The formation of an ion by the transfer of the bound electron is energy-dependent and particle-sensitive and seems to agree with the experimental results. Therefore, these reactions are adopted as a tentative mechanism for the production of the N_2^+ bands and the N II lines.

A summary of the consequences of adoption of these mechanisms is found in Table 5.

V. THE ORIGIN OF AURORAL EMISSIONS

One interesting point of the present experiment is that the spectrum produced by He^+ and Ne^+ ions shows stronger N II lines than that by protons. From Table 2 the value of I_{5004}/I_{5228} is about 10 for the He^+ excitation and is about 1.3 for the proton excitation. Thus the ratio for a spectrum excited by a mixture of He ions and protons of comparable velocity should lie between these values. This result provides a method for estimating the relative abundance of He to H in the primary auroral particle beam. If x is the ratio I_{5004}/I_{5228} and s is the ratio of the excitation cross-section of the emission of the 5228 A band by He^+ impact to that by proton impact, then the relative abundance of He to H is given by

$$f = \frac{x - 1.3}{s(10 - x)} .$$

The ratio of I_{5004}/I_{5228} for an aurora borealis spectrum is definitely higher than 1.3, which indicates that there must be some heavier ions present. If one neglects the contribution of any particles heavier than a helium-hydrogen ratio of 0.1, ($s = 1$) was estimated from an auroral spectrogram taken by Mr. Hugh M. Johnson by using the same spectrograph and film as was used in the laboratory experiments. This value is close to the relative abundance of *He* to *H* in the sun. Thus a more accurate determination of the relative abundance might shed some light on the possible origin of the high-energy particles responsible for the auroral emissions.

TABLE 5

	Reactions	Energy-dependent	Particle-dependent
Doppler-broadened $H\alpha$	$H^+ + e$ (bound) $\rightarrow H^* \rightarrow H + h\nu$	Very energy-dependent	
1PG, 2PG	(*a*) $N_2^+ + e \rightarrow (N_2)^*$ (radiative capture) $\rightarrow N_2 + h\nu$	Not dependent	Slightly
	(*b*) $N_2 + e \rightarrow (N_2)^* + e \rightarrow N_2 + e + h\nu$	Slightly dependent	Slightly
Negative system	(*a*) $N_2 + A^+ \rightarrow (N_2^+)^* + A \rightarrow N_2^+ + A + h\nu$	Very energy-dependent	Moderately
	(*b*) $N_2 + A^+$ (or A) $\rightarrow (N_2^+)^* + A^+$ (or A) $+ e \rightarrow N_2^+ + A^+$ (or A) $+ e + h\nu$	Less dependent	Slightly
NII lines	(*a*) $N_2 + A^+ \rightarrow N + (N^+)^* + A \rightarrow N + N^+ + A + h\nu$	Very energy-dependent	Very
	(*b*) $N_2 + A^+$ (or A) $\rightarrow N + (N^+)^* + A^+$ (or A) $+ e \rightarrow N + N^+ + A^+$ (or A) $+ e + h\nu$	Less dependent	Moderately

The authors wish to express their appreciation to Dr. S. K. Allison for his interest in this work and for the use of the Kevatron and the facilities of the Institute for Nuclear Studies. Thanks are also due to Dr. H. Casson, Dr. P. K. Weyl, Mr. G. DuFloth, Mr. S. Bowen, and Mr. H. L. Helfer for their assistance. This investigation has been supported in part by the Geophysical Research Directorate of the Air Force Cambridge Research Center under Contract No. 19(122)-480.

VIBRATION-ROTATION BANDS OF *OH**

ROBERT C. HERMAN AND GEORGE A. HORNBECK†
Applied Physics Laboratory, The Johns Hopkins University, Silver Spring, Maryland
Received March 18, 1953; revised May 14, 1953

ABSTRACT

The (4–0) sequence of the vibration-rotation bands of *OH* have been observed in the emission spectra of various oxy-hydrocarbon flames as well as the oxy-hydrogen flame. A set of molecular constants was determined from the (4–0), (5–1), and (6–2) bands taken together with the latest ultraviolet data of Dieke and Crosswhite. The constants obtained are as follows:

$$B_e = 18.867\ \text{cm}^{-1}; \qquad \omega_e = 3734.09\ \text{cm}^{-1};$$
$$\alpha_e = 0.708\ \text{cm}^{-1}; \qquad \omega_e x_e = 82.66\ \text{cm}^{-1};$$
$$\gamma_e = 0.00207\ \text{cm}^{-1}; \qquad \omega_e y_e = 0.094\ \text{cm}^{-1}.$$

In addition are given values of the coupling constant, lambda doubling, and band origins up to $v = 6$, as well as tables of the rotational and vibrational energy levels for $v = 4$, 5, and 6. These data should prove useful in predicting accurately the positions of some of the vibration-rotation lines of *OH* which are of astrophysical interest.

I. INTRODUCTION

In recent years the *OH* bands have become of increasingly greater importance for the measurement of temperature in flames and other combustion processes, as well as for general explorations of the physical conditions in flames, electrical discharges, and the upper atmosphere.[1] For these purposes it is necessary to have a knowledge of the band structure and constants. Dieke and Crosswhite[1] have given an excellent survey of the ultraviolet bands of the *OH* radical, including new wave-length and intensity measurements of lines in the entire region 2800–3550 A, a recalacultion of all band constants, a table of the rotational and vibrational energy levels, and a table of line positions in several vibration-rotation bands of *OH* as calculated from the data obtained from the ultraviolet bands.

The vibration-rotation bands of *OH* were first observed in emission in the spectrum of the night sky by Meinel.[2] These bands lie in the wave-length region ~6800–~9000A and include the vibrational transitions (7–2), (8–3), (9–4), (4–0), (5–1), (6–2), and (7–3). During the past several years there has been considerable attention given to the study of flame spectra, and during the course of these investigations the vibration-rotation bands of *OH* were identified. Plyler and Humphreys,[3] studying the oxy-acetylene flame at low dispersion in the near infrared, reported the appearance of some partially resolved rotational structure of *OH*, although the identification was not complete and there was some question whether the lines were emission lines of H_2O rather than *OH*. Recently,

* This work was supported by the U.S. Navy Bureau of Ordnance.

† Now at the National Bureau of Standards, Washington, D.C.

[1] G. H. Dieke and H. M. Crosswhite, *The Ultra-violet Bands of OH: Fundamental Data* ("Bumblebee Series," Rept. No.87 [The Johns Hopkins University, 1948]). Note that the notation employed in the present paper follows that employed by Herzberg in n. 13. This differs from that of Dieke and Crosswhite in several respects as follows: $f_{1e} \equiv f_1$, $f_{1d} \equiv f_1'$, $P_{1e} \equiv P_1$, $P_{1d} \equiv P_1'$, etc.; $Y_v \equiv a_v$, $A_v \equiv a_v B_v$; $q_1 \equiv b_1$; $\alpha_e \equiv \alpha$ and $\gamma_e \equiv \beta$.

[2] A. B. Meinel, *Ap. J.*, **111**, 555, 1950; **112**, 120, 1950. See also the recent work reported on *OH* in the airglow at high altitudes by J. W. Chamberlain and N. J. Oliver, *Phys. Rev.*, **90**, 1118, 1953.

[3] E. K. Plyler and C. J. Humphreys, *J. Res. Nat. Bur. Stand.*, **40**, 449, 1948.

Benedict, Plyler, and Humphreys[4] restudied the emission spectrum of the oxy-acetylene and oxy-hydrogen flames in the region from 1.4 to 1.7 μ at high resolution and identified many lines of the (2–0), (3–1), and (4–2) vibration-rotation bands of *OH*. The authors[5] have observed at high dispersion in emission from the outer cone of the oxy-acetylene flame the (4–0), (5–1), and (6–2) vibration-rotation bands of *OH* which appear in the photographic infrared between ~7450 and ~8750 A. Subsequently, Dejardin, Janin, and Peyron[6] studied the oxy-hydrogen and oxy-acetylene flames at low dispersion and reported a large number of vibration-rotation bands of *OH* in the photographic infrared. Recently, they have also resolved the structure of the (4–0), (5–1), and (6–2) bands and determined new band constants.[7] Their work will be discussed in a later portion of this paper. The purpose of the present paper is to report our measurements in detail, to derive a new set of molecular constants for the *OH* molecule, and to extend the tabulation of the rotational and vibrational energy levels of *OH* in the $^2\Pi$ ground state given by Dieke and Crosswhite,[1] with a listing of the levels for $v = 4$, 5, and 6.

II. EXPERIMENTAL

The measurements reported were obtained on a Baird 2-meter grating spectrograph containing a 15,000-line/inch grating ruled at The Johns Hopkins University. Spectra were taken in the first order at 8 A/mm, using a 25-μ slit and 1-*N* plates hypersensitized according to the procedure described by Meinel.[2] Using the outer cone of the oxy-acetylene flame as source, we were able to obtain spectrograms of the vibration-rotation bands of *OH* having good contrast and density, with exposure times of ~1½ hours under the conditions stated above. The vibration-rotation bands of *OH* in the spectral range ~7450–~8750 A can also be obtained from the outer cones of methane, ethylene, and hydrogen burning with oxygen. However, in these cases the *OH* lines are more badly overlapped by the intense H_2O vibration-rotation spectrum. We have achieved best results with the oxy-acetylene flame obtained from an ordinary torch burning the gases at stoichiometric proportions, when viewing the region of the outer cone closest to the tip of the reaction zone. A discussion of sources, fuel metering, and the effect of varying fuel and oxygen composition on the spectra of hydrocarbon flames has been given by the authors in an earlier publication.[8] The plates were measured under the comparator in the usual manner, using the iron-line standards. Measurements from different plates agree well, and the averages of line position listed in the next section should be accurate to ~0.05–0.10 cm^{-1}, depending on the extent to which the *OH* lines are blended with one another and with the lines of the H_2O vibration-rotation bands, as well as on the breadth of the line.

III. RESULTS AND DISCUSSION

In Figures 1, 2, and 3 are shown original microdensitometer tracings of the $\Delta v = 4$ sequence of the vibration-rotation bands of *OH* in the region ~7450–~8750 A. These curves were obtained with a Leeds and Northrup Knorr-Albers recording microphotometer. The *R* heads and various *Q* and *P* lines are indicated. Unprimed symbols are employed for the (4–0) lines, while primed and double-primed quantities refer to the (5–1) and (6–2) bands, respectively. These densitometer tracings show the character of $^2\Pi - ^2\Pi$ vibration-rotation bands and are useful for identification. They also provide a rough indication of relative line intensities obtained from the relatively high-temperature oxy-acetylene source. The temperature just above the tip of the inner cone is ~3000° K.

[4] W. S. Benedict, E. K. Plyler, and C. J. Humphreys, *J. Chem. Phys.*, **21**, 398, 1953.

[5] G. A. Hornbeck and R. C. Herman, *J. Chem. Phys.*, **19**, 512, 1951.

[6] G. Dejardin, J. Janin, and M. Peyron, *C.R.*, **234**, 1866, 1952.

[7] *Ibid.*, **235**, 538, 1952; *Phys. Rev.*, **90**, 359, 1953.

[8] G. A. Hornbeck and R. C. Herman, *Ind. and Eng. Chem.*, **43**, 2739, 1951.

The many background lines in Figures 1, 2, and 3 are lines in the vibration-rotation bands of H_2O.[9] Lines of the (0, 0) band of the $^1\Sigma - {}^3\Sigma$ system of O_2 and the resonance doublet of KI also appear.

Since the ground electronic state of the OH molecule is a $^2\Pi$ state, the vibration-rotation bands represent $^2\Pi - {}^2\Pi$ transitions, and the selection rules for such bands apply. According to Hill and Van Vleck,[10] the rotational energy of a $^2\Pi$ state is given by

$$f_{1,2}(J) = B_v\{(J+\tfrac{1}{2})^2 - 1 \pm \tfrac{1}{2}[(2J+1)^2 + Y_v(Y_v-4)]^{1/2}\}, \quad (1)$$

or

$$f_1(K) = B_v\{(K+1)^2 - 1 - \tfrac{1}{2}[4(K+1)^2 + Y_v(Y_v-4)]^{1/2}\} - D_v K^2(K+1)^2, \quad (J-\tfrac{1}{2}=K), \quad (2a)$$

and

$$f_2(K) = B_v\{K^2 - 1 + \tfrac{1}{2}[4K^2 + Y_v(Y_v-4)]^{1/2}\} - D_v K^2(K+1)^2, \quad (J+\tfrac{1}{2}=K), \quad (2b)$$

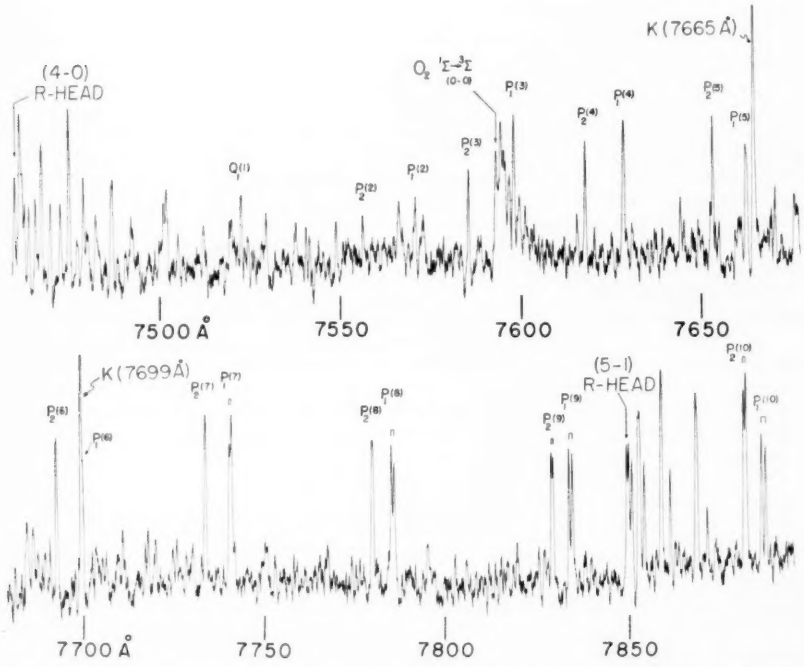

FIG. 1.—Densitometer tracing of the $^2\pi - {}^2\pi$, (4–0) sequence of the vibration-rotation bands of OH in the wave-length range 7450–7900 A. Unprimed, primed, and double-primed quantities refer to lines of the (4–0), (5–1), and (6–2) bands, respectively.

[9] The vibration-rotation bands of H_2O in the photographic infrared can be obtained with relatively high intensity from the outer cones of all hydrocarbon flames but are particularly strong in the oxymethane flame. Several bands have been measured and are being analyzed in collaboration with Dr. W. S. Benedict, The Johns Hopkins University.

[10] E. L. Hill and J. H. Van Vleck, *Phys. Rev.*, **32**, 250, 1928.

where Y_v is the coupling constant and the remaining symbols have their conventional spectroscopic meaning. Each of the rotational levels f_1 and f_2 is split because of Λ-doubling, and the two components are designated as f_{1c} and f_{1d}. In a $^2\Pi-{}^2\Pi$ transition there are 24 branches, including 4 each of P, Q, and R branches, for which $\Delta J = \Delta K$, and 12 satellite branches, for which $\Delta J \neq \Delta K$. In this type of transition the Q branches are weak relative to the P and R branches except for very low values of K, and the satellite branches are very weak. The rotational line strengths for the $^2\Pi-{}^2\Pi$ *OH* vibration-rotation bands with intermediate coupling have been evaluated according to the basic theory of Hill and Van Vleck by Benedict, Plyler, and Humphreys.[4] According to the above, the vibration-rotation bands of *OH* exhibit series of lines grouped in sets of four. These

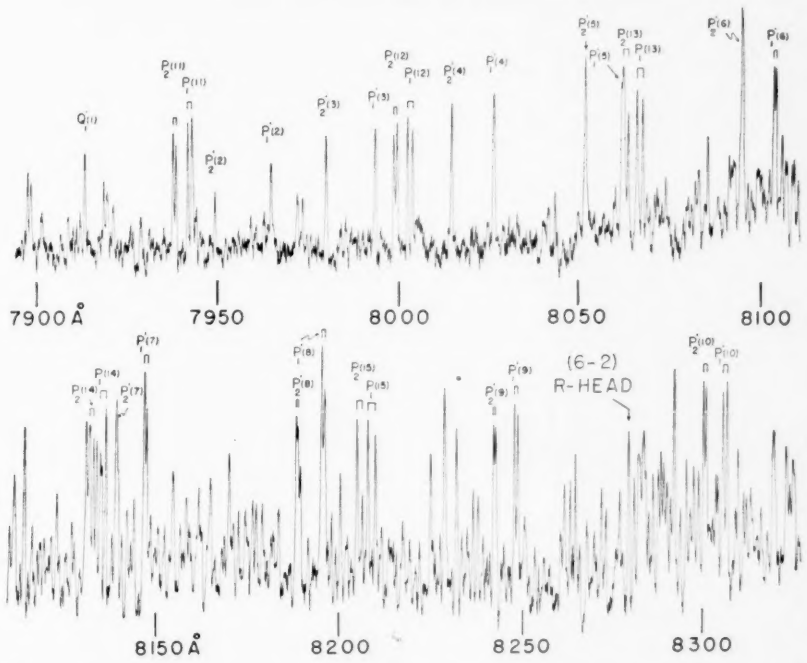

FIG. 2.—Densitometer tracing of the $^2\pi-{}^2\pi$, (4–0) sequence of the vibration-rotation bands of *OH* in the wave-length range 7900–8350 A. Unprimed, primed, and double-primed quantities refer to lines of the (4–0), (5–1), and (6–2) bands, respectively.

groups consist of pairs of spin doublets, whose separation decreases with increasing K. Each component of the spin doublet is itself a Λ-doublet, whose separation increases with increasing K. All these features are evident in the $\Delta v = 4$ sequence of bands shown in Figures 1, 2, and 3. The twelve main branches in a $^2\Pi-{}^2\Pi$ transition are for $i = 1, 2$, as follows:

$$P_{ic}(K) = f_{ic}(K-1) - f_{ic}(K), \quad (J-1 \rightarrow J), \tag{3a}$$

$$P_{id}(K) = f_{id}(K-1) - f_{id}(K), \quad (J-1 \rightarrow J), \tag{3a'}$$

$$Q_{ie}(K) = f_{ie}(K) - f_{id}(K), \quad (J \rightarrow J), \tag{3b}$$

$$Q_{id}(K) = f_{id}(K) - f_{ie}(K), \quad (J \rightarrow J), \tag{3b'}$$

$$R_{ie}(K) = f_{ie}(K+1) - f_{ie}(K), \quad (J+1 \rightarrow J), \tag{3c}$$

$$R_{id}(K) = f_{id}(K+1) - f_{id}(K), \quad (J+1 \rightarrow J), \tag{3c'}$$

with the first and second terms in f corresponding to the upper and lower vibrational states, respectively.

The wave length of the lines identified and measured in the (4–0), (5–1), and (6–2) bands of *OH* are given in Table 1. The frequency of the various lines arranged in branches are given in Tables 2, 3, and 4 for the (4–0), (5–1), and (6–2) bands, respectively. Both components of the Λ-doubling are given where resolved. In Tables 2, 3, and 4 some entries are given by ditto marks where the Λ-doubling is not resolved. Some entries are not given where the line has not been identified above the background. Identical entries in certain cases imply blending of lines. Wave lengths are listed in Å in air as measured and in cm^{-1} in vacuum as computed by means of Kayser's tables.[11] All the upperstate energy levels involved in the bands are listed in Tables 5, 6, and 7. These levels were calculated

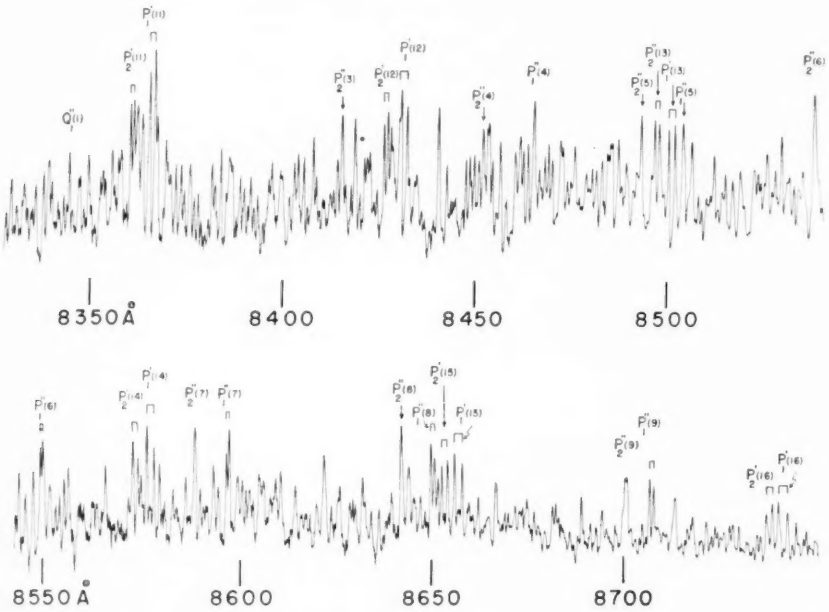

FIG. 3.—Densitometer tracing of the $^2\pi - ^2\pi$, (4–0) sequence of the vibration-rotation bands of *OH* in the wave-length range 8350–8750 Å. Unprimed, primed, and double-primed quantities refer to lines of the (4–0), (5–1), and (6–2) bands, respectively.

[11] H. Kayser, *Tabelle der Schwingungszahlen* (Ann Arbor, Mich.: J. W. Edwards, 1944).

TABLE 1

WAVE LENGTHS OF LINES IN THE (4-0) SEQUENCE OF *OH*

λ (A)	Identification		λ (A)	Identification	
	V'	Line		V'	Line
7461.31	4	R_{1c} (5), R_{1d} (5)	7860.78	5	R_{1c} (2), R_{1d} (2)
7462.55	4	R_{1c} (4), R_{1d} (4)	7868.07	5	R_{2c} (2), R_{2d} (2), R_{1c} (8), R_{1d} (8), R_{2c} (8), R_{2d} (8)
7463.19	4	R_{1c} (6), R_{2c} (5), R_{2d} (5)	7870.79	5	R_{1c} (1), R_{1d} (1)
7463.84	4	R_{1d} (6), R_{2c} (6), R_{2d} (6)	7881.08	4	P_{2c} (10)
7464.80	4	R_{2c} (4), R_{2d} (4)	7881.75	4	P_{2d} (10)
7466.71	4	R_{1c} (3), R_{1d} (3)		5	R_{2c} (1), R_{2d} (1), R_{1c} (9), R_{1d} (9), R_{2c} (9), R_{2d} (9)
7468.30	4	R_{1c} (7), R_{1d} (7), R_{2c} (7), R_{2d} (7)	7885.71	4	P_{1c} (10)
7470.83	4	R_{2c} (3), R_{2d} (3)	7886.74	4	P_{1d} (10)
7473.82	4	R_{1c} (2), R_{1d} (2)	7898.00	5	R_{1c} (10), R_{2c} (10)
7476.46	4	R_{1c} (8), R_{1d} (8), R_{2c} (8), R_{2d} (8)	7898.83	5	R_{1d} (10), R_{2d} (10)
7480.30	4	R_{2c} (2), R_{2d} (2)	7913.86	5	Q_{1c} (1)
7483.56	4	R_{1c} (1), R_{1d} (1)	7918.75	5	R_{2c} (11), R_{2d} (11)
7487.75	4	R_{2c} (9)	7919.72	5	R_{1c} (11), R_{1d} (11)
7488.13	4	R_{1c} (9), R_{2d} (9)	7921.33	5	Q_{1c} (2)
7489.67	4	R_{1d} (9)	7931.46	5	Q_{1c} (3)
7493.79	4	R_{2c} (1), R_{2d} (1)	7937.70	4	P_{2c} (11)
7502.39	4	R_{2c} (10)	7938.47	4	P_{2d} (11)
7503.17	4	R_{1c} (10), R_{2d} (10)	7941.78	4	P_{1c} (11)
7520.56	4	R_{2c} (11)	7943.04	4	P_{1d} (11)
7521.20	4	R_{1c} (11), R_{2d} (11)	7949.35	5	P_{2c} (2), P_{2d} (2)
7524.14	4	Q_{1c} (1)	7964.80	5	P_{1c} (2), P_{1d} (2)
7530.71	4	Q_{1c} (2)	7979.88	5	P_{2c} (3), P_{2d} (3)
7541.99	4	R_{2c} (12)	7993.46	5	P_{1c} (3), P_{1d} (3)
7542.99	4	R_{1c} (12), R_{1d} (12)	7998.15	4	P_{2c} (12)
7557.58	4	P_{2c} (2), P_{2d} (2)	7999.09	4	P_{2d} (12)
7571.83	4	P_{1c} (2), P_{1d} (2)	8001.89	4	P_{1c} (12)
7586.24	4	P_{2c} (3), P_{2d} (3)	8003.29	4	P_{1d} (12)
7598.58	4	P_{1c} (3), P_{1d} (3)	8014.20	5	P_{2c} (4), P_{2d} (4)
7618.17	4	P_{2c} (4), P_{2d} (4)	8025.98	5	P_{1c} (4), P_{1d} (4)
7628.78	4	P_{1c} (4), P_{1d} (4)	8052.14	5	P_{2c} (5), P_{2d} (5)
7653.48	4	P_{2c} (5), P_{2d} (5)	8062.75	4	P_{2c} (13)
7662.55	4	P_{1c} (5), P_{1d} (5)		5	P_{1c} (5), P_{1d} (5)
7691.98	4	P_{2c} (6), P_{2d} (6)	8063.84	4	P_{2d} (13)
7699.94	4	P_{1c} (6), P_{1d} (6)	8066.16	4	P_{1c} (13)
7734.05	4	P_{2c} (7), P_{2d} (7)	8067.77	4	P_{1d} (13)
7740.51	4	P_{1c} (7)	8093.79	5	P_{2c} (6), P_{2d} (6)
7741.08	4	P_{1d} (7)	8102.26	5	P_{1c} (6)
7779.51	4	P_{2c} (8), P_{2d} (8)	8102.92	5	P_{1d} (6)
7785.08	4	P_{1c} (8)	8131.63	4	P_{2c} (14)
7785.91	4	P_{1d} (8)	8132.74	4	P_{2d} (14)
7828.41	4	P_{2c} (9)	8134.74	4	P_{1c} (14)
7828.89	4	P_{2d} (9)	8136.36	4	P_{1d} (14)
7833.46	4	P_{1c} (9)	8139.19	5	P_{2c} (7)
7834.25	4	P_{1d} (9)	8139.76	5	P_{2d} (7)
7849.31	5	R_{1c} (5)	8146.59	5	P_{1c} (7)
7849.86	5	R_{1c} (4), R_{1d} (5)	8147.28	5	P_{1d} (7)
7850.67	5	R_{2c} (5), R_{2d} (5)	8188.32	5	P_{2c} (8)
7852.54	5	R_{2c} (4), R_{2d} (4), R_{1c} (6), R_{1d} (6), R_{2c} (6), R_{2d} (6)	8188.69	5	P_{2d} (8)
			8194.88	5	P_{1c} (8)
			8195.79	5	P_{1d} (8)
7853.75	5	R_{1c} (3), R_{1d} (3)	8204.68	4	P_{2c} (15)
7858.33	5	R_{2c} (3), R_{2d} (3), R_{1c} (7), R_{1d} (7), R_{2c} (7), R_{2d} (7)	8206.06	4	P_{2d} (15)
			8207.50	4	P_{1c} (15)
			8209.48	4	P_{1d} (15)

TABLE 1—*Continued*

λ (A)	Identification		λ (A)	Identification	
	V'	Line		V'	Line
8241.48	5	P_{2c} (9)	8432.17	5	P_{1d} (12)
8242.09	5	P_{2d} (9)	8452.21	6	P_{2c} (4), P_{2d} (4)
8247.33	5	P_{1c} (9)	8465.33	6	P_{1c} (4), P_{1d} (4)
8248.28	5	P_{1d} (9)	8493.50	6	P_{2c} (5), P_{2d} (5)
8278.56	6	R_{1c} (4), R_{1d} (4), R_{1c} (5), R_{1d} (5)	8496.99	5	P_{2c} (13)
			8498.16	5	P_{2d} (13)
8280.16	6	R_{2c} (5), R_{2d} (5)	8500.91	5	P_{1c} (13)
8281.56	6	R_{1c} (3), R_{1d} (3), R_{2c} (4), R_{2d} (4)	8502.62	5	P_{1d} (13)
			8504.81	6	P_{1c} (5), P_{1d} (5)
8282.22	4	P_{2c} (16)	8538.69	6	P_{2c} (6), P_{2d} (6)
8282.78	6	R_{1c} (6), R_{1d} (6), R_{2c} (6), R_{2d} (6)	8548.41	6	P_{1c} (6)
			8549.05	6	P_{1d} (6)
8283.93	4	P_{2d} (16)	8572.25	5	P_{2c} (14)
8285.06	4	P_{1c} (16)	8573.43	5	P_{2d} (14)
8287.04	4	P_{1d} (16)	8575.85	5	P_{1c} (14)
	6	R_{2c} (3), R_{2d} (3)	8577.67	5	P_{1d} (14)
8288.81	6	R_{1c} (2), R_{1d} (2)	8588.26	6	P_{2c} (7), P_{2d} (7)
8290.73	6	R_{1c} (7), R_{1d} (7), R_{2c} (7), R_{2d} (7)	8596.75	6	P_{1c} (7)
			8597.49	6	P_{1d} (7)
8296.46	6	R_{2c} (2), R_{2d} (2)	8642.07	6	P_{2c} (8), P_{2d} (8)
8298.96	5	P_{2c} (10)	8649.55	6	P_{1c} (8)
8299.59	5	P_{2d} (10)	8650.40	6	P_{1d} (8)
8302.08	6	R_{2c} (8)	8652.27	5	P_{2c} (15)
8302.71	6	R_{1c} (8), R_{1d} (8), R_{2d} (8)	8653.81	5	P_{2d} (15)
			8655.61	5	P_{1c} (15)
8304.18	5	P_{1c} (10)	8657.80	5	P_{1d} (15)
8305.23	5	P_{1d} (10)	8700.00	6	P_{2c} (9)
8344.68	6	Q_{1c} (1)	8700.71	6	P_{2d} (9)
8352.97	6	Q_{1c} (2)	8706.97	6	P_{1c} (9)
8360.48	5	P_{2c} (11)	8708.01	6	P_{1d} (9)
8361.30	5	P_{2d} (11)	8737.56	5	P_{2c} (16)
8365.10	5	P_{1c} (11)	8739.20	5	P_{2d} (16)
	6	Q_{1c} (3)	8740.83	5	P_{1c} (16)
8366.48	5	P_{1d} (11)	8743.03	5	P_{1d} (16)
8415.39	6	P_{2c} (3), P_{2d} (3)	8762.99	6	P_{2c} (10)
8426.43	5	P_{2c} (12)	8763.72	6	P_{2d} (10)
8427.41	5	P_{2d} (12)	8769.17	6	P_{1c} (10)
8430.20	6	P_{1c} (3), P_{1d} (3)	8770.35	6	P_{1d} (10)
8430.72	5	P_{1c} (12)			

from the line positions given in Tables 2, 3, and 4, using equations (3) and the energy levels for $v = 0$, 1, and 2 given by Dieke and Crosswhite.[1,12]

The constants B_v and D_v can be calculated for each vibrational level from the expressions for the rotational energy. Writing

$$\delta = f_{2c}(K+1) - f_{2c}(K-1) + f_{1c}(K) - f_{1c}(K-2), \tag{4a}$$

one has, using equations (2),

$$\frac{\delta}{8K} = B_v - D_v(2K^2+3). \tag{4b}$$

[12] See n. 1 for some details concerning the calculation of the energy levels. Also note in Tables 5, 6, and 7 for low values of K where the Λ-doubling components were not resolved in the (4-0) sequence, that the quantity $f_{1c} - f_{1d}$ reflects the Λ-doubling of the lower vibrational state only.

TABLE 2

FREQUENCIES OF IDENTIFIED LINES IN THE $^2\Pi - {}^2\Pi$, (4-0) BAND OF *OH*

K	P_{1c} P_{1d} (Cm^{-1})	P_{2c} P_{2d} (Cm^{-1})	R_{1c} R_{1d} (Cm^{-1})	R_{2c} R_{2d} (Cm^{-1})	Q_{1c} Q_{1d} (Cm^{-1})
1	.....	.....	13358.94	13340.72	13286.90
	.....	.....	"	"	"
2	13203.22	13228.11	13376.36	13364.78	13275.30
	"	"	"	"	"
3	13156.74	13178.14	13389.09	13381.72	.....
	"	"	"	"	.....
4	13104.66	13122.91	13396.55	13392.53	.....
	"	"	"	"	.....
5	13046.90	13062.35	13398.80	13395.41	.....
	"	"	"	"	.....
6	12983.55	12996.98	13395.41	13394.25	.....
	"	"	13394.25	"	.....
7	12915.50	12926.28	13386.25	13386.25	.....
	12914.55	"	"	"	.....
8	12841.55	12850.74	13371.64	13371.64	.....
	12840.19	"	"	"	.....
9	12762.24	12770.47	13350.80	13351.47	.....
	12760.95	12769.69	13348.06	13350.80	.....
10	12677.68	12685.13	13324.04	13325.42	.....
	12676.03	12684.06	.....	13324.04	.....
11	12588.18	12594.65	13292.09	13293.22	.....
	12586.17	12593.42	.....	13292.09	.....
12	12493.61	12499.45	13253.70	13255.46	.....
	12491.43	12498.00	.....	13253.70	.....
13	12394.06	12399.30	.....	.....	.....
	12391.60	12397.64	.....	.....	.....
14	12289.58	12294.28	.....	.....	.....
	12287.14	12292.60	.....	.....	.....
15	12180.63	12184.82	.....	.....	.....
	12177.70	12182.76	.....	.....	.....
16	12066.60	12070.74	.....	.....	.....
	12063.73	12068.26	.....	.....	.....

TABLE 3

FREQUENCIES OF IDENTIFIED LINES IN THE $^2\Pi - {}^2\Pi$, (5–1) BAND OF *OH*

K	P_{1c} P_{1d} (Cm^{-1})	P_{2c} P_{2d} (Cm^{-1})	R_{1c} R_{1d} (Cm^{-1})	R_{2c} R_{2d} (Cm^{-1})	Q_{1c} Q_{1d} (Cm^{-1})
1	.....	.....	12701.71	12684.06	12632.58
	.....	.....	"	"	"
2	12551.79	12576.20	12717.90	12706.11	12620.67
	"	"	"	"	"
3	12506.80	12528.08	12729.28	12721.86	12604.55
	"	"	"	"	"
4	12456.12	12474.43	12735.58	12731.24	.....
	"	"	12734.27	"	.....
5	12399.30	12415.64	12736.48	12734.27	.....
	"	"	12735.58	"	.....
6	12338.85	12351.77	12731.24	12731.24	.....
	12337.84	"	"	"	.....
7	12271.71	12282.85	12721.86	12721.86	.....
	12270.67	12282.00	"	"	.....
8	12199.40	12209.16	12706.11	12706.11	.....
	12198.03	12208.62	"	"	.....
9	12121.81	12130.42	12684.06	12684.06	.....
	12120.41	12129.52	"	"	.....
10	12038.82	12046.39	12657.95	12657.95	.....
	12037.30	12045.48	12656.62	12656.62	.....
11	11951.15	11957.75	12623.24	12624.79	.....
	11949.18	11956.58	"	"	.....
12	11858.13	11864.16	.....	.....	.....
	11856.09	11862.79	.....	.....	.....
13	11760.22	11765.65	.....	.....	.....
	11757.85	11764.02	.....	.....	.....
14	11657.45	11662.35	.....	.....	.....
	11654.98	11660.74	.....	.....	.....
15	11550.04	11554.48	.....	.....	.....
	11547.11	11552.43	.....	.....	.....
16	11437.42	11441.70	.....	.....	.....
	11434.55	11439.56	.....	.....	.....

TABLE 4

FREQUENCIES OF IDENTIFIED LINES IN THE $^2\Pi - {}^2\Pi$, (6-2) BAND OF *OH*

K	P_{1c} P_{1d} (Cm^{-1})	P_{2c} P_{2d} (Cm^{-1})	R_{1c} R_{1d} (Cm^{-1})	R_{2c} R_{2d} (Cm^{-1})	Q_{1c} Q_{1d} (Cm^{-1})
1	.....	.....	.....	.....	11980.39
	.....	.....	.....	.....	"
2	.....	.....	12061.15	12050.02	11968.51
	.....	.....	"	"	"
3	11858.86	11879.73	12071.71	12063.73	11951.15
	"	"	"	"	"
4	11809.64	11827.98	12076.08	12071.71	.....
	"	"	"	"	.....
5	11754.83	11770.48	12076.08	12073.74	.....
	"	"	"	"	.....
6	11694.88	11708.19	12069.92	12069.92	.....
	11694.00	"	"	"	.....
7	11629.12	11640.61	12058.35	12058.35	.....
	11628.10	"	"	"	.....
8	11558.12	11568.12	12040.95	12041.87	.....
	11556.99	"	"	12040.95	.....
9	11481.91	11491.10	.....	.....	.....
	11480.53	11490.16	.....	.....	.....
10	11400.46	11409.80	.....	.....	.....
	11398.93	11407.55	.....	.....	.....

TABLE 5

ENERGY LEVELS, $v = 4$ IN $^2\Pi$ STATE OF *OH*

K	f_{1c} (Cm^{-1})	f_{1d} (Cm^{-1})	f_{2c} (Cm^{-1})	f_{2d} (Cm^{-1})
1	13286.92	13287.12	13415.82	13415.58
2	13358.79	13359.04	13467.15	13466.90
3	13459.90	13460.39	13552.42	13552.19
4	13590.72	13591.59	13670.62	13670.53
5	13751.32	13752.57	13821.73	13821.75
6	13942.26	13943.64	14003.82	14004.16
7	14162.83	14164.50	14218.52	14219.20
8	14412.96	14415.40	14463.84	14464.63
9	14692.78	14695.72	14739.30	14740.41
10	15001.62	15003.89	15044.71	15046.06
11	15339.32	15343.68	15379.80	15381.23
12	15705.75	15711.03	15743.50	15745.76
13	16099.94	16106.10	16135.86	16138.45
14	16522.33	16528.89	16556.00	16560.01
15	16971.13	16978.77	17003.54	17007.91

Taking the quantities f_{ic} from Tables 5, 6, and 7 and employing the method of least squares, we obtain the values of B_v and D_v given in Table 8 for $v = 4$, 5, and 6. The quantities given in italics in Table 8 are the constants calculated by Dieke and Crosswhite[1] on the basis of the ultraviolet bands of *OH*. Following Dieke and Crosswhite,[1] we have determined the coupling constant from equations (2), written in the form

$$f_{2c}(K) - f_{1c}(K-1) = B_v[4K^2 + Y_v(Y_v-4)]^{1/2} - 4DK^3. \quad (5)$$

For each value of v, the quantity $Y_v(Y_v - 4)$ is calculated from equation (5) for the low values of K for two cases, namely, including and excluding the term in $4D_vK^3$. The true

TABLE 6

ENERGY LEVELS, $v = 5$ IN $^2\Pi$ STATE OF *OH*

K	f_{1c} (Cm^{-1})	f_{1d} (Cm^{-1})	f_{2c} (Cm^{-1})	f_{2d} (Cm^{-1})
1	16200.89	16201.07	16330.35	16330.15
2	16269.92	16270.20	16379.43	16379.14
3	16366.83	16367.28	16460.42	16460.24
4	16491.78	16492.54	16573.34	16573.18
5	16646.18	16646.20	16717.38	16717.44
6	16828.47	16829.64	16891.97	16891.83
7	17039.05	17040.64	17096.73	17097.13
8	17278.71	17280.95	17330.85	17331.49
9	17346.11	17548.97	17593.67	17594.73
10	17841.26	17844.75	17884.99	17886.58
11	18164.67	18168.19	18205.38	18206.68
12	18513.81	18518.78	18552.62	18555.28
13	18890.53	18896.04	18927.03	18930.26
14	19293.44	19299.59	19327.98	19331.62
15	19721.49	19728.64	19754.63	19759.08

TABLE 7

ENERGY LEVELS, $v = 6$ IN $^2\Pi$ STATE OF *OH*

K	f_{1c} (Cm^{-1})	f_{1d} (Cm^{-1})	f_{2c} (Cm^{-1})	f_{2d} (Cm^{-1})
1				
2	19017.46	19017.86	19127.93	19127.75
3	19110.07	19110.60	19205.30	19205.26
4	19230.06	19230.79	19312.25	19312.16
5	19376.80	19377.48	19449.50	19449.55
6	19550.99	19552.08	19615.84	19616.11
7	19752.09	19753.62	19811.05	19811.67
8	19980.20	19982.33	20033.73	20034.28
9	20235.10	20237.74	20284.99	20284.86

value of $Y_v(Y_v - 4)$ should lie between the two. The average values of Y_v determined in this manner are also given in Table 8. The Λ-doubling of the f_1 states is given approximately by

$$f_{1d}(K) - f_{1c}(K) = q_1K(K+1). \quad (6)$$

The constant q_1 for each vibration state determined from equation (6) is given in Table 8.

The values of B_v determined from the vibration-rotation bands of *OH* are in very good agreement with those calculated from Dieke and Crosswhite's values of B_e, α_e, and γ_e as

well as with the values determined by Dejardin, Janin, and Peyron,[7] also from the (4–0) sequence, and with the value of B_4 obtained by Benedict, Plyler, and Humphreys[4] from the (4–2) band. Furthermore, Table 8 shows, as expected from theory, that the absolute value of the coupling constant increases regularly with the vibrational quantum number and the Λ-doubling of the f_1 state decreases regularly with the vibrational quantum number.[1,13] The Λ-doubling of the f_2 state is smaller than that for the f_1 state, as can

TABLE 8

MOLECULAR CONSTANTS FOR THE $^2\Pi$ STATE OF *OH*

V	B_v (Cm^{-1})	D_v (Cm^{-1})	Y_v	A_v (Cm^{-1})	q_1 (Cm^{-1})	$\Delta G_{v+1/2}$ (Cm^{-1})
0	18.515	0.00187	−7.547	139.7	0.0417	3569.63
1	17.807	.00182	−7.876	140.2	.0399	3403.95
2	17.108	.00182	−8.214	140.5	.0377	3240.25
3	16.414	.0018	−8.568	140.6	.0351	3077.67
4	15.722	.00176	−8.941	140.6	.0313	2915.24
5	15.033	.00175	−9.368	140.8	.0287	2751.43
6	14.349	0.00181	−9.795	140.5	0.0269	.....

$B_e = 18.867\ cm^{-1}$; $\omega_e = 3734.09\ cm^{-1}$; $\omega_e = 3738.48\ cm^{-1}$

$a_e = 0.708\ cm^{-1}$; $\omega_e x_e = 82.665\ cm^{-1}$; $\omega_e x_e = 85.482\ cm^{-1}$

$\gamma_e = 0.00207\ cm^{-1}$; $\omega_e y_e = 0.0940\ cm^{-1}$; $\omega_e y_e = 0.7232\ cm^{-1}$

$\omega_e z_e = 0.04544\ cm^{-1}$

TABLE 9

EXTRAPOLATED VALUES OF CONSTANTS FOR THE $^2\Pi$ STATE OF *OH*

V	B_v (Cm^{-1})	D_v (Cm^{-1})	Y_v	q_1 (Cm^{-1})	$\Delta G_{v+1/2}$ (Cm^{-1})
6	.....	.....	.....	.....	2585.63
7	13.673	0.0018	−10.248	0.0234	2416.47
8	12.999	.0018	−10.726	.0203	2242.93
9	12.328	0.0018	−11.227	0.0171	.....

be seen in Figures 1, 2, and 3. While it does not follow a simple formula, it also decreases with the vibrational quantum number.

The constants B_e, a_e, and γ_e, which occur in the expression

$$B_v = B_e - a_e(v + \tfrac{1}{2}) + \gamma_e(v + \tfrac{1}{2})^2, \tag{7}$$

have been determined by the methods of least squares, taking B_v from Table 7, and have the following values:

$$B_e = 18.867\ cm^{-1}, \qquad a_e = 0.708\ cm^{-1}, \qquad \gamma_e = 0.00207\ cm^{-1}. \tag{7a}$$

For convenience to the investigator of the night-sky spectrum, we have extended Table 8 to higher values of the vibrational quantum number and give the results in Table 9. The

[13] G. Herzberg, *Molecular Spectra and Molecular Structure*, Vol. 1: *Spectra of Diatomic Molecules* (2d ed.; New York: D. Van Nostrand Co., Inc., 1950).

values of B_v are those computed with the aid of equation (7), while D_v is taken to be 0.0018 cm^{-1}. The values of Y_v and q_1 tabulated where calculated from the following expressions, which were obtained by a least-squares fit to the data in Table 8:

$$-Y_v = 0.01158\, v^2 + 0.3039\, v + 7.553 \tag{8}$$

and

$$q_1(\text{cm}^{-1}) = -5.238 \times 10^{-5}\, v^2 - 2.300 \times 10^{-3}\, v + 4.206 \times 10^{-2}.$$

The vibrational-term values for *OH* may be written, as customary, in the form

$$G(v) = \omega_e(v + \tfrac{1}{2}) - \omega_e x_e(v + \tfrac{1}{2})^2 + \omega_e y_e(v + \tfrac{1}{2})^3 + \ldots . \tag{9}$$

The separation between the successive vibrational levels v and $v + 1$ may be written as

$$\Delta G_{v+1/2} = G(v + 1) - G(v). \tag{10}$$

The values of $\Delta G_{v+1/2}$ given in Table 8 were obtained from the f_{1e} energy levels given by Dieke and Crosswhite[1] and the present paper for low values of K after subtraction of the rotational energy as given by equations (2). The values of $\Delta G_{1/2}$ and $\Delta G_{3/2}$ agree very closely with those given by Dieke and Crosswhite,[1] namely, 3569.59 and 3403.97 cm^{-1}, respectively. Writing equation (9) in the form

$$G_0(v) = G(v) - G(0) = \omega_0 v - \omega_0 x_0\, v^2 + \omega_0 y_0\, v^3 + \ldots \tag{11}$$

and, applying the method of least squares, we find

$$\omega_e = 3734.09 \text{ cm}^{-1}, \qquad \omega_e x_e = 82.66 \text{ cm}^{-1}, \qquad \omega_e y_e = 0.094 \text{ cm}^{-1}.$$

These values, like the other constants, are not very different from those of Dieke and Crosswhite.[1,14] If it is assumed that the experimental data are accurate enough to justify the inclusion of an additional term, viz., $-\omega_e z_e(v + \frac{1}{2})^4$ in equation (9), then least-squares methods yield the following values for the vibrational constants:

$$\omega_e = 3738.48 \text{ cm}^{-1}, \qquad \omega_e x_e = 85.482 \text{ cm}^{-1},$$

$$\omega_e y_e = 0.7232 \text{ cm}^{-1}, \qquad \text{and} \qquad \omega_e z_e = 0.04544 \text{ cm}^{-1}.$$

These constants are also listed in Table 8.

It should be pointed out that there is a systematic difference between our wave-length measurements of the lines in the (4–0) *OH* vibration-rotation band sequence and those of Meinel.[2] This discrepancy is probably due to the inaccuracies inherent in the low-dispersion night-sky spectra. It is felt that the molecular constants given in Tables 8 and 9 should prove of considerable value in predicting line and band head positions in the various bands of astrophysical interest. It may be noted that the values of $\Delta G_{v+1/2}$ given in Table 9 are those computed from the vibrational-term formula including the quantity $\omega_e z_e$. These values agree fairly well with Meinel's measurements.

We should also like to comment on the earlier paper of Dejardin, Janin, and Peyron[6] on the *OH* bands. Their wave-length measurements at low dispersion are consistent with ours in some cases. However, their resolution is insufficient to distinguish between the many strong lines in the vibration-rotation bands of H_2O and *OH* in this spectral region. Furthermore, some of their suggested assignments are not compatible with the relative intensities of lines within the *OH* vibration-rotation bands that are to be expected at the temperatures of the acetylene- and hydrogen-oxygen flames. It seems to us that there is

[14] Note that in n. 1, because of a misprint, $\omega_e x_e$ should be 82.81 instead of 82.21 as given. This quantity is quoted correctly by Herzberg in n. 13.

no positive evidence for some of these higher transitions. We find no evidence as yet of these higher bands on our plates, although one should first identify all the strong lines of H_2O in this region.[9] It would appear that some of these difficulties are now also appreciated by the above authors, who have more recently reported on higher-dispersion studies.[7]

In his analysis of the necessarily weak *OH* emission data obtained from the night-sky spectrum, Meinel[2] thought that it might be impossible to fit the vibration-term differences to the usual simple polynomial involving relatively few constants and that there might be peculiar properties associated with the potential function of the *OH* molecule. On the basis of the work reported in the present paper, the quantity $\Delta G_{v+1/2}$ (obs.) $-$ $\Delta G_{v+1/2}$ (calc.), determined on the basis of the constants ω_e, $\omega_e x_e$, and $\omega_e y_e$ given in Table 8, is in all cases less than 1 cm^{-1}. The average difference is $\sim$0.6 cm^{-1}. If the next highest term is added to the vibrational-term formula, viz., $\omega_e z_e$, then, using the appropriate constants given in Table 8, the average differences $\Delta G_{v+1/2}$ (obs.) $-$ $\Delta G_{v+1/2}$ (calc.) become $<$0.1 cm^{-1}. This result would imply that Meinel's findings are caused by inaccurate data and that there are no particularly peculiar properties associated with the potential function of the *OH* molecule.

Finally, we wish to thank Miss K. E. Pace for her assistance in measuring the plates and express our appreciation to Dr. W. S. Benedict for his interest in our work and his many profitable discussions and suggestions concerning the preparation and form of this paper.

VIBRATIONAL TRANSITION PROBABILITIES OF DIATOMIC MOLECULES: COLLECTED RESULTS N_2, N_2^+, NO, O_2^+*

W. R. JARMAIN, P. A. FRASER, AND R. W. NICHOLLS
Department of Physics, University of Western Ontario, London, Canada
Received March 25, 1953; revised May 8, 1953

ABSTRACT

Arrays of approximate vibrational transition probabilities, i.e., $p(v', v'')$ = (overlap integral)^2 are presented for the following transitions:

N_2: $B\,^3\Pi_g \rightarrow A\,^3\Sigma_u^+$ (first positive),
$C\,^3\Pi_u \rightarrow B\,^3\Pi_g$ (second positive),
$A\,^3\Sigma_u^+ \rightarrow X\,^1\Sigma_g^+$ (Vegard-Kaplan);
N_2^+: $B\,^2\Sigma_u^+ \rightarrow X\,^2\Sigma_g^+$ (first negative);
NO: $A\,^2\Sigma^+ \rightarrow X\,^2\Pi$ (γ-bands);
O_2^+: $A\,^2\Pi_u \rightarrow X\,^2\Pi_g$ (second negative).

The methods employed in computation of these values are indicated.

I. INTRODUCTION

It is well known that the spontaneous dipole transition probability of a diatomic molecular band is given by

$$P(v', v'') = \frac{4}{3}\frac{1}{c^3\hbar^4}E_{12}^{(v', v'')3}\left|\int_0^\infty \psi_1^{(v')} R_e \psi_2^{(v'')} d\boldsymbol{r}\right|^2,$$

where $\psi_1^{(v')}$ and $\psi_2^{(v'')}$ are vibrational wave functions of the two levels between which the transition takes place, $E_{12}^{(v', v'')}$ is the energy separation of the two levels, $\boldsymbol{r}$ is the internuclear separation, and $R_e(r)$ is the electronic dipole transition integral. Similar expressions give the transition probabilities for other multipoles.

The spontaneous transition probability is thus mainly controlled by integrals of the form

$$p(v', v'') = \left|\int_0^\infty \psi_1^{(v')} R_e \psi_2^{(v'')} d\boldsymbol{r}\right|^2 = (v', R_e v'')^2,$$

which will hereafter be called "vibrational transition probabilities." The dependence of $R_e(r)$ on r is generally unknown, but is assumed to be small, and $R_e(r)$ is taken to be of constant value in the important range of r as a first approximation. Hence, when *relative* vibrational transition probabilities are considered, a first approximation to p is given by

$$p(v', v'') = (v', v'')^2,$$

* The research reported in this paper has been sponsored by the Geophysics Research Directorate, Air Force Cambridge Research Centre, Air Research and Development Command under Contract AF-19(122)-470.

where

$$(v', v'') = \int_0^\infty \psi_1^{(v')} \psi_2^{(v'')} dr ,$$

the so-called "overlap" integral.

This paper presents arrays of such $p(v', v'')$, computed mainly by a recently developed approximate method[1] which applies to vibrational wave functions in Morse potentials. The Morse potentials for the two electronic states, 1 and 2, have the familiar form[2]

$$U_i(r) = D_i [1 - \exp - a_i (r - r_{ei})]^2 \qquad (i = 1, 2) .$$

The basis of the approximation is the replacement of a_1 and a_2 by a mean a, and the adjustment of all constants of both states that depend on a_i to correspond to the new a. This allows analytic evaluation of the overlap integrals. Substitution of numbers in the resulting general formulae is a rapid process, and the tedium of numerical evaluation of wave functions and subsequent numerical integration is thus avoided. In a few tables the results of numerical integrations of Morse wave functions are shown for comparison. The agreement is seen to be more than adequate and indicates the validity of the approximate method.

II. RESULTS

The extent of the tables is limited only by the capacity of a desk calculating machine, because of excessive cancellation of figures.[3] Methods of overcoming this cancellation are being sought with some success and will be used later to extend the tables. The p's for the Vegard-Kaplan band system have already been so extended.

Results by numerical methods are shown in parentheses below those calculated by the approximate method.

III. DISCUSSION

These results are part of a continuing program of calculation, by the rapid approximate method, of vibrational transition probabilities for band systems mainly of astrophysical interest. Diatomic molecules whose band systems have been studied or are under course of study include N_2, N_2^+, C_2, O_2^+, NO, OH, CH, CO, CO^+, CN, and C_2. The band systems may be classified into three groups according as the results derived by the approximate method are expected to be excellent (I), satisfactory (II), indicative of trends (III). The criteria for classification are discussed elsewhere[4] but may be qualitatively described as follows: The maximum error in the overlap integral is proportional to $|a_1 - a_2|$ and inversely proportional to $|r_{e1} - r_{e2}|$.

Over two-thirds of the band systems studied and under course of study are at least "satisfactory." Such classification of those band systems presented here is shown in the accompanying short table.

Transition	Classification
N_2 : B $^3\Pi_g \rightarrow$ A $^3\Sigma_u^+$ (first positive)	I
N_2 : C $^3\Pi_u \rightarrow$ B $^3\Pi_g$ (second positive)	II
N_2 : A $^3\Sigma_u^+ \rightarrow$ X $^1\Sigma_g^+$ (Vegard-Kaplan)	I
N_2^+ : B $^2\Sigma_u^+ \rightarrow$ X $^2\Sigma_g^+$ (first negative)	II
NO: A $^2\Sigma^+ \rightarrow$ X $^2\Pi$ (γ-bands)	I
O_2^+ : A $^2\Pi_u \rightarrow$ X $^2\Pi_g$ (second negative)	II

[1] P. A. Fraser and W. R. Jarmain, *Scientific Report No. 5* (Contract No. AF-19[122]-470, Department of Physics, University of Western Ontario, London, Canada); W. R. Jarmain and P. A. Fraser, *Scientific Report No. 7* (Contract No. AF-19[122]-470).

[2] G. Herzberg, *Spectra of Diatomic Molecules* (New York: D. Van Nostrand Co., 1950).

[3] Fraser and Jarmain, *op. cit.*; Jarmain and Fraser, *op. cit.*

[4] Jarmain and Fraser, *op. cit.*

TABLE 1

N_2, $B\ ^3\Pi_g \rightarrow A\ ^3\Sigma_u^+$ (First Positive)

$p(v', v'') = (v', v'')^2$

v'	v''						
	0	1	2	3	4	5	6
0	0.33_7 (0.34_0)†	0.32_4 (0.32_3)	0.19_6 (0.19_0)	0.08_9 (0.08_8)	0.03_7 (0.03_6)	0.01_4 (0.01_4)	0.00_5 (0.00_5)
1	0.40_6 (0.40_6)	0.00_2 (0.00_2)	0.10_5 (0.10_5)	0.17_7 (0.17_7)	0.14_5 (0.14_8)	0.08_7 (0.08_9)	
2	0.19_8 (0.20_0)	0.20_9 (0.21_2)	0.11_8 (0.11_5)	0.00_1 (0.00_2)	0.07_4 (0.07_4)		
3	0.05_1 (0.05_0)	0.29_9 (0.30_1)	0.03_6 (0.03_9)	0.15_9 (0.16_1)			
4	0.00_7 (0.00_6)	0.13_4 (0.13_4)	0.27_0 (0.27_2)				
5	0.00_1 (0.00_0)	0.02_9 (0.02_7)					
6	0.00_0 (0.00_0)						

† Results from numerical integration are shown in parentheses and are more fully reported in W. R. Jarmain and R. W. Nicholls, *Scientific Report*, No. 4 (Contract No. AF 19[122]-470).

TABLE 2

N_2, $C\ ^3\Pi_u \rightarrow B\ ^3\Pi_g$ (Second Positive)

$p(v', v'') = (v', v'')^2$

v'	v''						
	0	1	2	3	4	5	6
0	0.44_4 (0.44_5) †	0.32_8 (0.32_8)	0.14_9 (0.14_6)	0.05_4 (0.05_2)	0.01_8 (0.01_6)	0.00_5 (0.00_5)	0.00_2 (0.00_1)
1	0.38_9 (0.39_4)	0.01_5 (0.01_9)	0.19_6 (0.20_5)	0.19_9 (0.19_3)	0.11_6 (0.11_2)	0.05_2 (0.04_7)	
2	0.13_8 (0.13_5)	0.31_2 (0.32_3)	0.04_1 (0.03_2)	0.04_3 (0.06_2)	0.15_2 (0.15_8)		
3	0.02_6 (0.02_2)	0.25_6 (0.25_6)	0.14_3 (0.16_3)	0.13_1 (0.11_6)			
4	0.00_3 (0.00_2)	0.07_6 (0.07_6)	0.29_6 (0.30_3)				

† See footnote to Table 1.

TABLE 3

N_2, $A\,^3\Sigma_u^+ \rightarrow X\,^1\Sigma_g^+$ (VEGARD-KAPLAN)
$p(v', v'') = (v', v'')^2$

v'	v'' = 0	1	2	3	4	5	6	7	8	9	10	11	12	13	14	15	16	17	18	19	20
0	0.00$_0$ (0.00$_1$) *	0.00$_4$	0.01$_5$	0.05$_3$	0.10$_5$	0.15$_4$	0.18$_6$	0.17$_3$	0.13$_0$	0.08$_6$	0.04$_6$	0.02$_0$	0.00$_8$	0.00$_2$	0.00$_1$	0.00$_0$					
1	0.00$_1$ (0.00$_3$)	0.01$_3$	0.06$_0$	0.11$_1$	0.12$_4$	0.07$_6$	0.01$_4$	0.00$_0$	0.06$_1$	0.12$_5$	0.14$_6$	0.12$_0$	0.07$_3$	0.03$_7$	0.01$_3$	0.00$_5$	0.00$_1$	0.00$_0$			
2	0.00$_8$ (0.00$_5$)	0.04$_3$	0.09$_5$	0.10$_2$	0.04$_1$	0.00$_0$	0.04$_1$	0.08$_8$	0.06$_0$	0.00$_6$	0.01$_5$	0.08$_2$	0.13$_2$	0.12$_8$	0.08$_7$	0.04$_8$	0.01$_8$	0.00$_6$	0.00$_2$	0.00$_0$	
3	0.01$_2$ (0.01$_8$)	0.07$_0$	0.09$_9$	0.04$_8$	0.00$_0$	0.04$_8$	0.07$_0$	0.01$_3$	0.00$_1$	0.06$_2$	0.07$_8$	0.01$_9$	0.00$_8$	0.06$_3$	0.12$_3$	0.12$_7$	0.08$_9$	0.04$_6$	0.01$_8$	0.00$_6$	0.00$_1$
4	0.03$_0$ (0.03$_9$)	0.08$_2$	0.06$_6$																		
5	0.04$_3$ (0.04$_1$)	0.08$_2$	0.03$_0$																		
6	0.05$_8$ (0.06$_2$)	0.07$_6$																			
7	0.07$_1$ (0.07$_3$)	0.05$_4$																			
8	0.07$_8$ (0.08$_1$)																				
9	0.08$_3$ (0.08$_4$)																				

* Results from numerical integration are shown in parentheses.

TABLE 4

N_2^+, $B\,^2\Sigma_u^+ \rightarrow X\,^2\Sigma_g^+$ (FIRST NEGATIVE)

$p(v', v'') = (v', v'')^2$

v'	v''						
	0	1	2	3	4	5	6
0	0.66_6 (0.65)†	0.25_0 (0.26)	0.06_5 (0.07₁)	0.01_8	0.00_3	0.00_1	0.00_0
1	0.28_9 (0.30)	0.23_4 (0.22)	0.28_8 (0.29)	0.13_0	0.04_2	0.01_2	
2	0.04_3 (0.04₇)	0.39_9 (0.41)	0.04_8 (0.04₃)	0.23_1	0.16_6		
3	0.00_9 (0.00₅)	0.10_6 (0.11)	0.40_1 (0.41)	0.00_6			
4	0.00_0	0.00_9	0.17_5				
5	0.000	0.00_0					
6	0.000						

† Results from numerical integration are shown in parentheses, and have been taken from D. R. Bates, *Proc. R. Soc. London*, *A*, **169**, 217, 1949.

TABLE 5

NO, $A\,^2\Sigma^+ \rightarrow X\,^2\Pi$ (γ-BANDS)

$p(v', v'') = (v', v'')^2$

v'	v''						
	0	1	2	3	4	5	6
0	0.16_5	0.26_2	0.23_7	0.16_1	0.09_1	0.04_6	0.02_2
1	0.33_0	0.10_7	0.00_1	0.07_0	0.13_2	0.13_4	
2	0.29_1	0.01_4	0.11_2	0.07_7	0.00_1		
3	0.15_1	0.18_9	0.05_9	0.03_5			
4	0.05_1	0.23_7	0.03_5				
5	0.01_2	0.13_8					
6	0.00_2						

TABLE 6

O_2^+, $A\,^2\Pi_u \rightarrow X\,^2\Pi_g$ (SECOND NEGATIVE)

$p(v', v'') = (v', v'')^2$

v'	v''									
	0	1	2	3	4	5	6	7	8	9
0	0.000	0.000	0.000	0.00_7 (0.00_7)*	0.00_9 (0.00_9)	0.02_8 (0.02_5)	0.05_7 (0.05_8)	0.10_3	0.15_2	0.18_7
1	0.000	0.000	0.00_2 (0.00_2)	0.01_0 (0.01_0)	0.03_3 (0.03_2)	0.07_1 (0.06_7)	0.11_0 (0.10_1)	0.12_5	0.09_0	
2	0.000	0.00_1	0.00_7	0.02_3	0.06_3	0.09_6	0.09_2	0.04_4		
3	0.000	0.00_3	0.01_4	0.04_0	0.08_1	0.08_1	0.03_7			
4	0.00_1	0.00_6	0.02_4	0.05_3	0.07_8	0.04_1				
5	0.00_3	0.01_0	0.03_2	0.05_9	0.05_6					
6	0.00_7	0.01_4	0.04_1	0.05_4						
7	0.00_3	0.01_9	0.04_6							
8	0.00_4	0.02_4								
9	0.00_6									

* Results from numerical integration are shown in parentheses.

TABLE 7

BASIC MOLECULAR CONSTANTS

Molecule	State	$a(A^{-1})$	$K = \omega_e/\omega_e x_e$	$r_e(A)$
N_2*	$C\,^3\Pi_u$	2.6636	119.15	1.1482
	$B\,^3\Pi_g$	2.4517	119.84	1.2123
	$A\,^2\Sigma_u^+$	2.4021	105.13	1.293
	$X\,^1\Sigma_g^+$	2.4505	163.23	1.094
N_2^+**	$B\,^2\Sigma_u^+$	3.1036	104.35	1.075
	$X\,^2\Sigma_g^+$	2.5889	136.79	1.116
NO*	$A\,^2\Sigma^+$	2.5326	163.76	1.0637
	$X\,^2\Pi$	2.4876	136.28	1.1508
O_2^+†	$A\,^2\Pi_u$	2.5495	65.61	1.4089
	$X\,^2\Pi_g$	2.8005	113.52	1.1227

* G. Herzberg, *Spectra of Diatomic Molecules* (New York: D. Van Nostrand Co., 1950).

† M. W. Feast, *Proc. Phys. Soc. A.*, **63**, 557, 1950.

ETA CARINAE. II. THE SPECTRUM

E. GAVIOLA
Córdoba Observatory, Córdoba, Argentina
Received October 29, 1951; revised December 12, 1952

ABSTRACT

Wave lengths and identifications in the spectrum of η Carinae have been determined from 70 slit spectrograms obtained since January 9, 1944. The region 3255–7000 A is included; a slitless spectrogram extends the observed region toward the violet to 3029 A. A total of 903 emission lines and 76 absorption lines were measured, most of them on several plates. The intensities of the emission lines were determined with a semiquantitative objective scale. A small number of lines are almost perfectly sharp, while many are nebulous and very nebulous. Emission lines are multiple, showing two, three, and more components or satellites. They are unsymmetric. *Hα* is brighter, by a factor of several times, than the integrated remainder of the spectrum. Direct images obtained on panchromatic plates are thus monochromatic. An analysis of the Balmer series and a table of satellites are given. *Hα* shows components displaced about 1000 km/sec toward the violet and more than 1500 km/sec toward the red. The principal component is at +20 km/sec. Balmer absorption components vary in intensity and in relative position along the series. The true absorption spectrum studied by Cannon and Bok on the Harvard plates of 1892–1893 has been recorded. The emission spectrum covers it up partially; this suggests that the emission is produced by localized eruptions which do not—or do not completely—disturb the star's atmosphere. Comparison with earlier photographs shows that the spectrum has not changed much in the present century. Some transitory changes were observed in 1948. The *He* I emission lines are of variable intensity.

INTRODUCTION

The spectrum of η Carinae was first obtained on Harvard plates taken at Arequipa in 1892 with the 13-inch Boyden telescope and objective prism. The early results were described by Miss Cannon[1] and later by B. J. Bok;[2] and Miss Hoffleit[3] made a study of 40 plates taken at Arequipa between 1892 and 1930.

In 1893 the spectrum consisted almost entirely of absorption lines, of which Bok measured 70; he identified 42 of these as being due to *Fe* I, *Fe* II, *Ti* II, *Ca* II, *Mg* II, *Cr* II, *Sc* II, and *Sr* II; he classified the spectral type as probably cF5. Superposed on the absorption spectrum were strong emission lines of the Balmer series of hydrogen and a few other inconspicuous emission lines.

In 1895 the spectrum had changed and showed a large number of strong emission lines, as found at present. There was still a continuous background with some absorption lines, but it was much fainter than in 1892–1893. The magnitude of the star had decreased from 7.5 in 1893 to 8.3 in 1895, in spite of the increased intensity of the emission lines.

Slit spectra have been described by Gill,[4] Moore and Sanford,[5] Lunt,[6] and Spencer Jones.[7] Merrill[8] found that some of the strongest emission lines are due to forbidden ionized iron; he extended the identifications to 78 of the lines measured by Moore and Sanford and by Lunt between 4068 A and 5169 A. Spencer Jones extended the identifications into the red to *Hα*. Miss Hoffleit added and identified 44 new lines observed on an isochrom plate obtained in 1930.

A series of spectrograms was begun at Bosque Alegre, Córdoba, on January 9, 1944; a plane-grating reflecting spectrograph, designed and built at the observatory,[9] was

[1] *Harvard Ann.*, **28**, 175, 1901.
[2] *Pop. Astr.*, **38**, 399, 1930.
[3] *Harvard Bull.*, **893**, 11, 1933.
[4] *M.N.*, **61**, 66, 1901.
[5] *Lick Obs. Bull.*, **8**, 55, 1913; Sanford, *Lick Obs. Bull.*, **8**, 134, 1916.
[6] *M.N.*, **79**, 621, 1919.
[7] *M.N.*, **91**, 794, 1931.
[8] *Ap. J.*, **67**, 391, 1928.
[9] Gaviola, *Réunion d'opticiens, Paris 1946*, p. 127; *Rev. d'opt.*, March, 1948.

used in conjunction with the large reflector. Seventy slit and 33 slitless spectrograms have been taken since that date. The optical quality of the spectrograph, which gives a dispersion of 42 A mm, and the light-gathering power of the Bosque Alegre reflector allow a comprehensive analysis of the spectrum to be made; this was not possible hitherto. Both the emission-line spectrum, dominant since 1895, and the old absorption-line spectrum of 1893 have been observed. The plates show, on the whole, that the star has not changed much in the last 50 years.

THE CÓRDOBA SPECTROGRAMS

Of the 70 slit spectra obtained, the ones listed in Table 2, have been totally or partially measured. The short-exposure (under 30 minutes) panchromatic films and plates were measured only in the *Hα* region, to test for a possible change in the position of the main components of that line. No systematic changes have been detected so far.

The long-exposure films and plates, taken with the slit spectrograph, cover the wave-length band 3255–7000 A. The long-wave-length limit is given by the plate sensitivity; the ultraviolet limit is due to the silver film of the main mirror of the telescope. The two secondary mirrors of the telescope (Cassegrain and coudé) and the four reflecting surfaces of the spectrograph (including the plane grating) are aluminized, but Córdoba does not yet have a vacuum tank large enough for aluminizing the 60-inch mirror. The ultraviolet limit was nevertheless extended.

A technique had been developed for obtaining slitless spectra with a normal comparison spectrum. On nights with exceptionally good seeing the star was centered on a narrow slit; a thin wire reticule was centered on a near-by star in the guiding field of the spectrograph; the central star was then covered with the comparison-spectrum baffle, a plate was placed in position, and the iron-arc spectrum was exposed in the usual way; the slit was then opened wide, leaving a field of some 15″ radius free around the central star (as both slit jaws open symmetrically), and the baffle was removed while guiding the telescope by the near-by star. Upon completion of the desired exposure time, the baffle was replaced, the slit was narrowed to the previous value, and the comparison spectrum was exposed again. After the plate was covered and taken from the spectrograph, the baffle was removed, in order to see whether the star was still centered on the slit. With this technique an image of η Carinae appears on a panchromatic plate (Eastman 103A-F) with an exposure time of only 7 seconds. With longer exposure times, spectra of the star's nebulosity are obtained. These will be described in detail in a forthcoming publication.

When the spectrum of the star's nucleus to the red of 3255 A is strongly overexposed, a slitless spectrum to the violet of 3255 A is obtained. This is due either to a residual reflection of the silver mirror in that region or to reflection of the glass itself. One plate of exceptionally good quality (No. 47; see Table 2) taken as described above, has extended the measurable spectrum to 3029 A, for 355 A additionally. The precision of the wave lengths obtained in this extension is, of course, somewhat lower, on account of the wide slit. A small systematic error is also possible, due to guiding inaccuracies. This error, however, can be evaluated, since it is possible to measure the center of the slitless spectrum up to λ 3289, 34 A beyond the beginning of the slit spectrum. Each section then has one dozen lines in common.

No change in any wave length has been noticed since 1944. It is therefore permissible to take mean values for each line measured on several plates. As regards relative intensities, only the *He* I and the nebulium lines show some variation. The spectra of 1948 constitute an exception, as the Balmer absorption appears that year definitely enhanced (but not displaced) and the general continuum is probably stronger. After 1948 the spectrum returned to what it had been up to 1947. It is therefore justifiable to indicate a single scale of relative intensities.

Table 1 contains the results. The first column gives the number of plates (or films) on

TABLE 1

Wave Lengths and Identifications

No. of Plates	λ Star	Int	Identification
1	3028 8	0E	*Mn* II 29.04(50), *Zr* II 28.05(20)
1	3030 5	1E	*Zr* II 30.91(10)
1	3033 7	1E	*Fe* II 33.45(2n)
1	3039 6	1En	*Fe* II 38.78(3), *Mn* II 39.55(40), *Cr* II 40.92(70)
1	3042 3	1En	*Cr* II 42.79(25)
1	3045 6	1En	*Fe* II 44.84(5), *Mn* II 46.27(30), *Fe* II 46.68(1), *Fe* II 45.31(0)
1	3048 7	1En	*Fe* II 49.01(5n)
1	3050 5	1En	*Cr* II 50.14(100), *Mn* II 50.66(25)
1	3053 2	1En	*Cr* II 53.65(10)
1	3064 8	2Enn	*Fe* II 65.32(6)
1	3067 4	0E	*Fe* II 65.32r, *Cr* II 67.18(20)
1	3076 5	2En	*Fe* II 77.17(10), *Fe* II 76.46(6n), *Fe* II 78.70v
1	3078 1	3Enn	*Fe* II 78.70(8n), *Fe* II 77.17r
1	3080 2	2En	*Fe* II 78.70r, *Fe* II 80.41(2)
1	3084 7	1E	*Cr* II 84.46(15), *Cr* II 85.36(10)
1	3094 3	2E	*Zr* II 95.07(12)
1	3098 1	2En	*Fe* II 97.42(2), *Cr* II 98.16(18)
1	3102 7	1E	*Cr* II 03.48(30)
1	3106 8	2Enn	*Fe* II 05.55(5), *Fe* II 06.56(4), *Cr* II 07.58(50)
1	3111 0	1En	*Fe* II 14.30v, *Zr* II 10.87(10)
1	3113 1	1E	*Fe* II 14.30(7)
1	3115 9	2En	*Fe* II 16.59(6), *Fe* II 14.68(4)
1	3119 4	2En	*Cr* II 20.37(75), *Cr* II 18.65(60), *Fe* II 20.02(1)
1	3124 8	2En	[*Fe* II] 24.18, *Cr* II 24.98(100)
1	3131 4	1E	*Cr* II 32.06 (125), *Fe* II 31.72(4)
1	3132 8	1E	*Fe* II 33.05(4), *Fe* II 35.36v
1	3134 5	1E	*Fe* II 35.36(9)
1	3136 7	1En	*Cr* II 36.68(40)
1	3139 2	2Enn	*Zr* II 38.66(25), *Cr* II 40.21(25)
1	3145 9	1Enn	*Fe* II 44.75(5), *Fe* II 46.75(2)
1	3152 3	1E	*Cr* II 52.21(40), *Fe* II 54.20v
1	3154 0	2E	*Fe* II 54.20(12)
1	3155 8	1E	*Fe* II 54.20r, *Fe* II 55.95(2)
1	3158 3	1En	*Cr* II 58.03(20), *Cr* II 59.10(5)
1	3161 1	1E	*Fe* II 61.95(5)
1	3163 0	1E	*Fe* II 63.09(5)
1	3165 1	1Enn	*Fe* II 65.96(3u), *Fe* II 67.85v
1	3168 2	2E	*Fe* II 67.85(11)
1	3172 6	1E	*Cr* II 72.08(40), *Fe* II 67.85r
1	3180 2	1E	*Fe* II 79.50(8), *Fe* II 80.16(7), *Cr* II 80.73(75), [*Fe* II] 81.05
1	3182 5	1Enn	*Fe* II 83.12(8), *Cr* II 83.33(40), *Fe* II 82.86(35)
1	3184 6	1En	[*Fe* II] 85.01, *Fe* II 85.32(5)
1	3192 5	1E	*Fe* II 92.92(9)
1	3194 3	1Enn	*Fe* II 93.81(11), *Fe* II 96.07v, *Cr* II 97.12v
1	3196 4	2En	*Fe* II 96.07(10), *Cr* II 97.12(75)
1	3198 9	0En	*Fe* II 96.07r, *Cr* II 97.12r
1	3204 7	0En	*Cr* II 05.11(25)
1	3208 1	1Enn	*Cr* II 09.21(50), *Fe* II 10.45v, *Cr* II 08.62(20)
1	3211 4	2Enn	*Fe* II 10.45(10), *Fe* II 13.31v
1	3212 8	3En	*Fe* II 13.31(13)
1	3214 6	2Enn	*Fe* II 13.31r, [*Fe* II] 14.67, *Zr* II 14.19(40)
1	3217 2	0En	*Cr* II 17.44(50)
1	3218 7	0Enn	*Cr* II 19.13(18)
1	3222 3	0Enn	*Ti* II 22.84(35)
1	3223 4	0E	[*Ni* II] 23.3, *Fe* II 23.44(1)
1	3224 6	1E	[*Fe* II] 24.54
1	3226 2	2En	*Fe* II 27.73v, *Fe* II 26.38(2)
1	3228 2	4En	*Fe* II 27.73(13)
1	3229 8	2En	*Fe* II 27.73r, [*Fe* II] 30.17
1	3231 1	1E	*Fe* II 31.70(5), *Zr* II 31.69(30)
1	3232 5	1En	*Fe* II 32.79(7)
1	3236 9	0En	*Fe* II 37.82(8), *Fe* II 37.40(5), *Cr* II 38.77v
1	3239 0	2Enn	*Cr* II 38.77(50), *Ti* II 39.04(60)
1	3240 6	2Enn	*Cr* II 38.77r, *Fe* II 41.69(2), *Zr* II 41.01(25)
1	3242 8	0E	*Fe* II 43.72(8)
1	3244 4	1En	[*Fe* II] 44.18
1	3247 0	2E	*Fe* II 47.17(9), *Fe* II 47.39(3)
1	3248 9	3En	*Fe* II 49.66(4)
1	3250 6	2E	*Cr* II 50.79(10)
1	3252 5	2E	[*Fe* II] 54.24v, *Ti* II 52.91(40)
1	3254 2	3En	[*Fe* II] 54.24, *Ti* II 54.25(30)
2	3255 37	4En	*Fe* II 55.88(8)
1	3256 60	4E	*Fe* II 59.05v, [*Fe* II] 56.73, *Fe* II 58.77v
2	3258 48	5E	*Fe* II 59.05(10), *Fe* II 58.77(10)
1	3260 13	3En	*Fe* II 59.05r, *Fe* II 58.77r
1	3261 92	2En	*Ti* II 61.60(60), *Fe* II 59.05r, *Fe* II 58.77r
2	3264 39	3En	*Cr* II 64.26(35), [*Fe* II] 64.84
1	3266 41	2Enn	*Fe* II 66.94(4), *Fe* II 67.04(3)
1	3268 48	1En	*Fe* II 68.51(3), *Cr* II 70.14v
2	3269 74	3En	*Cr* II 70.14(40), *Fe* II 69.77(2)
1	3271 77	2E	*Ti* II 72.08(25), *Ti* II 71.65(25), *Cr* II 70.14r
1	3273 53	2En	*Zr* II 73.04(75), *Fe* II 73.50(3)
1	3275 53	3En	*Fe* II 76.61(5), *Fe* II 77.35v, *Ni* II 74.90(3)
3	3277 34	5En	*Fe* II 77.35(9), [*Fe* II] 77.12, [*Fe* II] 77.55
3	3280 75	4E	*Fe* II 81.29(7)
1	3283 53	2En	*Fe* II 81.29r
3	3284 95	3En	*Fe* II 85.43(3), *Fe* II 85.00(0)
2	3287 28	3E	*Ti* II 87.66(40), [*Fe* II] 87.45
3	3288 68	3E	*Fe* II 89.35(7), [*Fe* II] 89.46
1	3292 05	2E	*Fe* II 89.35r, *Fe* II 95.81v, *Mo* II 92.31(12)
2	3295 47	4En	*Fe* II 95.81(6), *Fe* II 95.24(4)
2	3302 75	4En	*Fe* II 02.86(4), *Fe* II 03.47(4), *Na* I 02.94(8R)
1	3305 19	3E	*Fe* II 05.63(1), *Zr* II 05.15(15), *Fe* II 02.86r
1	3306 79	3En	*Cr* II 07.04(50), *Cr* II 06.95(50)
1	3310 38	3En	*Cr* II 10.65(35), *Cr* II 10.65(35)
2	3313 52	3En	*Cr* II 14.57(35), *Fe* II 14.00(1), *Cr* II 13.08(20)
3	3323 30	4En	*Fe* II 23.07(8), *Cr* II 24.06(25), *Cr* II 24.10(20), *Cr* II 24.35(50)
1	3327 40	3E	*Fe* II 27.63, *Cr* II 24.06r
1	3332 86	3En	*Ni* II 33.16(2)
1	3338 60	5En	*Fe* II 38.52(3), [*Fe* II] 39.14, *Cr* II 39.80(50)
2	3342 39	5E	*Cr* II 42.51(50)
1	3344 66	3An	*Ti* II 49.40(125/), *Cr* II 47.84(40)
2	3347 06	4E	*Cr* II 47.84(40)
2	3349 42	4En	*Ti* II 49.40(125/), *Ni* II 50.42(5)
2	3352 41	3En	*Cr* II 53.12(20), *Co* II 52.80(30)
1	3354 92	3Ann	*Ti* II 61.21(125), *Cr* II 60.29(100), *Cr* II 58.50(75)
3	3359 19	5En	*Cr* II 60.29(100), *Fe* II 60.10(3)
2	3361 60	4Enn	*Ti* II 61.21(125), *Cr* II 61.77(30), *Cr* II 60.29r
2	3365 61	4E	*Fe* II 65.41(1), *Fe* II 65.64(0)
2	3368 78	5En	*Cr* II 68.05(150), *Fe* II 69.35(3)
1	3370 57	3Enn	*Cr* II 68.05r
3	3373 61	4En	*Ni* II 73.98(4), *Ti* II 72.80(100)
3	3376 22	6En	[*Fe* II] 76.20
1	3379 42	5En	*Cr* II 79.83(60), *Ti* II 80.28(30)
2	3381 25	4En	*Fe* II 81.00(4)
3	3386 42	4En	*Fe* II 86.72(2), *Fe* II 86.45(1), [*Fe* II] 87.10
2	3389 07	2Ann	*Ni* I 92.99(100r), *Cr* II 93.00(35), *Cr* II 93.86(30), *Ni* I 91.05(70r)
2	3391 38	5En	*Zr* II 91.96(100), *Cr* II 91.43(35)
3	3393 65	6En	*Cr* II 93.00(35), *Cr* II 93.86(30), *Cr* II 94.32(35)
2	3397 59	3E	*Fe* II 98.36(4), *Ni* II 97.82(1)
1	3398 71	2En	*Cr* II 99.54(18)
2	3400 75	4En	*Ni* II 01.76(2)?
2	3403 41	3En	*Cr* II 03.32(100)
2	3406 70	5En	*Ni* II 07.30(8)
2	3408 40	5En	*Cr* II 08.77(150)
1	3412 66	3An	*Ni* I 14.77(150R/), *Co* I 12.63 (80R), *Ni* I 15.05(150)
2	3415 38	4En	*Fe* II 16.02(5), *Co* II 15.78(75)

TABLE 1—*Continued*

No. of Plates	λ Star	Int.	Identification
1	3420 82	4Enn	*Cr* II 21.20(75), *Cr* II 22.74v
3	3422 65	6En	*Cr* II 22.74(125)
1	3425 81	4En	*Cr* II 22.74r, *Fe* II 25.58(3), [*Ve* V] 25.8(N)
2	3429 50	4Ann	*Ni* I 33.56(70r), *Cr* II 33.30(75), *Co* I 31.58
1	3430 64	3En	*Zr* II 30.53(30), *Cr* II 33.30v
2	3433 36	5En	*Cr* II 33.30(75), *Zr* II 33.90(8), *Ni* I 33.56(70)
2	3435 74	4E	*Fe* II 36.11(5)
1	3436 15	2An	*Fe* I 40.61(150R)
2	3438 48	6En	*Zr* II 38.23(100), [*Ni* II] 39.29
1	3440 72	4En	[*Fe* II] 40.99, *Fe* I 40.61, *Mn* II 41.98v
2	3441 92	6En	*Mn* II 41.98(100), *Fe* II 42.24(3)
2	3444 18	4E	*Mn* II 41.98r, *Ti* II 44.31(30)
3	3446 92	8Ann	*Ni* I 52.89(40R), *Ni* I 46.26(100r), *K* I 47.41(6R), *K* I 46.38(8R)
1	3448 69	4E	[*Fe* II] 52.30v, *Fe* II 48.43(1)
3	3451 88	6En	[*Fe* II] 52.30
3	3453 84	6En	*Ni* II 54.16(5), *Fe* II 53.60(2)
2	3458 03	5En	*Cr* II 57.62(30), *Mn* II 60.31v
2	3460 14	6En	*Mn* II 60.31(75), [*Fe* II] 60.20
3	3462 80	4An	*Co* I 62.80(60r), *Ni* I 61.65(125R)
3	3465 86	5En	*Fe* I 65.86(60r), *Mn* II 66.34(9), *Ni* II 65.62
1	3468 56	3E	*Fe* II 68.68(8)
1	3469 03	5A	*Ni* I 72.55(70r), *Co* I 74.02(100R)
3	3471 51	6Enn	*Ni* II 71.35(2), *He* I 71.80(1)
1	3474 88	7Enn	*Cr* II 75.13(20)
1	3477 20	4E	*Cr* II 75.13r, *Ti* II 77.18(15)
1	3478 14	5An	*Co* I 83.41(20r), *Ni* I 83.77(25R), *Mn* II 82.91(40)
2	3479 55	5Enn	*Fe* II 79.91(2)
3	3481 81	6Enn	*Fe* II 82.43(2), *Mn* II 82.91(40)
1	3483 88	4E	*Cr* II 84.15(20), *Fe* II 84.35(1), *Fe* II 82.43r
2	3484 94	4A	*Co* I 89.40(60r), *Fe* I 90.58(100r), *Ni* I 83.77(25R)
3	3486 20	5Enn	[*Fe* II] 89.98v
4	3489 02	6Enn	[*Fe* II] 89.98, *Fe* II 93.47v
2	3491 10	3An	*Fe* I 90.58(100r), *Co* I 95.68(50r), *Ni* I 92.96(150r)
2	3491 50	4E	*Fe* II 93.47v, [*Fe* II] 89.98r
3	3493 87	7Enn	*Fe* II 93.47(10), *Fe* II 94.67(5)
3	3495 26	6En	*Fe* II 95.62(4), *Mn* II 95.83(40), *Zr* II 96.18(50), *Cr* II 95.37(25)
1	3497 72	4E	[*Fe* II] 01.62v, *Fe* II 95.62r, *Mn* II 97.53(25)
3	3500 73	6En	[*Fe* II] 01.62, *Co* II 01.73(200)
4	3503 63	6E	[*Fe* II] 04.51, [*Fe* II] 04.02, *Fe* II 03.47(2)
1	3505 69	4En	[*Fe* II] 04.51r, [*Fe* II] 05.81
2	3507 53	4E	*Fe* II 07.39(3), *Fe* II 08.21(1)
1	3509 61	3En	*Cr* II 11.84v, *Ni* II 13.93v
2	3511 48	5E	*Cr* II 11.84(35), *Ni* II 13.93v
4	3513 70	6En	*Ni* II 13.93(8)
1	3516 12	4En	*Fe* II 15.82(2), *Ni* II 13.93r
1	3517 40	3En	*Ni* II 13.93r, *He* I 17.33(1)
1	3521 77	3Enn	[*Fe* II] 24.38v
1	3523 43	4En	[*Fe* II] 24.38
1	3525 89	3E	[*Fe* II] 24.38r, *Zr* II 25.81(8)
1	3527 34	2E	[*Fe* II] 24.38r, [*Fe* II] 28.28
2	3528 84	3En	*Cr* II 29.73(2)
1	3530 25	3En	*He* I 30.49(1)
1	3532 39	4En	*Fe* II 32.65(2)
1	3533 64	4Enn	[*Fe* II] 36.25v, *Fe* II 35.63v
3	3535 79	5Enn	[*Fe* II] 36.25, *Fe* II 35.63(2), *He* I 36.82(1)
4	3538 57	6En	[*Fe* II] 38.69, [*Fe* II] 39.19
3	3544 36	3Enn	.....
1	3550 60	3En	*Zr* II 51.94(18)?
4	3555 81	5Enn	*Zr* II 56.61(30)
1	3557 60	4En	*Fe* II 57.55(2), [*Ni* II] 59.86v
3	3559 30	6En	[*Ni* II] 59.86
1	3561 26	5En	[*Ni* II] 59.86r
1	3562 16	2An	*Ni* I 66.37(100R), *Fe* I 65.38(60r)
1	3562 70	4E	[*Ni* II] 59.86r, *He* I 62.95(1)
4	3565 04	5Enn	*Fe* II 66.05(2), *Fe* II 66.15(3), *Fe* I 65.38(60r)
1	3566 70	2An	*Fe* I 70.10(100R), *Ni* I 66.37 (100R), *Ni* I 71.87(50R)
3	3569 50	5En	*Fe* I 70.10(100R)
2	3573 63	5E	*Ni* II 76.76v, *Ti* II 73.74(20)
2	3576 31	6En	*Ni* II 76.76(3), *Zr* II 76.88(20)
1	3578 23	5Enn	*Ni* II 76.76r, *Cr* I 78.69(1000R)
1	3579 13	4En	*Ni* II 76.76r, [*Fe* II] 79.81
3	3581 96	2An	*Fe* I 81.20(250R), *Co* I 87.19(70R)
3	3584 90	6En	*Cr* II 85.31(60), *Cr* II 85.54(40)
2	3588 27	5En	*He* I 87.25(2), *Cr* II 85.31r, *Zr* II 88.32(6)
2	3593 47	4En	*Cr* I 93.49(900R)
3	3603 35	5Enn	*Cr* II 03.80(40), *Cr* II 03.86(20)
1	3607 99	4En	*Cr* II 03.80r, *Fe* I 08.86(100r)
1	3614 19	4E	*Fe* II 14.87(5), *He* I 13.64(3)
1	3621 08	5En	*Fe* II 21.27(6), *Co* II 21.22(100)
3	3626 30	7Enn	[*Ni* II] 27.35?, *Fe* II 27.17(1)
3	3631 28	7En	*Cr* II 31.49(50), *Cr* II 31.72(40)
1	3633 86	6E	*He* I 34.24(2)
2	3639 30	5Enn	*Cr* I 39.80(100), *Ti* II 41.33v
1	3641 83	6En	*Ti* II 41.33(100)?
1	3650 37	6En	*Cr* II 50.37(40)
1	3653 29	1An	*Ti* I 53.50
2	3655 69	5En	*Zr* II 55.56(7)
2	3659 67	5E	[*Fe* II] 59.96, *Ti* II 59.77(60)
1	3661 27	5En	*Ti* II 62.24(40)
2	3665 29	5En	*H*28 64.68, *Cr* II 64.95(30)
2	3670 85	5En	[*Fe* II] 70.62, *H*25 69.47
1	3672 19	4En	*H*24 71.48
1	3674 93	5E	*H*23 73.76, *Zr* II 74.74(40)
3	3677 48	6En	*H*22 76.37, *Cr* II 77.86(50), *Cr* II 77.69(40), *Cr* II 77.93(30)
2	3679 94	5En	*H*21 79.36
1	3680 79	2An	*Ti* II 85.20(250), *H*19 86.83
2	3683 45	5En	*H*20 82.81
1	3685 12	6En	*Ti* II 85.20(250), *H*19 86.83v
2	3686 78	1An	*H*18 91.56
1	3687 70	5E	*H*19 86.83, *Mo* II 88.31(15)
2	3690 84	5En	*H*18 91.56
3	3692 73	3An	*H*17 97.15
2	3696 27	5En	*H*17 97.15
2	3697 29	6En	*H*17 97.15
3	3699 58	3An	*H*16 03.86
2	3702 82	5En	*Mo* II 02.55(8), *H*16 03.86v
3	3703 85	6En	*H*16 03.86
1	3706 10	5En	*H*16 03.86r, *Fe* I 05.57(100r)
3	3707 81	4An	*H*15 11.97
2	3709 51	5Enn	*H*15 11.97v, *Zr* II 09.27(60), [*Fe* II] 09.14
4	3712 42	7En	*H*15 11.97, [*Fe* II] 12.26, *Cr* II 12.97(35)
2	3715 09	6E	*H*15 11.97r, *Cr* II 15.19(20), *Cr* II 15.45(20)
3	3717 24	3An	*H*14 21.94, *Fe* I 19.93(250R)
3	3720 24	6E	*H*14 21.94v, *Fe* I 19.93(250R)
2	3722 22	7En	*H*14 21.94, *Fe* I 22.56(50r)
1	3725 34	5E	*H*14 21.94r
4	3726 80	6E	*Cr* II 27.37(40), [*O* II] 26.16(N)
1	3728 45	3Ann	*Fe* I 33.32(40r), *Co* I 32.40, *Fe* I 27.62(50r)
1	3730 13	4E	[*O* II] 28.91(N)
1	3730 61	4A	*H*13 34.37, *Fe* I 34.87(300r)
3	3732 30	5En	*H*13 34.37v, *He* I 32.86(1), *He* I 32.99(1)
2	3734 45	7En	*H*13 34.37, *Fe* I 34.87(300r)
2	3736 18	6E	*H*13 34.37r, [*Fe* II] 36.17, *Fe* I 37.13(150R)
2	3738 13	5En	*Cr* II 38.38(25)
2	3741 05	5E	*Ti* II 41.63(50)
1	3744 77	4E	*Fe* I 45.56(100R)
3	3745 27	3A	*H*12 50.15, *Fe* I 49.49(200R)
3	3748 34	6En	*Fe* II 48.49(8), *H*12 50.15v
3	3750 45	6En	*H*12 50.15
3	3752 87	5En	*H*12 50.15r
1	3754 49	1A	*Fe* I 58.24(150R), *Ti* II 59.29(200)
1	3755 31	5En	*Fe* II 59.46v, *Ti* II 59.29v
2	3757 20	6En	*Ti* II 57.68(30), *Fe* II 59.46v, *Ti* II 59.29v
4	3759 00	6En	*Fe* II 59.46(6), *Ti* II 59.29(200)
3	3762 14	6En	*Fe* II 62.89(5), *Ti* II 61.32(200)
3	3764 15	6En	*Fe* II 62.89r, *Ti* II 61.32r
3	3765 34	6Ann	*H*11 70.63
2	3766 82	5E	*Zr* II 66.83(25), *Fe* I 67.19(80r), *Ni* II 69.46v

TABLE 1—*Continued*

No. of Plates	λ Star	Int.	Identification
2	3767.46	3A	*H* 11 70.63, *Fe* I 67.19(80r)
3	3769.28	7En	*Ni* II 69.46(5), *H* 11 70.63v
1	3772.41	5En	*Ni* II 69.46r, *H* 11 70.63r
2	3773.83	5Enn	*H* 11 70.63r
1	3775.00	4E	*Ni* I 75.57(30r)
2	3779.38	5E	*Fe* II 83.35v
4	3783.02	6Enn	*Fe* II 83.35(4)
1	3785.96	5En	*Fe* II 83.35r
2	3788.15	5Enn	*Fe* II 83.35r, *Fe* I 87.88(50)
3	3790.56	5E	*H* 10 97.90v
3	3792.75	7A	*H* 10 97.90, *Mo* I 98.26(50R//)
1	3796.60	5Enn	*H* 10 97.90v
4	3798.12	6Enn	*H* 10 97.90
3	3800.63	5Enn	*H* 10 97.90r, *Cr* II 01.21(10)
3	3805.62	5E	*He* I 05.76(1)
3	3813.18	5En	*Fe* II 14.12(4)
1	3816.00	2An	*Fe* I 20.43(250R), *Fe* I 15.84(100r)
1	3816.44	4E	*Fe* I 15.84(100r), *Cr* I 16.17(40)
1	3817.64	4En	*Zr* II 17.59(12), *He* I 19.61v
2	3819.27	5En	*He* I 19.61(4), *Fe* I 20.43(250R)
1	3821.59	4E	*He* I 19.61r
1	3823.26	5E	*Fe* II 24.91v, *Zr* II 23.41(3)
4	3824.73	6E	*Fe* II 24.91(4)
2	3827.11	5E	*Fe* II 27.08(4)
2	3828.45	4Enn	*Fe* II 27.08r, *H* 9 35.39v
4	3829.85	10An	*H* 9 35.39, *Fe* I 34.23(100r)
2	3832.85	5En	*H* 9 35.39v
3	3835.59	7En	*H* 9 35.39
3	3838.38	6En	*H* 9 35.39r
1	3841.42	2An	*Fe* I 41.05(80r), *Co* I 45.47
2	3843.91	5En	
2	3845.15	5E	*Fe* II 45.18(Fe)
2	3847.23	5En	[*Fe* II] 47.78, *Ni* II 49.58v
4	3849.41	6E	*Ni* II 49.58(2), *Mg* II 50.40(6)
2	3852.02	4An	*Fe* I 56.37(50r), *Ni* I 58.30(40r)
1	3853.91	5E	*Si* II 53.66(3), *Cr* I 54.22(50)
3	3855.26	6En	*Si* II 56.02(8), *Zr* II 55.43(3), *Cr* I 55.57(30)
1	3860.00	5E	*Fe* II 60.92(3), *Fe* I 59.91(300R)
1	3865.31	5E	*Cr* II 65.59(75)
5	3868.37	6En	[*Ne* III] 68.74(N), *He* I 67.48(2)
3	3872.56	5En	[*Ne* III] 68.74r, *Fe* I 72.50(60)
1	3874.03	3An	*Fe* I 78.58(100r)
1	3875.98	4E	*C* II 76.19(8), *C* II 76.41(7), *C* II 76.67(6), *C* II 76.05(6)
4	3877.94	5Enn	*Fe* I 78.58(100r), *He* I 78.18(1)
3	3881.04	5En	*H* 8 89.05r, *Ni* II 81.92(1)
5	3883.33	10An	*H* 8 89.05, *Fe* I 86.28(40r)
1	3885.92	5En	*H* 8 89.05v
2	3887.61	6En	*H* 8 89.05v, *He* I 88.65(10)
6	3889.55	7En	*H* 8 89.05
1	3891.29	5En	*H* 8 89.05r
2	3894.95	1Ann	*Fe* I 99.71(30R)
3	3899.76	4En	*Ti* II 00.55(70), *Fe* I 99.71(30R)
1	3902.83	5E	*Fe* II 06.04v
3	3905.60	6En	*Fe* II 06.04(5), [*Fe* II] 05.62
2	3910.51	5E	*Cr* II 11.32(3), *Ti* II 13.46v, *Fe* II 14.48v
1	3912.37	5E	*Fe* II 14.48v, *Ti* II 13.46(60)
4	3913.98	6En	*Fe* II 14.48(2)
1	3916.41	5En	*Fe* II 14.48r
1	3919.08	5Enn	*Cr* I 19.16(100), *C* II 18.98(9), *C* II 20.68(10), *Fe* I 20.26(20r)
1	3923.45	4En	*Si* II 23.48(7), *Zr* II 23.92(1)
2	3925.43	5Enn	*He* I 26.53(1)
7	3927.70	20An	*Ca* II 33.66(400R)
4	3929.94	4En	*Ca* II 33.66v, *Fe* I 30.30(25R)
4	3931.72	4En	*Ca* II 33.66v, [*Fe* II] 31.44, [*Fe* II] 32.72
7	3933.21	5A	*Ca* II 33.66(400R)
5	3934.46	5E	*Ca* II 33.66(400R), *Zr* II 34.80(20)
5	3935.38	5Enn	*Fe* II 35.94(6), *He* I 35.91(1)
7	3937.98	6En	*Fe* II 38.97(4), *Fe* II 38.29(2), [*Fe* II] 37.80
2	3940.72	4En	*Fe* II 38.97r
6	3944.89	5E	*Cr* II 45.11(1)
1	3948.34	4En	*La* II 49.10(600//), [*Fe* II] 49.27
1	3952.77	4En	*La* II 49.10r, *Zr* II 55.82v
3	3955.58	5Enn	*Zr* II 55.82(P), *Zr* II 58.24v
1	3957.61	5En	*Zr* II 58.24(50), *Fe* II 60.90v
3	3960.53	5En	*Fe* II 60.90(3)
7	3962.61	15An	*Ca* II 68.47(350R)
3	3964.11	4En	*He* I 64.73(4), *Ca* II 68.47v
5	3966.60	5En	[*Ne* III] 67.51(N), *He* I 70.07v, *Ca* II 68.47v
4	3967.82	4A	*Ca* II 68.47(350R)
6	3969.24	6En	*Ca* II 68.47(350R), *He* I 70.07v
5	3971.29	7Enn	*He* I 70.07
6	3973.75	5En	*Fe* II 74.16(3), *He* I 70.07r
2	3974.59	5En	*Fe* II 75.03(2), *He* I 70.07r
3	3979.43	4En	[*Fe* II] 79.93, [*Fe* II] 79.78, *Cr* II 79.51(20)
3	3982.00	5En	*Zr* II 82.01(3)
1	3984.30	3En	*Zr* II 84.76(4)
1	3986.65	3E	[*Fe* II] 86.38
3	3989.18	5En	*Ni* II 93.3v
3	3992.65	6En	*Ni* II 93.3, [*Ni* II] 93.65
3	3996.82	4E	*Ni* II 93.3r
4	4002.23	4En	*Fe* II 02.55(3), *Fe* II 02.07(2), *Cr* II 03.33(25)
3	4005.80	5E	*Fe* II 02.55r
1	4009.06	4E	*He* I 09.27(1), *Cr* II 12.50v
3	4011.94	4E	*Cr* II 12.50(30), *Fe* II 12.47(1), *Ni* II 15.50v
2	4015.06	4En	*Ni* II 15,50(1), *Cr* II 12.50r
2	4018.05	3En	*Ni* II 15,50r
3	4021.01	6A	*Ni* II 25.5, *Fe* I 21.87
1	4022.51	4En	*Ni* II 25.5v, *Fe* II 24.55v
1	4024.44	5En	*Ni* II 25.5, *Fe* II 24.55(5)
4	4025.80	5En	*He* I 26.19(5), [*Ni* II] 25.80
1	4028.09	4E	*He* I 26.19r, *Si* II 28.74(7)
3	4032.87	4En	*Ni* II 33.2, *Fe* II 32.95(3), [*Ni* II] 33.56
1	4035.31	3En	*Ni* II 33.2r
2	4040.40	1Ann	*Fe* I 45.82(60r), *K* I 44.14(8R)
1	4043.15	3E	*Fe* I 45.82v, *Zr* II 45.63v
2	4045.14	4En	*Fe* I 45.82(60r), *Zr* II 45.63(15)
2	4053.64	4E	*Cr* II 54.11(8), *Fe* II 57.46v
1	4057.96	4E	*Fe* II 57.46(2), *Cr* II 54.11r
1	4060.12	2An	*Fe* I 63.60(45)
1	4063.16	4E	*Ni* II 67.05v
1	4066.78	5En	*Ni* II 67.05(3), [*S* II] 68.62v(N)
5	4068.24	6E	[*S* II] 68.62(N)
2	4071.62	4En	[*S* II] 68.62r(N)
3	4075.72	5E	[*S* II] 76.22(N)
1	4079.27	4En	[*S* II] 76.22r, [*Fe* II] 80.00
1	4081.43	4En	[*Fe* II] 83.78v
2	4083.41	5Enn	[*Fe* II] 83.78
2	4093.88	4Enn	*Hδ* 01.74v
4	4095.90	4An	*Hδ* 01.74
1	4097.14	4En	*Hδ* 01.74v
2	4098.50	4En	*Hδ* 01.74v
3	4099.76	5En	*Hδ* 01.74v
6	4102.00	7E	*Hδ* 01.74
3	4104.58	5En	*Hδ* 01.74r
2	4106.49	3En	*Hδ* 01.74r
4	4111.28	4E	*Cr* II 11.01(18), *Fe* II 11.90(1), [*Fe* II] 14.48v
5	4114.11	5E	[*Fe* II] 14.48
1	4115.45	3En	[*Fe* II] 14.48r
3	4119.80	4En	*He* I 20.81(3), *Fe* II 22.64v
4	4122.17	5En	*Fe* II 22.64(4)
3	4125.59	2Ann	*V* I 28.07
4	4128.06	5En	*Fe* II 28.74(3)
1	4132.43	4Enn	*Cr* II 32.41(7), *Fe* II 28.74r
1	4136.73	3En	*Cr* II 32.41r
2	4140.30	2An	*Fe* I 43.87(30), *Fe* I 39.94
4	4143.31	5Enn	*He* I 43.76(2), *Fe* I 43.87(30), [*Ni* II] 43.17
2	4146.16	4En	[*Fe* II] 46.65
1	4148.13	3En	*Zr* II 49.22(75)
4	4152.07	5En	*Fe* II 52.98(P)?
2	4156.77	4En	*Fe* II 52.98r, *Zr* II 56.24(15)
1	4161.30	4E	*Zr* II 61.20(20), *Ti* II 63.64v
4	4163.02	5Enn	*Ti* II 63.64(40), *Si* II 62.70(10)
1	4165.69	4E	*Ti* II 63.64r
2	4168.42	2An	*Fe* II 73.45(8)
1	4171.24	4E	*Fe* II 73.45v, *Ti* II 71.90(30), *Cr* II 71.92(3)
4	4173.07	7E	*Fe* II 73.45(8)
2	4176.49	5En	*Fe* II 73.45r, [*Fe* II] 77.21, *Fe* II 78.86v
5	4178.13	8En	*Fe* II 78.86(8), [*Fe* II] 78.95
1	4180.88	5En	*Fe* II 78.86r

TABLE 1—*Continued*

No. of Plates	λ Star	Int.	Identification
3	4182 93	5En	*Fe* II 78.86r, *V* II 83.44(250)
2	4188 37	4En	[*Fe* II] 90.53v
2	4190 54	5En	[*Fe* II] 90.53
2	4193 21	4E	[*Fe* II] 90.53r
2	4198 89	5En	*Ni* II 01.4v, [*Ni* II] 01.74v
4	4200 59	6Enn	*Ni* II 01.4, [*Ni* II] 01.74
2	4202 67	5Enn	*Ni* II 01.4r, [*Ni* II] 01.74r
2	4205 16	5En	*Ni* II 01.4r, [*Ni* II] 01.74r
1	4210 64	4E	*Zr* II 10.62(5)
1	4215 08	4E	*Sr* II 15.52(300r)
1	4217 64	5Enn	*La* II 17.56(200)
1	4219 87	2Ann	*Ca* I 26.73(500R)
2	4221 09	4En	*Cr* II 24.85v
5	4224 75	5En	*Cr* II 24.85(20)
2	4226 52	2An	*Ca* I 26.73(500R), *Fe* II 33.17(11)
3	4228 28	5En	*Fe* II 33.17v, *Cr* II 24.85r
2	4230 15	5Enn	*Fe* II 33.17v
6	4232 80	8Enn	*Fe* II 33.17(11)
2	4235 92	5En	*Fe* II 33.17r
2	4240 12	6En	[*Fe* II] 43.98v, [*Fe* II] 44.81v
5	4243 75	9En	[*Fe* II] 43.98, [*Fe* II] 44.81
2	4246 67	6E	[*Fe* II] 43.98r, [*Fe* II] 44.81r
2	4248 98	5E	[*Ni* II] 49.48, [*Fe* II] 49.07, [*Fe* II] 43.98r
1	4253 63	1An	*Fe* II 58.16(3), *Fe* I 60.48, *Cr* I 54.35
2	4258 02	6En	*Fe* II 58.16(3)
5	4261 90	5E	*Cr* II 61.92(20), *Fe* II 58.16r
1	4265 88	4E	*Cr* II 61.92r, [*Fe* II] 66.34
1	4267 34	2An	*Fe* I 71.76
1	4268 68	4E	*Cr* II 69.28(10), [*Fe* II] 68.67
1	4270 53	4E	[*Fe* II] 70.62
3	4273 18	6E	[*Fe* II] 76.83v, *Fe* II 73.32(3)
5	4276 63	8En	[*Fe* II] 76.83
2	4279 08	5Enn	[*Fe* II] 76.83r
3	4283 34	6En	[*Fe* II] 87.40v
4	4287 02	10En	[*Fe* II] 87.40
2	4289 07	6Enn	[*Fe* II] 87.40r, *Ti* II 90.22(50)
4	4293 16	5E	*Fe* II 96.57v, *Ni* II 94.3, *Ti* II 94.10(40)
2	4294 45	5A	*Ti* II 00.05(60)
4	4296 41	6En	*Fe* II 96.57(6), *La* II 96.05(300)
2	4299 29	5E	*Ti* II 00.05(60), *Fe* II 96.57r, *Fe* II 03.17v
4	4302 49	6En	*Fe* II 03.17(8)
4	4305 59	6En	[*Fe* II] 05.90
1	4307 69	4En	[*Fe* II] 05.90r
2	4309 60	3An	*Ti* II 14.98(40), *Fe* I 07.91
4	4313 95	5En	*Fe* II 14.29(4)
4	4319 29	7En	[*Fe* II] 19.62, *Fe* II 19.72(1)
1	4322 64	2An	*Fe* I 25.77, *Sc* II 25.00
5	4325 45	5En	[*Ni* II] 26.85, *Fe* I 25.77(35)
4	4330 06	4En	
3	4333 11	6An	*Hγ* 40.47
4	4338 28	7En	*Hγ* 40.47v
4	4340 76	9En	*Hγ* 40.47
4	4342 58	7Enn	*Hγ* 40.47r
4	4346 29	6En	[*Fe* II] 46.85, [*Fe* II] 47.35
5	4351 56	8En	*Fe* II 51.76(9), [*Fe* II] 52.78
3	4354 94	7En	[*Fe* II] 59.34v–58.37v, *Fe* II 51.76r, [*Fe* II] 52.78r
5	4358 35	10En	[*Fe* II] 59.34, [*Fe* II] 58.37
1	4361 71	6En	[*Fe* II] 59.34r–58.37r
1	4364 26	6Enn	[*O* III] 63.21(N), *Mo* II 63.64(10), *La* II 64.66(100), double?
2	4366 68	2An	*Cr* I 71.28
3	4368 75	5En	*Fe* II 69.40(3), [*Fe* II] 72.43v
5	4371 95	6En	[*Fe* II] 72.43
1	4374 82	5E	[*Fe* II] 72.43r
1	4377 55	5En	*Mo* II 77.77(10)
4	4382 05	5En	[*Fe* II] 82.75, *Fe* II 85.38v
4	4384 69	6En	*Fe* II 85.38(7)
1	4387 58	5E	*He* I 87.93(3), *Fe* II 85.38r
1	4391 42	4En	*S* II 91.84(3), *Ti* II 95.04v
3	4394 09	5En	*Ti* II 95.04(60)
4	4399 41	5En	*Ti* II 99.77(35)
2	4403 12	4En	*Fe* II 02.87(2), *Zr* II 03.35(6)
2	4406 66	4An	*V* I 06.65
3	4409 80	5E	[*Fe* II] 13.78v, [*Fe* II] 09.86
2	4413 20	9En	[*Fe* II] 13.78, [*Fe* II] 14.45
3	4415 92	9En	[*Fe* II] 16.27, *Fe* II 16.82(7)
1	4422 21	4E	*Na* I 23.31(4n)
2	4426 41	4E	*La* II 27.52(100)
3	4429 17	4Enn	*La* II 29.90(200), [*Fe* II] 32.45v
3	4432 41	5En	[*Fe* II] 32.45
3	4442 18	4Enn	*Zr* II 42.99(25)
1	4443 59	5E	*Ti* II 43.80(50), *Fe* II 44.56(1)
1	4445 05	3A	*Fe* I 47.72(9)
3	4447 85	5En	[*Fe* II] 52.11v, *Fe* II 51.55v
4	4451 53	7En	[*Fe* II] 52.11, *Fe* II 51.55(4)
2	4455 35	5En	[*Fe* II] 52.11r, [*Fe* II] 57.95v, *Fe* II 55.26(3)
4	4457 40	7En	[*Fe* II] 57.95
2	4461 00	4En	[*Fe* II] 57.95r, [*Ni* II] 61.54
1	4463 85	4En	*S* II 63.58(7), *S* II 64.43(6)
2	4465 60	2An	*Ti* II 68.49(50), *Fe* I 66.56
2	4467 18	4En	*He* I 71.48v, [*Fe* II] 70.29v
3	4470 36	6Enn	*He* I 71.48(6), [*Fe* II] 70.29
2	4472 59	4Enn	*He* I 71.48r, *Fe* II 72.92(2), [*Fe* II] 74.91v
3	4474 20	6En	[*Fe* II] 74.91
3	4480 00	4Enn	*Fe* II 80.69(1)
2	4484 85	4Enn	*Fe* II 89.19v, [*Ni* II] 85.87, *Ni* II 85.4
3	4488 48	6E	*Fe* II 89.19(4), [*Fe* II] 88.75
2	4491 20	6En	*Fe* II 91.40(5)
2	4499 68	5Enn	*Cr* I 00.29(40)
1	4502 79	2An	*Fe* II 08.28(8)
4	4508 05	6En	*Fe* II 08.28(8)
1	4511 47	4En	*Fe* II 08.28r, *Fe* II 15.34v, *Cr* I 11.90(60)
4	4514 79	6En	*Fe* II 15.34(7), [*Fe* II] 14.90
4	4519 73	6E	*Fe* II 20.23(7)
4	4522 15	6E	*Fe* II 22.63(9), *La* II 22.37(400)
4	4527 72	5Enn	[*Fe* II] 28.39
4	4533 47	5Enn	*Fe* II 34.17(2), [*Fe* II] 33.00, *Ti* II 33.97(30)
4	4541 15	4E	*Fe* II 41.52(4), *Fe* II 49.47v
4	4549 06	7En	*Fe* II 49.47(10), *Fe* II 49.21(4), *Ti* II 49.62(60n)
1	4552 93	4En	*Fe* II 49.47r, *Fe* II 55.89v, *Ba* II 54.03(1000R)
4	4555 26	7E	*Fe* II 55.89(8)
3	4558 58	5En	*Cr* II 58.66(100), *Fe* II 55.89r
4	4563 01	4Enn	*Ti* II 63.76(30)
4	4570 34	5En	*Cr* I 71.10(25), *Cr* I 70.98(20), *Mg* I 71.10
1	4571 70	5En	*Ti* II 71.97(50n)
4	4575 97	5E	*Fe* II 76.33(4)
3	4579 90	5Enn	*Fe* II 83.83v, *Fe* II 80.06(1)
4	4583.32	8En	*Fe* II 83.83(11)
1	4586 18	4En	*Fe* II 83.83r
3	4587 64	4En	*Cr* II 88.22(75)
1	4592 07	4En	*Cr* II 92.09(20), *Cr* II 88.22r
2	4595 19	4En	*Cr* I 95.59(45)
1	4605 25	3E	*La* II 05.78(100)
1	4610 91	3E	*Cr* II 16.64v
1	4614 23	1An	*Fe* II 20.51(3), *Cr* II 18.83(35)
2	4616 22	4E	*Cr* II 16.64(18)
2	4618 50	4En	*Cr* II 18.83(35), *Fe* II 20.51v
3	4620 34	5En	*Fe* II 20.51(3)
2	4622 52	4En	*Fe* II 20.51r
1	4624 48	3E	*Fe* II 20.51r, *Fe* II 25.91(1)
4	4628 85	7En	*Fe* II 29.34(7)
3	4634 30	5Enn	*Fe* II 35.33(5), *Cr* II 34.11(25)
4	4639 42	6E	[*Fe* II] 39.68, *O* II 38.85(6)
1	4646 80	3En	*La* II 47.50(100)
2	4653 18	4E	*Fe* II 58.03v
4	4657 30	5En	*Fe* II 58.03, *Fe* II 56.97(1)
2	4660 74	3E	*Fe* II 58.03r
3	4662 45	3E	*La* II 62.51(200), *Cr* I 63.33(40), *O* II 61.64(9)
2	4664 18	4En	[*Fe* II] 64.45, *Na* I 64.81(3r), [*Fe* II] 64.97
4	4666 45	4E	*Fe* II 66.75(2)
4	4669 18	3Enn	*Fe* II 66.75r, *Fe* II 70.17(0), *La* II 68.91(250)
1	4670 89	3Enn	*La* II 71.82(200)
1	4676 43	3E	*O* II 76.23(8)
1	4678 74	4E	
1	4684 86	4Enn	*Zr* II 85.19(4)
1	4696 99	4En	*Cr* I 97.06(40), *Cr* II 97.62(2)
2	4701 38	4Enn	*Mg* I 02.98(40), *Ni* I 01.54, [*Fe* III] 01.54

TABLE 1—*Continued*

No. of Plates	λ Star	Int.	Identification
2	4712.40	4Enn	*He* I 13.14(3)
1	4716.49	4E	[*Fe* II] 16.36, *S* II 16.23(8)
1	4722.93	4En	[*Fe* II] 28.07v
2	4725.26	5En	[*Fe* II] 28.07v
4	4727.53	6E	[*Fe* II] 28.07
4	4731.14	5En	*Fe* II 31.49(3), [*Fe* II] 28.07r
3	4745.61	4En	[*Fe* II] 45.49
2	4746.73	4E	*Na* I 47.94(3n)
1	4749.40	3E	[*Fe* II] 50.57
1	4751.75	4E	*Cr* I 52.08(50)
2	4763.80	4Enn	*Cr* I 64.29(50)
2	4770.45	4Enn	[*Fe* II] 74.74v
4	4774.24	5En	[*Fe* II] 74.74
1	4778.94	4E	[*Fe* II] 74.74r, *S* II 79.11(2)
1	4782.98	3En	*Cr* I 83.06(15W)
2	4785.70	3En	*Ni* I 86.54(15)
1	4789.88	3E	*Cr* I 90.34(20)
1	4792.05	4En	*Au* I 92.63(100)
3	4798.01	3Enn	[*Fe* II] 98.28
2	4801.58	3E	
3	4803.78	3En	*La* II 04.04(80)
2	4806.63	3A	*Co* I 13.48(20), *Ni* I 07.00, *Zn* I 10.53
1	4808.66	3E	*La* II 09.00(100)
1	4809.98	5En	[*Fe* II] 14.55v, *Fe* II 10.76(0)
4	4814.04	6En	[*Fe* II] 14.55
1	4816.94	4En	[*Fe* II] 14.55r
1	4818.32	3E	[*Fe* II] 14.55r
2	4820.54	3En	*Cr* II 24.13v
3	4823.90	4En	*Cr* II 24.13(75), *La* II 24.05(100)
2	4828.14	3E	*Cr* II 24.13r
2	4832.76	3Enn	*Cr* II 36.22v
2	4835.86	4E	*Cr* II 36.22(25)
1	4839.20	3E	*Cr* II 36.22r, *Ti* II 39.25(1)
2	4841.92	3En	*Cr* II 36.22r
3	4847.74	4En	*Cr* II 48.24(60)
2	4852.12	4E	[*Fe* II] 52.73
1	4853.08	5An	*Hβ* 61.33
2	4858.70	7Enn	*Hβ* 61.33
6	4861.67	9En	*Hβ* 61.33
1	4868.81	4En	*Hβ* 61.33, [*Fe* II] 69.3
2	4872.62	5Enn	[*Fe* II] 74.49v, *Hβ* 61.33
5	4874.44	5E	[*Fe* II] 74.49, *Cr* II 76.41v
3	4876.07	4Enn	*Cr* II 76.41(50), [*Fe* II] 74.49r
1	4877.71	3E	*Cr* II 76.41r, *Hβ* 61.33
1	4884.02	3E	*Cr* II 84.37(10)
2	4885.55	5En	*S* II 85.63(2), [*Fe* II] 89.63v
6	4889.22	6En	[*Fe* II] 89.63
2	4892.41	4E	[*Fe* II] 89.63r, *Fe* II 93.78(0)
3	4898.00	3En	
2	4902.40	4En	[*Fe* II] 05.35v
5	4904.80	5En	[*Fe* II] 05.35
3	4908.10	4En	[*Fe* II] 05.35r
3	4909.08	4En	[*Fe* II] 05.35r
3	4910.79	3En	*Cr* II 12.49v, *Fe* II 13.37v
2	4912.44	4Enn	*Cr* II 12.49(12), *Fe* II 13.37(1)
2	4916.90	5An	*Fe* II 23.92(12), *Fe* I 20.51(60)
2	4918.26	4En	*Fe* II 23.92v
2	4920.16	5E	*Fe* II 23.92v
5	4923.48	7En	*Fe* II 23.92(12)
2	4926.30	5En	*Fe* II 23.92r
2	4929.04	4En	*Fe* II 23.92r
1	4936.30	3Enn	*Cr* I 36.33(150)
1	4943.85	3En	[*Fe* II] 47.38v
3	4946.70	4En	[*Fe* II] 47.38
3	4950.12	4En	[*Fe* II] 50.74
1	4956.74	3En	*Fe* I 57.60(60), *Fe* I 57.30(20)
3	4973.09	4En	[*Fe* II] 73.39
1	4978.92	2En	*Na* I 78.54(5r), [*Fe* II] 73.39r
1	4987.13	2E	[*Ti* II] 87.68, *Fe* II 93.36v
2	4992.35	3En	*Fe* II 93.36(1)
2	5000.82	3En	[*Fe* II] 05.52v
2	5004.46	4En	[*Fe* II] 05.52
4	5005.70	3En	[*Fe* II] 06.65
2	5009.09	5An	*Fe* II 18.43(12), *Ti* I 14.25
3	5013.65	5En	*Fe* II 18.43v
4	5018.07	8En	*Fe* II 18.43(12)
1	5022.17	4E	*Fe* II 18.43r
2	5024.59	5En	*Fe* II 18.43r
1	5030.60	3En	*Fe* II 30.74(3)
2	5035.15	3En	[*Fe* II] 35.50, *Fe* II 35.77(3)
1	5040.45	2E	[*Fe* II] 43.53v, *Si* II 41.06(8)
2	5043.13	3E	[*Fe* II] 43.53
1	5045.37	2E	*N* II 45.10(8), [*Fe* II] 43.53r
1	5047.34	2E	*He* I 47.74(2), [*Ti* II] 47.91
1	5053.71	3En	
2	5058.55	3Enn	
2	5064.54	2E	[*Ti* II] 65.43
1	5069.78	2En	*Fe* II 70.96(2), [*Fe* II] 72.40v
2	5072.19	3E	[*Fe* II] 72.40
1	5074.36	2En	[*Fe* II] 72.40r, *Fe* II 74.06(1)
1	5075.71	2E	*Fe* II 75.83(1), [*Fe* II] 76.57
2	5078.29	3En	*Cr* I 78.71(40)
1	5082.62	3E	[*Fe* II] 83.72
1	5087.08	3En	*Fe* II 87.25(3)
1	5095.98	2En	*Cr* II 97.29(15)
2	5100.30	3Enn	*Fe* II 00.84(4n), *Fe* II 00.95(15n)
1	5104.20	2En	[*Fe* II] 07.95v
3	5107.37	4En	[*Fe* II] 07.95
3	5111.05	4En	[*Fe* II] 11.63
1	5115.01	3En	[*Fe* II] 11.63r, *Cr* II 16.06(2)
1	5124.77	2En	*Zr* II 24.98(2)
2	5128.99	2En	
2	5132.79	3E	
1	5136.73	2En	*Cr* II 37.09(7), *Fe* II 36.79(tr)
1	5141.48	3En	
2	5145.38	3En	*Fe* II 46.12(P)
2	5153.96	5En	*Fe* II 58.81v
3	5158.47	7En	[*Fe* II] 58.81, [*Fe* II] 58.00
4	5162.12	4En	[*Fe* II] 58.81r
3	5163.92	5En	[*Fe* II] 58.81r, [*Fe* II] 63.94, *Fe* II 69.03v
1	5166.01	4En	*Fe* II 69.03v
3	5168.49	7Enn	*Fe* II 69.03(12)
1	5171.16	4En	*Fe* II 69.03r
1	5174.49	3E	*Fe* II 69.03r
1	5175.93	2En	[*Fe* II] 81.97v
2	5181.52	4En	[*Fe* II] 81.97
2	5183.37	3E	*Mg* I 83.60(125), *La* II 83.42(400), *Cr* I 84.59(100)
1	5186.08	3En	*La* II 88.21(500)?
1	5193.51	2E	*Fe* II 97.57v
3	5197.16	5E	*Fe* II 97.57(6)
1	5202.95	2En	*Fe* II 97.57r, *La* II 04.14(300)
1	5208.33	3An	*Cr* I 08.44(500R)
1	5210.92	2En	*Cr* II 10.87(7), *Ti* II 11.54
1	5215.50	3En	[*Fe* II] 20.06v
3	5219.76	4En	[*Fe* II] 20.06
2	5222.49	3En	[*Fe* II] 20.06r
2	5225.78	3En	[*Fe* II] 20.06r
2	5230.79	3En	*Fe* II 34.62v
3	5234.14	5E	*Fe* II 34.62(7)
1	5238.85	3En	*Fe* II 34.62r, *Cr* I 38.97(65)
1	5249.19	2E	*Cr* II 49.40(10)
2	5255.07	3En	[*Fe* II] 61.62v, *Cr* I 54.92(100), *Cr* I 55.13(125)
1	5258.25	4En	[*Fe* II] 61.62v
3	5260.98	6En	[*Fe* II] 61.62
2	5264.38	4E	*Fe* II 64.80(2), [*Fe* II] 61.62r
2	5267.50	4En	[*Fe* II] 61.62r, [*Fe* II] 73.38v
3	5268.76	4En	[*Fe* II] 68.88, [*Ni* II] 69.16, [*Fe* II] 73.38r
2	5272.51	6E	[*Fe* II] 73.38
2	5275.44	6E	*Fe* II 75.99(7), [*Ni* II] 75.83
3	5283.07	4En	*Fe* II 84.09(3), [*Fe* II] 83.11
3	5296.22	4En	[*Fe* II] 96.84
1	5302.85	3En	*Cr* II 05.85v, *Fe* II 03.42(0)
1	5306.36	3Enn	*Cr* II 05.85(25)
1	5307.62	3An	*Fe* II 16.61(8), *Fe* I 07.36(2), *Cr* II 13.59
2	5310.60	3E	*Fe* II 16.61v
1	5312.08	3E	*Fe* II 16.61v, *Cr* I 12.88(50)
3	5316.02	6E	*Fe* II 16.61(8), *Fe* II 16.78(4)
1	5322.56	3E	*Fe* II 16.61r
1	5323.71	4E	*Fe* I 24.19(30)
3	5333.14	5En	[*Fe* II] 33.65
1	5337.42	3En	*Fe* II 37.71(0), [*Fe* II] 33.65r
2	5346.89	4En	[*Fe* II] 47.67, *Fe* II 46.56(1)
1	5357.16	2En	*Fe* II 62.86v
3	5362.47	4En	*Fe* II 62.86(5)
1	5370.21	2Enn	[*Fe* II] 76.47v
1	5373.56	3En	[*Fe* II] 76.47v
4	5375.92	5En	[*Fe* II] 76.47
1	5381.30	2Enn	[*Fe* II] 76.47r

TABLE 1—*Continued*

No. of Plates	λ Star	Int.	Identification
2	5386.33	2Enn	*Fe* II 87.14(2)
2	5390.07	3En	
2	5396.11	2Enn	*Ti* II 96.3(1), *Ti* II 96.59(P)
2	5407.90	2Enn	*Cr* II 07.62(10), *Fe* II 08.84(1)
3	5410.23	3En	[*Fe* II] 12.64v
1	5412.25	4Enn	[*Fe* II] 12.64, [*Fe* II] 13.34
3	5415.02	2En	[*Fe* II] 12.64r
1	5417.68	2E	[*Fe* II] 12.64r
2	5424.99	3E	*Fe* II 25.27(2)
4	5427.85	2En	*Fe* II 27.83(u), [*Fe* II] 33.15v
3	5429.48	2E	[*Fe* II] 33.15v
1	5432.76	4En	[*Fe* II] 33.15
4	5437.83	2En	[*Fe* II] 33.15r
2	5440.50	2Enn	[*Fe* II] 40.45
2	5446.70	2En	*Fe* I 46.92(40)
1	5454.29	2E	*S* II 53.81(15)
2	5455.71	2An	*Fe* I 55.61(40), Atm. 5637?
1	5457.55	3En	
2	5473.32	2En	*S* II 73.59(15)
1	5477.37	3Enn	*Cr* II 78.35(15), [*Fe* II] 77.25
4	5483.10	2En	*Cr* II 78.35r
2	5492.19	2Enn	[*Fe* II] 95.82v
3	5495.76	3En	[*Fe* II] 95.82
1	5497.37	1E	*Fe* I 97.52(15)
2	5500.75	2En	*Cr* II 02.05(12)
1	5508.97	2E	*Cr* II 08.60(8), *S* II 09.67(15)
1	5518.00	3A	*Sc* II 26.81(75)
2	5522.63	2En	[*Fe* II] 27.33v, [*Fe* II] 23.28
2	5524.16	3E	[*Fe* II] 27.33v
4	5526.90	5Enn	[*Fe* II] 27.33, [*Fe* II] 27.61
2	5531.73	3En	[*Fe* II] 27.33r, *Fe* II 34.86v
3	5532.11	2A	*Ba* I 35.55
1	5534.42	4E	*Fe* II 34.86(4)
4	5539.70	2En	*Fe* II 34.86r
2	5551.29	3En	[*Fe* II] 51.31
3	5555.89	3En	[*Fe* II] 56.31
3	5562.52	2En	[*Fe* II] 56.31r
1	5564.30	2En	*S* II 64.94(8), *Fe* II 67.82v
2	5567.68	2En	*Fe* II 67.82(10)
1	5572.23	2En	*Fe* II 67.82r, *Fe* I 72.85(30)
1	5576.00	2En	[*Fe* II] 80.82v
1	5579.25	3Enn	[*Fe* II] 80.82, [*Cr* II] 79.06
1	5581.97	3E	[*Fe* II] 82.01
2	5584.53	2E	[*Fe* II] 82.01r
1	5586.04	2En	[*Fe* II] 82.01r
1	5605.94	1En	*S* II 06.11(15)
2	5608.86	1En	*S* II 06.11r, *Cr* I 09.19(35)
2	5613.14	2E	
2	5617.16	1En	
2	5622.64	2En	
1	5628.51	2En	*Cr* I 28.64(50)
1	5638.69	2En	*S* II 39.96(10), *S* II 40.32(10)
3	5643.76	2En	[*Fe* II] 44.00
2	5646.73	2E	[*Fe* II] 46.59, *S* II 46.98(8)
2	5649.81	2En	[*Fe* II] 50.39, [*Fe* II] 50.94
2	5653.85	3En	[*Fe* II] 54.85
2	5656.98	2E	[*Fe* II] 65.85r
3	5659.05	2E	[*Fe* II] 59.83
2	5661.04	2En	
4	5666.59	1En	
2	5668.84	2En	
1	5672.70	3En	
3	5675.56	2F	*N* II 76.02(6)
3	5678.48	2En	*Cr* II 78.42(10), *N* II 79.56(10)
1	5680.17	2En	*Na* I 88.20(10), *N* II 86.21(6)
2	5694.86	3En	*Cr* I 94.73(75), *Ni* I 95.00(6)
4	5707.20	2En	*Si* I 08.44 (75)
3	5711.98	1En	[*Fe* II] 13.35, *Cr* I 12.78(100)
2	5714.32	1E	*Ni* I 15.09(6)
2	5718.22	1En	*Cr* I 19.82(40)?
1	5721.49	1En	[*Fe* II] 21.35
1	5743.60	3En	[*Fe* II] 46.96v
2	5745.05	3Enn	[*Fe* II] 45.70, [*Fe* II] 46.96v
2	5746.77	4Enn	*N* II 47.29(4), [*Fe* II] 46.96
4	5748.43	3En	[*Fe* II] 46.96r, [*N* II] 54.8v
1	5753.99	5En	[*N* II] 54.8(N), [*Fe* II] 53.83
6	5757.32	3En	[*N* II] 54.8r
3	5758.50	2En	[*N* II] 54.8r
3	5775.10	1En	
1	5785.16	2En	*Fe* II 85.0(5N)
1	5808.12	1En	[*Fe* II] 09.43
1	5814.26	1En	*Ti* II 14.62(P)
2	5824.64	1En	
1	5831.02	1E	*Fe* II 35.61v
3	5833.10	2En	*Fe* II 35.61v
4	5835.11	3Enn	*Fe* II 35.61(3n)
2	5838.70	1En	*Fe* II 35.61r
2	5842.79	2E	[*Fe* II] 43.90
1	5844.30	1En	*Cr* I 44.61(40)
1	5865.96	2E	[*Fe* I] 67.17
2	5868.40	2E	*He* I 75.62v
2	5869.68	2E	*He* I 75.62v
1	5871.38	3En	*He* I 75.62v
3	5872.57	3Enn	*He* I 75.62v
6	5874.91	6E	*He* I 75.62(10)
3	5878.88	3Enn	*He* I 75.62r
5	5881.47	10An	*Na* I 89.95(10R), *Fe* II 91.36(8)
3	5886.23	2E	*Fe* II 91.36v, *Na* I 89.95v
2	5889.15	2En	*Na* I 89.95(10R), *Fe* II 91.36v
5	5889.71	3An	*Na* I 89.95(10R), *Na* I 95.92(9R)
3	5891.24	4Enn	*Fe* II 91.36(8)
5	5893.80	4Enn	*Fe* II 91.36r, *Na* I 89.95r
1	5894.65	1A	*Na* I 95.92(9R)
1	5895.35	2En	*Na* I 95.92(9R)
5	5897.86	2E	*Fe* II 91.36r, *Na* I 95.92r
4	5900.90	1E	[*Fe* II] 01.26
2	5902.20	2Enn	[*Fe* I] 02.64
1	5903.47	1En	*Fe* II 03.6(8)
1	5908.94	1En	*Fe* II 09.38(P), *Fe* II 03.6r
2	5913.13	2En	
1	5916.28	1E	*Cr* I 16.73(30)
1	5917.94	1E	
2	5922.70	1En	
2	5928.53	1En	[*Zr* II] 29.20
2	5932.77	2En	[*Zr* II] 32.88, *S* II 32.95(1)
2	5942.47	1En	*N* II 41.67(8)?
2	5944.96	1E	
2	5951.05	1En	*S* II 51.30(3)
2	5952.47	1En	*N* II 52.39(3)
2	5956.00	1E	*Si* II 57.61(5), *Fe* II 56.5(4)
1	5964.18	0En	
1	5966.96	0En	
1	5980.55	1En	*Ba* II 81.25(8)
2	5983.77	1En	
2	5985.26	0E	*Fe* II 91.38v
3	5986.92	1E	*Fe* II 91.38v
5	5991.11	3En	*Fe* II 91.38(10)
3	5994.60	1En	*Fe* II 91.38r
4	5999.00	1En	*Ba* II 99.85(3), [*Fe* I] 99.99
3	6007.91	1Enn	[*Ni* II] 07.34
1	6015.45	1En	[*Zr* II] 15.26
3	6039.95	1Enn	*Fe* II 45.50v
5	6044.10	2En	*Fe* II 45.50(6)
2	6049.01	0E	*Fe* II 45.50r
1	6052.78	0En	*Cr* II 53.48(10)
1	6068.36	0Enn	*Cr* II 68.00(7), *Cr* II 69.69(1)
1	6080.16	0En	*Cr* II 81.51(3), *Fe* II 84.11v
5	6083.66	2En	*Fe* II 84.11(5)
2	6089.37	1E	*Cr* II 89.69(15), *Fe* II 84.11r
1	6092.09	1En	*S* II 92.13(2), *Cr* II 89.69r
1	6094.42	0En	[*Ti* II] 95.96, *Cr* II 89.69r
2	6096.70	0En	*Fe* II 03.54v
1	6099.83	0E	*Fe* II 03.54v
2	6102.47	1Enn	*Fe* II 03.54(8)
1	6104.92	0E	*Fe* II 03.54r
2	6113.05	1E	*Fe* II 13.33(2)
1	6123.10	1En	[*Ti* II] 24.57, *S* II 23.41(1)
1	6129.48	0Enn	*Cr* II 29.23(7)
1	6133.75	1Enn	
2	6138.80	0En	*Cr* II 38.77(2)
2	6142.07	0En	*Ba* II 41.72(600r)
1	6144.53	1En	*Fe* II 47.74v, *Fe* II 49.24v
2	6147.28	3E	*Fe* II 47.74(30?)
2	6148.74	2Enn	*Fe* II 49.24(20)
2	6151.84	1En	*Fe* II 47.74r
2	6153.53	1En	*Na* I 5422(8r), *Fe* II 49.24r
2	6156.12	0Enn	*Fe* II 49.24r
4	6159.45	2En	*Na* I 60.75(8r)
2	6164.97	1En	*Na* I 60.75r, [*Zr* II] 65.35
1	6166.39	1En	
1	6178.68	1En	*Fe* II 79.38(5), *Cr* II 79.17(10)
1	6180.26	0E	*Fe* II 79.38r
2	6185.37	1En	[*Fe* II] 88.55v
4	6188.45	2Enn	[*Fe* II] 88.55

TABLE 1—*Continued*

No. of Plates	λ Star	Int.	Identification	No. of Plates	λ Star	Int.	Identification
1	6190.84	1En	[*Fe* II] 88.55r	2	6439.39	1En	[*Fe* II] 40.40
1	6193.70	0E	*Cr* II 95.18(3), [*Fe* II] 88.55r	1	6443.05	1En	*Fe* II 42.97(6)
2	6197.70	1En	*Fe* II 99.16(2)	6	6456.03	4E	*Fe* II 56.38(200)
1	6212.58	0En	*Ti* II 12.30(1)	2	6473.31	1E	[*Fe* II] 73.86
2	6218.80	1E	*Fe* II 19.35(P), *Fe* II 19.54(P)	3	6482.92	1Enn	
2	6228.00	0En	*Fe* II 29.34(P)	2	6492.73	2En	*Fe* II 93.05(8)
1	6232.42	1E	*Fe* II 38.38v, *Fe* II 33.52(3)	2	6501.85	1En	
5	6238.14	2En	*Fe* II 38.38(20)	2	6505.71	1Enn	*Fe* II 06.33(5)
1	6241.20	0En	*Fe* II 38.38r	1	6509.38	1Enn	*Fe* II 16.05v
4	6243.38	1E	*Fe* II 47.56v	6	6515.95	3En	*Fe* II 16.05(20), *Fe* II 17.01(5)
5	6247.29	3En	*Fe* II 47.56(80), *Fe* II 48.92(4)	1	6518.69	1En	*Fe* II 16.05r
4	6250.55	1E	*Fe* II 47.56r	2	6531.66	2En	*Ni* I 32.89(3)
3	6232.99	0E	*Fe* II 47.56r	1	6537.17	3En	*Cr* I 37.92(20), *Hα* 62.82
2	6254.37	1E		2	6539.39	3E	*Hα* 62.82
2	6256.06	1En		2	6541.76	4En	*Hα* 62.82
2	6261.44	1E	*La* II 62.30(300)	2	6543.61	4En	*Hα* 62.82
2	6265.09	0En		1	6545.32	4E	*Fe* I 46.25(200)
3	6269.28	1En		4	6547.81	5En	[*N* II] 48.1(N)
2	6271.20	1E	*Cr* II 71.83(5)	1	6552.13	2Ann	*Hα* 62.82
3	6274.68	1E	*Cr* II 74.94(1), *S* II 74.34(3)	1	6558.13	9E	[*Fe* II] 58.51, *Hα* 6282
1	6280.68	0En		9	6560.20	11En	*Hα* 62.82
1	6284.23	0En	*S* II 86.35(8)?	4	6561.48	3A	*Hα* 62.82
1	6291.49	0En		9	6563.26	13En	*Hα* 62.82
1	6296.95	1En	*La* II 96.08(300)?	2	6566.60	9E	*Hα* 62.82
4	6299.96	1En	[*O* I] 00.23(L)	2	6576.95	6Enn	*C* II 78.03(10), *Hα* 62.82
1	6302.52	1E		4	6582.87	7Enn	[*N* II] 83.6(N)
2	6304.53	1E	*Fe* II 05.32(15), *S* II 05.51(10)	1	6585.86	4E	*Hα* 62.82, *Fe* II 86.69(5), Max. Nubecula *k*
3	6311.70	2En	*S* II 12.68(10)	1	6587.95	4Enn	*Hα* 62.82
1	6314.27	1E	*S* II 12.68r, *Mg* I 18.23v	2	6591.27	3Enn	*Hα* 62.82
5	6317.39	3En	*Mg* I 18.23(5), *Mg* I 18.75(5), *Fe* II 17.98	1	6594.89	2En	*Hα* 62.82
2	6320.68	1En	*Mg* I 18.23r	3	6597.75	2En	*Cr* I 97.56(40), *Hα* 62.82
1	6325.72	0E	*Fe* II 31.97v	1	6626.22	2En	*Fe* II 27.28(5)
4	6331.91	1En	*Fe* II 31.97(12)	1	6649.63	1E	[*Ti* II] 50.61
2	6337.52	0En	*Fe* II 31.97r	1	6659.98	1E	[*Zr* II] 60.68, *Cr* I 61.08(50)
4	6346.13	2Enn	*Mg* II 46.67(5), *Zr* II 46.54(1)	1	6661.03	1En	[*Ni* II] 68.16v?
3	6352.43	1Enn	*Mg* II 46.67r	1	6663.56	2En	[*Ni* II] 68.16v?
1	6358.78	0En	[*Ni* II] 65.52v	2	6666.20	3En	[*Ni* II] 68.16?
5	6364.45	2En	[*Ni* II] 65.52	1	6676.79	2En	*Fe* II 77.33(3), *He* I 78.15(6), *Fe* I 77.99(600)
4	6369.30	2En	*Fe* II 69.45(4)				
1	6374.15	0En	*Fe* II 69.45r, *Fe* II 75.96(4n)	1	6697.64	0En	[*Fe* II] 98.02
3	6376.90	0E	*Fe* II 83.75v	1	6729.45	1Enn	[*Fe* II] 29.85
4	6383.43	2En	*Fe* II 83.75(15)	1	6746.65	0Enn	
2	6388.23	1En	*Fe* II 83.75r	1	6750.75	0Enn	*Fe* I 50.15(100), *Cr* I 51.28(40)
2	6395.18	1E	[*Fe* II] 96.30	1	6755.26	0Enn	*Si* I 57.16(10)
2	6399.10	1En	*Fe* I 00.01(800)	1	6809.28	1Enn	[*Fe* II] 09.21, [*Ni* II] 13.73v
2	6403.49	1E	[*Ni* I] 04.46	1	6813.10	2Enn	[*Ni* II] 13.73
2	6407.52	1E	*Fe* I 08.03(60)	1	6815.78	0Enn	[*Ni* II] 13.73r
2	6410.62	1E	*Fe* I 11.66(400), *Fe* II 16.91v	1	6868.52	4A	Atm. O 67-70 (B Band)
5	6416.44	3E	*Fe* II 16.91(20), *Cr* II 18.87(7)	1	6943.29	3Enn	[*Fe* II] 44.91
5	6432.27	3E	*Fe* II 32.65(8)	1	6966.00	2Enn	[*Fe* II] 66.32, *Fe* II 66.9(2)

which a line has been measured; the second contains the weighted mean value of the wave length, corrected only for the orbital velocity of the earth; the third column indicates the relative intensity of the line, on a scale described below; the fourth the identification, indicating element, laboratory wave length, and (in parentheses) laboratory relative intensity as written in Miss Moore's *Revised Multiplet Table*. Counting the components separately, we have 76 absorption and 903 emission lines listed, giving a total of 979 lines.

THE INTENSITY SCALE

As plates varying considerably in density had been used for Table 1, it appeared desirable to have some kind of uniform relative intensity scale covering the whole measured region from 3255 A to 7000 A. A series of slitless spectra was therefore exposed, taking advantage of the fact that the spectrum can be considered, to a first approximation, as a succession of monochromatic emission images of the star. This was done while guiding on a near-by star, as described above, on Eastman 103-F panchromatic plates. On a night with exceptionally good seeing, June 16, 1945, five plates were taken with

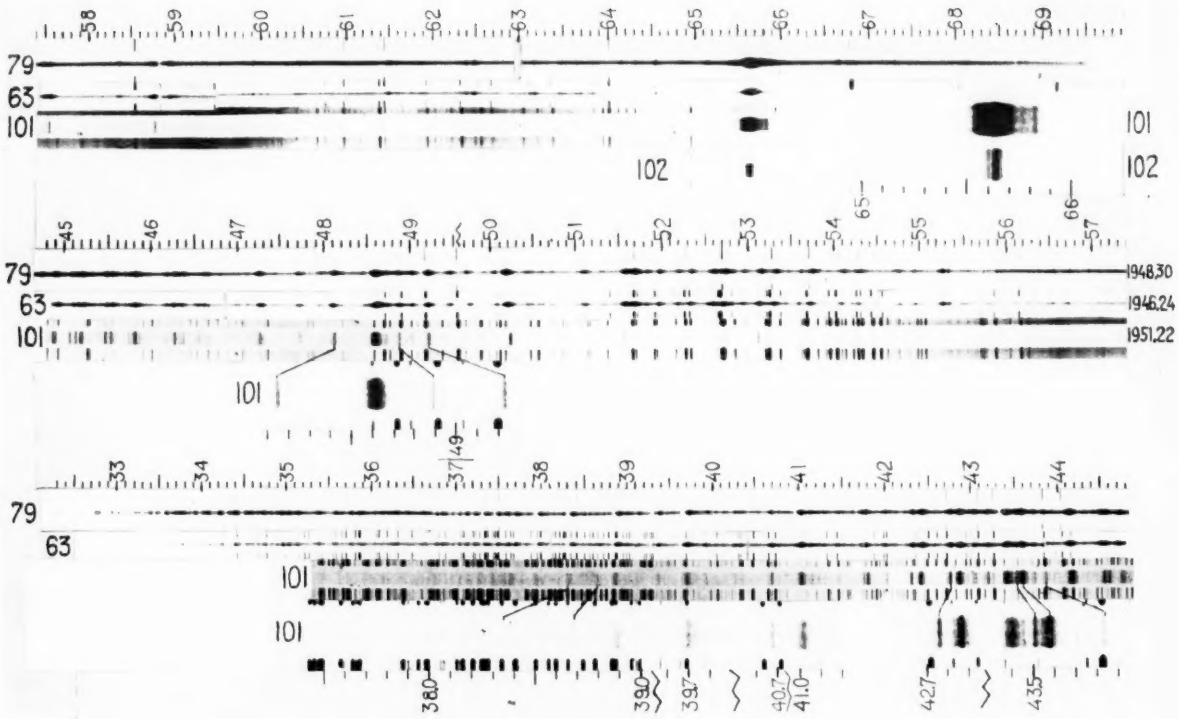

FIG. 1.—The spectrum of η Carinae

exposure times 1, 2, 4, 8, and 16 minutes. They were developed and fixed together under conditions as uniform as possible. The scale thus obtained was extended, on two similar nights, to 32, 64, and 128 minutes, on the one end, and to 30, 15, and 7½ seconds exposure, on the other. In this way an 11-step scale was obtained, which cannot claim any quantitative photometric value but which is better than the subjective evaluation of line intensities done while measuring plates. It permits the comparison of intensities of lines in diverse regions of the spectrum. On the 7.5-second plate, *Hα* is already well exposed, so well that it should just appear on a ½-second plate (step 14). The next brightest lines ([*Fe* II] 4287 and 4359) just begin to appear on step 10, requiring sixteen times more exposure time. This shows that all short-exposure-time photographs of the nebulosity around the star, on panchromatic plates, like the images reproduced in Figure 1 of "Eta Carinae. I. The Nebulosity,"[10] are monochromatic pictures taken in the light of *Hα*. A special *Hα* monochromatic filter would not change anything in them.

For the relative intensities of the slitless (or wide-slit) spectra to be comparable to the intensities of narrow-slit spectra, one of two conditions has to be fulfilled: either the spectral distribution of light of each line is the same, or the size of the star image is not much larger than the width of the slit. The first condition is not fulfilled: *Hα* and *Hβ* are wider than other lines; a few lines are comparatively sharp, while many lines are nebulous and very nebulous. The slitless spectra were therefore taken in such a way as to satisfy the second condition; on exceptional nights star images approach 1 second in diameter; this is equivalent to 1.3 A; the slit width was, in most cases, as shown in Table 2, only slightly smaller than this value; in some cases it was the same, or even larger. The slitless series can thus be used as an intensity scale. An increase in one unit means a doubling of the exposure time.

The band λλ 3028–3255 does not show on the scale series, owing to the reflection minimum of the silvered parabolic mirror at about 3100 A. The same cause reduces the intensities of the lines between λ 3255 and λ 3350 to a marked degree, as compared with an aluminized mirror. In order to extend the intensity scale to λ 3028, the estimated values of the band λλ 3028–3255 and the scale values of the band λλ 3255–3350 have been arbitrarily increased. The intensity scale of the absorption lines is independent and consists of ordinary estimates.

MEASUREMENT AND IDENTIFICATION OF THE LINES

Four spectra are reproduced in Figure 1, corresponding to plates 79, 63, 101, and 102 in Table 2. Plate 102 contains practically only the two main components of *Hα*; only that region is therefore reproduced. The negative prints are 10.7× enlargements of the original. The zones around certain areas of special interest are shown with 25.7× enlargement. The scale given at the side of the prints is for orientation only; for more accurate identifications the iron-arc and neon-lamp comparison spectra should be used.

The band λλ 3028–3255 will be reproduced in the next part of this paper, which deals with the slitless spectra.

For the identification of the lines the following facts need to be considered:

1. Emission lines differ in appearance. Sharp lines like [*S* II] 4069, [*Fe* II] 4114, *Fe* II 4297, and *Fe* II 5317 are about 1 A wide if the main line is subtracted from the background; nebulous lines like [*Fe* II] 4242, [*Fe* II] 4358, and the main components of the Balmer series are 2–3 A wide; very nebulous lines like *N* II 5747 and *He* I 5876 are wider still.

2. Lines are multiple: *Hα* has two main components and several secondary satellites; *Hβ* also has two main components, the weaker one being nearly indistinguishable from a dense continuous background; *Hγ* has three distinct main components; most of the

[10] E. Gaviola, *Ap. J.*, 111, 408, 1950.

stronger *Fe* II, [*Fe* II], *Cr* II, and other lines have two, three, four, and even five main components.

3. The intensity distribution of component lines and continuous background is unsymmetrical, as can be clearly seen in plates 101 and 102 for *Hα*, *Hβ*, *Hγ*, [*Fe* II] 4359, [*Fe* II] 4287, and [*S* II] 4069. This asymmetry produces the effect that the measured wave length changes with the density of the plate. Five dense plates gave for the main component of *Hβ*, for instance, λλ 4862.21, 4862.45, 4861.98, 4862.31, and 4862.30 (mean value 4862.25 ± 0.07); while two less dense plates gave λλ 4861.67 and 4861.67. The coincidence of the last two values is accidental, but the probable error of the mean value is smaller than 0.10. The mention of a few numbers representing the components of a

TABLE 2

No.	Date			Eq. Slit Width (A)	Ext. T.		Film or Plate	Measured Parts
	Year	Mo.	Day		Hr.	Min.		
5	1944	4	7	0 8		20	Eastman Super XX film	*Hα*
6	1944	4	7	0 8		30	Eastman Super XX film	*Hα*
8	1944	5	9	2 3	3	55	Eastman Super XX film, sensitized	3362–6565
9	1944	5	10	1 1	4	10	Eastman Super XX film, sensitized	3277–6583
10	1944	7	7	1 1	2	00	Eastman 103-F thin glass plate	3830–6698
11	1944	7	11	1 1		20	Eastman 103-F plate	*Hα*
15	1945	1	20	0 9		15	Eastman 103-F plate	*Hα*
16	1945	1	20	0 9		30	Eastman 103-F plate	*Hα*
17	1945	1	20	0 9		15	Eastman 103-F plate	*Hα*
18	1945	1	21	1 1	2	00	Eastman 103-F plate	5745–5875
19	1945	1	22	1 2	2	30	Eastman 103-O plate	3255–5093
47	1945	6	17	15 0	1	50	Eastman 103-O plate (slit-less)	3029–3289
48	1945	6	17	1 1		10	Eastman 103-F plate	*Hα*
59	1945	11	15	1 2		30	Eastman 103-O plate	3480–3565, 3925–3974, and 4903–4952
63	1946	3	28	1 4	3	00	Super XX film, sensitized	3928–3974 and 5658–6456
74	1947	4	26	1 2	2	00	Eastman 103A-O plate	*Hδ*, [*Fe* II] 4287, *Hγ*, *Hβ*
79	1948	4	18	1 1	3	00	Eastman 103A-F plate	*Hγ*, *Hβ*, *Hα*
80	1948	4	18	0 9		10	Eastman 103A-F plate	5831–7000; *H8*, *K*, *H*, *Hδ*, *Hγ*, *Hβ*
83	1949	1	27	1 1		60	Eastman 103A-O plate	*Fe* II 4233
101	1951	3	20	0 7		60	Eastman 103A-F plate	3665–4385, 4859–4909, 6548–6598
102	1951	3	20	0 7		8	Eastman 103A-F plate	*Hα*

"line" does not do justice to the continuous spread of intensity over a band 10–80 A wide.

4. The lines are unsymmetrical also in the east-west (slit) direction. This can be seen for *Hα* and *Hβ* on the prints of plates 79 and 63. On plate 79 the maximum density on the west side (side of the wave-length scale) is more to the violet than the maximum on the east side; on plate 63 the contrary seems to happen. This is not so. The apparent change is due to the fact that in April, 1946, between the dates of both plates, the plane grating of the spectrograph, that was normal to the optical axis of the collimator, was placed perpendicular to the optical axis of the camera, and it was rotated 180° around its own normal. This alteration improved the optical symmetry of the camera, but it changed the places of red and violet in regard to north and south. On the reproduction

of plate 79 west is on the side of the scale and south to the red; on plate 63 west is on the opposite side and south to the violet. Both plates show the same asymmetry. The density maximum on the west side is at λ 6563.3 for *Hα*, coinciding with the position of the main component λ 6563.26; the maximum density of the east side is at λ 6565.8, indicating a radial velocity of the nubeculae *f* and *d* (Fig. 5 of first paper) relative to the nucleus of +115 km/sec. The nubeculae *g* and *B* appear at rest with respect to the nucleus in radial velocity; transversely, *g* moves at 7".0 per century (see Fig. 6 of first paper) and *d* at 4".4 per century. If the star image is allowed to move along the slit, instead of being kept at the center by guiding, emission lines will appear slightly broadened when well exposed, and wider and displaced if overexposed.

The identification of the measured lines has been facilitated by the previous work of P. W. Merrill,[1] B. J. Bok, Spencer Jones, and D. Hoffleit, by the very useful *Revised Multiplet Tables* of Miss Moore, and by suggestions received from P. Swings regarding possible lines of [*Ni* II], [*V* II], [*Mn* II], and [*Cr* II].

THE BALMER SERIES

Hα.—*Hα* is by far the strongest line of the spectrum and gives to the star its visual color. The main component is over 2 A wide, having a comparatively sharp violet edge and a nebulous red edge, as can be seen in Figure 1. Its position corresponds to a radial velocity of 20 km/sec. The second component lies 3.06 A to the violet (at −120 km/sec); it is narrower and leaves a relatively unexposed space between the two lines, suggesting an absorption line. On denser plates a strong continuous background develops, extending from λ 6554.2 to λ 6572.4, upon which a relatively weak red component can be measured at +173 km/sec and a similar violet component at −214 km/sec. This background is shown by plate 101, where the two Nebulium lines, [*N* II] 6583.6 and [*N* II] 6548.1 also appear. The strong background ends on the violet side in a weak diffuse absorption, the position of which (−480 km/sec) could be measured only on the 1948 spectra. On the red side the continuum extends, with decreasing density, until it merges into the general continuum at about 6605 A (see pl. 79). On the violet side the *Hα* continuum can be traced to about 6535 A. The total width of the line is thus about 70 A. It is asymmetric, extending 28 A or 1280 km/sec toward the violet and 42 A or 1920 km/sec toward the red. While the brightest part of the nucleus has a negligible radial velocity in the light of *Hα*, the nebulosity around it moves, on the average, away from us at a speed of several hundred kilometers per second. The asymmetry may be due totally or partly to diffuse absorption on the violet side.

On plate 79 a cloud can be seen 23 A to the red of the center of *Hα*, separated from its main body. It is not a plate defect, as it can be seen on a few other slit plates and on many slitless spectra. Its origin is explained by Figure 2. While taking spectra of η Car, I used as a guiding baffle two thin wires about 10" apart, in order to leave most of the reflecting surface of the slit jaws uncovered and to be able to observe the surrounding nubeculae and stars during exposure. The nubecula *k* (first paper, Fig. 5) extends beyond the west wire. The cloud is the spectrum of the nubecula *k*. Its center is at λ 6585.86 (red displacement, 1050 km/sec). It extends from 980 to 1300 km/sec. The separation from the main body of *Hα* is the shadow of the west wire.

Nubecula *k* appears, therefore, as an eruption projecting to the west of the star and away from us at a resultant speed well in excess of 1000 km/sec. It has two weaker components with radial displacements of about 0 and −650 km/sec, which do not show on plate 79; they appear on several guided slitless plates. They somewhat complicate the model: a curving and dividing eruption would not do, as the emission components are separated by wide dark spaces in the spectra.

Hβ.—The integrated light of *Hβ* (lines plus continuum) forms the second brightest feature of the spectrum. If we do not count the continuous background, we find that the main components of [*Fe* II] 4287 and [*Fe* II] 4359 are brighter than the main compo-

nent of $H\beta$. The structure of $H\beta$ resembles that of $H\alpha$, with some differences: the violet component is displaced -163 km/sec instead of -120; the minimum of intensity between this and the main component is less marked at $H\beta$; no red component at or near $+173$ can be found; the absorption on the violet side (-509 km/sec) is better shown, particularly during 1948 (pl. 79).

$H\gamma$.—The continuous background is less intense. A narrower main component and two almost symmetrical satellites form a well-defined triplet (-151, 20, 146 km/sec). The violet absorption is stronger, the displacement being about the same.

$H\delta$.—The components are again nebulous. The violet absorption is weaker than that of $H\gamma$ or $H8$. No less than four nebulous violet emission components and two red components are probably present. The S-shape of the main component on plate 101 is due to local gelatin distortion. The violet displacement of the absorption has become smaller.

$H\epsilon$.—Most of the emission components belong probably to $H\epsilon$; the absorption, on the other hand, is mostly *Ca* II H.

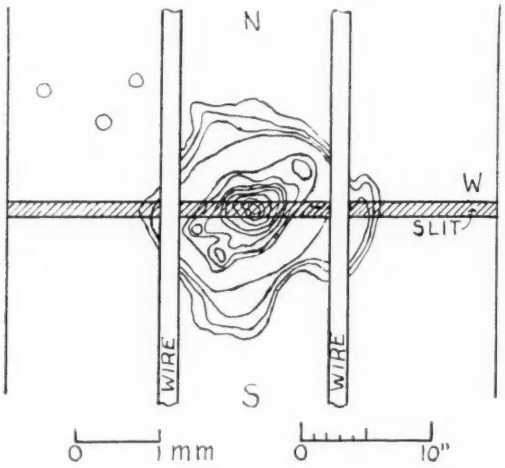

FIG. 2.—Environs of η Carinae. The positions of the slit and fiducial wires are shown

$H8$.—Shows clearly four emission components (-241 [5], -111 [6], 38 [7], and 173 [5] km/sec) and perhaps a fifth one at -617 km/sec. The violet absorption is at its maximum for the series. Its displacement is similar to $H\delta$ and $H9$ (about -434 km/sec).

$H11$.—The violet absorption appears divided in two by a weak emission line, perhaps a violet component of *Ni* II 3769.46. The main emission component, λ 3769.28, probably also belongs to *Ni* II. *Fe* I 3767.19 and *Zr* II 3766.83 are also probably present.

$H12$.—*Fe* II 3748.49 (emission) probably makes the violet emission component at -145 km/sec appear brighter than the main component at 24 km/sec. The violet absorption is weaker. Its position is possibly influenced by the absorption line *Fe* I 3749.49.

$H18$.—The principal emission component at about 20 km/sec is missing, appearing, instead, displaced to the violet at -59 km/sec; this is due probably to the violet absorption of $H17$.

$H19$.—The main emission component appears displaced to 71 km/sec (and weakened) by the absorption of $H18$. The violet emission component is perhaps enhanced by *Ti* II 3685.20. The violet absorption component of this titanium line increases the absorption shift, which, by $H15$, $H16$, and $H17$, had already become of the order of -347 km/sec, to a larger value: -492 km/sec.

H20–H25.—The absorption components are too weak for measurement. The main emission components have somewhat larger red shifts (about 50 km/sec). The still larger red shifts of *H22*, *H23*, and *H25* may be due to blends of *Cr* II, [*Fe* II], and *Zr* II lines.

Table 3 contains further details of the Balmer series. The following points deserve notice:

1. The multiple structure varies from line to line.
2. The main emission component has a red shift of about +20 km/sec for *Hα–H17*, moving afterward a little further to the red (+50 km/sec) for the higher members of the series.
3. The violet shift of the absorption component decreases from about −500 km/sec for the lower members to about −350 km/sec for the higher members of the series.
4. The diffuse background loses relative importance for the higher members.

THE METALLIC MULTIPLETS

Most of the bright metallic lines show multiple structure and a continuous background. This can be seen in Figure 1. The following general results for the metallic emission lines can be stated:

1. The main components have a violet shift of about −28 km/sec.
2. In most cases two satellites can be measured; in some cases only one; in a few cases three and even four.
3. The intensity of the two nearest satellites is generally two, sometimes one or three, units of our scale less than the main component. The further satellites, if any, are generally one unit less bright than the near ones.
4. The radial-velocity shifts of the satellites do not fall within narrow limits, as one would desire. The broad and diffuse character of the lines, the background, and the blends may account for this in part. The near satellites often have shifts in the range of ±140–200 km/sec; the farther components may lie between ±250 and ±350 km/sec.
5. There are bright lines that show a nebulous background, but no lines can be located upon it.

The large number of emission lines and their multiplicity makes identification difficult. The numerous blends that would show with single lines are multiplied by the uncertain number of violet and red components. These have been marked in Table 1 by a "v" or "r" on rhe right of the laboratory wave length of the line. Let us consider one example: in the series of star lines λλ 3486.02 (5E), 87.95 (5E), 91.50 (4E), 93.87 (7E), 95.26 (6E), 97.72 (4E), each one may be the violet component of the following line as well as the red component of the preceding one. The probable presence of main components for most of the measured wave lengths and rule 3 (above) for intensities of satellites leave only two possibilities: either λ 3491.50 is a red component of λ 3487.95, or it is a violet component of the following one, identified as *Fe* II 3493.47. The greater intensity of the latter eliminates the former alternative. All the red and violet satellites are, of course, there and blend with the main components, influencing the position and the intensity of the observed lines. Only a few of these blends have been indicated in Table 1.

THE ABSORPTION SPECTRUM

As the number of emission lines is large, it is easy to mistake the space between two of them for an absorption line. On a moderately exposed spectrum, like *101* of Figure 1, it is difficult to state whether there are any absorption lines. On denser plates a spurious continuum appears first, particularly in the blue-violet, formed by the blending of the numerous diffuse emission lines and their components. This effect is enhanced by a wide slit and low spectrographic dispersion. With the high definition of our instrument and an equivalent slit width of about 1 A, the true continuum appears with an exposure time about one hundred times longer than the one needed for showing *Hβ* and the brightest *Fe* II and [*Fe* II] lines, and about one thousand times longer than needed for showing *Hα* on an Eastman 103A-F plate. It is well shown in Figure 1, spectra *63* and *79*.

TABLE 3

THE BALMER SERIES

λ Lab.	Star	Int.	v	Blend
Hα	35 —	Emission begins		
6562.82	39.39	3E	−1060	
	41.76	4En	− 950	
	43.61	4En	− 865	
	45.32	4E	− 800	*Fe* I 46.25(200)
	47.81	5En	− 687	[*V* II] 48.1(−18)
	52.13	2Ann	− 480	
	58.13	9E	− 214	[*Fe* II] 58.51
	60.20	11E	− 120	
	61.48	3A?	− 61	
	63.26	13En	20	
	66.60	9E	173	
	76.95	6En	647	*C* II 78.03(10)
	82.87	7En	937	[*V* II] 83.6(−32)
	85.86	4E	1050	Max. Nubec. *k*
	87.95	4En	1155	
	91.27	3Enn	1288	
	94.89	2En	1450	
	97.75	2E	1596	*Cr* I 97.56(40)
	05 —	Emission ends		
Hβ	53.08	5A	− 509	
4861.33	58.70	7E	− 163	
	61.67	9E	21	
	68.81	4E	460	[*Fe* II] 69.3
	72.62	5E	698	
	74.44	5E	810	[*Fe* II] 74.49
	76.48	4E	935	[*Ti* II] 77.01
	77.71	3E	1010	
Hγ	30.06	4E	− 720	*Ti* II 30.71
4340.47	33.11	6A	− 509	
	38.28	7E	− 151	
	40.76	9E	20	
	42.58	7E	146	
Hδ	93.88	4E	− 575	
4101.74	95.90	4A	− 427	
	97.14	4E	− 336	
	98.50	4E	− 237	
	99.76	5E	− 145	
	02.00	7E	19	
	04.58	5E	208	
	06.49	3E	347	
Hε	66.60	5E	− 262	[*Ne* III] 67.51(N), *Ca* II 68.47 v
3970.07	69.24	6E	− 63	*Ca* II 68.47 (350R)
	71.29	7E	92	
	73.75	5E	278	*Fe* II 74.16 (3)
	74.59	5E	342	*Fe* II 75.03 (2)
H8	81.04	5E	− 617	*Ni* II 81.92 (1)
3889.05	83.33	10A	− 441	*Fe* I 86.28(40R)(−228)
	85.92	5E	− 241	*Fe* I 86.28 (40R)
	87.61	6E	− 111	*He* I 88.65 (10)
	89.55	7E	38	
	91.29	5E	173	
H9	28.45	4E	− 543	*Fe* II 27.08 r
3835.39	29.85	10A	− 433	*Fe* I 34.23(100r)(−343)
	32.85	5E	− 200	
	35.59	7E	16	
	38.38	6E	234	
H10	90.56	5E	− 580	
3797.90	92.75	7A	− 407	*Mo* I 98.26 (50R)
	96.60	5E	− 102	
	98.12	6E	17	
	00.63	5E	216	

λ Lab.	Star	Int.	v	Blend
H11	65.34	6A	− 421	
3770.63	66.82	5E	− 303	*Fe* I 67.19, *Zr* II 66.83
	67.46	3A	− 252	*Fe* I 67.19(80r)
	69.28	7E	− 107	*Ni* II 69.46 (5)
	72.41	5E	+ 142	*Ni* II 69.46 r
	73.83	5E	255	
H12	45.27	3A	− 391	*Fe* I 49.49(200R)
3750.15	48.34	7E	− 145	*Fe* II 48.49 (8)
	50.45	5E	24	
	52.87	5E	218	
H13	30.61	4A	− 302	*Fe* I 34.87(300r)(−343)
3734.37	32.30	5E	− 166	*He* I, *V* II
	34.45	7E	+ 6	*Fe* I 34.87(300r)
	36.18	6E	145	*Fe* I 37.13(150R), [*Fe* II] 36.17
H14	17.24	3A	− 379	*Fe* I 19.93(250R)
3721.94	20.24	6E	− 137	*Fe* I 19.93(250R)
	22.22	7E	23	*Fe* I 22.56(50r)
	25.34	5E	274	
H15	07.81	4A	− 336	
3711.97	09.51	5E	− 198	*Zr* II 09.27(60), [*Fe* II] 09.14
	12.42	7E	36	[*Fe* II] 12.26, *Cr* II 12.97 (35)
	15.09	6E	244	*Cr* II 15.19 (20)
H16	99.58	3A	− 347	
3703.86	02.82	5E	− 84	*Mo* II 02.55(8)
	03.85	6E	0	
	06.10	5E	181	*Fe* I 05.57(100R)
H17	92.73	3A	− 358	
3697.15	96.27	5E	− 71	
	97.29	6E	11	
H18	86.78	1A	− 388	*H*19 (E) 86.83
3691.56	90.84	5E	− 59	
H19	80.79	2A	− 492	*Ti* II 85.20 (250)
3686.83	87.70	5E	− 71	*Mo* II 88.31 (15)
	85.12	6E	− 139	*Ti* II 85.20 (250)
H20	83.45	5E	52	
3682.81				
H21	79.94	5E	47	
3679.36				
H22	77.48	6E	90	*Cr* II 77.86, .69, .93
3676.37				
H23	74.93	5E	96	*Zr* II 74.74 (40)
3673.76				
H24	72.19	4E	58	
3671.48				
H25	70.85	5E	112	[*Fe* II] 70.62
3669.47				
H28	65.29	5E	50	*Cr* II 64.95 (30)
3664.68				

Once the true continuum is photographed, the absorption lines appear. The diffuse absorptions to the violet of the Balmer lines have already been described.

The most conspicuous absorptions of the spectrum are *Ca* II K and H. They both appear twice, as displaced and as relatively undisplaced absorptions. Their contours are sharp, in contrast with the diffuse character of the Balmer absorption lines. The width of K in the −449 km/sec displaced position is 4 A and in the −34 km/sec "undisplaced" position, 1 A. The width of H in the −444 displaced position is only a little smaller, 3.4 A; in the "undisplaced" absorption position (−49 km/sec), on the other hand, the width of H is much smaller than that of K, so much smaller, that it looks just like a sharp edge of the main emission component of the line at λ 3969.24 (+58 km/sec). The absorption line appears partially covered up by the emission line λ 3966.60, which is probably a blend of the Nebulium line [*Ne* III] 3967.51 and a −262 km/sec violet emission component of *Hε*. If this is so, the undisplaced absorption of H and K must originate below a part at least of the emitting prominences or eruptions and cannot be interstellar. The displaced absorption cannot be interstellar either, as the sharp aspect of the lines may suggest, because they do not show on the near-by blue (probably B5) stars E and F (see Figs. 1 and 5 of first paper). Slitless spectra of these stars have been obtained; they show well-developed Balmer lines but no *Ca* II K absorption. The displaced absorptions may be those described by Miss Cannon[1] as "broad and dark." The shifts themselves agree with those of the near Balmer lines *Hδ* (−427), *H*8 (−441), and *H*9 (−433). Lines K and H appear also in emission, their main components being displaced to the red +61 and +58 km/sec, respectively. *Ca* I 4227 also appears twice in absorption, as a displaced line at −487 km/sec and in an undisplaced position at −15 km/sec. Both are nebulous and of equal intensity.

Na D_2 also appears broad (about 3 A) in a displaced position (−432 km/sec) and narrow in an undisplaced position (−12 km/sec). *Na* D_1, on the other hand, shows only ill-defined and weak undisplaced and displaced absorptions.

He I D_3 shows in emission, having a broad continuous background and a relatively sharp main component, but there is no definite absorption.

Fe I appears in emission and in absorption. The emission lines are displaced, on the average, −30 km/sec and are weak compared with the ionized iron lines. The absorption lines fall into three groups: undisplaced (+27 km/sec), half-displaced (−231), and displaced (−353 km/sec). *Ni* I and *Co* I behave like *Fe* I. *Ba* I, *V* I, and *Mo* I are represented by one line each: *Ba* I 5536 (−186), *V* I 4407 (0), *Mo* I 3798 (−435). The ionized elements are represented by displaced absorptions of 7 lines of *Ti* II, 8 lines of *Fe* II, *Ni* II 4026, and *Sc* II 5527.

COMPARISON WITH EARLIER SPECTRA

Lunt states (*op. cit.*, p. 622): "Comparison with Moore and Sanford's published photograph shows that the 1919 spectra are almost identical with the 1913 photographs." The Córdoba spectra are almost identical with the published photographs of Moore and Sanford and of Lunt, with the exception of the *He* I lines λλ 4026, 4144, and 4471. These lines have had the intensities, 5, 5, and 6 on our scale since 1944, save in 1948, when only a diffuse background remained. As can be seen on plates 101 and 63, the line λ 4471 is as bright as [*Fe* II] 4475, which has been measured by Lunt and by Moore and Sanford, who ascribed to it intensities 2 and 3, respectively. Spencer Jones, measuring a plate taken by H. E. Wood 13 days after the second plate of Lunt, finds a line of intensity 4 (his scale) at λ 4473.5, which he identifies as *Fe* II 4472.92 or [*Fe* II] 4474.91. Spencer Jones does not measure any lines at λ 4471 or λ 4475. As λ 4473 is 2 mag. weaker than λ 4475, his value suggests that *He* I 4471 was present on Wood's plate and that he measured a blend of all three lines. This is possible, as the *He* I lines are the most variable feature in the spectra of the recent years. A detailed study of the changes is not yet completed.

The multiple components were already present in the 1913 and 1919 spectra, and those of the Balmer lines were recognized as such. Moore and Sanford gave to $H\beta$ in their Table II the remark "double; strongly shaded to the red." This is exactly the present aspect, as it can be seen on the high enlargement of plate 101. But Sanford changed his mind nearly two years later (*op. cit.*, p. 134), influenced by a plate of March 2, 1914, which "was purposely underexposed." The radial velocity obtained for $H\beta$ on that plate was +17 km/sec, in good agreement with our value of +21 km/sec, derived from two not overexposed plates, while for the 1912 plate he found +46 km/sec and for the 1913 plates he found +37.8 km/sec for the mean of $H\beta$, $H\gamma$, and $H\delta$. The lines were therefore asymmetric then as they are now. For $H\gamma$ Moore and Sanford found two components which correspond well to ours, λ 4340.76 (9) and λ 4342.58 (7). For $H\delta$ they measured three components in fair agreement with our central triplet.

A number of multiple components of metallic lines were measured, but they were not recognized as such. This shows that the metallic lines in 1912, 1913, and 1919 already had components as they have now.

It has been possible to retain a great number of the identifications suggested by Lunt, Merrill, Hoffleit, and Spencer Jones. A number of emission lines identified previously as *Ti* II have been kept in our list, although I agree with Lunt, that this identification is not satisfactory, because many strong *Ti* II lines are not represented and because the dispersion in radial velocities is large. They should be considered as subject to eventual revision.

The comparison of relative intensities is difficult because of the different scales used. Our intensity 5, for instance, corresponds to lines of Lunt marked from 000 all the way to 3 and to lines of Moore and Sanford marked from 0⁻ to 3. Our intensity 6 corresponds to lines of Spencer Jones marked from 0 to 8. This disagreement is due probably mainly to the varied width and continuous background of the lines and to the different instruments, plates, and dispersions used.

The relative intensities of *Fe* II, [*Fe* II], and the Balmer lines agree, on the whole, with the curves of Hoffleit,[3] if we extrapolate from 1930 to 1950, keeping the tangent to the curve constant. This again shows that the spectrum has not changed much in the present century.

RADIAL VELOCITIES

Table 4 contains some mean radial velocities. The probably large number of blends and the multiple components of the lines make the values for the weaker elements less precise than one would desire.

CHANGES IN 1948

In 1948 three long-exposure spectra were taken, one on Eastman 103*a*-O plate, one on Process film, and one on an Eastman 103A-F plate. The latter is spectrum *79*, reproduced in Figure 1. Several changes were noticed on these spectra.

1. The general continuum had become stronger with respect to the emission lines.

2. The Balmer violet-displaced absorption series was considerably stronger. For $H\alpha$ and $H\beta$ it was difficult or impossible to determine precisely the position of the absorption maxima prior to 1948, as can be seen on spectrum *63*. In 1948 the $H\beta$ absorption was well developed and that of $H\alpha$ so far enhanced that its position could be measured. In the case of $H\gamma$ and $H\delta$ it had become as wide and deep as that of K and H. These last, on the other hand, and the *Na* D_2 absorption did not change. The wave length of the Balmer absorption lines had not changed detectably, in spite of the large change in intensity.

3. The sharp *He* I lines, particularly λ 5876 and λ 4471, which were previously distinct upon a broad diffuse background, had practically disappeared, leaving only the diffuse background. This can be seen in Figure 1. The variations of *He* I 4471 are easy to follow,

as it can be compared with [*Fe* II] 4475. In June 1947, *He* I 4471 was about ½ scale unit brighter than λ 4475; in 1948 it was more than 2 scale units fainter.

4. The line measured at λ 6515.9 and identified as *Fe* II 6516.05 had increased in brightness in comparison with other *Fe* II and [*Fe* II] lines. This fact makes the identification appear doubtful. No other *Fe* II or [*Fe* II] line has been found to change in magnitude or position.

5. The pair of lines λ 5747 and λ 5754 had apparently interchanged intensities. The first, which was fainter in 1947, had become somewhat brighter in 1948. The line λ 5754 had become definitely weaker. These two lines had been identified as [*Fe* II] 5746.96 and [*Fe* II] 5753.83. The changes suggested a better identification: *N* II 5747.29 and [*N* II] 5754.8N. The permitted line had grown at the expense of the nebulium line. The other two [*N* II] lines observed, λ 6548 and λ 6584, seem to have decreased in intensity during

TABLE 4

RADIAL VELOCITIES

ELEMENT	RADIAL VELOCITIES		ELEMENT	RADIAL VELOCITIES	
	Emission	Absorption		Emission	Absorption
Hα–*Hδ*	+20 ± 1		*Ti* II	−34 ± 9*	
Hα–*H*17		−480 to −350	*Cr* I	−23 ± 4	
He I	−32 ± 4		*Cr* II	−25 ± 3	
N II, [*N* II]	−26		*Fe* I	−30 ± 8	+27 ± 5 −353 ± 10
O II, [*O* II], [*O* III]	+53?				
[*Ne* III]	−29		*Fe* II	−27 ± 2	
Na I	−53	−432 − 12	[*Fe* II]	−28 ± 2	
			Ni II	−28 ± 4	
Mg I, *Mg* II	−28		[*Ni* II]	−38	
S II	−19 ± 8*		*Zr* II	−21 ± 8*	
[*S* II]	−32 ± 5		*Ba* II	−20	
Ca I		−487 − 15	*La* II	−36 ± 8*	
Ca II	+60	−449 − 41			

* The comparatively large least-squares error of the average radial velocity indicates that the presence of the lines of this element needs confirmation.

1948, too; the determination of the change is made difficult by the bright *Hα* continuous background.

6. Other nebulium lines have been examined. [*Ne* III] 3869 and 3967 have definitely reduced intensity in 1948. On the other hand [*O* II] 3726 and 3729, [*O* III] 4363, and [*S* II] 4069 and 4076 do not show any noticeable change.

The plates of 1949 show that the spectrum was coming slowly back to "normal": by July, 1949, the *He* I, the [*N* II], and the [*Ne* III] lines had changed again nearly to their old intensity; the continuous background and the Balmer absorptions remained still enhanced, though in a lesser degree than in 1948. The last and the present year seem to be normal.

My thanks are due, in the first place, to Dr. Ricardo Platzeck for his constant help, for taking some of the plates, and particularly for making possible, as acting director of the Observatory, the completion of this work; to Mr. David MacLeish, who measured and calculated a few of the spectra; to Miss Isabel Dobermont for typing Table 1, and to Mrs. Elena Dartayet de Gaviola for typing the text of the manuscript and the remaining tables.

THE BALMER DECREMENT IN SOME Be STARS*

G. R. BURBIDGE AND E. MARGARET BURBIDGE
Yerkes and McDonald Observatories
Received February 12, 1953; Revised March 20, 1953

ABSTRACT

Measurements of the Balmer decrement as far as the last visible emission line have been made for four Be stars. These measurements show that the strengths of the lines arising from the high levels ($> H\zeta$) are much greater than would be expected from the theory for a planetary nebula. The effect of self-absorption has been investigated for a simplified transfer problem, and it is shown that this effect could possibly explain the observed decrements, though unknown factors are involved.

I. INTRODUCTION

In a previous paper,[1] which will be referred to as "Paper I," the outer atmospheres of certain Be stars were discussed. In this work measurements of the Balmer emission lines $H\beta$–$H\zeta$ were made, and a tentative model of the outer atmosphere was suggested. Of the six stars studied in Paper I, 11 Cam alone had Balmer emission lines which were single and sharp and could be distinguished as far as *H*22. In the other cases the emission lines were double and appeared to fade out or could not be identified beyond $H\zeta$. In this paper we shall discuss measures of the Balmer emission lines arising from the high levels, in the spectrum of 11 Cam and in the spectra of three other Be stars—12 Aur,[2] HD 37998,[3] and HD 58050[4]—which were not discussed in Paper I.

Calibrated spectra of these latter three stars were obtained in January, 1952, at the McDonald Observatory with the Cassegrain quartz spectrograph (500-mm camera, dispersion 54 A/mm at $H\gamma$), on Eastman Kodak IIa-O plates. In all three of these stars, as in 11 Cam, emission lines superposed on broad absorption lines were visible from $H\beta$ to beyond the last observable hydrogen absorption line. Brief descriptions of the spectra of 12 Aur, HD 37998, and HD 58050 follow.

12 Aur.—The only description of the spectrum of this star is to be found in the *Catalogue and Bibliography of Be and Ae Stars*,[5] in the *Second Supplement*. Here Miczaika described the hydrogen lines as having sharp dark cores with a suspicion of emission at $H\beta$ in 1948 and 1949. The spectrum has evidently changed radically since then: on our plates no central absorption cores were visible. The emission lines were strong and rather broad (possibly unresolved doubles) and were visible as far as *H*22. A spectrogram obtained at Yerkes in January, 1953, with the one-prism spectrograph and 12-inch camera shows the spectrum of 12 Aur to be similar to its appearance a year previously.

HD 37998.—This star is described in the *Second Supplement*.[5] In 1945 $H\beta$, $H\gamma$, and $H\delta$ consisted of narrow emission components nearly centrally superposed on broad absorption lines, while the absorption lines of *He* I, *Mg* II, and *Si* II resembled those of β Orionis. From our plate this star is seen to be peculiar; a unique spectral classification cannot be assigned. *Si* II λλ 4128–4130 does not appear. The hydrogen lines have single, central narrow emission lines visible to *H*25, while the absorption lines are visible to *H*17.

* *Contributions from the McDonald Observatory*, No. 227.

[1] G. R. Burbidge and E. M. Burbidge, *Ap. J.*, **117**, 407, 1953.

[2] MWC 104, $\alpha_{1900} = 5^h09^m0$; $\delta_{1900} = +46°19'$; $m_v = 6.9$; Sp. B2 V.

[3] MWC 772, $\alpha_{1900} = 5^h37^m4$; $\delta_{1900} = +25°15'$; $m_v = 8.0$; Sp. B3–5p IV, V.

[4] MWC 176, $\alpha_{1900} = 7^h18^m8$; $\delta_{1900} = +15°43'$; $m_v = 6.4$; Sp. B2 V.

[5] P. W. Merrill and Cora G. Burwell, *Ap. J.*, **78**, 87, 1933; *Mt. W. Contr.*, No. 471; *Ap. J.*, **98**, 153, 1943; *Mt. W. Contr.*, No. 682; *Ap. J.*, **110**, 387, 1949; *Mt. Wilson and Palomar Reprints*, No. 8.

HD 58050.—This star was suggested by Dr. Morgan, from examination of his plates, as a typical "pole-on" star. In the *First Supplement*[5] there is a note that a spectrum obtained by Swings and Struve in 1943 showed hydrogen emission lines to *H*8 or *H*9, indicating that the emission was stronger then than in 1933. In the *Second Supplement* there is a note that Adams observed *Hβ*, *Hγ*, *Hδ*, and probably *Hε* to show broad double emission lines on a coudé spectrogram taken in 1945. On our plates the emission lines are single as far as *Hδ* or *Hε*, but the higher members are resolved as double, with a mean separation of 145 km/sec, and are visible as far as *H*19.

In the spectra of these three stars and 11 Cam we have found it possible to measure the equivalent widths of the hydrogen emission lines as far as the last visible line. The calibration technique was described in Paper I. The method of obtaining the equivalent widths of those emission lines which are superposed on absorption lines, by drawing in

TABLE 1

EMISSION-LINE EQUIVALENT WIDTHS, IN EQUIVALENT ANGSTROMS

Line	11 Cam	12 Aur	HD 37998	HD 58050
Hα	19.9	.....	.....	.....
Hβ	1.61	1.63	2.31	4.51
Hγ	0.60	.....	.....	2.07
Hδ	0.38	.....	.....	1.02
Hε	.....	.....	.....	0.92
Hζ	0.15	0.61	.....	0.71
*H*9	0.20	0.76	0.18	0.53
*H*10	0.18	0.68	.....	0.52
*H*11	0.22	0.69	0.15	0.59
*H*12	0.15	0.72	0.13	0.50
*H*13	0.20	0.86	.....	0.53
*H*14	0.17	0.63	0.12	0.44
*H*15	0.14	0.76	0.18	0.63
*H*16	0.20	0.43	0.14	0.44
*H*17	0.18	0.53	0.16	0.67
*H*18	0.15	0.34	0.15	0.40
*H*19	0.19	0.26	0.20	0.22
*H*20	0.13	0.25	0.17	.....
*H*21	0.15	0.21	.....	.....
*H*22	0.07	0.18	.....	.....
*H*23	.....	.....	0.10	.....
*H*24	.....	.....	0.14	.....
*H*25	.....	.....	0.06	.....

the central parts of the absorption lines, was also described in Paper I. For the reduction of all the lines arising from levels higher than $n = 7$, the calibration-curves for either *Hδ* or *Hε* were used. This does not introduce much inaccuracy, since the sensitivity varies only slightly with wave length in the range λλ 4000–3600. The equivalent width of the *Hα* line was measured in the spectrum of 11 Cam, from two plates obtained at Yerkes in November, 1952. For these, calibration-curves were obtained with the step-slit sensitometer at the Yerkes Observatory. The dispersion of these spectra was about 250 A/mm at *Hα* and about 90 A/mm at *Hβ*. In spite of this low dispersion, the two plates gave consistent results, and the equivalent width of the emission line at *Hβ* agreed well with the value obtained a year earlier from the McDonald coudé plate. We think it reasonable to suppose that the spectrum of 11 Cam has not shown significant variations in emission-line intensities in the 10 months' interval.

In Table 1 the equivalent width of *Hα* in 11 Cam is the mean of results from the two

Yerkes plates; the remainder of the lines in 11 Cam were measured from the single McDonald coudé plate. The values for HD 58050 are the means of the results from two plates (the mean difference between the two, from 14 lines for which measures were made for both spectra, was ±12 per cent). The values for 12 Aur and HD 37998 are from single plates. The lines from $H\gamma$ to $H\epsilon$ in 12 Aur and from $H\gamma$ to $H\zeta$ in HD 37998 were not measured, as the plates were rather too strongly exposed for spectrophotometric work in this region. Other gaps in the table are due to flaws on the plates.

It might be thought that systematic errors have been introduced by the process of drawing in the central parts of the underlying absorption lines. However, the last few lines, from *H*17 to *H*22 in 11 Cam, *H*15 to *H*22 in 12 Aur, *H*15 to *H*19 in HD 58050, and *H*18 to *H*25 in HD 37998, had no underlying absorption lines, and there is no appreciable systematic difference between these and the earlier lines.

II. THE BALMER DECREMENT

The energies emitted in the various lines have been obtained by assuming that the stellar continuum in each case is produced by a black body at the temperature given in the table by Keenan and Morgan[6] for the various spectral classes. (There is no evidence from their colors that any of these stars are intrinsically reddened.) The equivalent widths in Table 1 were referred to the apparent stellar continuum, which is depressed below the "true" continuum by the Balmer discontinuity, which occurs near λ 3700 and beyond which the broad absorption lines are no longer resolved. It is also depressed, to a lesser extent, on the long-wave-length side of this point, because of the overlapping of the hydrogen absorption wings. The measured equivalent widths of the higher Balmer emission lines have therefore to be multiplied by a factor giving the black-body intensity at that wave length and be divided by a factor giving the ratio of the "true" to apparent continuum at that wave length.

Barbier and Chalonge[7] give mean values of the Balmer discontinuity for normal stars of the various spectral types. The values for the types B2, B3, and B5 are 0.11, 0.17, and 0.25, respectively, where these figures give the logarithm of the ratio of the intensities on either side of λ 3700. In the four stars considered here, there is some continuous Balmer emission beyond the last resolved emission line (it is especially visible in HD 58050). We therefore took the continuum between the last few Balmer emission lines to represent the level from which the Balmer discontinuity should be measured. We plotted points representing the undepressed continuum on the microphotometer tracings, using the values 0.11 for 12 Aur and HD 58050; 0.17 for 11 Cam; and 0.25 for HD 37998 (since in this star the strength of the hydrogen absorption lines seemed consistent with a type B5 rather than B3). We joined these plotted points smoothly to the continuum between $H\zeta$ and *H*9, where the wings do not overlap; this curve now represents the "true," undepressed, continuum. The ratio of intensities in the "true" to the apparent continuum was obtained for each line, and these ratios were used as correcting factors in obtaining the energies in the various Balmer lines, thus reducing the values for the higher Balmer lines below those which would be obtained if no account were taken of the depression of the continuum. These correcting factors are likely to be over- rather than underestimated, since the hydrogen absorption lines are somewhat weaker in Be stars than in normal B stars.

The resultant energies, referred to $H\beta$ as unity, are given in Table 2 and are the Balmer decrements for the stars. If there is no self-absorption, the energies lead directly, by the method described in Paper I, to the relative populations of the various levels.

Baker and Menzel[8] tabulated the Balmer decrement for various values of T_e, calcu-

[6] *Astrophysics*, ed. J. A. Hynek (New York: McGraw-Hill Book Co., 1951), p. 23.

[7] *Ann. d'ap.*, **4**, 30, 1941.

[8] *Ap. J.*, **88**, 52, 1938.

lated for a gaseous nebula under the assumption that the nebula is excited by the absorption of stellar radiation beyond the Lyman limit. A temperature of 12,600° (T_e) was shown in Paper I to be a reasonable value for the outer atmospheres of Be stars. We have therefore interpolated from Baker and Menzel's tables for $T_e = 12{,}600°$ for their case B. This is the case in which the nebula is assumed to be opaque to Lyman radiation, and each Lyman transition is assumed to be balanced by an inverse transition. The resulting values of the Balmer decrement are also shown in Table 2.

This table shows that, although our observed values of the Balmer decrement in 11 Cam and HD 58050 are similar to the calculated nebular values for the first few lines,

TABLE 2

THE BALMER DECREMENT

Line	11 Cam	12 Aur	HD 37998	HD 58050	Calculated (Nebula)	γ Cas	
						a) $T =$ 25,000°	b) $T =$ 10,000°
$H\alpha$	4.8	.....	.....	.....	2.52	.....	.....
$H\beta$	1.00	1.00	1.00	1.00	1.00	1.00	1.00
$H\gamma$	0.52	.....	.....	0.65	0.51	0.33	0.28
$H\delta$	0.38	.....	.....	0.38	0.31	0.15	0.12
$H\epsilon$	.....	.....	.....	0.38	0.20	0.10	0.08
$H\zeta$	0.18	0.72	.....	0.31	0.14	0.17*	0.12*
$H9$	0.24	0.92	0.12	0.24	0.10	0.06	0.04
$H10$	0.22	0.80	.....	0.23	0.08	0.05	0.04
$H11$	0.28	0.80	0.14	0.27	.....	0.06	0.04
$H12$	0.17	0.81	0.11	0.22	.....	0.06	0.04
$H13$	0.22	0.96	.....	0.23	.....	0.08	0.05
$H14$	0.17	0.67	0.08	0.18	.....	0.09	0.06
$H15$	0.13	0.83	0.11	0.25	0.024	0.08	0.06
$H16$	0.19	0.48	0.08	0.17	.....	0.09	0.06
$H17$	0.18	0.61	0.09	0.27	.....	.....	.....
$H18$	0.15	0.41	0.08	0.17	.....	.....	.....
$H19$	0.19	0.32	0.10	0.09	.....	.....	.....
$H20$	0.13	0.31	0.09	.....	0.011	.....	.....
$H21$	0.15	0.27	.....	.....	.....	.....	.....
$H22$	0.07	0.24	.....	.....	.....	.....	.....
$H23$	.....	.....	0.05	.....	.....	.....	.....
$H24$	.....	.....	0.07	.....	.....	.....	.....
$H25$	.....	.....	0.03	.....	0.006	.....	.....

* Blended with *He* I.

the values for the higher lines all depart very considerably from the calculated values, and differ from star to star. If 11 Cam, for instance, had the calculated Balmer decrement, then the observed equivalent width of $H\beta$ is such that the equivalent width of $H20$ would be 0.01 equivalent angstroms, and would be quite unobservable on our plate. The slowness of the decrement in 12 Aur is remarkable.

Previous measures of the Balmer decrement[9] for $H\beta$–$H\epsilon$ in Be stars have been found not to depart much from those measured for planetary nebulae.[10] This has been interpreted to mean that, in spite of the greatly differing extent and density of the gas in Be

[9] E.g., O. Struve and H. F. Schwede, *Phys. Rev.*, **38**, 1195, 1931, and O. Struve, *Zs. f. Ap.*, **4**, 177, 1932; B. G. Karpov, *Lick Obs. Bull.*, **16**, 159, 1934; O. Mohler, *Pub. Obs. U. Michigan*, **5**, 43, 1934.

[10] See L. H. Aller, *Ap. J.*, **93**, 236, 1941, and references given in that paper; also Aller, *ibid.*, **113**, 125, 1951.

star atmospheres and in planetary nebulae, the conditions for the transmission of radiation are essentially similar. There are very few measures of equivalent widths of the Balmer emission lines of shorter wave length than $H\epsilon$. Walraven and Koelbloed[11] measured the emission lines $H\beta$–$H16$ of γ Cas in 1937 and 1938, when the emission was very strong. We have converted their published equivalent widths to relative energies by assuming that the continuous spectrum was that of a black body at (*a*) 25,000° (corresponding to a B0 star) and (*b*) 10,000° (since the star had appreciable intrinsic reddening at this time). The energies are sensibly constant from $H\epsilon$ to $H16$ in both cases. The decrement is shown in Table 2. The relative energies in the lines of shorter wave length are nearer to the calculated nebular values than in any of the four stars discussed here. Merrill and Wilson[12] give the central emission intensities (not equivalent widths) for some Balmer and Paschen lines in γ Cas; they do not vary appreciably for this star from $H10$ to $H16$. Perhaps the most striking feature shown by Table 2 is the general constancy, for any one star, of the energies emitted in the lines from $H8$ or $H9$ to the last observable line.

III. THE TRANSFER OF RADIATION

If there were no self-absorption, the decrements given here would indicate a considerable overpopulation of the higher levels of the hydrogen atoms. Such a distribution of populations, however, would seem to be very unlikely. We have therefore decided to examine the question of self-absorption of the line radiation as it passes through the outer atmosphere.

Miyamoto[13] has discussed self-absorption in Be stars in so far as it affects the strengths of $H\alpha$ and $H\beta$. This involved the solution of coupled equations of transfer for Lyman and Balmer frequencies. If we wish to discuss the strengths of the Balmer lines up to $\sim H20$ by this method, it would involve the solution of a large number of coupled equations, because of the conversion of radiation from one frequency to others by absorption and re-emission. Since it has not yet been possible to evolve a technique to handle such a situation, we shall consider, in order to determine some of the factors involved, the equation of transfer for one particular Balmer frequency ν.

Consider the transfer of radiation through a layer of geometrical thickness x. We will suppose that the layer is illuminated by a source emitting mainly in the ultraviolet. The gas in the layer absorbs radiation beyond the Lyman limit; it is ionized and recombines with the emission of the various line series. That part of this line radiation emitted in the frequency ν, together with that part of the absorbed Lyman radiation which is re-emitted at frequency ν, per unit volume per unit solid angle, will be denoted by J_1. The energy source is situated at the side of the layer, i.e., the line of sight which we are considering does not encounter the source (cf. Paper I, Fig. 13, *b*). J_1 may vary with lateral distance from the source, but this variation will be neglected.

If J_2 is the re-emission per unit volume per unit solid angle, then the equation of transfer in the frequency ν is

$$\cos\theta \frac{dI}{dx} = -\alpha N_2 I + J_1 + J_2 , \tag{1}$$

where α is the coefficient of line absorption per atom for the transition $2 - n$ corresponding to frequency ν, and N_2 is the number of atoms per unit volume in level 2. Then

$$J_2 = \frac{\varpi_0}{4\pi} \int_0^{\pi} \int_0^{2\pi} \alpha N_2 I \sin\theta \, d\theta \, d\phi ,$$

[11] *B.A.N.*, **8**, 299, 1938.

[12] *Ap. J.*, **80**, 19, 1934; *Mt. W. Contr.*, No. 494.

[13] *Jap. J. Astr.*, **1**, 17, 1949; *Pub. Astr. Soc. Japan*, **4**, 1, 28, 1952.

where ϖ_0 is the fraction of all absorbed radiation which is re-emitted at the same frequency. Put $d\tau = -\alpha N_2 dx$, $\mu = \cos\theta$, $J_1/\alpha N_2 = D$. Then the equation of transfer becomes

$$\mu \frac{dI}{d\tau} = I - \frac{\varpi_0}{2}\int_{-1}^{+1} I(\mu')\, d'\mu - D. \tag{2}$$

Following the method developed by Chandrasekhar,[14] we replace equation (2) by the $2n$ equations

$$\mu_i \frac{dI_i}{d\tau} = I_i - \frac{\varpi_0}{2}\sum_j a_j I_j - D, \tag{3}$$

where the μ_i's ($i = \pm 1, \ldots, \pm n$) are the zeros of the Legendre polynomials $P_{2n}(\mu)$ and the a_j's ($j = \pm 1, \ldots, \pm n$) are the corresponding Gaussian weights.

The solutions to equation (3) are given by

$$I_i = \frac{D}{1-\varpi_0}\left\{\sum_{\alpha=1}^{n}\frac{L_\alpha e^{-k_\alpha\tau}}{1+\mu_i k_\alpha} + \sum_{\alpha=1}^{n}\frac{L_{-\alpha} e^{+k_\alpha\tau}}{1-\mu_i k_\alpha} + 1\right\}. \tag{4}$$

We shall consider solutions for τ infinite and τ finite.

a) τ INFINITE

In this case we have the boundary conditions that $I_{-i} = 0$ at $\tau = 0$. Also, since none of the I_i's increases more rapidly than $\exp(\tau)$ as $\tau \to \infty$, we can omit the terms in $\exp(+k_\alpha\tau)$. In this case the solution can be obtained in closed form. If we write

$$S(\mu) = \sum_{\alpha=1}^{n}\frac{L_\alpha}{1-\mu k_\alpha} + 1,$$

then, following exactly the procedure devised by Chandrasekhar (*ibid.*, chap. iii), we have

$$S(-\mu) = (1-\varpi_0)^{1/2} H(\mu).$$

Hence

$$I(0, \mu) = \frac{D}{(1-\varpi_0)^{1/2}} H(\mu), \tag{5}$$

and therefore

$$\begin{aligned} F(\tau = 0) &= 2\int_0^1 I(0, \mu)\, \mu d\mu \\ &= \frac{2D}{(1-\varpi_0)^{1/2}}\, \alpha_1, \end{aligned} \tag{6}$$

where α_1 is the first moment of the H function and has been tabulated by Chandrasekhar (*ibid.*, p. 328) for different values of ϖ_0.

b) τ FINITE ($= \tau_1$)

In this case we have the boundary conditions that $I_{-i} = 0$ at $\tau = 0$, and $I_{+i} = 0$ at $\tau = \tau_1$. In the second approximation $n = 2$ ($i = \pm 1, \pm 2$; $j = \pm 1, \pm 2$) we find, by

[14] *Radiative Transfer* (Oxford: Clarendon Press, 1950).

evaluating the constants L_a and L_{-a} from the boundary conditions and using $F = 2\Sigma a_i \mu_i I_i$, that

$$F(\tau = 0) = \frac{-4D}{\varpi_0 A_5}\left\{\frac{1}{k_1}(A_1 - A_3) + \frac{1}{k_2}(A_4 - A_2)\right\}. \tag{7}$$

In equation (7)

$$\begin{aligned}
A_1 - A_3 = (e^{k_1\tau_1} - 1)\{\, & e^{k_2\tau_1}(a_2 - b_2)(a_1 b_2 - a_2 b_1) + e^{-k_1\tau_1}(a_3 - b_3)(a_2 b_4 - a_4 b_2) \\
& + e^{-k_2\tau_1}(a_4 - b_4)(a_4 b_1 - a_1 b_4) + e^{(k_2 - k_1)\tau_1}(a_2 - b_2)(a_2 b_3 - a_3 b_2) \\
& + (a_1 - b_1)(a_4 b_2 - a_2 b_4) + e^{-(k_1 + k_2)\tau_1}(a_4 - b_4)(a_3 b_4 - a_4 b_3)\,\}\,; \\
A_4 - A_2 = (e^{k_2\tau_1} - 1)\{\, & e^{k_1\tau_1}(a_1 - b_1)(a_2 b_1 - a_1 b_2) \\
& + e^{-k_2\tau_1}(a_4 - b_4)(a_1 b_3 - a_3 b_1) + e^{-k_1\tau_1}(a_3 - b_3)(a_3 b_2 - a_2 b_3) \\
& + e^{(k_1 - k_2)\tau_1}(a_1 - b_1)(a_1 b_4 - a_4 b_1) + (a_2 - b_2)(a_3 b_1 - a_1 b_3) \\
& + e^{-(k_1 + k_2)\tau_1}(a_3 - b_3)(a_4 b_3 - a_3 b_4)\,\}\,; \\
A_5 = e^{(k_1 + k_2)\tau_1}(a_1 b_2 - a_2 b_1)^2 & + e^{-(k_1 + k_2)\tau_1}(a_3 b_4 - a_4 b_3)^2 - e^{(k_1 - k_2)\tau_1}(a_1 b_4 - a_4 b_1)^2 \\
& - e^{(k_2 - k_1)\tau_1}(a_2 b_3 - a_3 b_2)^2 + 2(a_3 b_1 - a_1 b_3)(a_4 b_2 - a_2 b_4)
\end{aligned} \tag{8}$$

where

$$\begin{aligned}
a_1 &= (1 - \mu_1 k_1)^{-1}, & a_2 &= (1 - \mu_1 k_2)^{-1}, \\
a_3 &= (1 + \mu_1 k_1)^{-1}, & a_4 &= (1 + \mu_1 k_2)^{-1}, \\
b_1 &= (1 - \mu_2 k_1)^{-1}, & b_2 &= (1 - \mu_2 k_2)^{-1}, \\
b_3 &= (1 + \mu_2 k_1)^{-1}, & b_4 &= (1 + \mu_2 k_2)^{-1},
\end{aligned} \tag{9}$$

and k_1^2 and k_2^2 are the roots of the characteristic equation

$$\frac{1}{\varpi_0} = \frac{a_1}{(1 - \mu_1^2 k^2)} + \frac{a_2}{(1 - \mu_2^2 k^2)}.$$

For $\tau_1 \gg 1$, equation (7) becomes

$$F(\tau = 0) = \frac{4D}{\varpi_0}\left\{\frac{1}{k_1} + \frac{1}{k_2} - \mu_1 - \mu_2\right\}. \tag{7a}$$

The flux computed from equation (7*a*) will not exactly agree with that computed from equation (6), since (7*a*) is the solution in the second approximation only.

We have evaluated $F(\tau = 0)$ for several values of ϖ_0 and τ_1. These resulting fluxes from the atmosphere are shown in Table 3. In this table, the values of F for $\tau_1 = 1$ and 5 have been derived from equation (7), while the values for $\tau_1 > 5$ are from equation (6).

If there is no self-absorption, the equation of transfer becomes

$$\mu \frac{dI}{d\tau} = -D'. \tag{10}$$

Equation (10) has been derived from equation (2) by putting the first and second terms on the right-hand side equal to zero and by replacing D by D'. Now D' represents the original Balmer emission only, since it is now assumed that no Lyman radiation is absorbed and hence none is re-emitted at Balmer frequencies. The relative values $D'(H\alpha)$ $D'(H\beta)$ are equivalent to the Balmer decrement given by Baker and Menzel.[8]

From equation (10) we find that the outward flux

$$F(\tau = 0) = 2\int_0^1 I(\mu)\,\mu d\mu = 2D'\tau_1 . \tag{11}$$

The equivalent width of the emission line whose central frequency is ν can be written as

$$w = 2K\int_0^{\Delta\nu} F_\nu(\tau = 0)\,d\nu ,$$

TABLE 3

VALUES OF THE FLUX AND f/τ_1

ϖ_0	τ_1	$F(\tau=0)$	f/τ_1
0.9	1	$2D\times 0.87$	0.87
	5	2.38	.48
	10	2.61	.26
	10^3	2.61	.0026
0.7	1	$2D\times 0.70$	.70
	5	1.17	.23
	10	1.24	.12
	10^3	1.24	.0012
0.5	1	$2D\times 0.58$	.58
	5	0.87	.17
	10	0.85	.085
	10^3	0.85	0.0009

where $\Delta\nu$ is half the total extent of the line, which is considered symmetrical, and K is a factor of proportionality. Thus

$$w = 2K\int_0^{\Delta\nu} 2Df\,d\nu , \tag{12}$$

where

$$f = \frac{a_1}{(1-\varpi_0)^{1/2}} \quad \text{(for case } a\text{, from eq. [6])}$$

and

$$f = \frac{-2}{\varpi_0 A_5}\left\{\frac{1}{k_1}(A_1 - A_3) + \frac{1}{k_2}(A_4 - A_2)\right\} \quad \text{(for case } b\text{, from eq. [7])} .$$

Similarly, the equivalent width, if there were no self-absorption, would be

$$w = 2K\int_0^{\Delta\nu} 2D'\tau_1 d\nu \quad \text{(from eq. [11])} .$$

Thus the cut-down factor due to self-absorption is given by

$$\frac{\int_0^{\Delta\nu} D f \, d\nu}{\int_0^{\Delta\nu} D' \tau_1 d\nu} . \tag{13}$$

The optical depth $\tau_1 = N_2 a x$. The shape of the outer atmosphere is known only very approximately, and N_2 is one of the unknown quantities of the problem. From Paper I (Sec. X) we may put $x \approx 2R_* \approx 10R_\odot$. As a first approximation, a value of N_2 can be obtained from the work of Baker and Menzel,[8]

$$N_2 = b_2 N_2^{(0)} ,$$

where $N_2^{(0)}$ is the population of level 2 in thermodynamic equilibrium at $T_e = 12{,}600°$. From the tables of Baker and Menzel we estimate that $b_2 \approx 0.009$, so that $N_2 = 5.66 \times 10^4$/cc.

The line-absorption coefficients for the centers of some Balmer lines were computed from the well-known formula. These values, together with the values of N_2 and x, give the following representative values:

$$\tau_1(H\alpha) = 1.7 \times 10^4 , \qquad \tau_1(H\zeta) = 1.3 \times 10^2 ,$$

$$\tau_1(H\beta) = 2.4 \times 10^3 , \qquad \tau_1(H22) = 5.0 .$$

For all except the very high members of the series, the optical depths can be considered infinite, as far as the fluxes determined from the transfer equation are concerned.

The line-absorption coefficient varies rapidly over the line width because of damping and kinetic Doppler broadening. However, the observed line width of the emission line is governed by the Doppler width, owing to mass motions, and this is much greater than that due to the kinetic Doppler motion. Consequently, we can use the value of a_{ν_0} for the center of the line to determine the effective optical depth.

From equation (13), the cut-down factor now becomes

$$\frac{\int_0^{\Delta\nu} D f(a_{\nu_0}) \, d\nu}{\int_0^{\Delta\nu} D' \tau_1(a_{\nu_0}) \, d\nu} = \frac{f(a_{\nu_0}) \int_0^{\Delta\nu} D d\nu}{\tau_1(a_{\nu_0}) \int_0^{\Delta\nu} D' d\nu} = \frac{\overline{D} f(a_{\nu_0})}{\overline{D'} \tau_1(a_{\nu_0})} . \tag{14}$$

Thus the cut-down factor is directly proportional to $1/\tau_1$ for large values of τ_1. Some values of $f(a_{\nu_0})/\tau_1(a_{\nu_0})$ are given in Table 3.

Although the values of τ_1 are uncertain, the ratios from line to line are known. The dependence of the cut-down factor on $1/\tau_1$ acts in the right sense to explain the large intensities of the high-level lines; but if this were the only term involved, then the lines from the lower levels would be cut down by much too large factors. If one assumes that $a_1 \overline{D} / \overline{D'}(1 - \varpi_0)^{1/2}$ decreases on going to higher levels, then the observed Balmer decrements could be explained.

IV. CONCLUSION

We have shown that the effect of self-absorption will be to produce an apparent Balmer decrement in Be stars, which can depart considerably from that given in the ideal case of a planetary nebula and may approach that actually measured for the stars studied here. However, it is not possible to calculate the Balmer decrement exactly without set-

ting up and simultaneously solving equations of transfer for radiation in all the frequencies. Lack of precise knowledge of the geometry of the outer atmosphere would lead to difficulties, even if the equations could be set up and solved. We have not considered the variation of the effective radiation field with distance from the source, which can be expected to change the ratio $a_1\bar{D}/\bar{D}'(1-\varpi_0)^{1/2}$. This will correspond to a varying dilution factor. Miyamoto[13] has shown that the $H\alpha$/$H\beta$ ratio is very sensitive to variations in the assumed dilution factor.

It is important to realize that, of the "pole-on" stars studied in Paper I, 48 Per, 105 Tau, 56 Eri, ω CMa, and β Psc did not show this anomalous Balmer decrement. The complete decrement is not measurable in these stars, since the emission lines are too faint to measure beyond $H\zeta$; but it would appear that if these lines are so faint as to be unobservable, then the Balmer decrement is nearer to the ideal nebular case. Although, for the purpose of estimating the self-absorption effects, the physical characteristics of the atmospheres of the four stars studied here have been considered to be similar, we do not know what physical conditions they have in common which cause them to emit relatively so much more energy in the high-level Balmer lines than do the other five stars mentioned above. They are not a very homogeneous group: 11 Cam is a typical "pole-on" star with single emission lines, HD 58050 has double emission lines with a fairly large separation, 12 Aur has shown considerable changes in a three-year interval, and HD 37998 probably has a variable spectrum, to which a unique type cannot be assigned.

Since many of the Be stars show atmospheric variations with time, as measured by total emission strengths, for example, it will be important to look for possible changes in the Balmer decrement with time.

We are indebted to Dr. S. Chandrasekhar for helpful discussions of the transfer problem. We wish to thank Dr. W. W. Morgan for information about these stars. We are also grateful to Dr. G. R. Miczaika for letting us examine one of the Heidelberg spectrograms of 12 Aur, taken in March, 1949.

SPECTROGRAPHIC OBSERVATIONS OF SV CAMELOPARDALIS*

W. A. HILTNER
Yerkes and McDonald Observatories
Received April 29, 1953

ABSTRACT

The velocity-curve of SV Camelopardalis is given. $P = 0^d5930713$, $\gamma = -13$ km/sec, $K = 123$ km/sec, $e = 0.0$ (assumed), $a \sin i = 1.0 \times 10^6$ km, $f = 0.118\odot$.

In the 1952 *Preliminary Report of the International Astronomical Union*, interest was expressed in spectrographic observations of the eclipsing variable SV Camelopardalis. Since spectrograms of this star were available at the McDonald Observatory, they were measured and are herewith published. The star was originally placed on the McDonald spectrographic program because of the reported increase in total light shortly before primary minimum.[1] Both spectrographic and photometric observations were made.

The spectrograms—forty-seven in number—were obtained with the Cassegrain spectrograph, using two glass prisms and the 180-mm Schmidt camera. The dispersion is 76 A/mm at $H\gamma$. Usually, seven stellar lines were measured for radial velocity. These lines, with their assumed wave lengths, are as shown in the accompanying tabulation.

Identification	Adopted λ	Identification	Adopted λ	Identification	Adopted λ	Identification	Adopted λ
Fe I	4005.26	*Fe* I	4063.61	*Fe* I blend	4143.74	*Sc* II, *Fe* I	4325.76
Fe I	4045.83	*Hδ*	4101.75	*Ca* I	4226.74	*Fe* I	4383.56

The plate numbers, the Julian days of the observations, the phases, and the observed radial velocities are recorded in Table 1. The phases were computed from the formula

$$\text{Zero phase} = \text{Primary minimum} = \text{JD } 2432287.6261 + 0^d5930713E\,.$$

A period different from that previously employed was introduced in order to satisfy the photometric observations to be discussed later.

A detailed analysis of the velocity-curve in Figure 1 does not appear to be warranted at this time. A graphical solution gives the following elements:

$P = 0^d5930713$, $e = 0.0$ (assumed),
$\gamma = -13$ km/sec, $a \sin i = 1.0 \times 10^6$ km,
$K = 123$ km/sec, $f = 0.118\odot$.

The spectral class of the primary star was classified by Wyse[2] as dG3. This classification is confirmed, except that the primary may be somewhat above the main sequence. No classification of the secondary is available, although a spectrum was taken at primary eclipse. The brighter and larger star still dominates the spectrum at the annular

* *Contributions from the McDonald Observatory, University of Texas*, No. 226.

[1] F. B. Wood, *Pub. Princeton U. Obs.*, **21**, 41, 1946.

[2] *Lick Obs. Bull.*, **17**, 37, 1934.

TABLE 1

RADIAL VELOCITIES OF SV CAMELOPARDALIS

Plate No. G//2	JD 2432000+	Phase (Period)	Velocity (Km/Sec)	Plate No. G//2	JD 2432000+	Phase (Period)	Velocity (Km/Sec)
9324	244.582	0.423	− 70.8	9545	275.670	0.841	+ 87.3
9343	248.680	.333	−104.9	9546	275.689	.874	+ 73.4
9351	252.589	.924	+ 40.6	9615	284.590	.882	+ 62.3
9352	252.623	.981	+ 22.0	9616	284.608	.912	+ 42.3
9353	252.662	.047	− 69.0	9617	284.631	.951	+ 41.8
9354	252.702	.114	− 94.9	9618	284.663	.005	− 22.7
9355*	252.742	.182	−117.9	9619	284.696	.060	− 82.4
9356	252.776	.239	−138.4	9620	284.719	.099	− 88.1
9357	252.812	.300	−125.8	9621	284.738	.131	−105.6
9383	256.577	.648	+ 75.2	9622	284.756	.162	−115.6
9384	256.603	.692	+105.0	9623	284.776	.195	−129.9
9385	256.628	.734	+108.3	9679	293.690	.226	−150.3
9386	256.646	.764	+112.7	9680	293.712	.263	−145.5
9427	259.583	.717	+102.2	9681	293.735	.301	−131.9
9443	263.580	.456	− 46.7	9682	293.756	.337	−118.0
9444	263.603	.495	− 21.9	9697	295.594	.436	− 54.3
9445	263.626	.534	+ 10.0	9698	295.615	.471	− 51.1
9446	263.648	.571	+ 44.5	9699	295.633	.502	− 12.8
9447	263.669	.606	+ 56.3	9700	295.653	.535	− 7.3
9448	263.690	.642	+ 77.6	9701	295.676	.574	+ 11.6
9504	269.752	.863	+ 85.8	9702	295.709	.630	+ 77.2
9505	269.771	.895	+ 67.2	9703	295.749	0.697	+ 85.1
9515	270.732	.515	− 9.4				
9516	270.753	.551	+ 33.1				
9544	275.651	0.809	+104.9				

* Weak Ca II K emission.

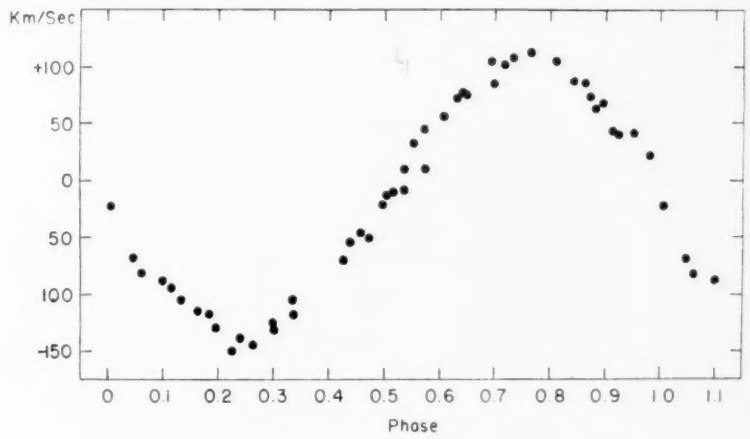

FIG. 1.—Velocity-curve of SV Camelopardalis

primary eclipse. The lines are broadened by rotation, and the velocity-curve gives some evidence of a rotation effect.

The photometric observations are not reported in detail, since no filter was employed with the 1P21 receiver. However, a few remarks should be made. The light-curve gives strong evidence at secondary minimum of irregular surface brightness similar to that reported by Kron[3] for AR Lacertae. Also, the secondary eclipse is significantly more shallow than that reported by Wood.[4] Four primary eclipses were observed as follows:

JD 2432253.8188, JD 2432265.6821, JD 2432268.6479, JD 2432287.6261.

These minima, with the first one receiving low weight, were combined with the available observed minima during 31,000 epochs to give the period recorded above. The difference

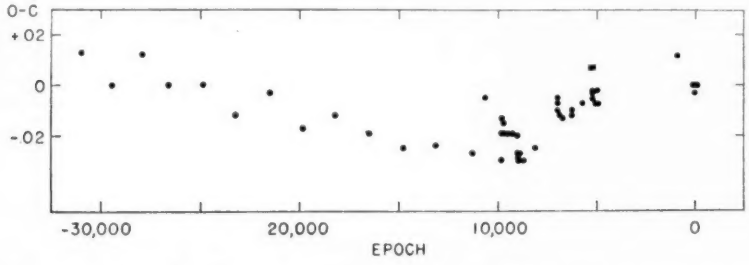

FIG. 2.—Plot of the observed *minus* the computed time of minimum (fraction of period) for the observed minima.

between the observed and the computed times of minima for the primary eclipses recorded by Wood[4] and the four above are shown in Figure 2. The elements given above represent the early and the current observations satisfactorily. However, because of a variable period,[5] the differences between the observed and the computed times of minima decrease to −0.025 (fraction of period) at JD 2425.500. An increase in total light shortly before primary minimum was not confirmed.

[3] *Pub. A.S.P.*, **59**, 261, 1947.

[4] *Ibid.*, p. 40.

[5] N. L. Pierce, *Pub. Princeton U. Obs.*, **18**, 3, 1938.

HD 50169, A SPECTRUM VARIABLE WITH EMISSION AT *Hα*

KENNETH R. W. BREWER
University of London Observatory*
Received February 27, 1953

ABSTRACT

A series of medium-dispersion spectrograms of HD 50169 is described and wave-length measures given. Emission at *Hα* is variable. The star has abnormally strong absorption lines of *Sr* II, *Cr* I, *Cr* II, and *Eu* II. An unidentified line at λ 4172 and possibly the lines of *Ti* II are variable. Other peculiarities include a group of fairly strong absorption lines which may originate from the ground state of *Co* I. Comparison is made with the rather similar spectrum variable 73 Draconis.

The peculiarities of HD 50169[1] were not recognized at the time of its inclusion in the *Henry Draper Catalogue*, where it is assigned the spectral type A2.

Merrill and Burwell, detecting variable emission at *Hα* and strong absorption lines of *Sr* II, included the star in the *Second Supplement* to their Mount Wilson *Catalogue* of Be and Ae stars[2] with the remark, "This star deserves further investigation." In order to make this possible, a series of eight spectrograms, taken with the 60-inch telescope and one-prism spectrograph by William C. Miller, was loaned to the University of London Observatory for measurement and analysis by the author.

TABLE 1*

THE RECORD OF OBSERVATIONS OF HD 50169

PLATE NO.	DATE (U.T.)	EXPOSURE TIME (MIN.)	CAMERA (INCH)	EXPOSURE† AT		EMULSION
				Hγ	*Hα*	
γ27497	1946 Mar 11.17	50	9	g	g	103*a*-E
γ28132	Oct. 20.49	20	9	o	O	103*a*-E baked
γ28162	Nov. 9.48	100	18	U	u	103*a*-E
γ28167	10.48	150	18	U	u	103*a*-E
γ28243	1947 Jan. 2.30	60	9	g	g	103*a*-E
γ28248	3.24	90	9	u	g	103*a*-E
γ28292	11.34	120	18	u	...	IIa-O
γ28296	12.30	240	18	g	..	IIa-O

* Dispersion using 9-inch camera = 78.6 A/mm at *Hγ*, 340 A/mm at *Hα*. Dispersion using 18-inch camera = 36.2 A/mm at *Hγ*, 162 A/mm at *Hα*.

† In these columns the following notation has been used: "U" = very badly underexposed; "u" = underexposed; "g" = well exposed; "o" = overexposed; "O" = very badly overexposed.

Table 1 shows the observer's record and the emulsion used for each spectrogram.

I. GENERAL CHARACTERISTICS OF THE SPECTRUM

If no account is taken of the emission at *Hα*, the star can be regarded as a typical member of a certain peculiar sequence of A-type stars described by Morgan,[3] containing

* Now at Commonwealth Observatory.

[1] HD 50169 = BD−1°1414 = MWC 823; 1900 R.A., 6h46m9s; dec., −1°32′; mag., 8.9.

[2] *Ap. J.*, **78**, 87, 1933; **98**, 153, 1943; **110**, 387, 1949.

[3] *Ap. J.*, **77**, 330, 1933.

stars with abnormally strong absorption lines of *Sr* II, *Cr* I with *Cr* II, singly and doubly ionized rare earths, *Si* II with the unidentified λ 4200 group, or *Mn* II, respectively. (Individual stars in this sequence are thus termed "strontium stars," "chromium stars," etc.; and, since the groups shown above tend to overlap, there are also "strontium-chromium stars," "strontium-chromium-europium stars," etc. Some confusion exists concerning a general term to cover all these stars, since the commonest term, "peculiar A stars," can also be used to describe this group and the metallic-line stars together. Mary Lee Woods, in some unpublished material, refers to the former as "enhanced-line stars," which name will be used throughout this paper.)

HD 50169, then, is a strontium-chromium-europium star and shows a strong resemblance to 73 Draconis, which has been studied in detail by Morgan,[4] using spectrograms of comparable dispersion. In common with many other stars of this type, both HD 50169 and 73 Draconis have variable spectra and a *Ca* II K line weak for their spectral type (A2). However, the writer was unable to find any enhanced-line star, other than HD 50169, which showed emission at *Hα* or any other line.

Most of the information about the absorption lines was derived from the spectrograms taken with IIa-O emulsion, for all the other six suffered from one or more of the following faults: overexposure, underexposure, narrowness of spectrum, and poor quality of emulsion. Unfortunately, the only spectrogram showing definite emission was so underexposed that the only observable line in the normal photographic region was *Hγ*, while the only other plate showing even doubtful emission was still more underexposed. Variability was made difficult to detect by the fact that the interval between the exposures of the two IIa-O plates was only 1 day.

For the radial velocity relative to the sun the spectrogram γ28296 gave $+23.0 \pm 0.9$ km/sec, and γ28292 gave $+22.2 \pm 1.3$ km/sec. Combining these values, we obtain $+22.8 \pm 0.7$ km/sec. The values derived from other spectrograms are far less reliable but do not differ significantly from this velocity. The wave lengths given in Table 4 are corrected for a value of +22.7 km/sec obtained in an earlier estimate.

The average probable error of the wave lengths in Table 4 is 0.14 A if measured on γ28292, 0.10 A if seen on γ28296, and 0.08 A if seen on both. A stain in the emulsion of γ28292 in the 4100–4200 A region distorted the apparent wave lengths by up to $\frac{1}{3}$ A. This was corrected by reference to the corresponding region in γ28296.

II. THE HYDROGEN LINES

In all the spectrograms taken with 103*a*-E emulsion, there is a strong absorption line at *Hα*. The radial velocity of this line, even when no emission is present, has measured values varying from +74 km/sec on October 20, 1946, to −217 km/sec on January 2, 1947. The numerical value of these variations is large compared with the probable error of measurement, for there can be no blending and a displacement of 0.004 mm, corresponding to about 65 km/sec on the spectrograms of low dispersion, is easily detectable. On November 10, 1946, there was a strong undisplaced emission line with a less strong absorption line having a measured velocity of −414 km/sec, part of which velocity is probably spurious and due to the filling-in by emission of the red absorption wing. The structure of the *Hα* region on the various spectrograms is shown in Table 2 (emission lines are marked "e" and some very doubtful components by ":"). The apparent variation in the intensity of the absorption component, with the exception of that in γ28167, can be entirely accounted for by the different qualities of the spectrograms.

It is interesting to note that this variation in radial velocity is entirely confined to the *Hα* line. (The measurement of *Hγ* in γ28167, over 1 A to the violet of the expected position, can be given no weight, on account of the breadth of the line and the extreme underexposure of the spectrogram in all save the *Hα* region.) Since the absorption coefficient

[4] *Ibid.*, p. 77.

in main-sequence A-type stars is dominated by ionization of hydrogen in the Paschen continuum, it increases considerably with wave length, and at *Hα* only the upper layers of the atmosphere can be seen. The evidence is, then, that these are moving more or less as a whole (for otherwise the absorption line would be vague and ill defined), with highly variable velocity of the order of +75 to −200 km/sec, and that a strong emission line can develop from nothing in the course of a day or so. Since on November 10, 1946, the emission line was undisplaced and the absorption line to the violet, it appears likely that in this case the outer atmosphere was behaving like an expanding shell, the absorption line arising from that part of the shell between the observer and the star, while the emission was coming mainly from the annulus beyond the star's limb.

The other hydrogen lines were normal for an A2 star. In γ28296 the *Ca* II H line was seen in the wing of *Hε*; however, in both the H*a*-O spectrograms of the stars an unidentified line at λ 4344 was observed in the wing of *Hγ*.

TABLE 2

THE *Hα* LINE

Plate No.	Date	Intensity and Appearance	Radial Velocity (Km/Sec)
γ27497	1946 Mar. 11	9	− 81
γ28132	Oct. 20	8	+ 74
γ28162	Nov. 9	9	+ 8
		4e::	−306
		2::	−469
γ28167	10	4::	+384
		8e	− 10
		6	−414
γ28243	1947 Jan. 2	9	−217
γ28248	3	11	− 43

III. OTHER ELEMENTS

Identification in the spectrum of HD 50169 was largely carried out by reference to previous identifications in related stars. The most useful papers for this purpose were Morgan's on 73 Draconis,[4] Hiltner's on β Coronae Borealis,[5] Frost, Struve, and Elvey's on ε Aurigae,[6] and Morgan's on 13 A-type stars.[7] Multiplet tables by Miss Moore[8] and Allen[9] were used extensively. Reference was also made to the lists of wave lengths found in A-type stars prepared by the Wavelength Sub-committee of Commission No. 30 (Stellar Radial Velocity) of the I.A.U.[10]

In the following discussion comparison is made with the very similar star 73 Draconis. This latter was compared, by Morgan, with ε Serpentis,[4] of which a study had been made by himself and Miss Farnsworth.[11] At that time it (ε Serpentis) was thought to be a normal A2 dwarf, but Morgan, Keenan, and Kellman have since classified it as a metallic-line star, with the *Ca* II K line indicating a spectral type of A2 and the other metallic

[5] *Ap. J.*, **102**, 438, 1945.

[6] *Pub. Yerkes Obs.*, Vol. **7**, Part II, 1932.

[7] *Pub. Yerkes Obs.*, Vol. **7**, Part III, 1935.

[8] *Princeton Obs. Contr.*, No. 20, 1945.

[9] *Commonwealth Obs. Mem.*, No. 5, 1934.

[10] *Trans. I.A.U.*, **4**, 188, 1932.

[11] *Ap. J.*, **76**, 299, 1932.

lines the type A7.[12] On the other hand, 73 Draconis is, like HD 50169, an enhanced-line (strontium-chromium-europium) star.

The intensities in Table 4 are eye estimates on a scale of 10. No direct comparison could be made between Morgan's intensities in 73 Draconis and the writer's in HD 50169, but comparison was made between the recorded intensities of several of the medium and strong lines (chiefly of iron and chromium) in the two stars. No significant difference between the two scales was detected, but the possibility that the lines of the one star are uniformly stronger than those of the other cannot be excluded.

No reference is made by Morgan to *O* I, *Al* II, *Si* I, *S* II, *Ti* I, *Mn* II, or *Co* I in his study of 73 Draconis.[4] It may be safely assumed that lines of these elements are very faint or absent in that star.

O I.—This line is never strong in the photographic region of the spectra of A stars. In the infrared region Keenan, Hynek, and Deutsch[13] and later Slettebak[14] showed that *O* I is particularly weak in enhanced-line stars. No real evidence for the presence of this atom could be found in HD 50169, but λ 4368 may contribute to a blend.

Mg I.—All the *Mg* I singlets numbered from (12) to (21) in Miss Moore's *Revised Multiplet Table*[8] were seen in γ28296, but only λ 4167 was seen in γ28292. *Mg* I is about as strong as in 73 Draconis.

Mg II.—The strong doublet at λ 4481 is of intensity 8 on both the II*a*-O spectrograms. Morgan assigns an intensity 10 to this line in 73 Draconis. A few fainter lines are present in both stars.

Al I.—The presence of the ultimate doublet at λ 3944 and λ 3962 is very doubtful in both stars.

Al II.—Three multiplets—(45), (46), and (47)—may contribute to blends of moderate intensity. *Al* II is weak, if present.

Si I.—It is impossible to say definitely whether *Si* I is present or not or to estimate its strength. The evidence suggests that a considerable portion of the line of intensity 8 at λ 3906 is due to neutral silicon. The line λ 4103 is masked by *Hδ*, and there are no other lines in the observable region to shed any further light on the problem.

Si II.—This is present in considerable strength at λλ 3854, 3856, 3863, and again at λλ 4128–4131. The line at λ 4131 is unblended and that at λ 3856 nearly so. Their intensities are 5–6, and 8 respectively. *Si* II is definitely stronger in this star than in 73 Draconis and probably even stronger than in *β* Coronae Borealis.

S II.—The strongest multiplet, (44) in Miss Moore's table, is definitely absent. Multiplet (49) is less definitely absent, but the cumulative evidence is sufficient for one to conclude that no substantial portion of any blended line is attributable to *S* II.

Ca I.—The ultimate line at λ 4227 is a doubtful contributor to a blend. It is remarkably weak in HD 50169, weaker than in 73 Draconis.

Ca II.—The K line is of intensity 9, that is to say, as strong as λ 4233 of *Fe* II and slightly weaker than the strong *Sr* II doublet. By comparing with photographs of other spectra, the ratio of this line to *Hε* + *Ca* II H is similar to that of B8 or B9 stars. The H line is readily visible in the wing of *Hε*, and *Ca* II is not so weak as in 73 Draconis.

Sc II.—Five lines, λλ 4247, 4314, 4321, 4325, and 4374 all probably contribute to blends and shadings of lines of moderate intensity. *Sc* II may also contribute to a broad line at λ 4400. No trace is seen of λ 4416. *Sc* II is faint in HD 50169: its presence in 73 Draconis is doubtful.

Ti I.—May be present in HD 50169, but, if so, it is very faint.

Ti II.—This ion is responsible for a number of fairly strong lines in HD 50169, including λ 3901 of intensity 7. There is also a strong *Fe* II–*Ti* II blend at λ 4550, intensity 8. No change is observed in the intensity of the *Ti* II lines between the two II*a*-O spectro-

[12] *Atlas of Stellar Spectra* (Chicago: University of Chicago Press, 1943).

[13] *Ap. J.*, **111**, 1, 1950. [14] *Ap. J.*, **113**, 437, 1951.

grams, but they cannot be seen on the 103*a*-E plates, though they should be sufficiently strong for observation on the four taken with the 9-inch camera. The evidence is not conclusive but strongly suggests that *Ti* II is variable in intensity, as also in several enhanced-line stars, such as 73 Draconis, α^2 Canum Venaticorum, and possibly ϵ Ursae Majoris.[15]

V II.—This ion is almost certainly absent. In 73 Draconis it is doubtfully present.

Cr I.—Chromium and iron together are responsible for the great majority of lines in both stars. The intensity and excitation of *Cr* I in HD 50169 are comparable with the corresponding values in 73 Draconis.

Cr II.—As with *Cr* I, excitation and intensity are comparable with 73 Draconis. Both are very high.

TABLE 3

COMPARISON OF INTENSITIES OF *Fe* I LINES IN 73 DRACONIS GIVEN BY MORGAN AND IN HD 50169 ON JANUARY 12, 1947

Laboratory Wave Length (A)	Intensity in 73 Draconis	Intensity in HD 50169	Excitation Potential of Lower Level (Volts)
4005.25	6	8	1.56
4260.49	6	Blended, 4	2.40
4045.82	5	6	1.49
4235.94	5	5	2.42
4181.76	5	3	2.83
4227.43	5	3	3.33
4202.03	4	4	1.49
4063.60	4	6	1.55
4156.80	3–4	3	2.82
3948.78	3	Blended, 5	2.18
4282.41	3	1	2.18
4447.72	3	3	2.22
4104.14	3	Masked, *Hδ*	3.26
4147.68	2–3	Absent	1.49
4067.98	2–3	Blended, 5	3.21
4118.56	2–3	3	3.58
4219.36	2–3	2	3.58
4383.55	2	Blended, 6	1.49
4404.75	2	2	1.56
3997.40	2	5	2.73
3951.17	2	Absent	3.27
4149.37	2	Absent	3.33
4264.21	2	Absent	3.36

Mn I.—The ultimate lines at λλ 4030, 4033, and 4034 are present, and others at λλ 4036–4041. Blending with lines from other elements is almost certain in every case. A group of lines in this region appears abnormally strong on γ28292. This may be due to some fault in the emulsion or to some variable and unidentified multiplet.

Fe I.—There is a sufficient number of *Fe* I lines in both stars to construct a table comparing intensities. The recorded differences can be largely explained by the fact that the writer has tended to overestimate intensities in underexposed regions. When this has been allowed for, the evidence, which on the surface points to a lower excitation temperature in HD 50169, becomes of little significance. All but the faintest lines of *Fe* I unblended in 73 Draconis are contained in Table 3.

[15] Deutsch, *Ap. J.*, **105**, 283, 1946.

Fe II.—Quite strong in both stars, λ 4233 being among the strongest lines in their respective spectra.

Co I.—Miss Moore's tables indicate that five strong lines originating from the ground state of *Co* I are present in the normal photographic region. These are λ 4191 and λ 4252 in multiplet (1) and λλ 3910, 3980, and 4027 in multiplet (3). There are lines in HD 50169 at all five of these wave lengths, and λ 3910 (intensity 6) and λ 4027 (intensity 5) have no satisfactory alternative identification. The intensities of the other three star lines are compatible with their having a contribution from *Co* I. No trace could be found of other *Co* I lines. If present, it is at an exceedingly low excitation temperature.

Ni I.—There is a weak line in the spectrum at λ 4714; but, even if this is due to *Ni* I, the neutral nickel spectrum must be very weak in HD 50169. Despite a line of intensity 5 at λ 4714, Morgan considered the presence of *Ni* I in 73 Draconis to be very doubtful.

Ni II.—The presence of *Ni* II is very doubtful in both stars.

Sr II.—After the hydrogen lines, those of *Sr* II are the strongest in the spectrum. There is no great difference between the intensities of the two most important lines, as there is in 73 Draconis. (Anomalous intensities such as this are, however, not absent from HD 50169; in the *Cr* I spectrum, in particular, this phenomenon caused considerable difficulty in identification. It is common in enhanced-line stars.)

As well as the strong ultimate doublet, fainter lines are also seen at λ 4161 and λ 4305.

Y II.—Weaker than in 73 Draconis. All the lines which appear most conspicuous in A-type stars are weak, blended, or absent.

Zr II.—A few lines in Table 4 are ascribed to *Zr* II, but the strong multiplet $a^2F - z^2F^\circ$ is absent. Nearly all the suspected *Zr* II lines derive from the a^2P and a^2D levels. *Zr* II is absent from 73 Draconis.

Ba II.—Absent from HD 50169; presence in 73 Draconis very doubtful.

La II.—Probably absent from both stars.

Singly ionized rare earths.—The *Eu* II lines are about as strong as in 73 Draconis but not so strong as in β Coronae Borealis or HD 125248. A peculiar feature is the absence of λ 4130: this is an example of the phenomenon, referred to above in the discussion of *Sr* II, of anomalous intensities within multiplets. The lines λ 4436 and λ 4523 were apparently present on January 11, 1947, and absent the following night.

Because of the relative weakness of *Eu* II in this star as compared with β Coronae Borealis, the comparative faintness of other rare-earth spectra in the latter star and the small dispersion available compared with that used by Hiltner,[5] the only other rare-earth spectra investigated were those of *Ce* II and *Gd* II. The presence of both these ions in HD 50169 is very doubtful. None of the rare-earth elements is able to account for the residue of lines for which the identifications remain unsatisfactory.

IV. UNIDENTIFIED LINES

Some of the lines for which the identifications given in Table 4 are inadequate play such an important role in this spectrum that it was considered desirable to discuss them in the text rather than as notes to a table.

λλ *4034, 4036, 4038, 4039, 4040, 4041, 4043.*—These lines are all stronger in γ28292 than in γ28296. In some cases the identifications shown are quite sufficient to explain the intensity in the latter plate, but inadequate for that in the former. In the discussion of *Mn* I above, two explanations are put forward. If there is, indeed, an extensive flaw in the emulsion at this wave length, it is not easily detectable. More good-quality spectrograms are needed before any conclusion can be drawn.

λ *4172.*—Although the identifications given are sufficient to explain the intensities recorded for the two H*a*-O spectrograms, the remarkable strength of this line on the four plates taken with the 9-inch camera is not accounted for. Apart from *Hα*, this is the only line to provide indisputable evidence that the spectrum is variable. On January 2 and 3, 1947, it was the most outstanding feature of the spectrum after the hydrogen lines. If the

TABLE 4

λ	No.	Int.[1]	Int.[2]	Ident.
3853.99	1	-	5i	Si II 3.66 Cr I 4.22 Ti I
55.97	1	-	8	Si II 6.02 Fe I 6.37 Cr I
59.53	2	-	8n	Mg I 9.24 Fe I 9.91 Fe I
62.51	1	-	6N	Si II 2.59 Fe II Cr II Ti I
63.70	1	-	4	Fe II 3.41 Fe II 3.95
65.49	1	-	7r	Cr II 5.59 Fe I 5.53 Cr II 6.01
			RW	Cr II 6.54 Ti I
72.67	2	-	7v	Fe I 2.50
			VW	Fe I 1.75
74.75	1	-	6N	Cr I 4.57 Ti I Fe I Cr II Cr II Ti I
78.42	2	-	8nv	Mg I 8.58 Fe I 8.58 Fe I
			VW	Fe I 8.02
88.50	2	-	H	H_8 9.05
97.68	1	-	6N	Ti I 5.24 Fe I 5.66 Fe I 7.90 Cr II Cr II Gd II Fe I
3900.68	1	-	7	Ti II 0.55 Fe I 9.71
02.72	2	-	6	Fe I 2.95
03.74	1	-	7	Fe I 3.90 Mg I 4.02
05.75	1	-	8	Si I 5.53 Cr II 5.64 Fe II 6.04 Cr II
06.96	1	-	4i	Eu II 7.10 Fe I
3908.06	1	-	5i	Cr I 7.78 Fe I 7.94 Cr I
09.72	1	-	6	Co I 9.93 Fe I
11.57	2	-	7n	Cr II 1.32 Cr I 1.95 Ti I
10.83) to 17.59)	1	-	9N	(Ti II 3.46 (Zr II 5.94 (Fe I 6.73 (Ce II Ti I (Fe II Ti I (Cr I Gd II
18.83	1	-	7n	Fe I 8.64 Cr I 9.16 Fe I Fe I
20.52	1	-	7n	Fe I 0.26 Ti I
23.22	1	-	6N	Fe I 2.91
25.86	2	-	6N	Fe I 5.65 Fe I 5.95 Ti I
			VW	Ti I 4.53
27.91	2	-	6	Fe I 7.92
30.44	2	-	7	Fe I 0.30 Eu II 0.50 Y II Cr II
32.09	1	-	4:	Ti II 2.01 Fe I 2.63
33.62	3	-	9	Ca II 3.66
35.79	3	-	6	Fe II 5.94 Fe I 5.82
36.96	1	-	5	Cr II 6.95 Fe I 7.33
38.59	3	-	7n	Fe II 8.97 Fe II 8.29 Mg I 8.40
41.22	1	-	5	Fe I 0.88 Fe I 1.28
43.0:	2	-	7N	Fe I 2.44 Al I 4.01
44.81	1	-	5	Fe I 4.89 Fe I 5.12 Cr II

TABLE 4 – Continued

λ	No.	Int.[1]	Int.[2]	Ident.
3948.27	2	-	5nI	Fe I 7.53 Fe I 8.11 Fe I 8.78 Ti I
52.38	2	-	6	Cr I 2.40 Fe I 2.61
56.62	2	-	6	Fe I 6.46 Fe I 6.68 Fe I 7.03 Ti I
58.43	1	-	5n:	Zr II 8.24 Cr I 8.08 Ti I 8.21
68.32	1	-	8i	Ca II 8.47 Fe I Fe I
70.03	4	-	H	Hε 0.07
76.46	2	-	7	Cr I 6.67 Fe I 6.62 Cr I
77.81	1	-	5	Fe I 7.74
79.28	2	-	6	Cr II 9.51 Co I 9.52 Cr I Cr I
81.88	2	-	6N	Fe I 1.78 Ti I 1.76 Ti II Ti I Y II
84.02	2	-	7	Cr I 3.91 Fe I 3.96 Cr I
86.09	2	-	5n	Fe I 6.18 VW Fe I 5.39 RW Mg I 6.75
89.87	2	-	5	Cr I 9.99 Ti I 9.76
91.30	3	-	5R	Cr I 1.12 Zr II 1.14 Cr I RW Cr I 2.85
94.12	1	-	5	Cr I 3.97 Fe I
95.95	1	-	4:	Al II 5.86 Fe I 6.00 Al II 6.16 Al II 6.38 Co I
3997.35	2	-	5r	Fe I 7.39 RW Fe I 8.05
98.85	1	-	3N:	Ti I 8.64 Cr I 8.85 Zr II 8.98 Ce II
4002.35	5	7i	6N:	Cr I 1.44 Cr II 2.48 Cr II 3.33 Fe I Fe II Fe II Ti I Cr I
05.04	4	8n	8	Fe I 5.25
06.89	4	6n	7	Fe I 6.31 Cr II 7.04 Fe I 7.28
09.53	1	-	3n:	Fe I 9.71 Ti I 8.93
12.43	4	-	8	Cr I 2.49 Cr II 2.50 Ti II Ce II Fe II
14.64	2	-	2i::	Fe I 4.53 Cr I 4.67
17.86	3	-	7v	Cr II 7.96 Fe I 8.28 Ti I Mn I VW Fe I 7.16
19.95	1	-	2n::	Unid.
22.22	4	-	7	Fe I 1.87 Cr I 2.26 Cr II 2.36
24.80	4	-	7n	Fe II 4.55 Fe I 4.74 Ti I Ti II
27.08	2	6	5	Co I 7.03 Cr I
28.35	1	-	6	Ti II 8.33
30.48	3	9	9	Mn I 0.76 Fe I 0.50 Cr II Ti I
32.89	4	6i	7	Mn I 3.07 Fe I 2.64 Fe II 2.95

TABLE 4 – Continued

λ	No.	Int.[1]	Int.[2]	Ident.
4034.18[X]	2	6	3	Mn I 4.49 Ti I Ti I (Unid.)
35.83[X]	2	6	2nI::	Unid. Mn I Ti I
37.83[X]	3	8ni	4	Cr II 8.03 (Unid.)
39.10[X]	2	8	3	Cr I 9.10 (Unid.)
40.07[X]	1	6:	-	Unid.
41.46[X]	2	7n:	6	Unid. Mn I
42.77[X]	3	5	2:	Unid. Ce II La II
44.05	2	-	3i:	Cr I 3.70 Fe I 3.90 Fe I 4.61
45.79	3	7:	6v	Fe I 5.82 Zr II
46.90	2	8	4	Unid.
48.88	4	9	7	Cr I 8.78 Cr II 9.14 Fe II
51.76	2	7	5	Cr II 1.97 Fe I
53.75	3	9n	6	Cr II 4.11 Cr II 3.45 Ti II 3.81
55.91	1	-	2::	Cr II 6.07 Mn I Ti II
57.39	1	-	1I::	Fe II 7.46 Mg I 7.51
61.74	2	6::	5	Cr II 1.77
63.71	4	8	6	Fe I 3.60 Cr II 3.94 Fe I
67.72	2	-	5N	Fe I 7.98 Fe I 6.98 Cr II 7.05 Fe I 7.28
70.72	1	-	5	Cr II 0.90 Fe I 0.77 Cr I 1.00
72.57	2	-	5	Cr II 2.56
4074.76	1	-	1::	Fe I 4.79
75.73	2	-	5	Cr II 5.63 Cr I 6.06 Ce II Ce II
77.59	6	10	10	Sr II 7.71 Cr II Cr I
79.47	1	-	2:	Mn I 9.24 Mn I 9.42 Ti I 9.71 Fe I 9.85
81.27	1	-	2:	Cr II 1.21
82.11	1	-	3	Cr II 2.30
83.54	1	-	3	Mn I 3.63 Ce II
85.56	2	-	5n	Fe I 5.01 Fe I 5.31 Cr II 6.14 Gd II
87.43	1	-	2:	Fe II 7.27 Cr II 7.63
89.20	1	-	2i::	Cr II 8.90 Cr II 9.49
92.95	1	-	1::	Cr I 3.06
4101.89	6	H	H	Hδ 1.74
09.38	1	-	3	Cr I 9.58
11.06	4	-	6	Cr II 1.01 Cr I Cr I Cr I
12.89	2	-	6	Cr II 3.24 Cr II Fe I
15.09	1	-	1I::	Unid.
16.77	2	-	2i:	Cr II 6.66
18.56:	5	-	3)	(Fe I 8.55
19.65:	2	-	3)	(Fe II 9.53
22.73	3	-	6	Fe II 2.64 Fe I Ti I Fe I Ti I
28.19	4	-	8N	Cr II 7.08 Si II 8.05 Fe II 8.74 Cr I 9.21 Ti I Fe I Cr I Fe I

TABLE 4 – Continued

λ	No.	Int.[1]	Int.[2]	Ident.	λ	No.	Int.[1]	Int.[2]	Ident.
4130.96	4	6	5	Si II 0.88 Cr I	4177.75	3	-	3	Y II 7.54 Fe I
32.30	3	8	7	Fe I 2.06 Cr II 2.41	79.35	5	8r	5	Fe II 8.86 Cr I 9.26 Cr II 9.43
34.67	3	5:	2i	Fe I 4.68					Cr I Cr II
35.67	1	5:	-	Unid. Cr II Fe I	81.64	1	-	3n	Fe I 1.76 Cr II 1.50
42.28	1	21::	-	Cr I 2.19	84.50	1	-	4	Cr I 4.90 Fe I 4.90
43.61	4	6	5v	Fe I 3.42 Fe I 3.83 Fe I 3.87 Cr I					(Unid)
					87.10	2	-	5	Ce II 6.60 Fe I 7.04 Fe I 7.80
45.95	5	6	6	Cr I 5.77 Cr I 6.20	91.23	6	5:	4nI	Co I 0.71 Fe I 1.44 Cr I
51.30	2	-	2N::	Cr II 1.00 Fe I					
					93.71	1	-	2:	Cr I 3.66
54.20	4	-	4	Fe I 3.91 Fe I 4.50 Fe I 4.81 Cr I	95.41	5	7ir	6	Cr II 5.41 Cr I 4.95 Fe I 5.34
								RW	Fe I 6.22
56.75	1	-	3n	Fe I 6.80	98.47	6	8	7	Fe I 8.31 Cr I 8.53 Fe I 8.65 Fe I 9.10
58.98	1	-	3	Fe I 8.80					
61.55	5	7	6	Cr I 1.42 Sr II 1.80 Cr II Cr II	4200.65	3	5n:	3	Cr I 0.10 Fe I 0.93
63.60	2	6	4	Ti II 3.64 Cr I	02.16	3	3::	4	Fe I 2.03
65.51	2	5	2i:	Cr I 5.52	03.97	1	-	1::	Fe I 3.99
67.25	2	5r	2:	Mg I 7.27	05.33	3	4i::	5	Eu II 5.05 Fe I
70.57	4	5nv	5	Cr I 0.20 Cr II 0.58 Cr II 0.86 Fe I 0.91	07.21	2	-	2i::	Cr I 6.90 Fe I 7.13 Cr II 7.35
72.02[X]	6	2::	5R	Unid. Cr I 1.68 Ti II 1.90 Cr II 1.92 Fe I 2.13	09.32	2	6n	4n	Cr II 9.02 Cr I 9.37 Cr I 9.76 Cr II
				Cr II 2.60 RW Fe II 3.45	11.40	1	4n:	-	Cr I 1.35
75.44	1	-	0::	Cr I 5.23 Fe I 5.64	13.29	1	3:	-	Cr I 3.18 Fe I 3.65

TABLE 4 – Continued

λ	No.	Int.[1]	Int.[2]	Ident.
4215.53	6	6i	10	Sr II 5.52 Cr II
17.59	5	5	4	Fe I 7.55 Cr I 7.63
19.08	2	3N	2i::	Fe I 9.36
21.95	3	4	3n	Cr I 1.57 Fe I 2.22
				Cr I 2.73 Cr II
24.44	5	5r	4n	Cr II 4.85 Fe I 4.18
				Cr I 4.51 Cr II Fe I
			RW	Fe I 5.46 Fe I 5.96
27.39	3	6	3n	Fe I 7.43 Al II 6.83
				Al II 7.51 Al II 8.00
				Ca I Cr II
29.94	2	4N	5n	Cr II 9.81 Cr I 0.48
31.80	1	1::	-	Unid.
33.26	6	8	9	Fe II 3.17 Cr II 3.25
				Fe I 3.61 Cr II
36.04	3	7n	5n	Fe I 5.94 Cr I Cr II
39.10	3	-	4n	Fe I 8.82 Cr I 8.96
				Cr II Fe I
42.55	4	8	7	Cr II 2.38
44.35	1	-	2n:	Cr I 4.33
46.20	5	6N	4ir	Fe I 5.26 Fe I 6.09
				Cr II 6.41
			RW	Sc II 6.83 Fe I 7.43
50.43	3	8	6	Fe I 0.13 Fe I 0.79
52.62	3	5	6	Co I 2.30 Cr II 2.62
54.45	3	7	6	Cr I 4.35
4255.99	2	5	2	Cr II 6.16 Ti I Fe I
58.09	5	4I	4	Zr II 8.05 Fe II 8.16
59.18	4	2:)	4n	(Cr I 9.15
60.45	4	5)		(Fe I 0.48
61.85	3	5i	3	Cr I 1.62 Cr II 1.92
				Cr II
63.78	1	-	0::	Cr II 3.49 Fe II 3.90
				Cr II 4.19
66.28	1	-	0:	Cr II 6.23
69.13	3	6	6	Cr I 8.79 Cr II 9.28
				Cr II
71.41	3	8	5	Fe I 1.16 Fe I 1.76
				Cr I
73.40	2	7r	4	Fe II 3.32
74.6:	2	4n)	5	(Cr I 4.80
75.71	2	3::)		(Cr II 5.57 (Cr I 5.97
78.06[X]	2	6	5	Unid. Cr II Fe II Ti I
80.33	2)	6N	(2	Cr II 0.33 Cr I 0.41
82.57	2)		(1v:	Fe I 2.41 Ti I 2.70
84.13	2	5i::	5	Cr II 4.21
88.18	1	-	2i:	Fe I 8.15
89.90	4	8	6	Cr I 9.72 Ti II 0.22
91.99	1	-	2:	Cr I 1.96
94.08	1	-	1:	Ti II 4.10 Fe I 4.13
96.67	3	4:	3	Fe II 6.57
98.19	1	3i::	-	Cr I 7.74 Fe I
99.90	3	4I:	6	Ti II 0.05 Cr I

TABLE 4 – Continued

λ	No.	Int.[1]	Int.[2]	Ident.
4303.26	3	4v	5	Fe II 3.17
			VW	Ti II 1.93
05.45	3	4	4	Sr II 5.45
				Cr I Fe I
07.91	3	4	4	Ti II 7.90
				Fe I 7.91
09.50	2	5	4	Fe I 9.38
				Y II 9.62
10.59	1	1I::	-	Unid.
12.94	2	5	4	Ti II 2.86
				Fe II
15.06	3	5v	5	Ti II 4.98
				Fe I 5.09
			VW	Sc II 4.08
				Fe II 4.29
17.12	1	-	1:	Zr II 7.32
				Ti II 6.81
18.97	1	-	3	Ti I 8.63
				Cr II 8.77
21.07	2	4ni	5i	Sc II 0.75
				Cr I Ti II
				Cr I Ti I
23.55	1	4ni	-	Cr I 3.52
25.54	3	7	7	Fe I 5.77
				Sc I 5.01
30.52[x]	2	5i	4	Unid. Ti II
				Ti II
37.69	1	-	4::	Ti II 7.92
				Cr I 7.57
40.55	7	H	H	Hγ 0.47
44.04[x]	2	8:	7	Unid.
51.85	3	-	5n	Fe II 1.76
				Mg I 1.89
				Mg I 1.91
				Cr I Cr I
				Fe I
54.33	2	-	2	Cr I 3.98
				Mg I 4.54
				Fe II
57.31	1	-	4nr	Cr I 7.53
				Fe II 7.57
			RW	Fe I 8.51
4360.3:	1	-	5N	Cr I 9.63
				Cr I 9.99
				Fe II 1.25
63.21	2	3i::	2i::	Cr II 2.93
				Cr I 3.13
65.34	1	5I::	-	Cr I 4.87
67.83	3	4nI::	4	Fe I 7.58
				Ti II 7.66
				Cr I 8.25
71.06	3	-	4:	Cr I 1.28
74.81	4	4ni:	4n	Sc II 4.46
				Y II 4.94
				Cr II
77.12	2	3i::	3n	Cr I 6.80
				Cr I 7.55
80.51	2	-	3n	Mg I 0.38
84.87	4	8N	6n	Fe I 3.55
				Fe II 5.38
				Mg II Cr I
91.33	2	6n	3n	Mg II 0.59
				Fe I 0.95
				Ce II 1.66
				Cr I 1.75
95.09	2	5N	3n	Ti II 5.03
				Cr I 5.42
97.88	1	4i:	-	Cr I 7.25
				Y II 8.02
4400.47	2	5n	-	Ti II 9.77
				Sc II 0.36
				Fe I 1.29
03.09	2	6	-	Fe II 2.88
				Cr I 3.37
				Cr I 3.50
04.85	2	6	2:	Fe I 4.75
08.50	1	5N	-	Fe I 7.71
				Cr I 7.72
				Fe I 8.42
				Mg I 9.84
11.26	1	3n	-	Ti II 1.08
				Cr I 1.09
14.02	2	5n	5n	Cr I 3.87
17.25	2	4N	4	Fe II 6.82
				Ti II 7.72

TABLE 4 – Continued

λ	No.	Int.[1]	Int.[2]	Ident.
4419.41	1	–	4	Cr I 9.10
22.77	2	6	5	Fe I 2.57 Cr I 2.70 Cr I 3.32 Y II
25.74	1	2i:	–	Unid.
27.46	2	5i:	3	Fe I 7.31 Mg II 8.00
30.38	3	7	4	Cr I 9.94 Cr I 0.49 Fe I 0.62
32.31	2	3:	–	Fe I 2.57
33.53	2	5	2	Fe I 3.22 Fe I 3.79 Cr I 3.97 Mg II 3.99
36.32	1	4d	–	Eu II 5.58 (Unid.)
43.35	2	6N	4d	Fe I 3.20 Ti II 3.80
47.38	1	–	3n:	Fe I 7.72
50.61	1	–	3n:	Ti II 0.49 Fe II 1.55 Fe I
58.45[X]	2	5	3nV	Cr I 8.54 Fe I
			VW	Unid.
61.70	2	6	5	Fe I 1.65 Fe I 1.99 Fe I
65.20	2	4n	12N	Cr I 4.67 Cr I 4.91 Cr I 5.15 Cr I 5.36 Cr II 5.78 Cr I 6.17 Fe I 6.55 Ti I Fe I
69.19	2	4:		Ti II 8.49 Fe I 9.38
72.90	2	5		Fe II 2.92 Fe I
75.98	3	5I:		Cr I 5.35 Fe I 6.02 Fe I 6.08
78.61	1	3N:	–	Unid.
4481.30	5	8	8	Mg II 1.13 Mg II 1.33 Ti I Cr I
89.19	3	3ni	2i:	Fe II 9.19 Ti I 9.09
91.82	3	3n	1:	Fe II 1.40 Cr I 1.68 Cr I 2.31
94.37	2	4n	1::	Fe I 4.57
96.05	1	–	1::	Ti I 6.15
4500.71	1	–	3	Cr I 0.30 Cr I 1.11 Ti II 1.27
04.23[X]	1	–	3	Cr II 4.52 (Unid.)
07.43	2	5n:	4	Cr I 6.85 Fe II 8.28 Cr II
12.14	2	4nI	2:	Cr I 1.90 Cr II
15.64	2	7n	6	Fe II 5.34 Cr I 5.44 Cr II
22.85	1	3	–	Eu II 2.59 Fe II 2.63
24.08	1	4n	–	Fe I 3.40 Cr I 4.84
26.14	1	–	3n	Cr I 6.11 Cr I 6.47
29.60	2	–	2n:	Cr I 9.85
34.10	2	4:	4	Ti II 3.97 Fe II 4.17
40.29	2	6n	5d	Cr II 9.62 Cr I 0.72 Cr I Cr I
45.35	3	4N	3n	Cr I 4.62 Cr II 4.70 Cr I 5.34 Cr II 5.49 Ti II Cr I
49.66	3	8	8	Fe II 9.47 Ti II 9.62 Fe II

TABLE 4 – Continued

λ	No.	Int.[1]	Int.[2]	Ident.
4552.36	2	2i	2:	Ti I 2.45
55.44	2	7	7	Cr II 5.02 Fe II 5.89 Cr I
58.72	4	8	8	Cr II 8.66 Cr II
62.14	1	4i	-	Ce II 2.36
63.85	2	5	-	Cr I 3.66 Ti II 3.76 Cr I 4.17
64.74	1	-	5d VW	Same as the line above
			RW	Cr II 5.78
71.94	2	5	5	Ti II 1.97 Cr I 1.83
75.15	1	-	1::	Cr I 5.12
76.86	1	-	3I::	Fe II 6.33
80.11	2	3:	3i::	Fe II 0.06 Cr I 0.06
83.28	2	4N	5	Fe II 3.83 Fe II 2.84 Al II
88.15	2	4	5	Cr II 8.22 Al II
90.1:	1	3N	-	Al II 9.75 Cr II 9.89 Cr II 0.00
92.08	3	4	2	Cr II 2.09 Cr I 2.54
95.90	2	4n	2:	Cr I 5.59 Fe I 6.06
4600.94	2	3N:	2I::	Cr I 1.02 Cr I 1.15
05.36	1	3N:	-	Unid.
11.15	1	3N:	-	Fe I 1.29
16.51	2	5	5	Cr II 6.64
19.14	1	6N	4	Cr II 8.83 Fe I Cr I Fe II 0.51
20.75	1			
21.95	1		3	Cr I 1.89 Cr I 1.96

λ	No.	Int.[1]	Int.[2]	Ident.
4625.73	2	5n	3:	Cr I 5.93
29.69	1	-	3i	Fe II 9.34
34.33	1	-	4	Cr II 4.11
38.21	2	2::	2	Fe I 8.02
46.70	2	3:	3ir	Cr I 6.50 Cr I 6.81
			RW	Fe I 7.44
55.94	1	-	4d	Fe I 4.63 Cr I 4.74 Cr I 6.19 Cr I 6.84
63.80	2	3	2	Cr I 3.33 Cr I 3.83
66.67	2	2::	3	Cr I 6.22 Cr I 6.51 Fe II 6.75 Cr I 7.18
70.22	1	-	3	Sc II 0.40 (Unid.)
73.11	2	2:	3	Fe I 3.17
89.83	1	-	2	Cr I 9.37 Fe I 0.15
98.71	2	3:	2	Cr I 8.46 Cr I 8.62 Cr I 8.95 Cr I 9.59
4701.62	1	-	1::	Unid.
08.38	2	3:	2n:	Cr I 7.75 Cr I 8.04 Fe I 9.09
14.47	1	-	3n:	Ni I 4.42
23.81	1	-	1::	Cr I 4.42 Cr I 3.06 Cr I 3.18
27.08	1	-	1i::	Cr I 7.15 Fe I 7.41
31.26	2	3n	4	Cr I 0.71 Fe II 1.44
37.50	2	5nir	4	Cr I 7.35 Fe I 6.78
55.24	1	-	4N	Cr I 6.11 Mn I 4.04

TABLE 4 – Continued

λ	No.	Int.[1]	Int.[2]	Ident.
4759.00	1	-	1:	Unid.
61.64	1	-	21	Cr II 1.42
65.40	2	1::	4	Unid.
79.77	1	2::	-	Unid.
83.53	1	2::	-	Mn I 3.42
89.99	1	-	2	Fe I 9.65
4805.34	1	-	2	Cr I 5.24
24.26	2	5	3	Cr II 4.13 Mn I
48.77	1	-	3	Cr II 8.24
52.26	1	-	2	Cr I 1.47
61.33	6	H	H	Hβ 1.33
71.72	1	-	2:	Fe I 1.32
75.98	1	-	4	Cr II 6.41
86.25	2	-	6N	Y II 3.69 Cr II 4.57 Cr I 4.95 Cr I 5.96 Cr I 7.01 Fe I Gd II Fe I Ti I Fe I
4911.26	1	-	5N	Cr II 2.49 Fe I Ti II Fe II Ti I
21.10	2	6N	6N	Fe I 9.00 Fe I 0.51 Cr I 0.95 Cr I 2.27 Fe II 3.92 Ti I Cr II Ti I
84.27	1	-	3	Fe I 2.51 Fe I 3.26 Fe I 3.86 Fe I 5.26 Cr II
90.82	1	-	31	Fe I 8.96 Fe I 1.28
94.65	1	-	31	Unid.
5004.87	1	-	4N	Fe I 1.87 Fe I 2.80 Fe II 4.26 Cr I 4.38 Fe I 5.72 Fe I 6.13 Fe I
18.69	1	-	3	Fe II 8.43
22.21	1	-	1::	Fe I 2.24
6562:	6	-	-	Hα 2.82 See Table 2

NOTES TO TABLE 4

The columns show (1) the wave length; (2) the number of spectrograms on which the line was observed, either distinctly or as part of a blend; (3) the intensity in γ28292 ("Int.[1]"); (4) the intensity in γ28296 ("Int.[2]"); and (5) the identifications.

The wave length given is, where possible, the mean of the wave lengths measured on the two II*a*-O spectrograms; but where a line has been measured on only one of these, that wave length is given, measures on the 103*a*-E spectrograms being ignored throughout. With the exception of *Hα*, all lines invisible on the II*a*-O plates were seen on one spectrogram only and could in each case easily be explained away as defects in the emulsion; such lines have consequently been omitted. The superscript "x" following a wave length indicates that there is a note on the line in Section IV of the text.

In the intensity columns, "n" = nebulous, "i" = irregularity in the emulsion, "d" = double, "r" = shaded to red, "v" = shaded to violet, ":" = doubtful, "::" = very doubtful, and "H" = hydrogen line (very strong and broad). Other capital letters, such as "N" and "I," indicate that the nebulosity, irregularity, etc., are very pronounced.

Identifications include the element, the stage of ionization, and the laboratory wave length as given in Miss Moore's *Revised Multiplet Table* (*Princeton Obs. Contr.*, No. 20, 1945). The predominant contributor (if any) is listed first and underlined. Then follow the other important contributors in order of increasing wave length. Minor contributors are indicated by the element and stage of ionization alone and are also listed in order of increasing wave length. Lines entirely or mainly unidentified are marked "Unid.," while others which may have an unidentified component are marked "(Unid.)." "VW" and "RW" precede the identification of the violet and red wings of a given line, respectively.

Ti II lines are indeed variable, they change out of phase with λ 4172. A number of stars in the *Henry Draper Catalogue* have this line prominent, including the strontium stars HD 110066, HD 125335, and ω Herculis (=HD 148112).

λ *4278.*—Line, intensity 5, at this wave length in 73 Draconis.

λ *4330.*—Line, intensity 3, at this wave length in 73 Draconis.

λ *4344.*—This coincides closely with a wave length observed in manganese stars at the other end of Morgan's sequence. It is a strong laboratory line of *Mn* II, noted for being comparatively weak in such stars.[16] A few lines in HD 50169 do coincide in wave length with some of the lines observed in manganese stars, but these can all be sufficiently explained by alternative identifications.

λ *4458, violet wing.*—Line, intensity 2–3, at 4457 A in 73 Draconis.

λ *4504.*—The line is 0.3 A to the violet of the suggested identification both in this star and in 73 Draconis.

V. CONCLUSIONS

This star has much in common with 73 Draconis. The relative intensities of the strongest lines of *Sr* II, *Cr* I, *Cr* II, *Eu* II, *Fe* I, *Fe* II, and *Ti* II are about the same in each star, and they share unidentified lines at λλ 4278, 4330, 4457, and possibly 4504.

Deutsch[15] records that the *Eu* II and *Ca* II lines and possibly λ 4423 vary in phase with the *Ti* II lines in 73 Draconis. In HD 50169 the spectrograms taken with the 9-inch camera, in which the *Ti* II lines do not appear, are not of sufficient quality to record the comparatively faint *Eu* II lines, whether they vary in phase with *Ti* II or not; little weight can be placed on the nonappearance of λ 4423, and the K line seems no weaker than usual. There is no evidence that λ 4423, strong and variable in 73 Draconis, is in any way abnormal in HD 50169.

Other points of difference are the peculiar nature of the *Hα* line, the slight relative weakness of *Mg* II λ 4481, the somewhat greater strength of *Si* II, the presence of a group of lines which appear to originate from the ground state of *Co* I, the strength of *Sr* II λ 4078, the weakness of *V* II, the possible presence of *Zr* II, the absence of *Eu* II λ 4130, a strong variable unidentified line at λ 4172, and another strong unidentified line at λ 4344.

The writer received financial support during the course of this research from a London County Council Scholarship and the Coopers' Company's Jubilee Exhibition. The spectrograms on which the research was based were taken by Mr. William C. Miller and loaned by Mount Wilson and Palomar Observatories. The writer is also indebted to Dr. E. M. Burbidge, Professor R. W. B. Pearse, and Professor C. W. Allen for supervising various stages of his work.

[16] Morgan, *Ap. J.*, **73**, 104, 1931.

VARIATION IN LIGHT OF THE SPECTRUM VARIABLE 56 ARIETIS*

SANFORD S. PROVIN
Yerkes Observatory
Received April 13, 1953

ABSTRACT

Observations at three effective wave lengths, λλ 5500, 4400, and 3550, show amplitudes of variation of 0.04, 0.06, and 0.06 mag. respectively. The observations give a period of 0.728 day for the light-variation.

The star 56 Arietis (5.65 mag.) is designated as A0p in the *Henry Draper Catalogue;* its noted peculiarity is a feature at λ 4129. Deutsch[1] found that lines of *He* I vary in intensity and that the changes are periodic.[2]

The photometric observations reported here were made with the 13-inch reflector of the McDonald Observatory. An RCA 1P21 multiplier was used as the light-sensitive element of the photometer. Observations were made at three effective wave lengths: λ 5500, isolated by a Corning 3384 filter; λ 4400, isolated by a Corning 5030 and a Schott GG-13 filter; and λ 3550, isolated by a Corning 9863 filter.

In this work, two comparison stars were used. They were HR 944 (B9; 5.60 mag.) and HR 945 (A0; 6.38 mag.). The former was used for most of the comparisons with 56 Ari, and HR 945 was observed only occasionally as a check on HR 944.

Scattered observations made in 1951 at Yerkes Observatory indicated that either there were large errors in the observations or the period of 2.563 days given by Deutsch[2] did not apply to the total light. It was found that a period of 0.64 day[3] was in better agreement with the observations than 2.563 days. The possibility of a short period was investigated during the months of November and December, 1952. Observations made in this interval show that the period of light-variation is less than 1 day with the following elements:

$$\text{Light-minimum} = \text{JD } 2434355.806 + 0.728E.^{4}$$

The observations are compiled in Table 1, where the dates of the observations are in universal time. The phases were calculated according to the period above, with November 6.000 U.T. taken arbitrarily as zero phase. The magnitude difference 56 Ari *minus* HR 944 is given for the yellow, blue, and ultraviolet observations and also for $B-V$ and $U-B$. Only the observations made in the yellow are given for the comparisons of HR 944 with HR 945.[5] The observations are plotted against phase in Figure 1.

* *Contributions from the McDonald Observatory, University of Texas*, No. 225.

[1] *Ap. J.*, **105**, 296, 1947.

[2] *Ap. J.*, **105**, 503, 1947.

[3] The reciprocal period less than 1 day which can be derived from the period 2.563 days is 0.72 day.

[4] At the December, 1952, meeting of the American Astronomical Society, Deutsch announced a similar period for the spectral variations.

[5] In combining individual comparisons into an observational point, the mean of the comparisons made during intervals of about ½ hour has been taken. Since HR 944 was observed as frequently as 56 Ari, the number of comparisons (equal to the number of observations of 56 Ari) per interval is 4 or 5. From the comparisons of HR 944 with HR 945 (all single comparisons), the mean error of a single comparison is about ±0.005 mag. for the yellow and ±0.006 mag. for the blue and ultraviolet. It is estimated, therefore, that the mean error of each observational point is ±0.0025 mag. for the yellow and ±0.003 mag. for the blue and ultraviolet.

TABLE 1

PHOTOMETRIC OBSERVATIONS OF 56 ARI

DATE U.T. 1952	PHASE ($P = 0.4728$)	56 ARI *minus* HR 944					HR 945 *minus* HR 944
		V	B	U	$B-V$	$U-B$	
Nov. 6.218	0.299	0.044	−0.182	−0.510	−0.226	−0.328	0.182
.290	.398	.044	− .175	− .515	− .219	− .340	.184
11.226	.179	.039	− .194	− .510	− .233	− .316	.182
.358	.360	.036	− .186	− .515	− .222	− .329	.179
12.321	.683	.072	− .149	− .479	− .221	− .330	.182
15.277	.743	.071	− .143	− .462	− .214	− .319	.196
19.277	.238	.044	− .185	− .506	− .229	− .321	.182
20.267	.598	.048	− .178	− .507	− .226	− .329	.182
27.135	.032	.034	− .198	− .513	− .232	− .315	.186
Dec. 1.175	.581	.049	− .171	− .499	− .220	− .328	.178
.333	.798	.062	− .151	− .452	− .213	− .301	.188
2.083	.828	.069	− .158	− .455	− .227	− .297	.182
.216	.011	.038	− .190	− .497	− .228	− .307	.182
.350	.195	.036	− .194	− .510	− .230	− .316	.185
4.100	.599	.051	− .174	− .503	− .225	− .329	.183
.179	.707	.070	− .147	− .459	− .217	− .312	.187
5.039	.894	.059	− .161	− .452	− .220	− .291	. . . . .
.065	.924	.059	− .168	− .454	− .227	− .286	.182
.091	.960	.047	− .183	− .479	− .230	− .296	. . . . .
.117	.996	.038	− .188	− .491	− .226	− .303	.185
.142	.030	.037	− .198	− .504	− .235	− .306	. . . . .
.168	.066	.027	− .198	− .514	− .225	− .316	.186
.196	.104	.028	− .208	− .513	− .236	− .305	. . . . .
.219	.136	.033	− .203	− .517	− .236	− .314	.191
.267	.202	.036	− .190	− .509	− .226	− .319	. . . . .
.287	.229	.035	− .197	− .512	− .232	− .315	.181
.314	.266	.046	− .182	− .505	− .228	− .323	. . . . .
.340	.302	.046	− .185	− .511	− .231	− .326	.185
.366	.338	.042	− .183	− .507	− .225	− .324	. . . . .
.398	.382	.037	− .193	− .502	− .230	− .309	.189
8.076	.061	.033	− .200	− .518	− .233	− .318	.186
.104	.099	.031	− .211	− .513	− .241	− .302	.184
9.075	.432	.031	− .196	− .527	− .227	− .331	.180
.194	.596	.044	− .177	− .509	− .221	− .332	. . . . .
.286	.722	.072	− .148	− .470	− .220	− .322	.185
.306	.750	.071	− .149	− .457	− .220	− .308	. . . . .
.325	.775	.070	− .142	− .454	− .212	− .312	.180
10.065	.792	.068	− .142	− .439	− .210	− .297	. . . . .
.150	.909	.052	− .165	− .469	− .217	− .304	.192
.170	.936	.054	− .170	− .472	− .224	− .302	. . . . .
.280	.088	.030	− .198	− .513	− .228	− .315	.181
.297	.112	.031	− .206	− .508	− .237	− .302	.188
15.196	.840	.068	− .147	− .459	− .215	− .312	.187
.289	.968	.048	− .182	− .483	− .230	− .301	.192
16.075	.048	.040	− .199	− .500	− .239	− .301	.195
.120	.110	.035	− .204	− .516	− .239	− .312	.190
24.065	.023	.038	− .194	− .494	− .232	− .300	.192
.106	.080	.030	− .205	− .510	− .235	− .305	.196
.154	.146	.032	− .195	− .512	− .227	− .317	.186
.202	.212	.047	− .189	− .510	− .236	− .321	.187
.244	0.269	0.040	−0.187	−0.509	−0.227	−0.322	0.175

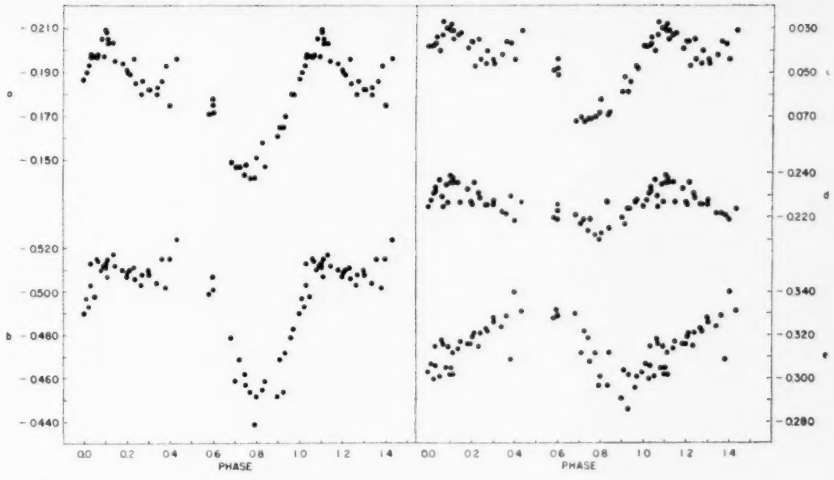

FIG. 1.—56 Ari *minus* HR 944: *a*, $\lambda_{\text{eff}} = 4400$; *b*, $\lambda_{\text{eff}} = 3550$; *c*, $\lambda_{\text{eff}} = 5500$; *d*, $B-Y$; *e*, $U-B$

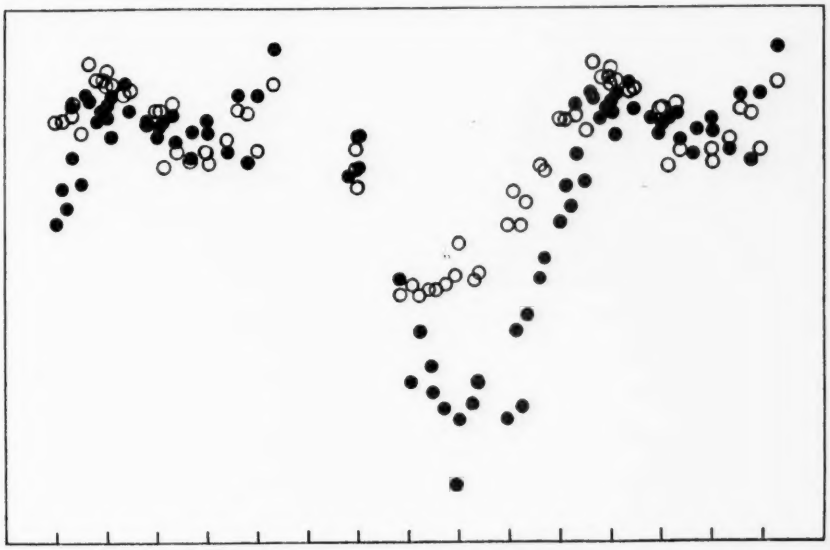

FIG. 2.—The yellow observations are shown by the open circles; the ultraviolet, by the filled circles

The observations show that 56 Arietis varies in light with an amplitude of 0.04 mag. in the visual and 0.06 mag. in the blue and ultraviolet. The depth of the minima in the blue and ultraviolet does not appear to repeat, whereas in the yellow the minima are in good agreement. The observations give evidence for a second minimum near phase 0.3. The color change $B-V$ is 0.02 mag., and the change in $U-B$ is about 0.04 mag. The star is bluest at phase 0.1 and most ultraviolet at phase 0.5.

A feature of the light-curves is a delay in the time at which the ultraviolet reaches minimum as compared to the yellow. The minimum in the ultraviolet occurs about 0.04 later in phase than the minimum in the yellow. In Figure 2 the ultraviolet and the yellow observations are superposed. The shift then becomes quite evident.

The phase shift is such that the star remains relatively faint in the ultraviolet, while the blue and yellow have recovered. This suggests that absorption due to hydrogen may be involved. It is noted that the phase shift found here is in the sense opposite to the shifts found by Stebbins[6] for δ Cephei.

In conclusion, I wish to thank Dr. W. A. Hiltner for helpful suggestions in the preparation of this paper.

[6] *Ap. J.*, **101**, 47, 1945.

A STATISTICAL STUDY OF THE ROTATION OF THE STARS*

SU-SHU HUANG†
Berkeley Astronomical Department, University of California
Received December 16, 1952; revised February 2, 1953

ABSTRACT

The line widths in the spectra of about 1550 stars have been measured on Lick plates, and a simple procedure for converting the line width to the rotational velocity is advanced. The results of our measurements, given in Tables 1 and 2, have been compared with the results by other authors. Some statistical data, such as the frequency distribution, the mean value, etc., which can be derived from the present measurements are also given. We have also discussed the problem of the correlation between the space motion and the rotational motion of the stars.

I. INTRODUCTION

A systematic study of the rotation of the stars was first carried out by G. Shajn and O. Struve. In their paper[1] we can also find a summary of the earlier investigations on the subject. Meanwhile, O. Struve and C. T. Elvey[2] initiated the quantitative spectroscopic study of a line contour broadened by rotation. A survey of the spectra of stars of various types shows[2] that, although rapid rotation is peculiar to the earliest spectral classes, a number of spectroscopic binaries of later types, such as the W Ursae Majoris stars, rotate rapidly. Subsequently, several authors have investigated the problem in one way or another; among them we should mention C. Westgate,[3] E. van Dien,[4] and A. Slettebak.[5]

In the present paper we shall give some observational results concerning the rotational velocities measured at the Lick Observatory. Our investigation is an extension of the work of Miss Westgate. She had used Yerkes single-prism spectrograms with a linear dispersion of 30 A/mm at λ 4500, and had measured 275 O and B stars, 413 A stars, and 112 F stars. The Lick (three-prism and two-prism) plates which we have used were taken for the radial-velocity program and have already been described in great detail elsewhere.[6] The three-prism plates have a linear dispersion of 10.4 A/mm (at Lick) and 13.3 A/mm (at the Chile station) at λ 4481, and the two-prism plates have a linear dispersion of 26.5 A/mm at the same wave length. Hence the instrumental broadening is much smaller for the three-prism plates than for the one-prism or the two-prism plates. The result derived from the three-prism plates would therefore seem to be the most trustworthy.

Next we consider the problem of calibration of the line width measured directly on the photographic plate. As the standard for calibration, Westgate used the values of the rotational velocities derived from a line-profile study.[2] This would be a good method, provided that one had obtained a fairly well-defined curve of calibration. As a matter of

* The observational material used in the present investigation was contained in the large collection of spectrograms at the Lick Observatory.

† A part of the present investigation was performed when the author was a Guggenheim Fellow during the academic year 1951–1952.

[1] *M.N.*, **89**, 222, 1929.

[2] *M.N.*, **91**, 663, 1931; C. T. Elvey, *Ap. J.*, **70**, 141, 1929; **71**, 221, 1930; O. Struve, *Ap. J.*, **72**, 1, 1930.

[3] *Ap. J.*, **77**, 141, 1933; **78**, 46, 1933; **79**, 357, 1934.

[4] *J.R.A.S. Canada*, **42**, 249, 1948.

[5] *Ap. J.*, **110**, 498, 1949.

[6] J. H. Moore, *Pub. Lick Obs.*, Vol. **18**, 1932.

fact, the calibration points are so scattered that it is difficult to draw a definite calibration-curve. Moreover, the accuracy involved in the determination of rotational velocities by the line-profile study is itself subject to some uncertainties.[1, 2] We shall therefore introduce a new method for converting the measured width into the rotational velocity.

Let us first define a fictitious line without rotational broadening as the line that would be recorded on the photographic plate, were the star concerned to stop its rotation completely but to remain the same otherwise. Hence this fictitious line is broadened by all the physical processes in the stellar atmosphere (except, of course, the rotation) as well as by the instrument. Let $\Delta\lambda_I$ be half the average width of this fictitious line. If the intrinsic stellar line (before it is broadened by the rotation) is narrow compared with the width of the instrumental broadening, $\Delta\lambda_I$ can be regarded as half the average width of a weak comparison line. Further, let $\Delta\lambda_R$ be the rotational width:

$$\Delta\lambda_R = \frac{\lambda}{c}\,\xi_r \sin i\,. \tag{1}$$

For convenience we put $\beta = \Delta\lambda_R / \Delta\lambda_I$. Denoting by v the wave length in the unit of ΔI_λ and by x that in the unit of $\Delta\lambda_R$, we have $v = \beta x$.

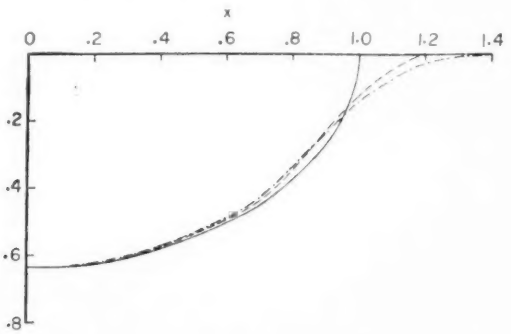

FIG. 1.—Line profiles broadened by fast rotation ($\beta = 5$). The different profiles are drawn according to the different forms of the original line: (1) an infinitely narrow line (the solid curve, i.e., a pure rotational profile); (2) a rectangular line of finite width (the broken line); and (3) a line having the form of a triangle (the broken line with dots). The abscissa is plotted in units of the rotational width; hence the greater the rotation, the more the broadened profiles approach the pure rotational contours, no matter what the shape of the original line. In other words, an absorption line of a rapidly rotating star always has a pure rotational profile. We have plotted the profiles in the figure in such a way that the areas bounded by them are all unity. Compressing these curves everywhere vertically by a constant factor, one can obtain a series of profiles representing lines of different strengths broadened by the same amount of rotation.

In Figure 1 are plotted final profiles, assuming the fictitious line without rotational broadening to be rectangular and triangular, respectively. For comparison the pure rotational profile also has been drawn. From the figure we can see that the relevant parts of the three contours are nearly the same. For convenience of comparison we have normalized the equivalent width of all the three contours to unity in the x-scale instead of in the v-scale (in which it would be observed). Since we are ultimately interested only in the relative slope of the line profile, the normalization makes no difference to our argument. Now the measurement of the line width by a measuring machine is determined by the apparent visual edge of the absorption line on the photographic plate, and the apparent visual edge of the absorption line might be expected to be approximately the place where the density of the plate declines most rapidly. Hence it depends not only on

the true contour of the line but also on the characteristic curve of the photographic plate. In any case the apparent visual edge of the line must be somewhere between $x = 0.5$ and $x = 1$, depending on the type of the emulsion, the exposure time, etc. The true rotational width is unity in all cases; hence we must multiply the measured width by a factor γ in order to get the true rotational width. If $\Delta\lambda_M$ is half the measured line width, then the true rotational width would be $\Delta\lambda_R = \gamma\Delta\lambda_M$ for large values of $\Delta\lambda_R$. Although γ may change from plate to plate, we shall regard it, nevertheless, as a constant for all the plates taken by the same spectrograph with the same dispersion. In doing so, we overestimate the rotational velocity obtained from a strong absorption line and underestimate that obtained from a weak line, because with the same amount of rotational broadening the stronger line always appears to the eye to be broader. (See also the discussion concerning Fig. 3.) Returning to the relation between the rotational velocity and the measured width, we should further note that the observed line width does not go to zero as the rotational velocity vanishes. It is limited by the width $\Delta\lambda_I$ of the instrumental broadening and can be estimated by the width of the weak comparison line. Therefore, we propose a simple interpolation formula for the relation between the measured width $\Delta\lambda_M$ and the rotational width $\Delta\lambda_R$ as follows:

$$\Delta\lambda_R = \gamma\,[\,(\Delta\lambda_M)^2 - (\Delta\lambda_I)^2\,]^{1/2}. \qquad (2)$$

We cannot expect this formula to hold very well when $\Delta\lambda_R \approx \Delta\lambda_I$. As a matter of fact, no method can yield a good result when this is the case.[2, 4, 5]

II. RESULTS OF THE MEASUREMENTS

In Table 1 we give the line widths of 1103 stars, all measured on the three-prism plates. This number includes 389 O and B stars, 446 A stars, 251 F stars, 10 G stars, and 7 stars with double spectra. We have listed all the stars between O and F, inclusive, that we have measured, including those which do not show any kind of broadening.

Some of the spectra investigated show such large broadening that it is extremely hard to tell where the absorption line begins. Or they show no lines (except the *H* lines) on the three-prism plates, but the spectra of the same stars on the one-prism plate show large broadening. In both cases we write "Large" under the heading of the measured widths. If the spectra show no line on the three-prism plates and at the same time we have no other evidence to establish the fact that the broadening is really very large, we write "No line" under the same heading. Very likely the broadening in such cases is also great. The line we have measured is *Mg* II λ4481, except for the early-type stars, in which we have used *He* I λ 4472. In the latter case we have put a dagger (†) after the measured width. An asterisk (*) after the measured width indicates a doubtful measurement due either to the poor quality of the plate or to some other difficulty. For such measurement the error cannot be estimated. Otherwise, the difference in the line widths of the same star measured on different plates cannot be greater than 20 per cent.

We have made two estimates of the rotational velocity. The first estimate is based on the assumption that the edge of the absorption line that we see on the plate corresponds to $x = 0.8$ in Figure 1, and the second corresponds to $x = 0.5$. In other words, we have $\gamma = 1.25$ for the first case and $\gamma = 2$ in the second case. The total width ($2\Delta\lambda_I$) of a weak comparison line is about 0.52 A. With these values, the rotational velocities can be computed directly from equation (2) and are therefore not given in the table. We found by comparison with the results of other investigators[2, 5] that the first estimate is too low and that the second estimate agrees approximately with both Elvey's and Slettebak's determination of the rotational velocities. Hence in all the following discussions of rotational velocities derived from the three-prism plates the second estimate is always used.

TABLE 1

LINE WIDTHS OBTAINED FROM THE THREE-PRISM PLATES

Boss (PGC)	Measured Width $2\Delta\lambda_M$ (A)	Boss (PGC)	Measured Width $2\Delta\lambda_M$ (A)	Boss (PGC)	Measured Width $2\Delta\lambda_M$ (A)	Boss (PGC)	Measured Width $2\Delta\lambda_M$ (A)
5	2.26*	384	Large	679	Large	926	2.03
10	1.12	411	1.80	681	2.06	931	0.75
12	1.71	419	1.25	682	3.10*	932	1.27
19	1.27	421	2.82	694	0.52	934	1.65
22	0.52	422	1.38	696	2.13*	935	0.79
27	0.52	428	1.68	700	3.08	937	0.52
43	1.87	433	0.52	705	No line	938	Large
50	1.94	440	Large	708	1.15	944	1.62
55	0.52	441	1.91	721	1.68*	947	2.68
57	1.31	446	1.00	722	0.52	955	0.52
68	Large	449	2.05	723	0.52	957	Large
77	4.02	452	3.18	730	3.32	963	1.39
89	0.73	458	4.18	739	1.47	967	0.61
97	No line	459	1.99	740	Large	971	1.55
101	2.00	463	1.86	741	Large	974	3.85*
103	1.35†	466	1.99	742	2.39	975	No line*
116	0.67	474	1.87	744	Large*	981	2.10
118	1.55	476	0.52	757	2.16	986	1.47
122	0.76	480	2.47*	761	0.63	989	1.26
123	0.87	482	1.61	767	3.27†	995	1.91
141	2.36*†	483	3.77	772	0.52	997	0.52
145	1.95	497	0.64	780	1.76	998	1.08
152	2.84*†	501	0.52	781	1.00	1001	0.92
155	0.84	508	3.53*	784	0.76	1003	1.02
168	0.52	517	3.28*	786	0.94	HD 27429	2.23
169	1.03	522	1.32	790	Large	1023	1.82
172	1.15	526	0.77	791	4.69	1024	3.60
174	0.52	534	1.09	805	0.99	1026	1.58
175	1.14	550	0.94	806	1.97	1027	2.42*
179	0.52	551	2.08*	812	0.52	1029	0.52
181	0.52	559	2.10	816	1.58	1033	2.48
189	0.52	560	1.65	825	0.52	1039	2.92*†
199	No line	563	0.52	838	Large	1046	1.73
203	1.34	575	0.52	842	0.52	1047	1.84
212	0.63	580	0.94	844	1.91	1048	0.68
224	1.49	597	2.45	847	2.18	1052	Large
246	1.87	604	1.05	850	0.96	1055	0.71
257	1.67	605	0.60	858	2.73	1056	1.57
258	No line	606	2.36	860	0.89	1067	2.31
263	0.84	617	0.52	865	Large	1076	0.96
264	1.75	620	1.96*†	869	3.19*	1079	0.67
269	1.98	621	2.16	873	0.54	1081	3.28
285	0.62	622	4.15	877	Large	1083	2.98
294	2.55	627	0.74	883	0.92	1084	1.92
295	3.12	628	1.54	893	3.26*	1087	1.85
298	0.90	629	1.70	894	1.21	1088	2.08
300	2.22	631	0.72	896	1.99	1089	1.39
314	2.32	643	1.94*	898	3.69*	1095	0.76
318	1.86	644	3.05	900	1.32	1097	1.88
321	2.11	648	3.32	902	0.92	1103	4.15
325	0.52	654	1.52	904	Large*	1110	1.13
350	0.52	664	0.56	910	2.15	1114	2.32
363	6.53†	666	4.80*	914	0.59	1117	1.25
369	1.77	668	No line	920	1.61	1122	2.08
371	2.39	674	1.36	923	0.74	1123	2.44
379	1.12	677	1.46	924	0.53	1139	1.63

TABLE 1—*Continued*

Boss (PGC)	Measured Width $2\Delta\lambda_M$ (A)	Boss (PGC)	Measured Width $2\Delta\lambda_M$ (A)	Boss (PGC)	Measured Width $2\Delta\lambda_M$ (A)	Boss (PGC)	Measured Width $2\Delta\lambda_M$ (A)
1140	0.52	1340	0.85	1609	0.90	1952	1.44
1141	5.00	1343	0.63	1611	2.13	1956	4.49
1147	1.36	1345	3.50†	1622	0.52	1968	0.73
1153	3.80*	1347	0.52	1629	0.52	1974	1.31
1159	2.40	1352	2.18	1634	1.98	1977	4.47*
1160	3.42*	1353	1.34	1635	3.12	1979f	0.78
1161	1.09	1354	2.09	1640	3.43	1979b	0.52
1163	1.72*	1357	1.46	1646	1.54	1988	0.52
1178	2.25	1362	1.10	1647	2.28	1994	3.76
1185	0.74	1364	1.60*†	1657	0.67	1999	0.58
1187	1.02	1368	1.58	1660	0.73*	2001	2.02
1189	3.30*	1370	1.64	1666	3.79†	2008	0.52
1190	0.68*	1372	2.46	1668	3.47	2009	4.94*
1192	1.10	1384	0.52	1682	2.61	2010	Large
1193	3.80*†	1388	1.23	1686	Large	2011	1.48
1194	3.00	1389	1.56	1688	2.88	2012	2.16*
1195	3.34	1391	3.06	1690	0.56	2022	5.62*
1202	0.61	1392	1.92*	1702	3.12	2035	1.24
1203	1.04	1396	1.80	1714	2.26	2045	5.08*
1204	2.49†	1398	2.19	1716	Large	2051	2.31
1206	0.99	1411	0.87	1724	0.52	2071	0.52
1213	0.62	1420	0.52	1725	1.94	2078	2.36
1214	2.04	1428	1.49	1732	0.52	2088	0.52
1216	1.76	1432	3.71*	1734	5.11	2091	1.71
1219	1.29	1433	2.38	1739	4.14	2111	1.73
1220	3.40	1435	1.63	1744	Large	2119	3.44*
1224	0.52	1438	0.70	1753	0.78*	2138	3.04
1226	0.52	1443	4.37	1759	2.72	2141	No line
1227	1.12	1446	2.20	1761	No line	2145	3.06
1231	Large	1452	1.95	1763	2.86	2153	0.52
1235	0.52	1453	1.65	1769	2.93*	2158	3.07*
1236	1.54	1454	2.82†	1778	3.04	2167	No line
1239	3.02*	1457	0.53	1781	1.39	2168	0.52
1241	0.52	1476	0.52	1782	1.14	2177	0.52
1242	2.10*	1478	0.68	1786	4.36*	2202	0.52
1244	0.63	1482	1.34	1789	2.73	2207	2.21
1250	1.14	1488	0.99	1793	1.32	2237	2.46
1252	1.62	1501	0.58	1804	0.80	2246	0.60
1260	1.32	1503	0.60	1812	4.65†	2264	0.55
1262	0.75	1504	0.58	1817	1.29	2295	4.48
1268	0.52	1507	1.50	1819	0.83	2324	1.00
1271	1.74	1515	1.03	1831	2.87†	2325	0.52
1274	2.38	1522	3.62*	1848	2.77	2327	1.93
1276	4.28*	1523	1.04	1853	3.95*	2330	2.08
1277	1.19	1525	1.25	1872	2.72	2331	1.32
1278	Large	1548	3.65*†	1879	4.93*	2342	0.52
1281	1.18	1550	Large	1886	2.98	2354	0.52
1297	0.52	1554	1.20	1898	3.13	2356	No line
1301	Large	1564	0.67	1901	1.99	2357	3.39*
1302	Large	1568	1.48	1917	0.52	2358	0.52
1303	1.02	1572	1.00	1924	2.36	2361	2.98
1304	0.92	1575	1.07	1928	0.78	2365	0.87
1313	3.04	1577	0.57	1930	3.08	2398	2.80
1315	0.92	1580	No line	1934	1.10	2400	1.80
1331	2.89*	1581	4.90*	1944	Large	2402	2.04
1336	No line	1593	0.67	1945	1.00	2404	2.38
1338	1.38	1598	2.40	1948	0.52	2407	1.51
1339	2.89	1603	5.51*	1950	1.22	2413	0.52

TABLE 1—*Continued*

Boss (PGC)	Measured Width $2\Delta\lambda_M$ (A)	Boss (PGC)	Measured Width $2\Delta\lambda_M$ (A)	Boss (PGC)	Measured Width $2\Delta\lambda_M$ (A)	Boss (PGC)	Measured Width $2\Delta\lambda_M$ (A)
2421	0.52	2804	1.70	3256	3.90*	3633	1.10
2424	Large	2811	5.99	3260	1.87	3635	0.52
2426	0.63	2813	1.10	3272	1.43	3650	0.52
2440	0.76	2830	0.52	3277	2.30	3654	2.44
2441	0.52	2853	1.27	3281	Large	3660	0.52
2443	0.76	2854	3.54	3283	1.50	3667	2.39
2446	0.65*	2862	3.24†	3289	3.14†	3668	5.88†
2458	1.30	2883	No line	3292	2.44*	3670	1.10
2463	0.52	2926	1.70	3302	1.63	3672	1.00
2465	1.11	2928	1.56	3307s	0.77	3679	0.86
2473	0.52	2930	1.22	3307n	0.84	3692	3.22
2476	3.52	2932	0.53	3309	Large	3697	4.65
2479	1.93	2942	0.79	3310	3.18	3699	0.52
2491	2.30	2960	0.74	3320	1.60†	3700	0.52
2493	3.48	2964	1.36	HD 111456	0.89	3704	0.85
2495	4.02	2966	0.93	3347	2.19	3705	0.99
2503	0.52	2970	3.22	3352	1.73	3707	Large
2526	0.74	2972	3.60	3356	Large	3710	0.52
2540	2.44	2974	0.52	3363	0.93	3716	2.06
2541	0.77	2982	3.62*	3370	0.52	3722	2.72
2552	0.52	2984	0.52	3371	0.52	3724	No line
2559	1.64	2987	0.81	3372	3.00	3729	0.52
2565	4.15	2990	1.38	3382	2.54	3732	3.84†
2584	1.76	2997	0.52	3392	Large	3739	0.52
2590	2.86	2999	0.52	3409	0.56	3744	2.13
2600	2.88	3005	2.16	3412	0.73	3745	0.52
2602	0.52	3023	3.90*	3422	0.52	3749	0.63
2604	1.26	3033	0.52	3447	0.52	3758	1.46
2605	6.89†	3054	Large	3450	1.77	3771f	3.08
2632	2.61	3055	Large	3452	1.87	3779	0.92
2635	0.52	3068	0.52	3474	0.72	3783	1.00
2637	0.52	3088	3.68	3475	1.33	3784	0.52
2642	2.86	3092	1.46	3476	Large*	3814	2.48
2650	2.17	3097	1.14	3480	4.82	3815	2.16†
2655	3.59	3098	0.52*	3494	4.65	3818	1.14†
2665	0.52	3101	3.32	3506	0.52	3838	3.60†
2672	2.44	3105	0.52	3508	Large	3852	2.73†
2674	0.77	3117	3.12	3509	3.90	3855	0.98
2690	1.24	3135	1.54	3511	0.52	3866	1.22
2692	3.75	3139	1.50	3512	2.73	3879	No line
2694	0.62	3143	2.03	3518	3.46	3880	1.63
2697	0.65	3160	1.40	3530	4.31	3883	1.66
2698	5.98*	3165	3.65	3544	2.44	3890	Large
2723	2.08	3166	0.64	3558	0.52	3895	0.52
2724	Large	3182	1.02	3564	1.77†	3896	4.24
2729	1.62	3187	3.50†	3565	3.15†	3905	2.44
2730	2.32	3190	2.84	3566	3.28	3915	4.83
2735	1.78	3191	1.03	3577	0.52	3919	0.52
2741	0.52	3192	2.75*	3586	1.22	3926	1.68
2762	2.44	3207	Large	3593	3.07†	3928	2.16
2768	0.94	3210	0.52	3596	0.52	3939	2.42
2778	1.40	3224	0.52*	3602	2.68†	3940	0.52
2783	1.08	3231	1.31	3606	1.64	3943	0.81
2784	0.72	3237	2.04†	3610	0.52	3955	0.69
2785	0.52	3238	No line	3612	2.86	3960f	1.68
2788	2.89	3244	2.03	3615	2.60*†	3960b	1.92
2792	2.66	3251	0.89	3621	0.52	3961	3.00
2802	3.14	3254	2.68	3626	0.60	3973	4.26†

TABLE 1—*Continued*

Boss (PGC)	Measured Width $2\Delta\lambda_M$ (A)	Boss (PGC)	Measured Width $2\Delta\lambda_M$ (A)	Boss (PGC)	Measured Width $2\Delta\lambda_M$ (A)	Boss (PGC)	Measured Width $2\Delta\lambda_M$ (A)
3980	2.03	4285	1.22	4553	0.72	4851	0.52
3988	2.38	4287	1.78†	4557	Large	4859	3.95
3994	2.01	4300	1.50	4559	0.58	4865	4.17†
3998	2.98	4302	1.45	4564	0.77	4869	3.48
4004	2.11	4322	0.52	4565	2.26†	4872	2.89
4016	1.04*	4327	0.76	4566	0.52	4874	0.63
4017	0.66	4328	0.94	4581	1.37	4875	2.38
4018	0.52	4332	0.94	4582	0.52	4883	3.56†
4026	0.89	4334	2.58†	4584	Large	4887	0.67
4028	Large	4346	2.44	4590	0.55	4891	0.52
4030	1.85	4354sp	0.59	4591	3.31	4897	0.65
4033	2.44	4354nf	0.52	4592	0.94	4902	1.46
4038	Large	4358	1.41	4603	0.52	4905	3.46
4042	0.52	4360	0.52	4604	1.47	4906	2.52
4052	2.49†	4361	3.96	4620	2.80	4911	1.33
4055	0.52	4368	0.86	4623	0.52	4914	1.77
4057	2.00	4374	0.70	4632	0.66	4917	6.05†
4058	No line	4382	2.72	4645	Large	4924	1.59
4059	No line	4391	2.96	4657	0.52	4928	1.40
4062	2.19	4394	0.52	4661	3.00	4929	1.67
4066	2.70	4395	2.23	4670	0.88	4932	1.62
4072	2.68	4399	1.01†	4671	3.54*	4933	2.87
4077	0.52	4401	0.52	4672	0.52	4934	0.87*
4081	2.45	4402	2.31	4674	2.18*	4936	1.64
4082	0.61	4403	0.52	4685	No line	4942	0.78
4086	2.04†	4405	5.62*†	4702	1.22	4948	0.73
4087	1.52†	4419f	Large	4707	0.60	4949	3.08†
4089	0.52	4419b	1.45	4712	0.53	4953	1.90
4090	0.68	4421	0.85	4713	1.51	4962	0.52
4093	2.20†	4423	1.47	4721	0.95	4972	0.84
4112	0.52	4427	4.05†	4722	0.52	4992	0.58
4113	No line	4428	2.30	4731	0.68	4998	Large
4117	3.36	4429	1.73†	4734	0.74	4999	1.26
4119	0.75	4439	3.80†	4739	0.91	5000	0.52
4143	1.14	4457	2.40	4740	4.10	5002	1.65
4158	1.10†	4458	1.98	4745	0.52	5004	1.51
4162	0.70	4459	4.59	4752	0.70	5014	0.52
4163	2.14	4460	0.98	4753	0.52	5023	0.52
4165	3.02	4462	0.52	4756	0.57	5024	0.85
4178	2.91†	4465	1.73	4761	0.91	5028	2.96
4181	2.18	4466	0.52	4762	3.48†	5031	1.16
4182	1.27	4474	2.04†	4775	3.18	5032	0.56
4183	2.18†	4475	1.99	4779	0.52	5033	0.52
4189	0.63	4479	0.52	4783	0.61	5048	4.80*
4198	4.50†	4481	0.52	4784	2.57†	5051b	0.52
4200	1.60†	4483	0.74	4788	0.77	5058	No line
4203	2.46	4492	0.96	4797	0.52	5062	3.65
4206	0.95	4493	0.75	4802	2.62	5068	2.70
4213	3.29	4498	0.92	4803	3.40	5071	0.52
4218	0.52	4503	0.52	4804	0.60	5086	1.54
4225	Large	4504	0.52	4816	0.62	5097	2.01†
4269	1.01	4511	2.83	4817	0.65	5099	0.65
4270	1.18	4528	0.70	4820	0.69	5101	1.97
4273	0.63	4539	0.52	4824	1.30	5102	0.82
4277	3.24†	4542	0.68	4832	2.17	5105	No line
4280	0.52	4544	1.61	4839	4.38†	5107	1.33
4281	2.07†	4545	3.85†	4842	0.52	5108	1.36†
4284	0.80	4548	0.84	4846	2.13	5122	3.13*

TABLE 1—*Continued*

Boss (PGC)	Measured Width $2\Delta\lambda_M$ (A)	Boss (PGC)	Measured Width $2\Delta\lambda_M$ (A)	Boss (PGC)	Measured Width $2\Delta\lambda_M$ (A)	Boss (PGC)	Measured Width $2\Delta\lambda_M$ (A)
5127	Large†	5365	1.14	5624	1.10	5910	2.31
5132	0.52	5366	0.68	5627	2.66†	5913	0.63
5134	2.76	5371	1.42	5635	2.52	5916	1.92
5139	0.62	5393	No line	5661	0.72	5918	No line
5156	2.44†	5399	1.21	5667	Large	5931	1.16
5170	No line	5405	Large	5671	0.52	5933	3.16*
5171	1.19	5414	Large†	5679	1.19	5936	No line
5173	0.99	5417	1.60	5680	1.84	5939	2.02
5182	2.49	5427	2.27	5687	1.43†	5944	2.41
5185	5.34	5432	0.52	5688	0.52	5949	1.52
5186	3.44	5443	0.52	5706	0.80	5955	1.17†
5188	1.90	5455	0.52	5709	2.49	5958	0.57
5190	3.60†	5460	1.91	5713	1.87	5967	2.94*
5191	4.20	5461	0.84	5719	2.66*†	5973	Large
5199	0.62	5465	0.63	5721	0.52	5975	1.34
5208	1.37	5467	2.78	5742	1.68	5985	1.52
5213	0.52	5469	0.92	5755	1.51	5992	3.60*
5214	0.66	5471	3.18†	5757	0.78	5997	2.49
5216	0.52	5473	1.13	5761	1.91	6005	3.69
5223	0.66	5480	4.97	5762	2.58†	6009	2.45
5240	1.01	5488	2.33†	5763	1.36	6010	3.14
5244	2.37	5491	1.32	5764	0.84	6023	2.10
5249	2.56	5493	0.52	5777	No line	6024	2.28
5255	0.52	5515	1.79	5779	0.87	6031	0.94
5265	2.86†	5516	2.52†	5784	2.56*	6054	0.87
5268	2.58	5517	0.52	5793	1.89	6062	0.70
5270	1.21	5525	Large	5794	1.37	6063	2.30
5272	1.05	5532	0.84†	5800	1.64	6072	4.60
5275	1.30	5549	3.33†	5803	0.86	6073	0.92
5282	2.34	5551	2.10	5805	2.46	6075	3.24*
5290	0.52	5553	3.44	5807	0.56	6076	1.80
5291	0.96	5555	2.86	5808	0.52	6077	0.52
5298	0.62	5562	0.78	5813	2.28	6084	1.31
5301	1.05	5563	1.77†	5818	2.29*	6087	2.59*
5303	Large	5579	2.13	5819	0.67	6095	No line
5310	3.16	5580	1.76	5837	1.88	6099	1.37
5318	2.68	5587	0.52	5838	1.95	6108	3.28
5320	0.78	5592	0.52	5844	0.92†	6119	0.77
5323	0.58	5596	4.12	5850	1.52	6128	2.54
5325	1.16	5600	1.92	5853	2.52	6135	0.91
5328	0.98	5605	2.90*	5858	0.52	6155	2.82*†
5334	0.52	5608	0.89	5874	0.53	6156	0.91
5337	2.25	5609	1.19	5880	4.76	6169	1.28
5344	0.52	5616	2.46	5893	1.16	6173	1.25
5350	1.77†	5617	1.75	5894	0.52	6179	1.70*
5361	1.35†	5623	2.01	5904	1.78		

Among the 800 stars measured by Westgate and 1103 stars measured by us, there are about 600 stars in common. In Figure 2 we have plotted her measurements against ours for these 600 stars. The points are scattered widely. But we discern a general trend. First, for very large widths the points are more or less scattered along a 45° line passing through the origin. But for the intermediate and small widths, Westgate's values are statistically much higher than those from the present measurement. This is not difficult to explain, since there is a tendency to overestimate the width on small-dispersion

plates. We have plotted in Figure 3 the rotational velocities determined by Elvey and by us for those stars we have both investigated. In Figure 4 we have a similar plotting of Slettebak's determination against ours. In Figure 3 the dots, the half-filled circles, and the circles represent, respectively, the cases for which the total strength of the measured line is strong, medium, and weak. Since we overestimate the rotational velocity obtained from a strong line, the dots should occur more frequently below the straight line (of 45° inclination passing through the origin) than above it. The contrary should be the case for the population of the circles. There certainly exists such a tendency in Figure 3, although this tendency is mixed up with the correlation between the rotational velocity

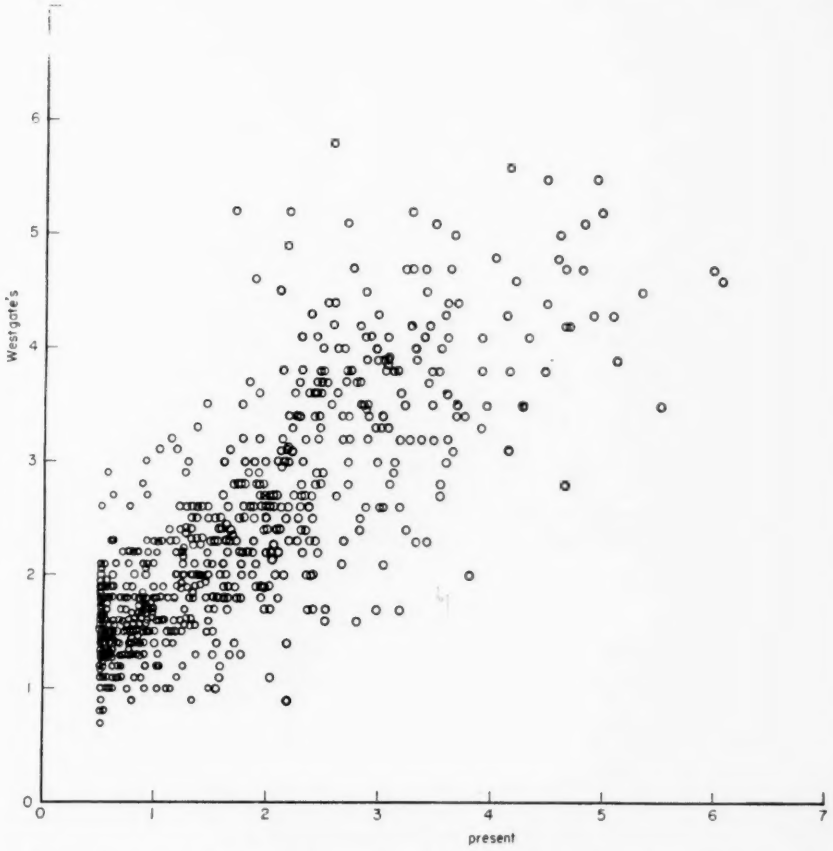

FIG. 2.—Comparison of the present measurements with Miss Westgate's for about 600 stars investigated in common. For very large widths the points are more or less scattered along a 45° line passing through the origin, as was to be expected. For the intermediate and small widths, Westgate's values are statistically much higher than those from the present measurements. This may be due to the overestimation of line widths on the low-dispersion plates. A cutoff at 0.52 A represents the instrumental width for the three-prism plates we have used.

and the estimated line strength. The latter correlation may be the result of inaccurate estimation of the equivalent width of the measured line.

In Table 2 we give a list of the line widths for 445 stars, of which 231 are O and B stars, 152 are A stars, and 62 are F stars (F0–F5). The line widths were measured on two-prism plates taken at the Chile station of the Lick Observatory. The notation has the same meaning as that in Table 1. The total instrumental width ($2\,\Delta\lambda_I$) in the present case is 1.12 A. We have chosen a value for γ such that the average value of rotational velocities for the O–F5 stars listed in Table 2 will be approximately equal to that

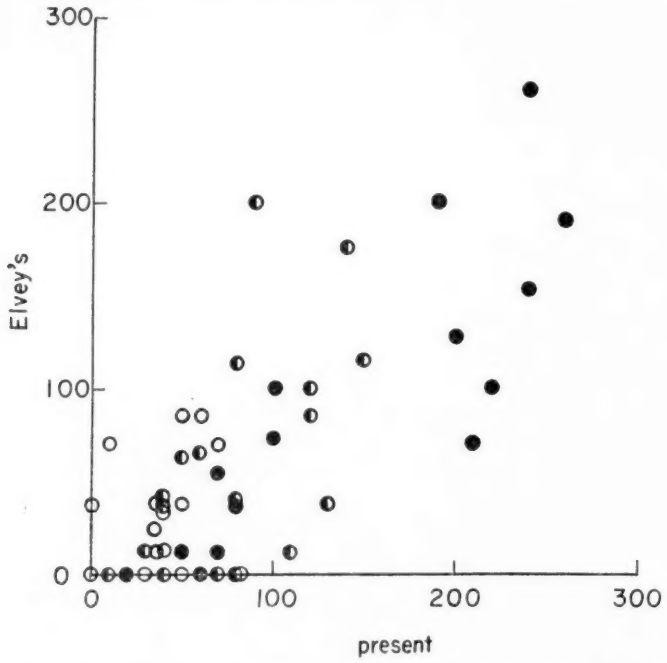

FIG. 3.—Comparison of the present estimate ($\gamma = 2$) of rotational velocities with Elvey's. The dots, the half-filled circles, and the circles represent, respectively, the cases for which the total strength of the measured line is strong, medium, and weak. The error of overestimating the rotational velocity obtained from a strong line and underestimating that from a weak line is mixed in the diagram with the correlation between the rotational velocity and the estimated line strength. The latter correlation may be the result of inaccurate estimation of the line strength on the photographic plate.

of the second estimate for the same types of stars listed in Table 1. In this way we get $\gamma = 1.3$, and the rotational velocity can be directly computed. Even with $\gamma = 1.3$, we cannot take the rotational velocities thus determined as being on the same scale as those of the second estimate used in reducing the line width for the three-prism plates. It is therefore advisable not to combine the two tables in the statistical study.

Finally, we shall present some statistics concerning our results. The average values of the observed rotational velocities for different types of stars have been computed and given in Table 3. The spectral classes used in the study are taken directly from the catalogue of radial velocities.[6] We use the *Henry Draper* classification in general but fol-

low the revised one if there is any. Hence the spectral classes used are not based on a uniform system. The average values of the true rotational velocities given in parentheses in Table 3 are computed from S. Chandrasekhar and G. Münch's formula.[7] In evaluating the average, we have taken all stars designated "No line" and "Large" in our measurement to have a mean rotational velocity of 400 km/sec both for the three-prism plates and for the two-prism plates. These estimates may be subject to considerable uncertainty. We have plotted the mean rotational velocity against the spectral class in Figure 5. The full line is obtained from Table 1, the broken line from Table 2. There is a

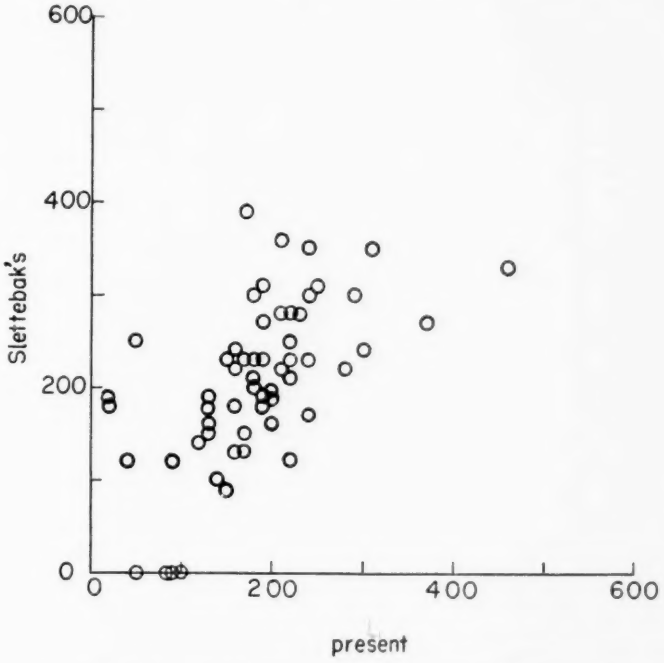

FIG. 4.—Comparison of the present estimate ($\gamma = 2$) of rotational velocities with Slettebak's. This applies only to a limited range of spectral classes (B2–B5 and B2e–B5e); hence the line strength is nearly the same for all the stars considered here.

certain arbitrariness in grouping spectral subdivisions to obtain the mean value, when there are not enough stars to make the average value of every single subdivision meaningful. The mean rotational velocity seems to assume high values at B3 and B9 and then decreases gradually from A0 down toward the later spectral classes. At F2 there appears to be a further sudden drop in rotational velocities as observed by Westgate. The high values of the rotational velocity at B3 may be a result of the systematic error of the classification system we used, for, according to this classification, all B1 and B2 spectra in which weak *O* III lines have been washed away by rotation would be classified as B3. This explanation is further supported by the fact that there are far too few B1 and B2

[7] *Ap. J.*, 111, 142, 1950.

TABLE 2

LINE WIDTHS OBTAINED FROM THE TWO-PRISM PLATES

Boss (PGC)	Measured Width $2\Delta\lambda_M$ (A)	Boss (PGC)	Measured Width $2\Delta\lambda_M$ (A)	Boss (PGC)	Measured Width $2\Delta\lambda_M$ (A)	Boss (PGC)	Measured Width $2\Delta\lambda_M$ (A)
15	3.17	1430	2.64†	2060	1.66	2389	2.65
24	1.13	1467	2.29	2061	No line	2395	2.52
99	3.28	1480	2.12	2062	3.66†	2399	2.34
100	4.06	1481	1.13	2070	1.27†	2408	1.13
107	2.21	1509	1.13	2086	1.13	2414	1.13
111	1.63	1512	6.12†	2089	5.11*†	2418	1.76
120	1.13	1516	1.59	2094	6.30†	2427	1.87
146	1.13	1517	2.94†	2095	5.95*†	2428	1.13
260	2.40	1529	1.68	2096	2.16*	2433	1.13
354	1.82	1537	No line	2108	1.13	2457	2.76†
396	2.26	1538	Large	2109	3.48*†	2460	3.12
401	1.70	1539	5.71	2110	1.13	2467	1.34
HD 12563	1.13	1558	6.21†	2125	3.04	2475	8.71
506	No line	1566	2.60	2136	1.13	2477	1.13
524	5.56	1594	2.65	2137	2.62	2483	4.68
557	2.66	1605	4.90	2151	1.13	2486	2.16
564	3.09	1619	1.13	HD 67536	6.68†	2504	No line
603	7.18	1641	3.33	2165	4.52†	2513	1.13
611	4.43*	1642	Large	2166	3.78	2517	1.13
630	1.58	1655	3.22	2171	4.39†	2523	1.37
642	2.53	1669	2.94	2179	1.13	2537	4.69
647	6.00	1696	1.13	2181	1.13	2557	No line
652	3.95	1749	4.07	2187	3.95†	2558	4.69*
671	2.16	1754	4.69†	2188	4.89†	2563	3.00
680	1.72	1767	1.13	2191	1.72	2575	No line
684	2.33	1792	5.71†	2200	4.64*	2577	4.81†
690	2.22	1795	3.14*	2217	1.96†	2581	1.13
706	2.48	1799	2.37	2226	3.98†	2606	2.29
711	1.51	1802	3.05†	2228	1.60	2607	1.44
728	3.59	1805	1.40	2244	1.13	2619	1.19
738	1.56	1807	1.90†	2249	1.26	2629	2.82†
776	1.13	1826	2.34	2250	3.74†	2640	3.16*
HD 21882	4.61	1829	1.76	2252	No line	2699	2.06
824	4.44	1833	1.13	2259	2.98	2702	5.04†
846	5.33†	1845	1.13	2266	1.88†	2705	3.54
880	1.13	1863	1.87	2267	3.86†	2722	3.86
884	1.13	1874	1.54,	2273	1.43	2725	1.26
885	5.05	1877	5.69†	2274	No line	2733	No line
903	1.39	1882	1.13	2298	4.24†	2738	No line
948	2.50	1883	3.40	2303	4.73	2755	1.26
956	1.13	1884	No line	2307	1.13	2763	4.84
966	4.50	1891	3.20†	2320	1.13	2767	2.12*
1012	4.06	1907	6.36†	2326	Large	2790	1.13
1066	1.13	1910	3.02†	2329	1.13	2809	1.13
1111	3.37	1911	1.31	2332	1.55	2835	1.13
1130	4.16	1925	1.31*	2334	2.18	2856	3.17
1158	1.72	1932	1.31	2337	6.54	2859	5.09†
1172	2.61	1935	1.56†	2340	No line	2860	1.95†
1205	5.02	1969	1.42	2341	1.13	2867	7.54
1207	1.13	1991	6.79†	2347	6.60†	2876	Large
1225	1.13	2004	2.14	2363	6.75†	2878	Large
1257	2.76	2015	1.21	2366	6.88	2879	5.06
1390	1.34	2017	3.33†	2376	2.08	2880	4.75†
1401	3.68	2026	2.53	2382	1.83†	2889	1.13
1414	1.47	2033	No line	2388	1.21	2901	1.46

TABLE 2—*Continued*

Boss (PGC)	Measured Width $2\Delta\lambda_M$ (A)	Boss (PGC)	Measured Width $2\Delta\lambda_M$ (A)	Boss (PGC)	Measured Width $2\Delta\lambda_M$ (A)	Boss (PGC)	Measured Width $2\Delta\lambda_M$ (A)
2902	1.13	3366	3.31†	3950	7.95†	4792	1.13
2929	2.77	3369	5.86†	3954	2.66†	4796	1.99
2945	4.70	3384	4.34	3965	1.13	4810	3.20*
2947	4.36	3390	5.02†	3991	1.13	4830	No line
2948	4.51	3393	1.44†	4019	5.83†	4836	4.72
2954	1.70	3399	2.66*	4037	6.51	4843	2.68
2957	5.25	3419	5.00*†	4049	2.09	4844	1.54
2961	1.13	3427	1.13	4050	5.02	4854	2.69
2965	3.10	3429	5.66	4064	5.81	4868	4.33*
2969	4.78	3451	1.35	4071	3.60	4913	3.75*†
2992	7.97†	3457	6.21*†	4076	5.26	4922	7.38
3001	2.10	3468	1.13	4084	1.13	4943	1.92
3013	2.22	3486	5.60*	4091	7.66†	4997	1.13
3016	4.77†	HD 117360	1.13	4094	2.45	5003	7.15†
3024	1.13	3513	2.76	4100	4.25	5034	1.98
3036	1.13	3528	6.45*	4120	4.14	5050	1.60
3043	3.30	3529	5.27*	4128	5.78†	5060	1.13
3048	4.46	3549	9.91	4148	1.13	5081	1.62
3053	1.50	3576	4.35	4155	1.13	5084	3.20
3073	4.39*	3587	1.13	4156	3.68	5110	1.13
3079	1.13	3603	3.63†	4167	3.80*	5115	2.25
3091	1.71	3604	Large	4174	1.13	5286	1.13
3103	6.21	3643	6.90†	4180	2.68†	5315	2.02
3111	1.59	3657	5.88†	4190	2.37†	5326	No line
3126	2.48	3665	1.13	4199	3.18†	5332	2.22
3127	3.84	3677	1.36	4208	3.21†	5390	1.72
3134	4.77	3680	2.80	4249	5.08†	5411	1.56
3138	3.40†	3685	No line	4253	2.69	5435	4.64*
3146	1.13	3686	1.13	4288	3.68†	5446	1.13
3148	1.13	3688	1.13	4320	1.74	5464	2.61
3151	1.25	3712	1.13	4321	No line	5506	1.66
3152	4.37	3713	4.10	4369	4.89†	5582	1.13
3162	3.55	3747	4.21†	4375	1.13	5604	3.56
3168	4.74	3755	3.71	4398	8.76†	5634	5.15
3174	3.02	3759	10.32	4404	3.58*†	5652	No line
3176	3.52	3766	3.82	4415	No line	5684	6.65†
3199	5.31*†	3774	1.13	4420	1.76	5689	5.47
3200	4.39†	3776	4.28	4426	No line	5695	4.68
3215	No line	3796	2.44	4431	6.60*†	5726	1.43
3220	2.25	3802	Large†	4434	No line	5778	Large
3222	No line	3805	2.65	4445	No line	5831	1.74
3227	1.52	3807	4.70	4454	1.58	5836	1.13
3236	3.30†	3832	1.13	4537	4.46	5849	6.65
3245	5.34†	3862	5.53	4599	4.59*†	5873	1.13
3249	4.09	3863	4.40	4612	2.17†	5921	2.33
3269	6.38†	3865	1.13	4637	1.13	5935	1.13
3286	2.16	3871	1.13	4642	6.62†	5937	2.28
3293	1.13	3874	5.80*†	4666	2.36	5951	No line
3300	1.30	3886	3.17†	4677	1.13	5991	1.13
3305	4.34*	3888	7.05*†	4679	2.94	6027	1.13
3324	1.13	3892	2.50*	4680	1.13	6057	6.80
3328	1.38	3899	1.13	4682	3.60	6068	3.06
3342	4.19*	3901	6.38†	4697	4.08†	6103	5.04†
3349	1.47	3910	4.65†	4725	3.24	6110	No line
3357	7.78†	3916	1.13	4732	3.18	6149	4.46
3358	1.19	3921	5.34	4738	4.45	6160	4.10*†
3359	3.02*†						

stars as compared with B3 stars (see Table 3). The curves in Figure 5 represent a general variation in rotational velocity with spectral class which can be plotted from the observational results. We have tentatively drawn two distribution-curves—one for stars earlier than F2 and another for stars later than F2—because of the sudden drop in the mean rotational velocity at that subdivision.

The distributions of the observed rotational velocities are given in Figure 6. Two sets, each with three histograms (respectively for O and B stars, for A stars, and for early F stars), are given. One set is derived from Table 1, the other from Table 2. The cases of

TABLE 3

MEAN VALUES OF ROTATIONAL VELOCITIES FOR DIFFERENT SPECTRAL CLASSES

Sp. Class	Three-Prism Plates		Two-Prism Plates	
	No. of Stars	Mean Rot. Vel. (Km/Sec)	No. of Stars	Mean Rot. Vel. (Km/Sec)
O	8	179	5	172
B0	14	200	7	120
B1	19	111	5	116
B2	30	126	6	190
B3	96	194	68	177
B4	4	157	2	90
B5	52	178	46	156
B6	7	127	2	75
B7	17	130	8	74
B8	71	150	49	204
B9	71	170	33	177
O–B9	389	166 (211)	231	170 (216)
A0	139	154	61	146
A1	39	158	2	170
A2	104	140	44	102
A3	57	133	19	62
A4	24	110	0	.....
A5	50	127	18	101
A6	9	119	1	400
A7	10	133	3	110
A8	10	86	1	200
A9	4	107	3	103
A0–A9	446	140 (178)	152	118 (150)
F0	50	93	18	82
F1	17	83	6	92
F2	30	71	10	49
F3	8	25	4	32
F4	28	21	8	7
F5	47	26	16	32
F0–F5	180	57 (72)	62	52 (66)
F6	20	24		
F7	16	11		
F8	20	12		
F9	15	5		
F0–F9	251	45 (57)		

"Large" and "No line" in the tables are not considered in the histograms. The two sets of diagrams derived from the two tables agree reasonably well, but we should give greater weight to the first set, i.e., that derived from Table 1.

Several authors have discussed the distribution of the true rotational velocities. As has been pointed out by A. Brown,[8] the shape of the frequency distribution of true rotational velocities can vary appreciably, yet still lead to distributions of the apparent rotational velocities which are compatible with the observations. Hence it seems to be impossible, with the accuracy attained by the observations at the present time, to determine the distribution of true rotational velocities from the distribution of observed ones. But we might indulge in a little speculation: It is highly probable that the spin vector of the star follows a Maxwellian distribution. This was suggested by van Dien[4]

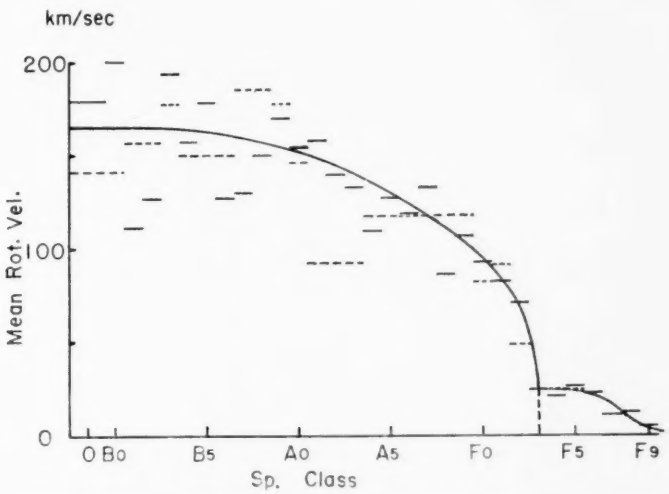

FIG. 5.—Observed mean rotational velocities at different spectral classes. The full lines and the broken lines represent the mean values of rotational velocities derived from Tables 1 and 2, respectively. The solid curves are drawn to represent a general variation of mean rotational velocity with spectral class. The sudden drop of rotational velocities at F2 necessitates the introduction of two distribution-curves. These curves are drawn tentatively and could be modified if the spectral classification were based on a uniform system.

(the second of her three assumptions concerning the distribution of true rotational velocities). Or, making it a little broader, we can assume that the distribution of angular velocities in our neighborhood of the galaxy is of the form of an ellipsoid like the distribution of the residual velocities. There are some reasons for believing this. First, what we have asserted here amounts only to the statement that the distribution of the components of the angular velocities along three mutually perpendicular axes is of the form of the error function. Second, along the three axes (say one perpendicular to the galactic plane, one in the plane toward the center of the galaxy, and one in the plane following the direction of the galactic rotation) a newly born star could conceivably acquire different amounts of rotational velocity because of the anisotropic structure of the galaxy. Afterward the stars will lose their rotation at different rates along the three directions for

[8] *Ap. J.*, **111**, 366, 1950.

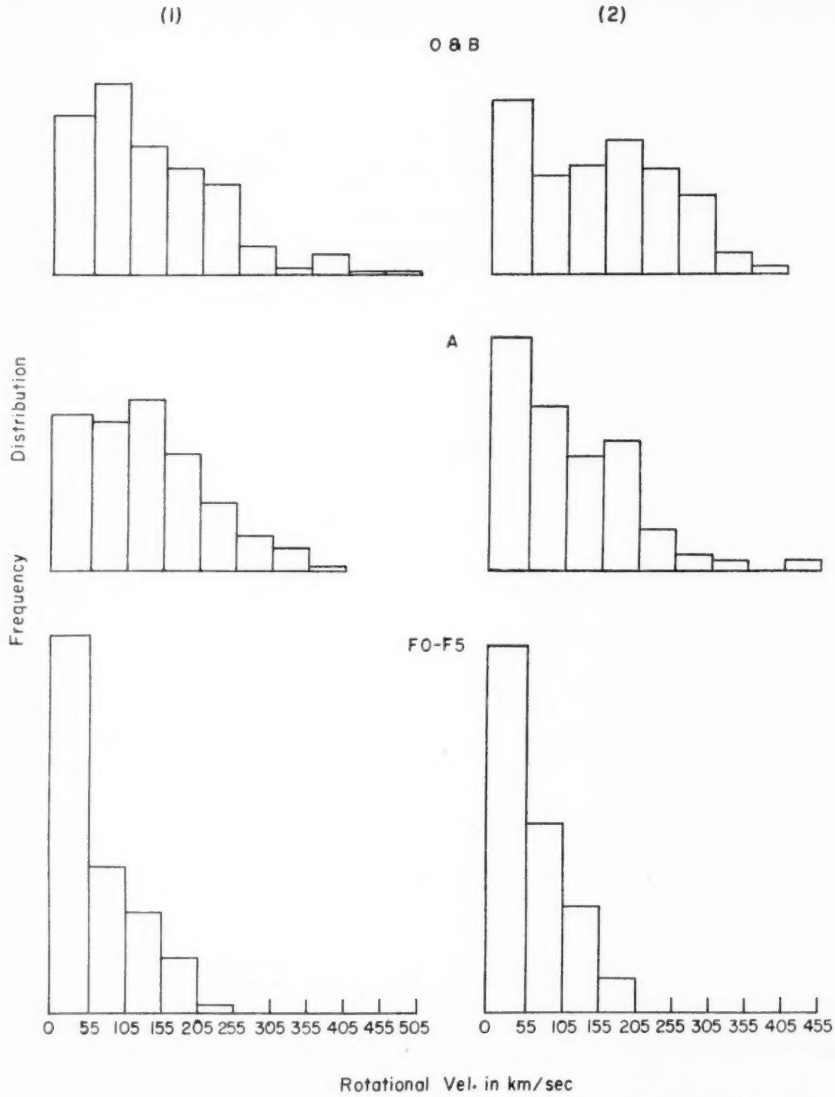

FIG. 6.—The distributions of the observed rotational velocities. The first set (*left-hand side*) of three histograms (respectively for O and B stars, for A stars, and for early F stars) is derived from an estimate ($\gamma = 2$) of rotational velocities for the stars listed in Table 1 (three-prism plates). The second set (*right-hand side*) of three similar histograms is derived from an estimate ($\gamma = 1.3$) of rotational velocities for the stars listed in Table 2 (two-prism plates). The two estimates for the two different kinds of plates are approximately, but not exactly, on the same scale.

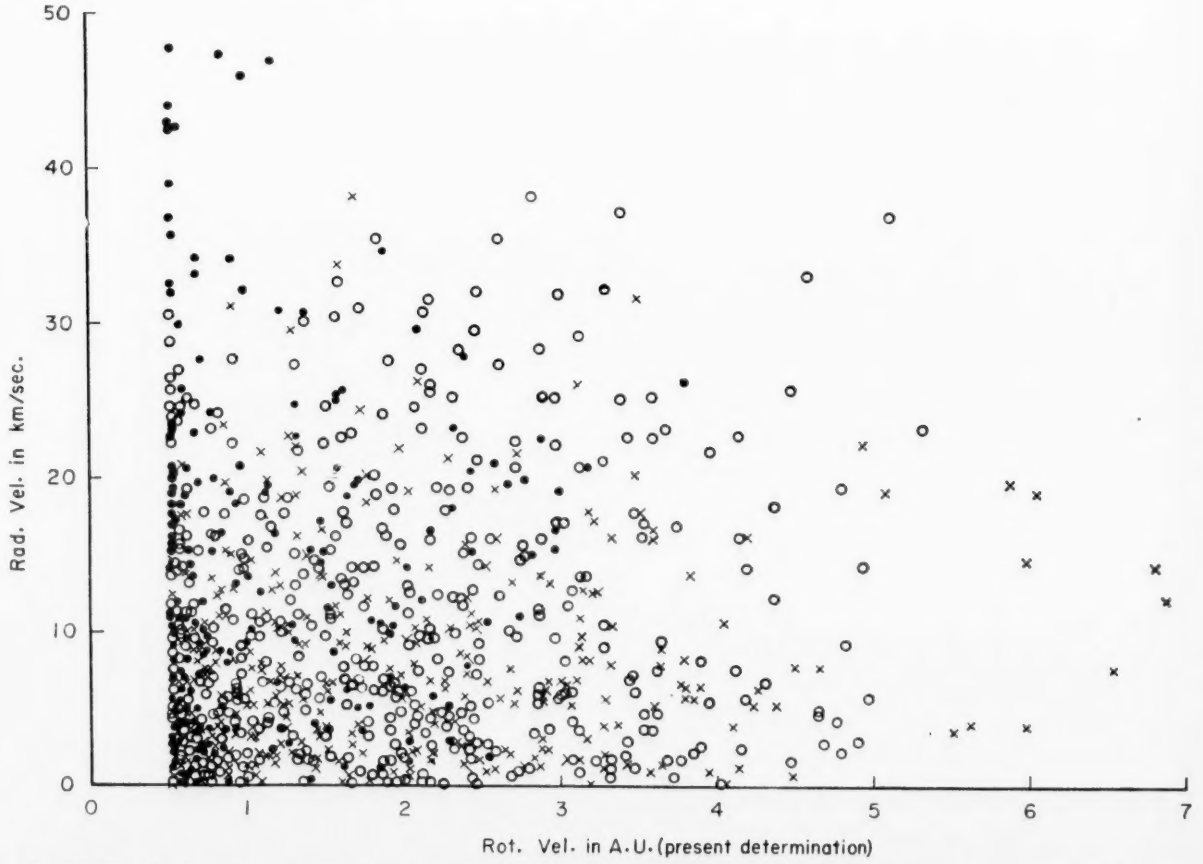

FIG. 7.—Plot of radial velocity (corrected for the solar motion) against measured line width (from Table 1). The crosses represent B stars, the circles A stars, and the dots F stars.

the same reason. Therefore, we could expect the components of the rotational velocities to have different mean absolute values for different directions. The difference may be small, so that it is not surprising that no correlation between the observed rotational velocity of the star and its position in the sky has been found.[8]

If we assume an ellipsoidal distribution of the angular velocities of the stars, the distribution of the observed rotational velocity would approach zero as the observed rotational velocity goes to zero. This does not seem to be the case in the diagrams in Figure 6, which show the distribution function of the observed rotational velocities. Since we cannot measure exactly the rotational velocities less than 30 km/sec, the exact distribution function for velocities less than this amount is unknown, and our result does not present a serious objection to the assumption of an ellipsoidal distribution of rotational velocities. Moreover, the distributions of the observed rotational velocities for B2e–B5e stars and for B2–B5 stars obtained by Slettebak[5] have a clear tendency to go to

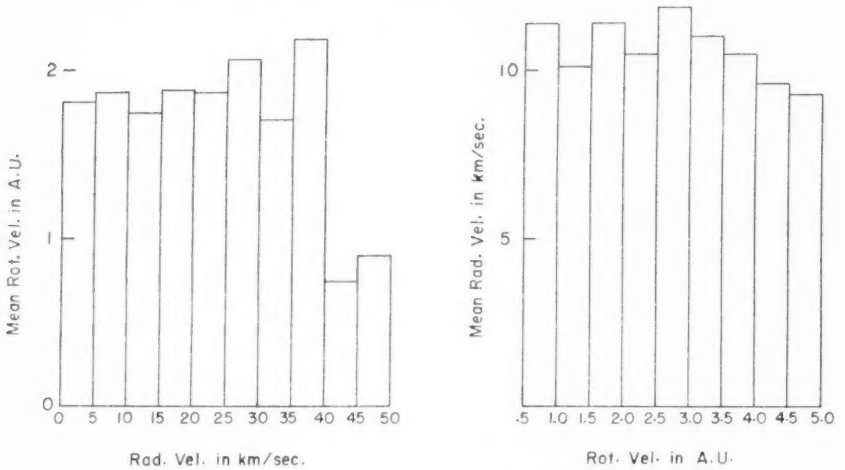

FIG. 8.—Mean rotational velocity against radial velocity (corrected for the solar motion), and mean radial velocity (corrected for the solar motion) against rotational velocity. These two diagrams show that there exists, in general, no correlation between the space motion and the rotational motion. But the rotation may drop suddenly at a certain space velocity (40 km/sec).

zero as the velocity approaches zero. This supports our view but is far from being strong evidence in favor of our assumption. Further study is necessary before it can be proved or disproved

Finally, attention should be called to the fact that, although we have regarded the broadening of the measured line as solely due to rotation, it is possible that the lines of some of the stars listed in Tables 1 and 2 are broadened by turbulent motion in stellar atmospheres.[9]

If the rotational velocity decreases[10] while the space velocity increases[11] as the stars become older, we might expect some correlation between the rotational velocity and the

[9] Studies of the line profiles for distinguishing macroscopic motion from rotation are now being carried out here by Dr. O. Struve and myself.

[10] O. Struve, *Stellar Evolution* (Princeton: Princeton University Press, 1950), p. 147.

[11] L. Spitzer, Jr., and M. Schwarzschild, *Ap. J.*, **114**, 385, 1951.

space velocity. Hence we have plotted in Figure 7 the measured line width against the radial velocity corrected for the solar motion.[12] We have used $\alpha = 270°$ and $\delta = 30°$ as the position of the solar apex and 20 km/sec as the magnitude of the solar motion.[13] The line widths used are taken from Table 1, the radial velocities from the Lick *Catalogue*. When the average value of the observed rotational (or radial) velocity is plotted against the radial (or rotational) velocity, we find that there exists no correlation. From these plots (Fig. 8) it seems to us that the rotation may drop suddenly at a certain space velocity (40 km/sec). Of course, this suggestion is only tentative and cannot be taken too seriously at present. Also, in Figure 8 the average radial velocities for stars with line widths greater than 5A have not been considered, because the radial velocities determined for these stars are extremely inaccurate, and the number of these stars is not large enough to make the average value meaningful.

It is a pleasure to thank Professor Otto Struve for his suggestion of the present problem and for valuable discussions during the present investigation. I am also indebted to Dr. C. D. Shane, director of the Lick Observatory, and to other members of that observatory for their hospitality and their interest in this problem. They not only permitted me to use freely the plates from which the material contained in this paper was obtained, but also gave me every conceivable convenience during the six weeks in the fall of 1951 which I spent on Mount Hamilton.

[12] The density of points in the diagram represents the frequency function $\phi(y_1, y_2)$ of the observed rotational velocity, y_1, and the radial velocity (corrected for the solar motion), y_2. The function $\phi(y_1, y_2)$ is related to the true frequency function $f(x_1, x_2)$ of the equatorial rotational velocity, x_1, and the space velocity, x_2, by the following integral equation:

$$\phi(y_1, y_2)\, dy_1 dy_2 = dy_1 dy_2 \int_{y_1}^{\infty} \int_{y_2}^{\infty} f(x_1, x_2) \frac{y_1}{(x_1^2 - y_1^2)^{1/2}} \frac{dx_1}{x_1} \frac{dx_2}{x_2}.$$

[13] E.g., W. W. Campbell, *Stellar Motions* (New Haven: Yale University Press, 1913); J. H. Oort, *M.N.*, **99**, 369, 1939; S. Chandrasekhar, *Principles of Stellar Dynamics* (Chicago: University of Chicago Press, 1942).

A RADIO MODEL OF THE GALAXY

STANLEY P. WYATT, JR.
Observatory, University of Michigan
Received July 28, 1952; revised March 31, 1953

ABSTRACT

An analysis is carried out to determine the structure of the galaxy as it is defined by the intensity distribution of continuous radio emission at 100 Mc/sec. Observational data are the radio isophotes of Bolton and Westfold. Results depend on the likely assumptions that the radio galaxy is axially symmetric and that it is transparent at 100 Mc/sec.

The density function in the galactic plane turns out to be approximately Gaussian in character, with a fairly "flat" nucleus, the sharpest decay in the regions of 2–4 kiloparsecs from the center, and a nearly linear decrease in the vicinity of the sun. The curve agrees with that found by Bolton and Westfold for the inner part of the galaxy. The density of radio sources in the galactic core is 5.4 ± 1.2 (p.e.) *times* the local density near the sun; and the average emission in our part of the Milky Way system is 1.1×10^{-39} ergs cm^{-2} sec^{-1} (cycles/sec)$^{-1}$. Superposed on the smooth radio galaxy are two additional features: first, a constant component with brightness temperature about 450° K, to be identified with the spherically distributed excess radiation discovered by Westerhout and Oort; second, an asymmetric component in the anticenter directions, probably originating from *H* II clouds in the Morgan-Osterbrock-Sharpless spiral arm that passes about 300 parsecs exterior to the sun.

The density distribution in the z-direction is assumed to follow a Gaussian law. From this approximation, it is found that in the nuclear part of the galaxy the precision modulus of the distribution at right angles to the galactic plane is five times its value in the plane. In the solar neighborhood the ratio is only about 3.

I. INTRODUCTION

Some insight into the over-all structure of the radio galaxy can be gained from an examination of the distribution of the continuous radio radiation, at some selected frequency, across the celestial sphere. The problem under investigation in the present paper is this: Given the intensity or brightness temperature of radiation at 100 Mc/sec at all galactic latitudes and longitudes, as observed from our eccentric station in the galaxy, and assuming a basic symmetry for our galaxy, we wish to solve for the three-dimensional distribution of radio-emitting sources.

Several investigations have already been devoted to the derivation of a model radio galaxy. Since the discovery of galactic radio radiation by Jansky[1] in 1931, it has become increasingly clear, from radio surveys by Reber[2] and by Hey, Parsons, and Phillips,[3] that the maximum power is received from the direction of the galactic nucleus in Sagittarius and that the radio Milky Way tapers off in intensity rather rapidly in latitude, but fairly slowly in longitude. The era of galactic analysis at radio frequencies was launched in 1950 by Bolton and Westfold[4] in Australia, who used the data of their own survey at 100 Mc/sec[5] in a way that is basically similar to Herschel's pioneering interpretations at visual wave lengths by star-gauging. On the assumption that the observed intensity in any direction is proportional to the radial extent of radiating matter in that direction, these authors found the equatorial section of the inner galaxy to be somewhat ovoid in shape and its meridian section to be a flattened ellipse with axis ratio about 0.15.

Westerhout and Oort,[6] utilizing the Bolton-Westfold data,[5] examined the changing density distribution of radio sources with distance from the sun. They sought a corre-

[1] *Proc. I.R.E.*, **20**, 1920, 1932.
[2] *Ap. J.*, **91**, 621, 1940; **100**, 279, 1944.
[3] *Proc. R. Soc. London*, *A*, **192**, 425, 1948.
[4] *Australian J. Sci. Res.*, *A*, **3**, 251, 1950.
[5] *Ibid.*, p. 19.
[6] *B.A.N.*, **11**, 323, 1951.

spondence between the observed radio isophotes and those predicted from a mass model of the galaxy that had been derived earlier by Oort and van Woerkom[7] from the distribution of G and K stars and dynamical considerations. The adopted model, adjusted to conform with the radio findings, comprises a set of superposed constant-density spheroids centered on the galactic nucleus. The innermost and densest of these spheroids has semiaxes of 2.8 and 1.0 kpc, with density 3.5 times that near the sun; the outermost and least dense has semiaxes of 32.5 and 10.3 kpc and a density of 0.00075. Additionally, Westerhout and Oort discovered a spherically distributed excess of radiation, with brightness temperature about 600° K, that could not be fitted to their model and thus is probably nongalactic in origin.

Bolton and Westfold[8] have recently completed an analysis of the distribution of sources of galactic noise in the galactic plane by solving Abel's integral equation. Although these authors subtract 1000° from the observed brightness temperatures, as being "extranuclear" in origin, and therefore are limited to a solution in the interior regions of the galaxy, their derived curve is of great interest. It shows that the nucleus is five or six times as dense as the outermost point of their solution—nine-tenths of the way from nucleus to sun. The inner core is roughly of constant density, and the steepest gradient occurs from 0.2 to 0.5 in terms of the sun's distance. Bolton and Westfold conclude that away from the galactic plane the observed isophotes fail to conform to a single spheroidal source distribution.

II. OBSERVATIONAL DATA

The present analysis utilizes the Bolton-Westfold 100 Mc/sec data,[5] which are presented as contours of constant temperature in galactic co-ordinates. This survey is the most complete presently available, with contours covering the entire Sagittarius region, both galactic polar caps, and about three-quarters of the equator (all except the northern arc from Sagitta to Auriga). Moreover, the integral equation expressing observed intensities as a function of true intensities and antenna pattern was solved carefully by graphical techniques. In the final derived temperature contours, the relative error at any point is estimated as not more than 5 per cent.

III. ASSUMPTIONS

In solving for a model of the radio galaxy, one needs to introduce several assumptions, some to render the analysis possible, some to render it tractable.

First, we assume that the galaxy is axially symmetric with respect to its polar axis of rotation. A second assumption is that the solar system is located in the galactic plane. Although evidence has accumulated from optical studies[9] and from the analysis by Seeger and Williamson[10] at radio frequencies that the sun may lie a few parsecs north of the plane, the effect of overlooking this possibility is negligible in examining the over-all form of the Milky Way system.

Third, we assume that interstellar space is essentially transparent to 100 Mc/sec radiation. Supplied with a general picture of the densities and spatial extent of Strömgren's *H* II regions,[11] Westerhout and Oort[6] find that, for 100 Mc/sec radiation, the optical depth per kiloparsec of "cloudy" structure is only about 0.017. Bolton and Westfold[8] conclude that the "intercloud" regions would have, at most, an optical depth of only

[7] *B.A.N.*, **9**, 185, 193, 1941.

[8] *Australian J. Sci. Res.*, *A*, **4**, 476, 1951.

[9] See J. J. M. van Tulder, *B.A.N.*, **9**, 315, 1942.

[10] *Ap. J.*, **113**, 21, 1951.

[11] *Problems of Cosmical Aerodynamics* (Dayton: Central Air Documents Office, 1951), p. 7.

0.0072 over a 20-kpc path. It thus seems warranted to disregard absorption effects completely in our analysis.

A final point, while not an assumption, ought to be mentioned. Results will be stated in terms of the total amount of energy emitted per second over unit frequency interval by an average volume of space located at some point, independently, of course, of the specific nature of the source or sources of the radiation at that point.

IV. DENSITIES IN THE GALACTIC PLANE

The first step in the analysis is to solve for the density distribution of radio sources in the plane of the galaxy as a function of distance from the center, inasmuch as the relevant integral equation is much simplified and offers symmetry properties that do not obtain at nonzero latitudes. From inspection of the Bolton-Westfold isophotes, we adopt the longitude of the center as 327° and define $\alpha = 327° - l$.

Let $E_\nu d\nu$ represent the total energy radiated per second in all directions by an average radio source in elementary frequency interval, and let there be $n(a)$ such sources per unit volume in the galactic plane at a distance a from the center. Now consider a region of space that subtends a small solid angle $d\omega$ at the antenna. Then the total radiation emitted per second in the frequency range $d\nu$ by elementary volume, $d\tau = r^2 dr d\omega$, will be

$$E_\nu d\nu n(a)\, r^2 dr\, d\omega . \tag{1}$$

This radiation is diluted in reaching unit area of the antenna by a factor of $1/4\pi r^2$, so that the energy per second received by 1 cm^2 of the antenna, originating from $d\tau$, is

$$\frac{E_\nu d\nu d\omega n(a) dr}{4\pi} = \frac{E_\nu d\nu d\omega n(a)\, a\, da}{4\pi (a^2 - a_0^2 \sin^2 \alpha)^{1/2}}, \tag{2}$$

where the differential dr is transformed into a function of distance from the galactic center, a, distance of sun from center, a_0, and longitude difference, α.

Now the specific intensity of radiation from the direction α ($0 \leq \alpha \leq \pi/2$) and, by symmetry, from $-\alpha$ is then the integral of this function evaluated from the sun across the galaxy and out to infinity:

$$I(\pm\alpha) = \frac{2E_\nu}{4\pi} \int_{a_0 \sin \alpha}^{a_0} \frac{n(a)\, a\, da}{(a^2 - a_0^2 \sin^2 \alpha)^{1/2}} + \frac{E_\nu}{4\pi} \int_{a_0}^{\infty} \frac{n(a)\, a\, da}{(a^2 - a_0^2 \sin^2 \alpha)^{1/2}}. \tag{3}$$

In opposite directions ($\pi/2 \leq \alpha \leq \pi$), where we integrate only through regions farther than the sun from the galactic nucleus, we find by a similar construction that

$$I(\pi \pm \alpha) = \frac{E_\nu}{4\pi} \int_{a_0}^{\infty} \frac{n(a)\, a\, da}{(a^2 - a_0^2 \sin^2 \alpha)^{1/2}}. \tag{4}$$

From these two relations, it is clear that within the framework of our assumptions we can subtract the "exterior" intensity from the "interior" intensity and deal with the residual, which is simply the total contribution originating inside a circle of radius a_0 about the galactic center. If we subtract equation (4) from equation (3), the interior intensity is

$$I(\pm\alpha) - I(\pi \pm \alpha) = \frac{E_\nu}{2\pi} \int_{a_0 \sin \alpha}^{a_0} \frac{n(a)\, a\, da}{(a^2 - a_0^2 \sin^2 \alpha)^{1/2}}. \tag{5}$$

The procedure here not only restricts our attention to high-density regions of the galaxy but also eliminates the effect of any excess nongalactic radiation that may be spherically

distributed over the celestial sphere. What remains is an integral equation, wherein the left member comprises a set of known observational data for all values of α less than $\pi/2$ and the integrand contains the sought-for function, $n(a)$.

The first procedure in the solution of this equation requires finding a well-behaved curve for the Bolton-Westfold brightness temperatures[5] as a function of longitude difference, α. The points in Figure 1 are taken from the published isophotes and plotted against α. Open circles refer to points at longitudes less than 327°; filled circles, to longitudes greater than 327°. The smooth curve joining these points is shown as a dotted line. The curve-drawing was governed by several considerations. First, departures from equality at equal angular distances on either side of the center were viewed as arising from the

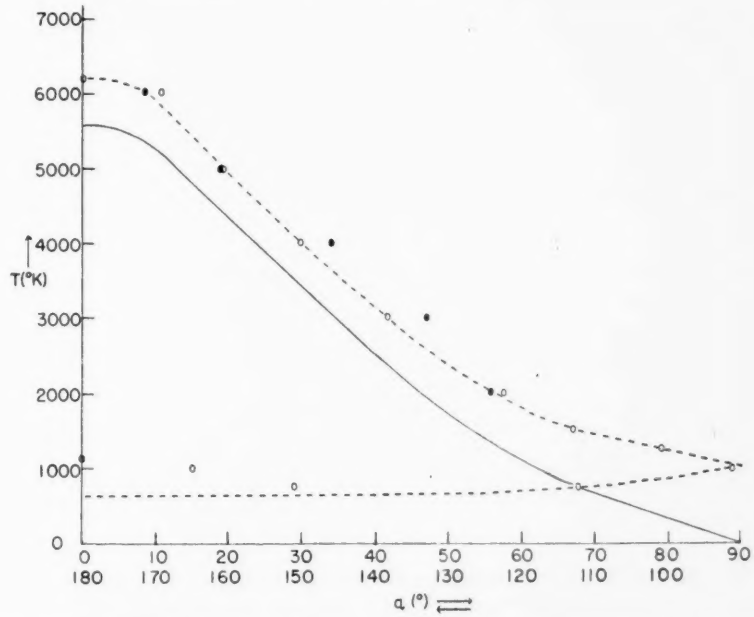

FIG. 1.—Radio temperatures at 100 Mc/sec as a function of longitude difference, α, in the galactic plane. Open circles are observed temperatures at longitudes less than 327°; filled circles those at longitudes greater than 327°. The upper dotted curve shows the adopted temperature function for $0° \leq \alpha \leq 90°$, while the lower dotted curve represents the adopted distribution for $90° \leq \alpha \leq 180°$. The solid curve is the difference between the two dotted curves and represents that part of the total temperature originating interior to a circle of radius a_0 centered on the galactic nucleus.

integrated effects of asymmetrically distributed *H* II regions. Thus, regarding inequalities as being excesses rather than deficiencies, the curve was guided pretty much along the lower set of observed points. Additionally, the role of symmetry and the likely prospect that $n(a)$ is a decreasing function of a demand a temperature function that decreases monotonically with α. Thus the trend of rising temperature observed toward the anticenter ($150° \leq \alpha \leq 180°$) has again been supposed to originate from *H* II clouds in spiral structure. An asymptote was drawn in this region, governed by the fact that the smoothed anticenter temperature will very probably not fall below the 600° temperature observed at the galactic poles. The final adopted temperature distribution arising from

the "interior" galaxy is derived, according to equation (5), by simply differencing the two dotted curves. This function is drawn as a solid line in Figure 1.

The next step involves finding a preliminary solution of the equatorial density function. To achieve this, the interior galaxy was divided into ten circular rings of constant density, each of width $a_0/10$. The density in the ring externally tangent to the sun is proportional to the temperature observed at $\alpha = \sin^{-1} 0.9$ and inversely to the path length in this direction. The density of the next ring can then be found in terms of the density just evaluated, the observed temperature at $\alpha = \sin^{-1} 0.8$, and the relative path lengths across both rings in this direction. One then solves successively for the relative density in each ring until finally the central density is found. Normalizing so that the density at

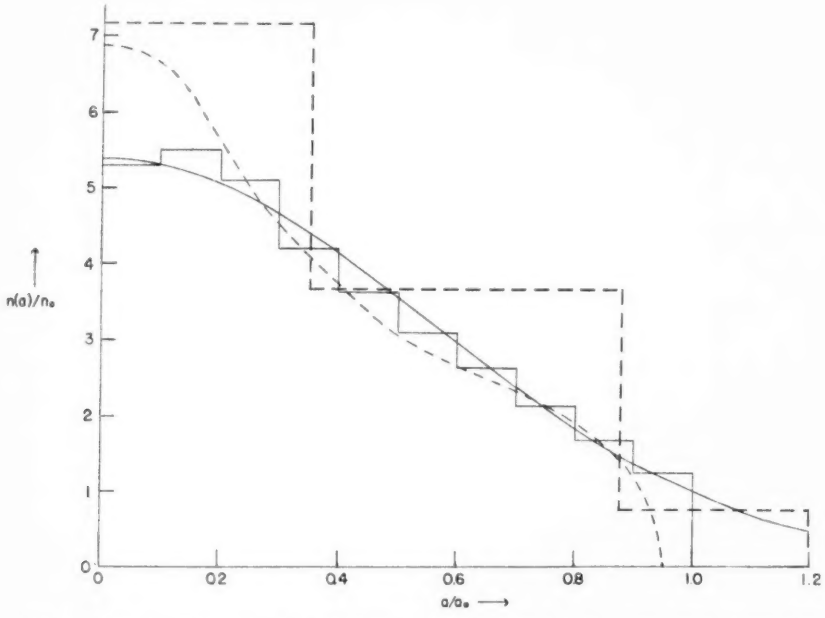

FIG. 2.—The density distribution of radio emission in the galactic plane as a function of distance from the center, in terms of the density near the sun. The solid histogram represents the preliminary numerical solution; the solid curve is the best Gaussian fit to the observations. The density of the Westerhout-Oort model of homogeneous spheroids is shown as the dotted histogram; the dotted curve gives the results of Bolton and Westfold.

the sun is unity, one finds the first approximation to the desired function, $n(a)$, with results as shown by the solid histogram in Figure 2. The noteworthy features of the distribution are threefold: (1) a rather "flat" galactic core of density about five times that near the solar system, (2) a rather sharp gradient at distances $0.2a_0$–$0.4a_0$, and (3) an approximately linear decrease in the regions $0.6a_0$–$1.0a_0$. The central density cannot be very adequately determined, since each integration depends on all those that preceded it and, moreover, the central value is conditioned by the smoothing process over the entire range of the observed function. However, an independent trial of the solution, using nine rings, and another trial, using the Hey, Phillips, and Parsons isophotes at 64 Mc/sec, agree in giving a central density of 5.

Finally, we wish to adopt, if possible, a suitable analytic form for the density function and try direct solutions in order to reproduce the solid curve of Figure 1. The first trials were in terms of a linear decrease, but this form proved unsuitable. For no straight-line function is it possible to recover the observed curve. Intensities at small α are satisfied for central density 7 or 8, whereas those at large α demand a central density of only 4 or 5. The observations can be closely satisfied by no less than three separate legs: a flattish one in the nucleus, a steep one farther out, and a moderate one in the regions $0.5a_0$–$1.0a_0$. Such a representation seems artificial and is laborious to integrate.

With the qualitative knowledge gained from this attempt, however, it appeared that a single Gaussian function might fit the observed temperature-curve rather well. Let us adopt for the density function the relation

$$n(a) = n_c e^{-h^2 a^2}, \tag{6}$$

where the precision modulus, h, is related to the central density, n_c, by the condition that the density near the sun be $n(a_0) = n_0$. Thus

$$n_c = n_0 e^{h^2 a_0^2}. \tag{7}$$

Substituting equation (6) in equation (5) and transforming to r and α as variables, it is found that

$$I(\pm\alpha) - I(\pi \pm \alpha) = \frac{E_\nu n_c e^{-h^2 a_0^2}}{2\pi e^{-h^2 a_0^2 \cos^2 \alpha}} \int_0^{a_0 \cos \alpha} e^{-h^2 (r - a_0 \cos \alpha)^2} dr$$

$$= \frac{E_\nu n_0}{2\pi h} \frac{H(h a_0 \cos \alpha)}{H'(h a_0 \cos \alpha)}, \tag{8}$$

where

$$H(x) = \frac{2}{\sqrt{\pi}} \int_0^x e^{-t^2} dt$$

is the error function and where

$$H'(x) = \frac{2}{\sqrt{\pi}} e^{-x^2}$$

is the derivative of the error function. With tables of these functions,[12] calculated intensity-curves were constructed for values of $ha_0 = 1.2$, 1.3, 1.4, and 1.5, normalized approximately and superposed on the observed curve. From the preliminary values of $E_\nu n_0 / 2\pi h$ and ha_0 found in this way, the most probable values of these quantities were found by least squares from the observed intensities at each 10° in α. The resulting values, with their probable errors, are

$$\frac{E_\nu n_0}{2\pi h} = 3.73 \pm 0.15 \times 10^{-18} \text{ erg cm}^{-2} \text{ sec}^{-1} \text{ (cycles/sec)}^{-1}, \tag{9}$$

$$h a_0 = 1.30 \pm 0.09. \tag{10}$$

The latter quantity leads, on substitution in equation (7), to a central density of 5.4 ± 1.2 in terms of the density near the solar system. If we now adopt 9 kpc as the distance from the sun to galactic center, we find that $h = 0.144$ kpc^{-1}. With this value, one can determine the absolute emission per unit volume at this frequency for the vicinity of the

[12] *Tables of Probability Functions* (New York: Federal Works Agency, Work Projects Administration, 1941), Vol. 1.

sun. Converting h into centimeters and substituting in equation (9), we find readily that this emission is

$$E_\nu n_0 = 1.1 \times 10^{-39} \text{ erg cm}^{-3} \text{ sec}^{-1} \text{ (cycles/sec)}^{-1} . \tag{11}$$

If, instead, we adopt $a_0 = 8$ kpc, in order to compare these results with those of previous investigations, the emission per unit volume is, in the same units, 1.2×10^{-39}. The result of Westerhout and Oort,[6] reduced to these units, is 1.0×10^{-39}. Although Bolton and Westfold do not evaluate the emission near the sun, it is possible to intercompare values at the galactic center. The nuclear emission found in the present paper is 5.4 times the value near the sun, or 6.5×10^{-39}; that of Bolton and Westfold,[8] after conversion of units, is 8.4×10^{-39}. The density functions of the three analyses are plotted in Figure 2.

One often finds data presented in terms of brightness temperature rather than specific intensity, and the transformation is readily carried out by using the Rayleigh-Jeans approximation to Planck's law,

$$I_\nu d\nu = \frac{2\nu^2}{c^2} kT d\nu . \tag{12}$$

On this basis, the value of equation (9) becomes $1220° \pm 50°$, and may be used to calculate interior temperatures by equation (8). Calculated Gaussian temperatures and observed temperatures agree rather well at all values of α, the average absolute difference being 70°.

Now that we have settled on values to represent the equatorial density function and if we assume the Gaussian function to hold in regions exterior to the sun, it is found readily that, for example, the density of radio sources falls to half the local density at distance $1.19a_0$ and to one-tenth the local density at distance $1.53a_0$ from the galactic nucleus. Moreover, it becomes possible to integrate for the total temperatures, interior and exterior, arising from the galaxy, for any value of longitude. The integral for any interior longitude is

$$I(\pm\alpha) = \frac{E_\nu n_0}{4\pi h} \frac{1 + H(ha_0 \cos \alpha)}{H'(ha_0 \cos \alpha)} . \tag{13}$$

And the integral for any exterior longitude is simply the difference of equations (13) and (8). The contributions in the galactic plane due to the smooth galaxy range from 5650° at the center through a monotonically decreasing function to 190° at the anticenter, with a value at $\alpha = \pm 90°$ of 540°.

Upon comparison of calculated temperatures with the observed total temperatures, two features stand out. First, there exists an approximately uniform excess radiation at all longitudes. Comparing the smoothed temperatures in Figure 1, shown as dotted lines, with those calculated from equations (8) and (13), at every 10° of longitude around the galactic circle, the mean value of the excess brightness temperature is found to be 450°, with an average deviation of $\pm 55°$. It must be stressed that this result rests on the unchecked extrapolation of the Gaussian density function to exterior regions of the galaxy. It is possible that some or all of this excess arises from the smooth galaxy itself if the exterior density decays less rapidly than the adopted function. However, this same excess of 450° appears also at the galactic poles, as will be shown subsequently, and we identify it provisionally with the general spherical excess first discovered by Westerhout and Oort[6] in 1951. It should be remembered that this component of the emission remains in the smoothed data, only canceling out when we use the symmetry properties of the integral equation to examine the interior galaxy.

Another aspect of the equatorial temperatures is the specific run of the local excesses

previously subtracted for the purpose of analyzing the smooth and symmetric component of the galaxy. It will be seen from Figure 1 that there is a run of rising intensity near the anticenter, increasing steadily from Monoceros to Auriga, where one finds a maximum brightness temperature of about 500°, over and above the smooth galaxy and the spherical excess of 450°. It appears also that there may be some tendency to local excesses in the Aquila region, 30°–50° from the galactic center.

The run of increased temperatures toward the anticenter may well be due to the Morgan-Osterbrock-Sharpless[13] spiral arm, defined by *H* II clouds, which extends past the sun and exterior to it about 300 parsecs distant. There is no obvious correspondence with specific individual clouds, and none should be expected, inasmuch as the beam width of the Bolton-Westfold antenna is 17°. The general decrease in intensity with angular distance from the anticenter may, however, be anticipated because of the inverse-square law. As the arm winds out and away from the sun, the average number of clouds cut by the antenna cone will increase roughly by a secant law, but the increasing distance overcompensates for this, and the integrated intensity of *H* II ought to decrease gradually to zero by the time we are looking out between the arms—perhaps in the Canis Major direction. It is possible to calculate readily the emission measure at radio frequencies for ionized regions (see, e.g., Westerhout and Oort[6]). For the anticenter region with its *H* II excess of 50°, this quantity, $\int N_e^2 ds$, is, in Strömgren's units, about 1000 cm^{-6} pc. This value agrees approximately with one of the average extended emission regions measured by Strömgren and Hiltner[11] and corresponds, if the antenna pattern is completely filled with *H* II spheres, to an average density of 3 electrons/cm^3 over a path of 100 pc or 10/cm^3 over a path of 10 pc. These values accord in a rough way with results from studies at optical wave lengths.

The local excesses shown in Figure 1 in the Aquila region are not very pronounced and may be unreal. Certainly, one cannot expect much correlation with Balmer emission from *H* II clouds, since the Great Rift lies in this direction. W. Becker[14] has supposed, however, that in this direction we may be looking tangentially along an inner spiral arm. If this were true, one would expect the radio-emission measure to reach a peak at these longitudes.

It will be interesting to see whether from future high-resolution surveys there emerges any detailed correspondence in position and emission measured between asymmetric radio excesses and the locations of specific *H* II clouds.

V. DENSITIES AWAY FROM THE GALACTIC PLANE

Analysis of the density distribution from data at nonzero latitudes is complicated by the fact that the integral equation offers no simplifying symmetry properties. Moreover, one is dealing with low-intensity levels, subject to the uncertainties entailed in subtracting a uniform 450° over the celestial sphere. Results for the density function in the z coordinate are chiefly qualitative in character.

As an approximation to the density function, we assume that the density in the z direction decreases according to a Gaussian law. We then solve for k, the precision modulus of this distribution, and attempt to ascertain whether this value remains constant or how it changes in the galaxy. Some such assumption as to the form of the density decay is mandatory if the integrations are to be kept at all tractable. Actually, the Gaussian law has some basis in dynamical theory,[15] except that it holds strictly only at small distances from the galactic plane. Moreover, there is no certainty that the distribution of radio emission follows the distribution of mass.

[13] *Sky and Telescope*, **11**, 138, 1952.

[14] *Zs. f. Ap.*, **29**, 269, 1951.

[15] See, e.g., S. Chandrasekhar, *Principles of Stellar Dynamics* (Chicago: University of Chicago Press, 1942), p. 190.

The first step in solving for the density distribution in the z co-ordinate, under the assumption stated above, involves the selection of an approximate value of k, calculating a model galaxy with this single value of k, and comparing with the observed isophotes. The total emission from any cube in the galaxy can be represented by the function

$$n(a, z) = n_c e^{-h^2a^2-k^2z^2}. \tag{14}$$

As in Section IV, we integrate this function from the sun to infinity to calculate the total intensity received at the earth. Transforming to r, a, and b as variables, where b is galactic latitude, and integrating over r, we find, after some reduction, a generalization of equation (13) for nonzero latitudes. The energy received from (a, b) is

$$I(a, b) = \frac{E_v n_0}{4\pi (h^2 \cos^2 b + k^2 \sin^2 b)^{1/2}} \frac{1 + H(x)}{H'(x)}, \tag{15}$$

where

$$x = h a_0 \frac{h \cos b \cos a}{(h^2 \cos^2 b + k^2 \sin^2 b)^{1/2}}. \tag{16}$$

The initial choice of k is governed by the flattening of the observed high-intensity isophotes in the Sagittarius region. The ratio of minor to major axis of the observed isophotes approaches as a limit the value h/k, the ratio of the precision modulus in a to that in z, as the magnitude of the axes approaches zero. This result will be vitiated by any appreciable excess radiations, but in the present instance the effect will be very small, since the spherical excess of 450° is only about 8 per cent as strong as the temperature of the galaxy itself in the direction of the center. Now the average value of the axis ratio for the five innermost isophotes is 0.20 ± 0.005 (p.e. of mean), with, however, a slight indication for an asymptotic approach to a value as low as 0.17. Thus the ratio of the precision modulus in z to that in a is $1/0.20 = 5$, or perhaps as high as $1/0.17 = 6$. That is, the density decays in the z direction 5 or 6 times as sharply as in the equatorial direction. A galaxy model constructed with $k/h = 5$ shows generally good agreement with the observed isophotes in the high-intensity regions near Sagittarius, but it fails to reproduce the brightness temperatures over the galactic polar caps, after the spherical excess of 450° is subtracted from the isophotes. More relevantly, the constructed model shows little conformity with the temperature gradient across the galactic caps, as pointed out to the author during a conversation with Professor Oort. It is apparent that a pure spheroidal model, corresponding to a single choice of k, fails to represent the galaxy. The value $k/h = 5$, selected from the characteristics of the high-density galactic core, is thus representative only of the material in the inner regions of the Milky Way system.

In order to evaluate k/h in our part of the galaxy, the best procedure seems to be to try reproducing the observed temperature gradient across the polar caps, inasmuch as this gradient is independent of any spherical source distribution. By a trial-and-error procedure, the value for k/h in our neighborhood is found to be about 3. The decay of density is less steep than for central regions. A check on the excess radiation in the polar caps can be made by calculating the anticipated temperature due to the galaxy alone, using a value of 3, and subtracting the result from the observed 600°. One finds again an excess of about 450°.

Although there is little doubt that k is a markedly varying function of distance from the center, the approximate values found here should be taken *cum grano salis*, since they are based on an assumed Gaussian decay. Indeed, the slower decay in z in the solar regions leads to the anomalous result that the emission at a point, for example, 3 kpc above the solar system, is greater than the emission 3 kpc above the galactic core.

An interesting feature of the computed models is that the points of minimum temperature on the celestial sphere ought to occur not at the galactic poles but at points dis-

placed from them toward the anticenter. The radio observations seem to confirm this effect, with the minimum point (averaged for both galactic hemispheres) occurring very roughly at $l = 180°$, $b = 45°$. A displaced minimum also appears in van Rhijn's tables of stellar distribution,[16] at about $l = 160°$, $b = 65°$. The latitude effect here is expected, by virtue of the density decay in both z and a; the fact that the minimum longitude is not exactly at the anticenter, however, must arise from asymmetric effects superposed on the smooth galaxy.

VI. CONCLUSIONS

The observed distribution of radio emission at 100 Mc/sec appears to be compounded of three parts: a component arising from the axially symmetric galaxy, another from spiral structure in the Milky Way system, and a third from a roughly spherical distribution of sources.

The dominance of the first component in regions near Saggittarius permits the derivation of a smooth model galaxy. The best Gaussian fit to the observed equatorial temperatures indicates that the emission per unit volume near the sun is about 1.1×10^{-39} erg cm^{-3} sec^{-1} (cycles/sec)$^{-1}$ and in the galactic nucleus it is five or six times this value. These results agree reasonably well with those of Westerhout and Oort[6] and Bolton and Westfold.[8] An entirely different approach to galactic structure, undertaken by Oort and van Woerkom[7] and Parenago,[17] utilizing dynamical theory and the observed distribution and velocities of the common stars, yields the distribution of mass in the galaxy. Parenago finds that $\rho_c/\rho_0 = 5.5$, in close agreement with the value $n_c/n_0 = 5.4 \pm 1.2$ from the present investigation. Moreover, the Oort–van Woerkom mass model is found to fit closely the radio observations. It thus appears that the axially symmetric component of the 100 Mc/sec emission is distributed in much the same way as is the mass of the galaxy.

The second component of the radiation probably originates in the spiral arms. Although there is rough agreement at optical and radio wave lengths between the location and the observed emission measure of *H* II clouds along spiral arms, a check on the detailed correspondence in both wave-length regions must await radio surveys of higher resolution.

The third component, a spherical excess of about 450°, is evaluated in the present paper by extrapolating the Gaussian equatorial density function beyond the sun and also from the observed temperature gradient over the galactic polar caps. The value of 600° discovered by Westerhout and Oort[6] rests on the assumption, which appears to be a good one, that mass and radio emission are distributed similarly in the galaxy. Bolton and Westfold[8] also find evidence for an isotropic background of the same order of magnitude. Since, however, all three investigations are based on the same observational data it is important that the existence and magnitude of this spherical excess be checked from other surveys at neighboring frequencies.

[16] *Groningen Pub.*, Vol. **43**, 1929.

[17] *A.J. Soviet Union*, **29**, 245, 1952.

PHOTOELECTRIC MAGNITUDE SEQUENCES FOR THE MAGELLANIC CLOUDS*

ARTHUR N. COX AND KENNETH L. HALLAM†
Goethe Link Observatory, Indiana University
Received March 18, 1953

ABSTRACT

Photoelectric magnitudes and colors of stars in the Harvard sequences for the Magellanic Clouds have been observed with the 24-inch Victoria telescope at the Royal Observatory, Cape of Good Hope. Comparisons were made with stars in the Harvard Standard Regions E2, E3, and E4. Use has been made of a previous tie of these E-region stars to the NPS.

An attempt is made in this paper to establish an accurate photoelectric system of magnitudes and colors for the brighter stars in the regions of the Magellanic Clouds. Previous work on magnitude standards has been done by Mohr,[1] McKibben,[2] and van Wijk;[3] numerous references to these standards appear in other Harvard publications. The apparatus used for these observations was identical to that described by Cox.[4] Figure 1 identifies the ten standard stars for the Small Magellanic Cloud; the eight standard stars for the Large Magellanic Cloud are designated in Figure 2. For the sake of completeness, all the bright standard stars are marked. Other nomenclature for the sequence stars can be found in Table 1. Standard stars used in the regions E2, E3, and E4 are the same as those used previously.[4]

TABLE 1

NOMENCLATURE AND POSITIONS OF THE SEQUENCE STARS

HARVARD LETTER SMC	GC OR CPD	1950 α	1950 δ	HARVARD LETTER LMC	GC OR CPD	1950 α	1950 δ
a	777	0^h36^m7	−73° 25′	a	6795	5^h27^m3	−68° 40′
b	1435	1 08.5	−73 13	b	7177	5 41.8	−67 26
c	771	0 36.4	−74 14	c	6682	5 23.2	−71 33
d	1329	1 03.7	−72 49	d	−70°399	5 29.8	−70 52
e	1238	0 59.3	−72 58	e	6157	5 00.1	−68 39
f	1306	1 02.7	−72 31	f	6542	5 17.8	−68 39
g	−72°68	0 48.4	−71 46	g	6443	5 13.8	−68 05
h	−73°44	0 42.2	−72 38	h	−68°345	5 17.6	−68 31
k	−72°65	0 44.7	−72 29	l	−68°352	5 18.6	−68 31
l	−72°66	0 44.8	−72 34	m	−68°349	5 18.2	−68 34
m	−73°49	0 48.9	−72 36	n	−68°346	5 17.8	−68 25
n		0 45.1	−72 27	o		5 19.1	−68 31

* *Publications of the Goethe Link Observatory, Indiana University*. No. 11.

† Now at the University of Wisconsin.

[1] *Harvard Ann.*, **105**, 237, 1937.

[2] *Harvard Ann.*, **108**, 13, 1940.

[3] *Harvard Bull.*, **921**, 7, 1952.

[4] *Ap. J.*, **117**, 83, 1953.

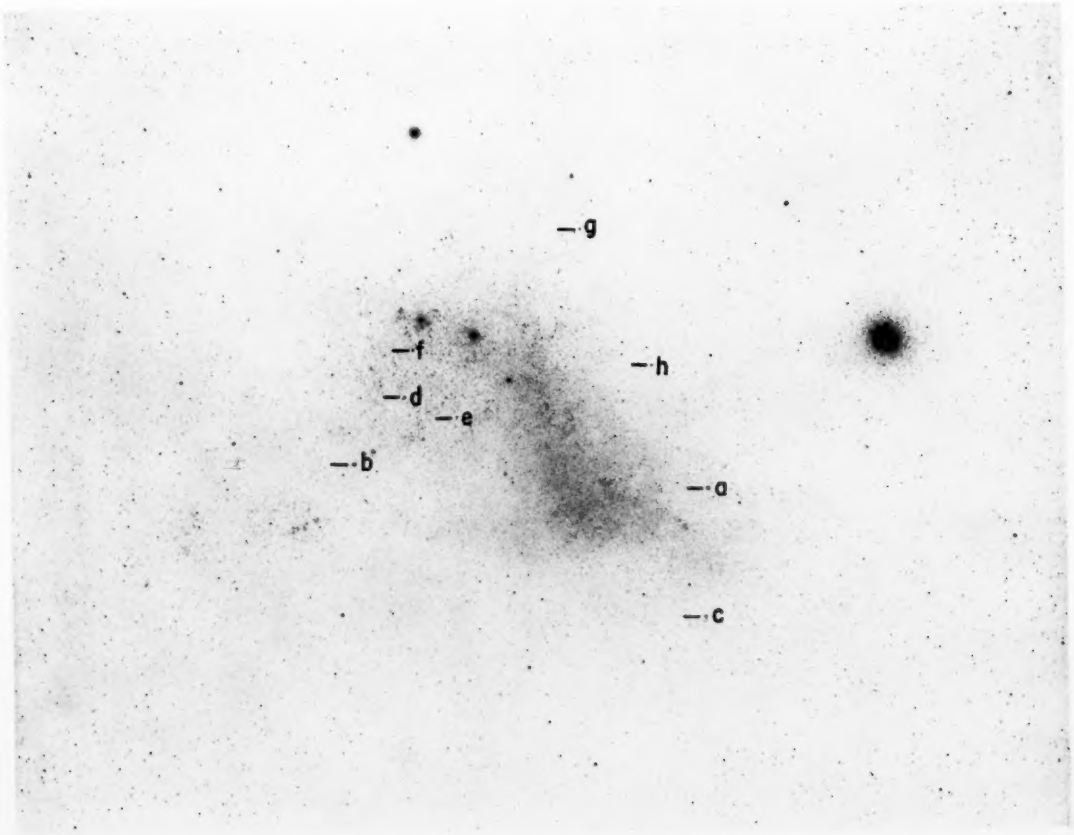

FIG. 1*a*.—A photograph of the Small Magellanic Cloud. All the bright standard stars are marked

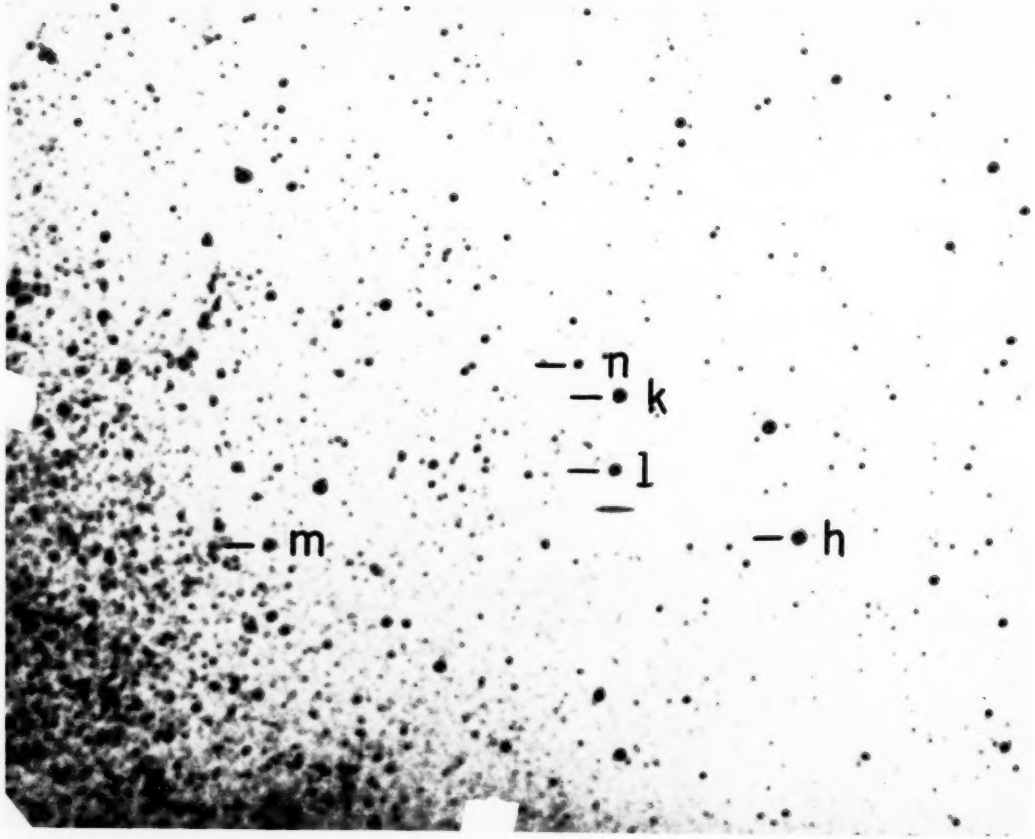

FIG. 1*b*.—An enlargement of the Harvard sequence region in the Small Magellanic Cloud. All the bright standard stars are marked.

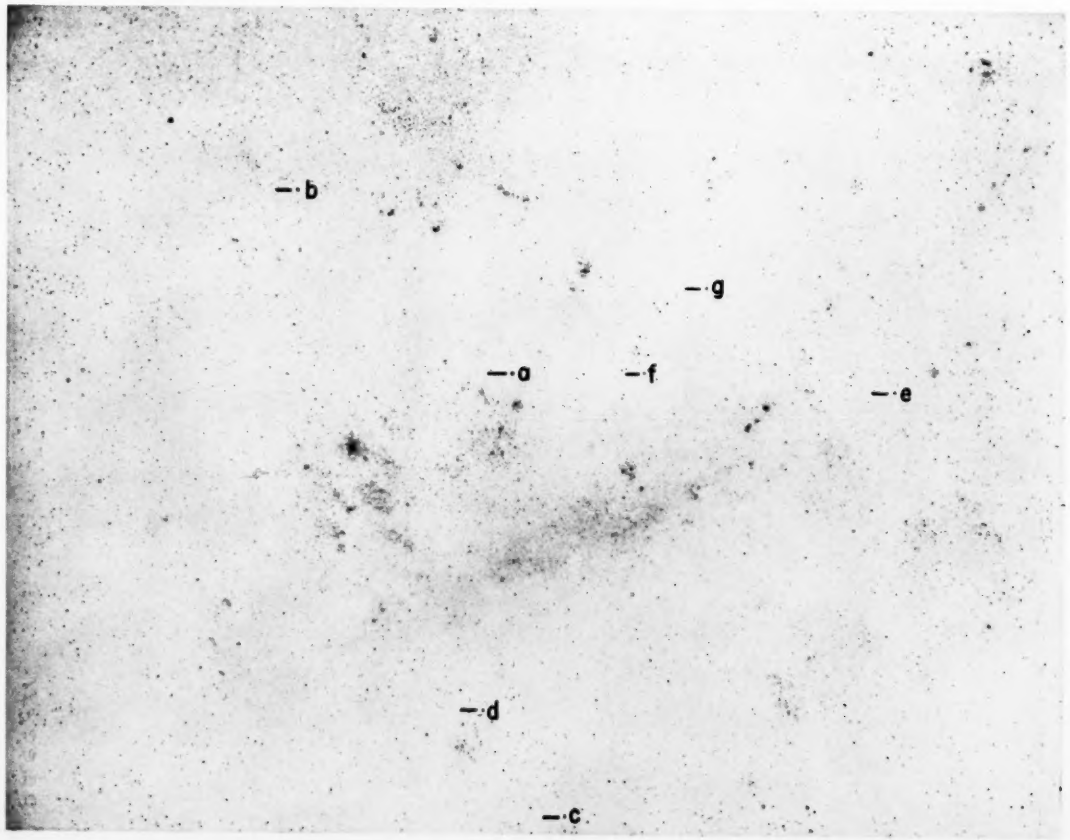

FIG. 2*a*.—A photograph of the Large Magellanic Cloud. All the bright standard stars are marked

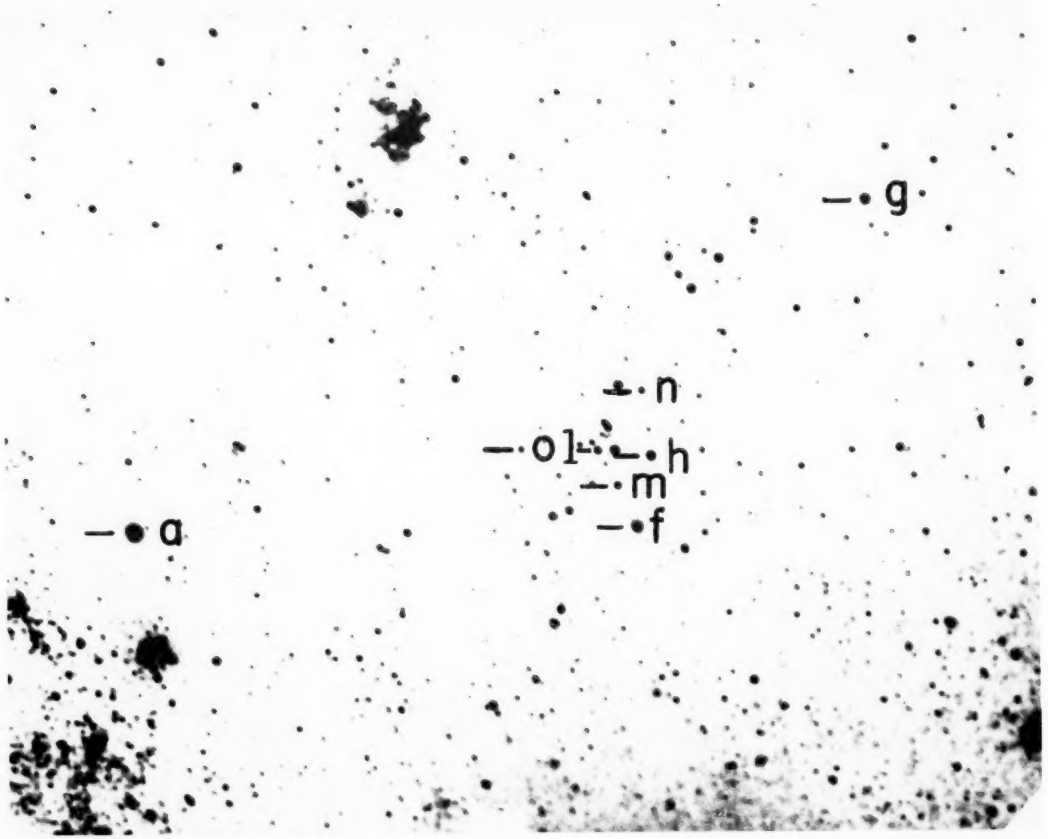

FIG. 2*b*.—An enlargement of the Harvard sequence regions in the Large Magellanic Cloud. All the bright standard stars are marked.

A comparison between a Cloud sequence and an E region was made so that all observations were at nearly equal altitudes. Transfers were obtained to the SMC on four nights and to the LMC on six nights. Measures were made of stars in both Clouds on four other nights. Four bright stars of Harvard Sequence I of the SMC and of Harvard Sequence V of the LMC, together with the four stars of each E region, were used to establish the zero points of magnitude and color in the Clouds. A typical comparison was: SMC c, d, e, f, c; E2 B, G, H, K, B; SMC c, d, e, f, c.

A differential correction due to atmospheric extinction of the form $m - m_0 = k(\sec z - \sec z_0)$ was applied individually to each observation. In the above expression, m is the observed magnitude at a zenith distance z, and m_0 is the magnitude corrected to the zenith distance z_0. The values of sec z_0 were chosen to be the means of the observed secants of the zenith distance, 1.29 and 1.23 for the SMC and LMC, respectively. The coefficients of extinction, k, were 0.155 mag. for the yellow light and 0.270 mag. for the blue light. These coefficients were adopted from the average of values obtained on many nights at the Cape in the eastern sky. An analysis of the resulting magnitudes during each night led to a further extinction correction which was made to depend on the time of observation.

TABLE 2

MAGNITUDE AND COLOR ZERO-POINT RESIDUALS

Date	Transfer	Weight	$B-\bar{B}$	$V-\bar{V}$	$C-\bar{C}$
Nov. 20–21, 1950	SMC-E2-SMC-E3	½	+0.005	+0.008	−0.003
Dec. 4–5	SMC-E2-SMC	1	− .023	− .025	+ .002
8–9	SMC-E3-SMC	1	+ .006	+ .007	− .001
17–18	SMC-E3-SMC-E2	1	+ .015	+ .015	.000
Nov. 12–13, 1950	E2-LMC	1	+ .043	+ .034	+ .009
13–14	E2-LMC	1	+ .008	+ .014	− .006
20–21	LMC-E3-LMC-E3	1	− .001	− .004	+ .003
26–27	LMC-E3-LMC	1	− .009	− .006	− .003
Dec. 4–5	LMC-E3-LMC	1	− .024	− .025	+ .001
Jan. 19–20, 1951	LMC-E4-LMC	½	−0.030	−0.025	−0.005

In the reductions, relative magnitudes for the E-region stars were known for a sec z of 1.55. By means of a linear color relation, allowance was made in tying the Cloud magnitudes to the E regions at a sec z near 1.26. Raw relative Cloud magnitudes are therefore known for sec $z = 1.55$.

Because of small flexure of the optical system during the transfers, it was necessary to apply corrections to the observed magnitudes. The form of this correction was assumed to be $F_{E-C} = -K(\cos t_E \sin \delta_E - \cos t_C \sin \delta_C)$ mag., where K is a constant equal to 0.033 mag., t_E and t_C are the hour angles of the E region and the Cloud, respectively, and δ_E and δ_C are the corresponding declinations of the E region and the Cloud sequence. The flexure corrections ranged from 0.007 to 0.049 mag. More details about the observing and reduction procedures can be found elsewhere.

The zero-point residuals from the final means are given in Table 2. In the second column the regions are given in order of observation. Weights were assigned according to the quality of the night. The zero-point residuals show that the probable error of each determination of the zero point in the SMC is ±0.011 mag. in the blue, ±0.012 mag. in the yellow, and ±0.001 mag. in the color index; in the LMC it is ±0.017 mag. in the blue, ±0.015 mag. in the yellow, and ±0.004 mag. in the color index. An examination of the relative magnitudes of the stars gives no positive evidence of variability of any of the stars in either Cloud sequence. The magnitudes and colors of the standard stars in

the Cloud sequences and the number of observations of each are given in Table 3. The (B, C) values listed are on the natural color system of the photometer at sec $z = 1.55$. This (B, C) system is identical to that used by Cox.[4] The magnitudes on the $(\boldsymbol{P}, \boldsymbol{V})$ system of Stebbins, Whitford, and Johnson[5] were determined from the relations which hold at sec $z = 1.55$: $\boldsymbol{P} = B + 0.084C + 4.18$, $(\boldsymbol{P} - \boldsymbol{V}) = 1.165C - 0.14$. In Table 4

TABLE 3

MAGNITUDES AND COLORS OF THE SEQUENCE STARS

	Star	B	C	$\boldsymbol{P}$	$(\boldsymbol{P}-\boldsymbol{V})$	No. of Obs.
SMC	c	3.55	+0.42	7.77	+0.35	36
	d	4.25	+0.50	8.47	+0.44	19
	e	4.66	+1.21	8.94	+1.27	10
	f	5.06	+0.92	9.32	+0.93	20
	g	5.78	+0.49	10.00	+0.43	22
	h	5.91	+0.42	10.13	+0.35	4
	k	6.14	+0.17	10.33	+0.06	3
	l	6.84	+0.36	11.05	+0.28	2
	m	7.22	+0.03	11.40	−0.11	2
	n	7.49	+1.11	11.76	+1.15	2
LMC	e	3.97	+0.21	8.17	+0.10	39
	f	4.14	+0.80	8.39	+0.79	23
	g	4.40	+0.28	8.60	+0.19	11
	h	4.99	+0.12	9.18	0.00	23
	l	6.15	+0.19	10.35	+0.08	29
	m	6.44	+0.25	10.64	+0.15	3
	n	6.81	+0.27	11.01	+0.17	3
	o	7.41	+0.40	11.62	+0.33	3

TABLE 4

MAGNITUDES AND COLORS OF THE E-REGION STARS

	Star	B	C	$\boldsymbol{P}$	$(\boldsymbol{P}-\boldsymbol{V})$
E2	B	3.47	+0.20	7.67	+0.09
	G	4.31	+0.44	8.53	+0.37
	H	4.44	+1.12	8.71	+1.16
	K	4.61	+0.10	8.80	−0.02
E3	E	3.64	−0.10	7.81	−0.26
	H	4.60	+0.23	8.80	+0.13
	L	5.25	+0.51	9.47	+0.45
	M	5.27	+0.92	9.53	+0.93
E4	C	3.67	+0.05	7.85	−0.08
	F	3.86	+0.17	8.05	+0.06
	I	5.08	+0.19	9.28	+0.08
	O	5.49	+0.88	9.74	+0.89

[5] *Ap. J.*, **112**, 469, 1950.

the magnitudes and colors of the E-region stars are copied from the results of Cox.[4] It is entirely on these E-region values that the Cloud sequence magnitudes depend.

A comparison of these magnitudes with those determined by McKibben for the SMC and van Wijk for the LMC is given in Table 5. The overlap is poor and the agreement disappointing. More work on standard magnitudes in the Magellanic Clouds with a large reflector is badly needed.

TABLE 5

COMPARISONS WITH MCKIBBEN AND VAN WIJK

Star		P	$(P-V)$	P_{g_p}*	C_p*	P_g†	$P-P_{g_p}$	$(P-V)-C_p$	$P-P_g$
SMC	k	10.33	+0.06	.....	.....	10.18	.....	.....	+0.15
	l	11.05	+0.28	.....	.....	10.80	.....	.....	+ .25
	m	11.40	−0.11	.....	.....	11.15	.....	.....	+ .25
	n	11.76	+1.15	.....	.....	11.41	.....	.....	+0.35
LMC	l	10.35	+0.08	10.30	−0.03	.....	+0.05	+0.11	.....
	m	10.64	+0.15	10.56	− .01	.....	+ .08	+ .16	.....
	n	11.01	+0.17	11.06	+ .07	.....	− .05	+ .10	.....
	o	11.62	+0.33	11.53	+0.22	.....	+0.09	+0.11	.....

* *Harvard Bull.*, **921**, 7, 1952.

† *Harvard Ann.*, **108**, 13, 1940.

This program was supported by several grants from the Indiana University Graduate School, and a grant from Research Corporation made it possible to construct some of the photoelectric equipment. Considerable assistance in the observing was given by H.M. Astronomer at the Cape of Good Hope, Dr. R. H. Stoy, and Mr. A. W. J. Cousins. The authors wish to thank Dr. James Cuffey for many helpful suggestions and discussions.

STUDIES IN GALACTIC STRUCTURE. I. A PRELIMINARY DETERMINATION OF THE SPACE DISTRIBUTION OF THE BLUE GIANTS

W. W. Morgan, A. E. Whitford, and A. D. Code
Yerkes and Washburn Observatories
Received February 26, 1953; revised May 25, 1953

ABSTRACT

Distances of a preliminary list of high-luminosity stars of classes O–A have been determined spectroscopically. A total of twenty-seven separate large-scale clusterings, or aggregates, are catalogued.

Seven of the aggregates, located between galactic longitudes 311° and 346°, define part of a spiral arm located between the sun and the galactic center, at a distance from the sun of around 1400 psc. This confirms the tentative identification of an inner arm announced earlier by Morgan, Sharpless, and Osterbrock.

The arm in which the sun is located appears to branch into two; this is in qualitative agreement with the 21-cm *H* observations of Oort, van de Hulst, and Muller.

A catalogue of some probable members of the aggregates is included.

The present paper is the first of a series dealing with certain investigations of galactic structure being carried out at the Yerkes and Washburn Observatories. A preliminary

TABLE 1

DATA ON AGGREGATES

No.	Name	l (Degrees)	b (Degrees)	r (Kpc)	Associated Feature
1	I Sco	311	0	1.4	NGC 6231
2	II Sco	315–321	+11 to +22	0.21	σ Sco
3	I Sgr	333.7	−2.7	1.3	M 8
4	II Sgr	334.9	−1.7	1.4	M 20
5	III Sgr	338.9–340.4	−2.0 to −2.9	2.3	Small Sgr cloud
6	IV Sgr	341.2	−0.5	1.7	NGC 6561
7	I Ser	344.6	−0.7	2.3	M 16
8	II Ser	346.1	+0.2	2.0	NGC 6604
9	I Vul	28	−1	1.8	NGC 6823
10	I Cyg	40.2	+1.4	2.3	NGC 6871
11	II Cyg	42–45	+2 to −1	1.5	P Cyg
12	III Cyg	44.6	−0.2	2.0	M 29
13	IV Cyg	49–52	−7 to −9	1.0	σ Cyg
14	I Lac	64–66	−16 to −19	0.46	10 Lac
15	I Cep	60–72	+1 to +9	0.72	ν Cep
16	II Cep	66–76	−1 to −3	3.6	
17	III Cep	77.6	+2.6	0.96	
18	I Cas	82.8–84.0	−0.4 to +0.7	2.5	6 Cas
19	II Cas	87.2	−0.3	2.2	
20	III Cas	89.5–91.5	+0.5 to +2.5	2.5	
21	I Per	100–104	−2 to −4.5	2.3	Double cluster in Per
22	I Cam	108–119	−2.5 to +4	0.9	
23	II Per	124–131	−12 to −17	0.36	ζ Per
24	I Aur	137–145	−1.5 to +2	1.15	χ Aur
25	I Gem	155–158	+0.5 to +5.5	1.5	3 Gem
26	I Ori	166–182	−12 to −24	0.5	ϵ Ori
27	I Mon	174–177	−1.5 to +1.5	1.4	NGC 2244

TABLE 2

SOME PROBABLE MEMBERS OF THE AGGREGATES

Star	MK	Aggregate	Star	MK	Aggregate
151804	O8f	1	190429 (ft.)	O9.5 *Ib* p	10
152003	B0 I	1	190864	O6	10
152076	B0 IV, V	1	190918	O9.5 I+WR	10
152147	B0 I	1	190919	B1 *Ib*	10
152218	O9 IV, V	1	+35°3955	B1 *Ib*	10
152233	O6	1	+35°3956	B0.5 V	10
152234	B0.5 I	1	227634	B0 II–III	10
152235	B1 I	1	190967	B1 *Ib*–II	10
152247	O9	1	227696	B0.5 IV:	10
152248	O8	1	227704	B0 III	10
152249	O9 I	1	192422	B0.5 *Ib*	11
152314	O9 IV, V	1	192639	O8f	11
152408	O8fp	1	193183	B1.5 *Ib*	11
152424	O9 I	1	193237	Bp	11
π Sco	B1 V	2	228841	O6.5	11
δ Sco	B0 V	2	193443	O9 III	11
β Sco (br.)	B0.5 V	2	193514	O7f	11
ω^1 Sco	B1 V	2	193595	O7	11
σ Sco	B1 III	2	193682	O5	11
τ Sco	B0 V	2	193855	B2 III	11
164794	O5	3	229059	B1.5 *Ia* p	11
164816	B0 V	3	194153	B1 *Iab*	11
164906	B1 IV: pe	3	229221	B0: I: pe	12
165052	O7	3	229227	B0 II	12
164402	B0 *Ib*	4	229234	O9.5 III	12
164492	O8	4	229238	B0.5 *Ib*	12
164514	A5 *Ia*	4	229239	B1 *Iab*	12
164637	B0.5 III	4	201795	B1 V	13
164833	B0 III	4	201819	B1 Vp	13
166628	B3 *Ia*	5	202349	B0.5 V	13
166965	B3 II	5	σ Cyg	B9 *Iab*	13
167224	B3 II	5	8 Lac (br.)	B1 Ve	14
167287	B1 *Ib*	5	10 Lac	O9 V	14
167336	B0 II	5	12 Lac	B2 III	14
167659	O8	5	198895	B1 V	15
167771	O8	5	200857	B3 III	15
168021	B0 *Ib*	5	202214	B0 V	15
166286	B1 II	6	203025	B2 III	15
166287	B0.5 III	6	203374	B0 IV pe	15
166304	B1 V	6	204116	B1 Ve	15
166540	B0.5 IV	6	204827	B0 V	15
168075	O7	7	205139	B1 II	15
168076	O5	7	9 Cep	B2 *Ib*	15
168137	O8.5V	7	206267	O6	15
168504	O8	7	206773	B0 V: pe	15
−12°4970	B0.5 *Ia*	8	207198	O9 II	15
−11°4586	O8 (I²)	8	ν Cep	A2 *Ia*	15
−12°4982	B0 II	8	207538	B0 V	15
167971	O8f	8	208218	B1 III:	15
168112	O5	8	208392	B1 IV:	15
186841	B1 *Ia*	9	13 Cep	B8 *Ib*	15
186745–6	B8 *Ia*	9	208905	B1 Vp?	15
+23°3745	B0.5 *Ib*	9	209339	B0 IV	15
+23°3759	B0 II	9	14 Cep	O9 V	15
+22°3782	O6	9	209744	B1 V	15
+23°3761	B0 II:	9	235673	O7	16
190429 (br.)	O5f	10			

TABLE 2—*Continued*

Star	MK	Aggregate	Star	MK	Aggregate
209678	B2 I	16	14302	B1 II–III	21
209900	A0 *Ib*–II	16	14322	B8 *Ib*	21
210809	O9 *Ib*	16	14433	A1 *Ia*	21
+53°2827	B2 III:	16	14480	A2 *Ia*	21
+53°2833	B1 III	16	14535	A1 *Ia*	21
+54°2726	B1 II	16	14542	B8 *Ia*	21
235781	B6 *Ib*	16	14818	B2 *Ia*	21
235783	B1 *Ib*	16	14956	B2 *Ia*	21
211853	B0: I: +WR	16	15316	A3 *Iab*	21
+53°2843	O8	16	15497	B6 *Ia*	21
235813	B0 III	16	15571	B1 II:	21
212455	B5 *Iab*	16	19820	O9 IV	22
235825	O9 V	16	21291	B9 *Ia*	22
+54°2764	B1 *Ib*	16	21389	A0 *Ia*	22
213470-1	A3 *Ia*	16	22253	B0.5 III	22
214419	O7+WR	16	23675	B0.5 III	22
215835	O6 nn	16	23800	B1 IV	22
+55°2840	O7	16	24431	O9 IV–V	22
216927	B9 *Ia*	16	24432	B3 II	22
216532	O8	17	21856	B1 V	23
216658	B0 V	17	40 Per	B0.5 V	23
216711	B1 V	17	o Per	B1 III	23
217035	B0 V	17	24131	B1 V	23
217061	B1 V	17	ζ Per	B1 *Ib*	23
217086	O7	17	24534	O pev	23
+61°2509	B0.5 *Ib*	18	ξ Per	O7	23
+60°2615	B0.5 *Ib*	18	34656	O7	24
+61°2526	B2 *Ib*	18	34921	B0 IV: pe	24
+61°2529	B1 *Ib*	18	35345	B1 Vpe	24
6 Cas	A3 *Ia*+	18	35600	B9 *Ib*	24
+61°2550	B0 IV	18	35633	B0.5 IV	24
+61°2559	O9 V	18	35653	B0.5 V	24
223087	B1.5 *Iab*	18	35921	O9.5 III	24
224055	B3 *Ia*	18	χ Aur	B5 *Iab*	24
1383	B1 II	19	χ^2 Ori	B2 *Ia*	25
1544	B0 III:	19	3 Gem	B2.5 *Ib*	25
+61°39	B0.5 IV	19	42088	O6	25
1743	B0 III	19	42379	B1 II	25
1810	B0 IV	19	42400	B5 II	25
2451	B0.5 IV	19	9 Gem	B3 *Iab*	25
3940	A1 *Ia*	20	43753	B0.5 III	25
4694	B3 *Ia*	20	43818	B0 II	25
4717	A0 *Ib*	20	46056	O8	27
4841	B5 *Ia*	20	46106	B0.5 V	27
5551	B1.5 *Ib*	20	46149	O8	27
5689	O7	20	46150	O6	27
12953	A1 *Ia*	21	46202	O9 V	27
13267	B5 *Ia*	21	46223	O5	27
13476	A3 *Iab*	21	13 Mon	A0 *Ib*	27
13744	A0 *Iab*	21	46485	O8	27
13745	B0 III	21	46573	O7	27
13841	B2 *Ib*	21	46711	B3 II	27
13854	B1 *Iab*	21	46847	B0 III: p	27
13866	B2 *Ib*	21	46966	O8	27
14134	B3 *Ia*	21	47129	O8	27
14143	B2 *Ia*	21	47240	B1 *Ib*	27

discussion of the arrangement in space of the high-luminosity stars of classes O–A, as carried out at the Yerkes Observatory, is given here; later papers in the series will include a catalogue of distances of the early-type stars of high luminosity and an investigation of the blue giants and *H* II regions now being observed in South Africa by Code.

The program of spectroscopic absolute magnitudes and color indices of the O, B, and A stars of high luminosity has now reached a point at which certain conclusions on galactic structure are apparent. Details of the observing procedure and a general catalogue of the stars will be given later.

FIG. 1.—Space distribution of aggregates (*solid circles*). Eight distant stars (*open circles*) are also plotted. Oort's value of 9 kpc for the distance to the galactic center has been adopted. The longitude index lines are 500 psc long.

The stars included in the present discussion are those whose spectral types and luminosity classes (on the Yerkes revised *Atlas* system) are as follows: (1) all stars of classes O5–B1, inclusive; (2) classes B2 Ia–A5 Ia, B2 Ib–A5 Ib, B2 II–B5 II, and B2 III–B3 III. The visual absolute magnitude of the lower limit of this group is in the neighborhood of −3.0.

The majority of these stars fall into well-defined clusterings, or aggregates. It is possible at this time to give preliminary distances for a total of twenty-seven aggregates. A number of these are already well known; in addition, there are some which are probably new.

The locations and distances of the aggregates are given in Table 1. The first column gives a running serial number; the second denotes the aggregate by a roman numeral and the constellation abbreviation; the third and fourth give the galactic co-ordinates; the fifth lists the distance in kiloparsecs; and the sixth identifies an associated cluster or bright star, if either exists.

TABLE 3

SOME DISTANT STARS BETWEEN $l = 347°$ AND $l = 5°$

Star	l (Degrees)	b (Degrees)	MK	r (Kpc)	Star	l (Degrees)	b (Degrees)	MK	r (Kpc)
170716	347.4	−2.7	B0.5 Ib	6.0	173438	355.9	−2.3	B0.5 Ia	3.8
173783	351.9	−4.9	O9 I	3:	−0°3584	0.5	−2.3	O8	4:
172275	352.7	−2.1	O6	2.9:	177812	5.2	−3.2	B1 Ib	3.4
173987	354.6	−3.8	B0.5 Iab	6.6	178129	5.5	−3.4	B3 Ia	3.5

Table 2 lists some probable members of the various aggregates, with the exception of I Ori: for this, the recent paper of Sharpless[1] should be consulted. The third column identifies the aggregates by means of the numbers in Table 1.

The positions of the aggregates are plotted in Figure 1. The small *s* identifies the position of the sun; the distance of the sun from the galactic center has been taken to be 9 kpc, from the determination of Oort.[2] The inner circle at the galactic center corresponds to the galactic nuclear region shown in the infrared observations by Stebbins and Whitford;[3] the outer circle, representing a region of lower intensity, was plotted from wide-angle photographs by Sharpless and Osterbrock.

The two outer arms are shown well, and, in addition, a third well-marked arm segment can be seen; the latter is located some 1400 psc from the sun in the direction of the galactic center. Eight very distant stars are listed in Table 3 and are plotted in Figure 1; their distances are, of course, less accurately known than are those for the aggregates.

The aggregates III Cep, I Cam, I Aur, I Gem, and I Mon appear to form a branch to the arm in which the sun is located. The observations of Oort, van de Hulst, and Muller[2] indicate a similar branching.

The present observations confirm and extend the conclusions reached earlier[4] by Morgan, Sharpless, and Osterbrock.

The data for I Sco are (in part) from a paper by Brownlee and Cox, now in press. We are indebted to Dr. Stewart Sharpless for a series of spectrograms obtained at the McDonald Observatory in July, 1952. Part of the spectral classification was carried out by Mrs. Irene Hansen Osterbrock.

[1] *Ap. J.*, **116**, 251, 1952.

[2] *Koninkl. Nederl. Akad. Wetenschappen, Amsterdam*, Vol. **61**, No. 8, 1952.

[3] *Ap. J.*, **106**, 235, 1947.

[4] *A.J.*, **57**, 3, 1952.

BLUE GIANTS IN THE NEIGHBORHOOD OF NGC 6231

W. W. Morgan, Graciela González, and Guillermina González
Tonantzintla Observatory, Mexico, and Yerkes Observatory
Received April 22, 1953

ABSTRACT

A total of eighty-eight OB stars have been found on a Tonantzintla Schmidt camera plate in an area of 25 square degrees surrounding NGC 6231. Of these, seventy are located in a region $1° \times 2°$ in size, and form an interesting aggregate showing strong elongation in the approximate direction of galactic longitude.

The gaseous nebula IC 4628 is located at the northern end of the aggregate, and the cluster NGC 6231 is near the southern end. On the assumption that the distance of NGC 6231 is 1400 psc (Cox and Brownlee; Morgan), the true projected dimensions of the elongated system are about 25×50 psc.

The Milky Way in the region of MGC 6231[1] is especially interesting and complex. The early literature on the subject is summarized by MacRae.[2] Distances ranging from 300 to 1260 psc have been derived for the cluster and nearby early-type stars. The most recent determinations of the distance of NGC 6231 are those of Cox and Brownlee[3] and those of Morgan (unpublished). Both values are near 1400 psc; it is unlikely that this value is in error by much more than 10 per cent.

The earlier investigations have been concerned principally with stars in the immediate neighborhood of NGC 6231. An objective-prism plate obtained with the Tonantzintla Schmidt camera by B. Iriarte shows, however, that the cluster itself is located near the southern end of an elongated system of blue giant stars. This system is illustrated in Figure 1.

On this plate, which has an area of about 25 square degrees, eighty-eight OB stars have been classified. Seventy of these form a pronounced clustering about 2° long and 1° wide; the major axis of the clustering is approximately parallel to the direction of galactic longitude. The gaseous nebula IC 4628 is located at the northern end of the elongated clustering. Plate 16 of Barnard's Milky Way *Atlas* shows the region well.

Table 1 lists the OB stars in the field of 25 square degrees. The columns give (1) a running number, (2) the HD or HDE number, and (3) the visual magnitude. These are, in general, taken from the *Henry Draper Catalogue;* new approximate values have been estimated for some stars which appear to have catalogue errors, and all magnitudes given to one decimal are to be considered very rough values. The fourth column lists the Draper types. Approximate types and luminosity classes on the revised Yerkes *Atlas* system are given in the fifth column; these were determined from McDonald spectrograms obtained by Struve for the measurement of radial velocities.[4] Star No. 38 was classified as Of on the Tonantzintla objective-prism plate. The last column gives the number from Struve's paper.[4] The relative positions of NGC 6231 and IC 4628 are shown in Figure 2; the clustering of OB stars extends from NGC 6231 to IC 4628. Figure 3 gives a negative reproduction of IC 4628; it is from the same original plate as Figure 2. The plate was obtained by E. Chavira, using the Tonantzintla Schmidt camera on

[1] α (1875) = 16^h45^m3; δ (1875) = $-41°35'$.

[2] *Harvard Bull.*, No. 914, 1940.

[3] *Ap. J.* (in press).

[4] *Ap. J.*, **100**, 189, 1944.

TABLE 1

BLUE GIANTS

No.	HD	m_{vis}	Sp.		Struve No.	No.	HD	m_{vis}	Sp.		Struve No.
			HD	Morgan					HD	Morgan	
1	151003	7.1	B1	.....	.....	46	152591	8.1	B5	.....	.....
2	151139	7.5	B2	.....	.....	47	152622	8.1	B5	.....	.....
3	151212	9.5	B2	.....	.....	48	152623	7.0	B3	.....	.....
4	151515	7.4	B2	.....	.....	49	152667	6.40	B0	.....	.....
5	151564	8.1	B2	.....	.....	50	152685	7.5	B5	.....	.....
6	151804	5.37	Oe	O9f	18	51	152723	7.20	B3	.....	.....
7	151805	9.1	B8	.....	.....	52	152756	9.5	(B0)	.....	.....
8	151932	6.56	Oc	WR	20	53	153178	9.0	(B0)	.....	.....
9	152003	7.1	B0	B0 I	1	54	153199	8.0	B5	.....	.....
10	152042	8.3	B2	.....	2	55	153295	9.9	B0	.....	.....
11	152060	10.1	B2	.....	.....	56	153677	8.1	B3	.....	.....
12	152076	8.5	B2	B0 V	3	57	154313	10.1	B0	.....	.....
13	152077	9.0	B5	.....	.....	58	155051	8.0	B0	.....	.....
14	152096	10.1	B9	.....	.....	59	155134	9.3	B0	.....	.....
15	152147	7.3	B0	B0 I	4	60	322089	.....	B0	.....	.....
16	152182	8.7	B8	.....	.....	61	322211	.....	B	.....	.....
17	152198	8.8	B8	.....	.....	62	322277	.....	B8	.....	.....
18	152199	8.6	B0	.....	.....	63	322282	.....	B0	.....	.....
19	152200	8.7	B8	.....	.....	64	322307	.....	B5	.....	.....
20	152217	8.8	(B0)	.....	.....	65	322417	.....	B0	.....	.....
21	152218	7.7	B5	O9 V	5	66	322422	.....	B3	.....	.....
22	152219	8.6	B	.....	.....	67	322432	.....	B5	.....	.....
23	152233	6.6	B	O6	6	68	322433	.....	B3	.....	.....
24	152234	5.5	B0	B0.5 I	7	69	322447	.....	B3	.....	.....
25	152235	6.18	B0	B1 I	8	70	322454	.....	B5	.....	.....
26	152236	4.88	B1p	.....	.....	71	323333	.....	B5	.....	.....
27	152245	7.9	B5	.....	.....	72	325916	.....	B0	.....	.....
28	152246	7.0	B3	.....	.....	73	326176	.....	B0	.....	.....
29	152247	7.3	B2	O9	9	74	326306	.....	B0	.....	.....
30	152248	6.1	B	O8	10	75	326309	.....	B5	.....	.....
31	152249	6.5	B0	O9 I	11	76	326310	.....	B3	.....	.....
32	152268	7.8	B8	.....	.....	77	326327	.....	B2	.....	.....
33	152270	6.72	Oa	WR	19	78	326328	.....	B3	.....	.....
34	152291	8.8	B8	.....	.....	79	326329	7.9	B0	O9 V	12
35	152292	9.1	B5	.....	.....	80	326331	7.5	(B)	O8	14
36	152314	7.8	B	O9 V	15	81	326332	.....	B9	.....	.....
37	152333	8.0	B3	.....	.....	82	326340	.....	B5	.....	.....
38	152386	8.08	Oe	(Of)	.....	83	326348	.....	B0	.....	.....
39	152405	7.31	B3	.....	.....	84	326351	.....	B3	.....	.....
40	152408	6.03	Oep	O7–8fp	17	85	326364	.....	B0	.....	.....
41	152424	6.4	B0	O9 I	16	86	326476	.....	B2	.....	.....
42	152553	8.4	B3	.....	.....	87	326823	.....	Oe5	.....	.....
43	152559	8.2	B5	.....	.....	88	Anon.*	.....	.....	.....	.....
44	152560	8.2	B5	.....	.....						
45	152590	8.1	B5	.....	.....						

* Brightest of three unmarked stars preceding HD 152249 in small insert map on Chart 196 of *Harvard Annals 112.*

FIG. 1.—OB stars located in the range α (1875) = 16^h39^m—16^h52^m; δ (1875) = $-39°40'$ to $-42°45'$. The bright star near the right edge is ζ^1 Sco; the cluster at right center is NGC 6231. North is at left; east is at bottom.

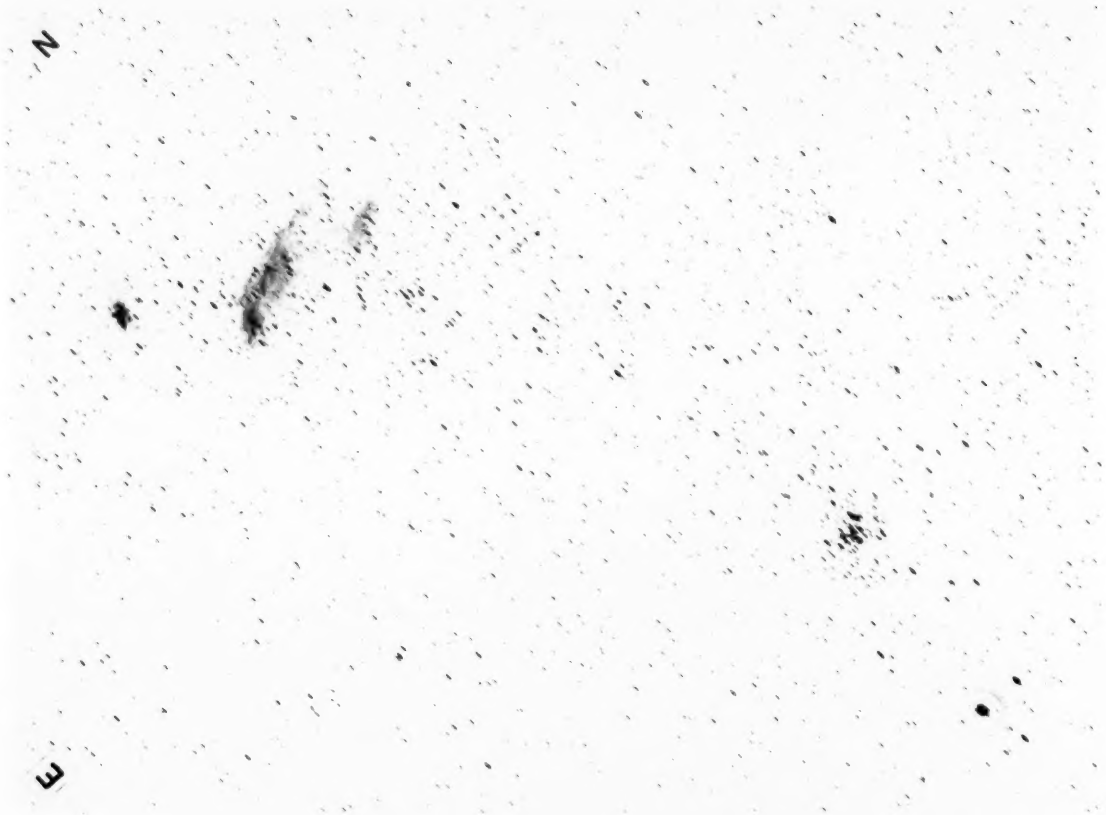

FIG. 2.—Negative reproduction of red spectrum plate, showing positions of NGC 6231 (*lower right*) and IC 4628 (*upper left*). The brightest star near the lower-right corner is ζ^2 Sco. The aggregate of OB stars extends from ζ^1 Sco (above and to the right of ζ^2 Sco) to IC 4628.

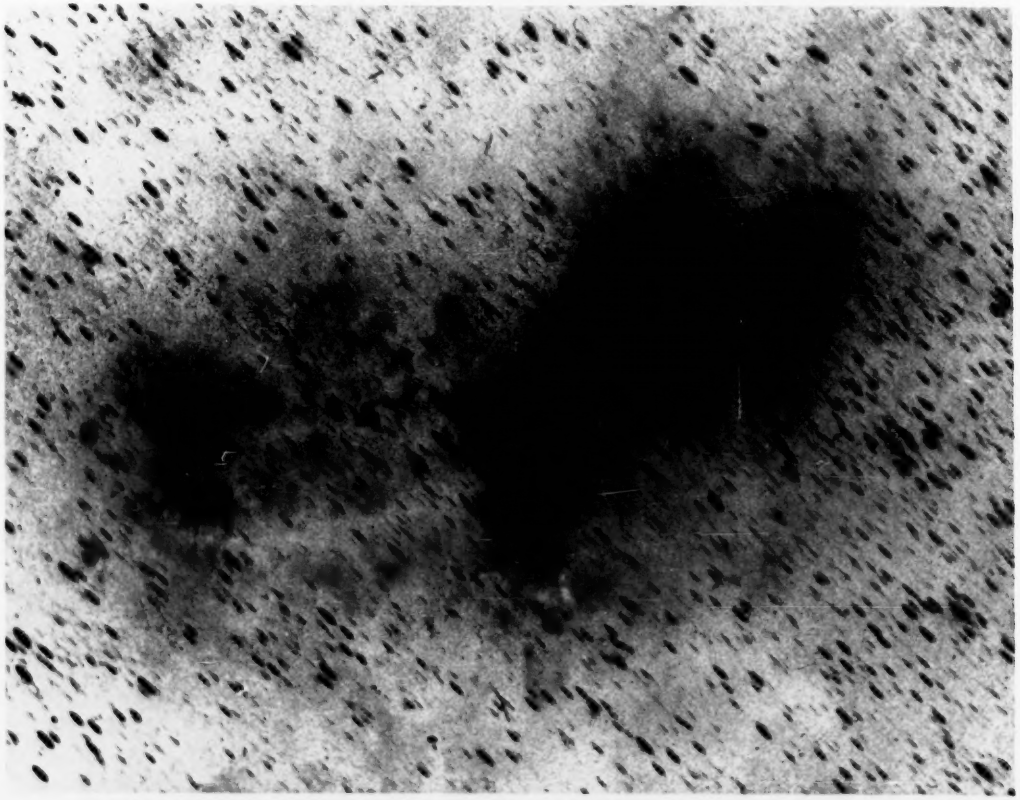

FIG. 3.—Negative reproduction of IC 4628 from Tonantzintla Schmidt plate. Red-spectrum plate and red filter. Eastman 103*a*-E emulsion. The images of the emission nebulosities are due effectively to $H\alpha$.

Eastman 103*a*-E emulsion, with objective prism and red filter. The images of the emission nebulosities are essentially due to $H\alpha$. The true projected length of the aggregate of OB stars is around 50 psc; the width is around 25 psc; these dimensions are derived from an assumed distance of 1400 psc.

The aggregate appears to be in a spiral arm located about 1500 psc from the sun in the direction of the galactic center;[5] it is of unusual interest because of its location and is in need of accurate observations—both photometric and for the determination of precise spectral types and luminosity classes.

[5] Morgan, Whitford, and Code, *Ap. J.*, **118**, 318, 1953.

INHOMOGENEOUS STELLAR MODELS. III. MODELS WITH PARTIALLY DEGENERATE ISOTHERMAL CORES*

M. SCHWARZSCHILD, I. RABINOWITZ, AND R. HÄRM
Princeton University Observatory
Received March 30, 1953

ABSTRACT

A search was made for conditions under which models with partially degenerate isothermal cores could give radii as large as those of red giants. Special conditions were found for which detailed computations gave, indeed, models fitting well the red giants in radius and luminosity. But it has not been investigated whether the special conditions are likely to be realized in the evolution of a star.

I. INTRODUCTION

If a star during the early stages of its evolution possesses no appreciable mixing currents in its interior, the central portion of this star will in time burn out of fuel, and an exhausted, isothermal core will form. Stellar models with isothermal nondegenerate cores were investigated by Schönberg and Chandrasekhar;[1] they found that these models were fairly similar to the Cowling model and that, hence, stars built according to these models should fall reasonably close to the main sequence in the Hertzsprung-Russell diagram. Following this investigation, Gamow and Keller[2] made approximate computations regarding models with isothermal cores in a partially degenerate state; these computations appear to indicate that under certain circumstances such models could give very large radii—large enough to fit the red giants. Subsequently M. H. Harrison[3] accurately computed an array of models with partially degenerate isothermal cores; none of these models showed large radii. This result, however, is not certain to be general, since the cases considered by Mrs. Harrison were selected according to certain considerations regarding stellar evolution.

At present the internal evolution of a star still seems quite uncertain; in particular, the existence, extent, and strength of mixing currents as a function of time during the evolution are still fairly unknown. It therefore appeared useful to extend the earlier accurate computations without restrictions following from evolutionary considerations. A first such extension was carried out by M. Hayashi,[4] who, however, restricted himself to a particular composition for the envelopes. A more general extension is presented in this paper.

It is the purpose of the present investigation to check by accurate computations under which circumstances models with partially degenerate isothermal cores will give radii as large as those of red giants.

II. APPROXIMATIONS AND BASIC EQUATIONS

The models here to be considered consist of two zones: (1) a partially degenerate isothermal core with a composition of 98 per cent helium and 2 per cent heavy elements,

* This research was supported in part by funds of the Eugene Higgins Trust allocated to Princeton University and in part by contract with the Office of Naval Research.

[1] *Ap. J.*, **96**, 161, 1942.

[2] *Rev. Mod. Phys.*, **17**, 125, 1945.

[3] *Ap. J.*, **103**, 193, 1946.

[4] *Phys. Rev.*, **75**, 1619, 1949.

i.e., without nuclear fuel (accordingly, the molecular weight in the core is $\mu_i = 1.342$, the same for all models); (2) a radiative envelope of composition different from the core (whenever the envelope is given the same molecular weight as the core, this is meant as a limit for a small hydrogen content in the envelope but is not meant to represent an exhausted envelope).

In order to facilitate the integration of the equations and the fitting of the models, the following simplifying approximations are made:

a) The energy generation takes place in an infinitesimally thin shell at the interface between core and envelope.

b) The temperature of this shell—and hence in the entire core—is 30,000,000°, so that the carbon cycle can proceed at the required rate.

c) The composition changes discontinuously at the interface between the hydrogen-containing envelope and the burned-out core.

d) The absorption coefficient in the radiative envelope is given by Kramers' law as

$$\kappa = \kappa_0 \rho T^{-3.5} \qquad \text{with} \qquad \kappa_0 = 2 \times 10^{25} Z(1 + X)\,, \tag{1}$$

corresponding to a guillotine factor of $(l/\bar{g}) = 2$.

e) Radiation pressure is negligible.

f) The mean molecular weight in the core, μ_i, is computed to correspond to the total number of particles, not of the electrons alone. Thus the correct equation of state is used in the outer, nondegenerate portion of the core, while in the inner portion the degenerate pressure is exaggerated by a factor of 1.5 for helium—an error presumably tolerable for the present purpose.

The following definitions and equations form the basis for the computations.

Subscripts:

i for the core (interior),
e for the envelope,
1 for the interface,
c for the center (except for the central degeneracy, which is ψ_0).

Dimensionless variables p, t, q, and x for the envelope:

$$P = p\,\frac{GM^2}{4\pi R^4}\,, \qquad T = t\,\frac{\mu_e H}{k}\,\frac{GM}{R}\,, \qquad M_r = qM\,, \qquad r = xR\,. \tag{2}$$

Differential equations for the envelope:

$$\frac{dp}{dx} = -\frac{pq}{tx^2}\,, \qquad \frac{dq}{dx} = \frac{px^2}{t}\,, \qquad \frac{dt}{dx} = -C\,\frac{p^2}{x^2 t^{8.5}}\,, \tag{3}$$

with

$$C = \frac{3\kappa_0}{4ac}\left(\frac{k}{\mu_e H G}\right)^{7.5}\left(\frac{1}{4\pi}\right)^3 \frac{LR^{0.5}}{M^{5.5}}\,. \tag{4}$$

Homology invariants in envelope:

$$U = \frac{px^3}{tq}\,, \qquad V = \frac{q}{tx}\,. \tag{5}$$

Dimensionless variables ξ and ψ for the core:

$$r = \frac{h^{3/2}}{4\pi\mu_i H}(2mkT)^{-1/4}(2mG)^{-1/2}\xi\,, \tag{6}$$

$$\rho = \frac{4\pi}{h^3}(2mkT)^{3/2}\mu_i H F_{1/2}(\psi)\,, \tag{7}$$

$$P = \frac{8\pi}{3h^3}(2mkT)^{3/2}kTF_{3/2}(\psi)\,, \tag{8}$$

where the Fermi-Dirac integral is defined by

$$F_\nu(\psi)\int_0^\infty \frac{u^\nu}{e^{u-\psi}+1}\,du\,. \tag{9}$$

Differential equation for core:

$$\frac{1}{\xi^2}\frac{d}{a\xi}\left(\xi^2\frac{d\psi}{a\xi}\right) = -F_{1/2}(\psi)\,. \tag{10}$$

Homology invariants for core:

$$U = \frac{F_{1/2}(\psi)\,\xi^3}{\left(-\xi^2\dfrac{d\psi}{d\xi}\right)}, \qquad V = \frac{F_{1/2}(\psi)}{F_{3/2}(\psi)}\cdot\frac{3}{2\xi}\cdot\left(-\xi^2\frac{d\psi}{d\xi}\right). \tag{11}$$

Fitting conditions at the interface between core and envelope, where the jump in molecular weight occurs:

$$\frac{U_{1i}}{U_{1e}} = \frac{V_{1i}}{V_{1e}} = l \qquad \text{with} \qquad l = \frac{\mu_i}{\mu_e}. \tag{12}$$

For the envelope, ten particular solutions of equations (3) (corresponding to ten values of the parameter C), with the boundary conditions that $p = t = 0$ and $q = 1$ at $x = 1$, were obtained by numerical integration.[5] Five of these solutions are shown in Figure 1 in terms of the U–V plane.

For the core, G. W. Wares[6] has obtained eight particular solutions of equation (10) (corresponding to eight values of ψ_0, the degeneracy at the center). Five of these solutions are shown in Figure 1 in terms of the U–V plane.

III. PRELIMINARY ORIENTATION IN THE U–V PLANE

The family of models here to be considered has three free parameters. In dimensionless terms, one may use for these parameters ψ_0 (which fixes the particular core solution to be used); ξ_1 (which fixes the end-point on the core solution, i.e., U_{1i} and V_{1i}, at which the jump to the envelope solution should occur); and l (which, according to eq. [12], gives the length of the jump in the U–V plane and hence the starting point U_{1e} and V_{1e}, from which the envelope solution should be followed out to the surface). In physical terms, the three free parameters are the total mass of the star, M; the fraction of the total mass in the exhausted core, q_1; and the ratio of the molecular weights in core and envelope, l. The explicit occurrence of M as an independent parameter here is caused by

[5] To be published in a forthcoming *Princeton U. Obs. Contr.*

[6] *Ap. J.*, **100**, 158, 1944; also "Partially Degenerate Stellar Models" (dissertation, University of Chicago, 1940).

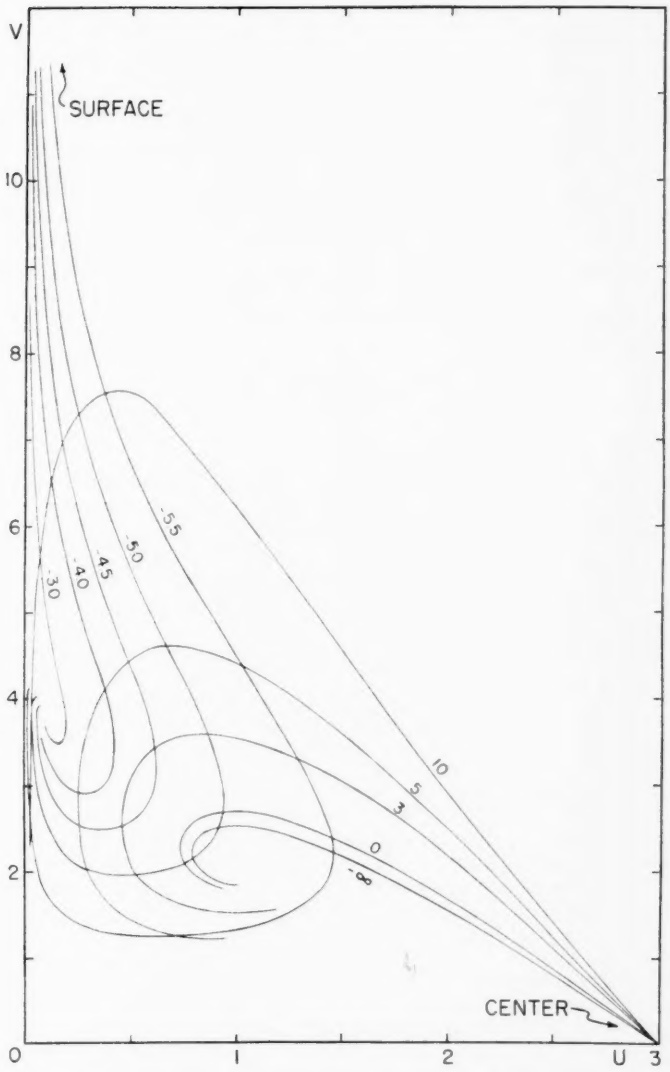

FIG. 1.—Solutions for the cores and envelopes in the U−V plane. The envelope solutions are labeled by values of log C, the core solutions by ψ_0. The solution labeled $-\infty$ is the nondegenerate isothermal core.

the complicated equation of state here used. It introduces a computational complication not found in such nondegenerate models as those discussed in the preceding papers of this series, where the mass could be transformed away by a homology transformation.

Since it does not seem practicable at present to cover the three-parameter family of models completely by individual numerical examples, it appears necessary, first, to find out in which part of the U–V plane the physically interesting cases are to be found. Such a survey was carried out as follows.

If for this survey $l = 1$ is used, any model can be represented in the U–V plane by the point U_1, V_1, which characterizes the interface between core and envelope. The representative points of all the models which have the same value of the mass will form a curve in the U–V plane. Such curves of constant mass may be derived as follows: The value of the density at the interface can be expressed in terms of p_1 and t_1 by the first two equations (2). The same density value can also be expressed in terms of $F_{1/2}(\psi_1)$ by equation (7). Setting the two expressions equal, one obtains an equation which, besides dimensionless variables, involves M and R. Eliminating R with the help of the second equation (2), one obtains for M

$$M = \frac{p_1^{1/2}}{t_1^2} F_{1/2}^{-1/2}(\psi_1) \left(\frac{h^2 k T_1}{2G^2 m}\right)^{3/4} \left(\frac{1}{2\pi^{1/2}\mu_e H}\right)^2. \tag{13}$$

With $\mu_e = 1.342$ and $T_1 = 30{,}000{,}000°$, the two right-hand factors in this equation are known constants. Regarding the first factor, p_1 and t_1 can be interpolated from the envelope solutions for any point in the U–V plane. Similarly for the second factor, $F_{1/2}(\psi_1)$ can be interpolated from the core solutions. Therefore, M can be computed for any point in the U–V plane, and points of equal M can then be connected by curves. These curves of constant M are shown in Figure 2, *a*. The curve corresponding to 1.8 solar masses may be thought of as the center line of a strip containing all the models with masses of the right order for red giants.

Next, curves connecting all representative points corresponding to the same mass fraction in the exhausted core may be obtained. Since for any point in the U–V plane the value of q_1 is directly given by the value of q on that envelope solution which goes through the point in question, the curves of constant q_1 are the curves of constant q drawn across the envelope solutions. These curves are shown in Figure 2, *b*. The approximate parallelity of the curves of constant M and those of constant q_1 indicates that for a given mass a small change in q_1 can produce large changes in the model.

Finally, to be able to judge which of these models may have large radii to fit the red giants, the curves of t_1 are to be constructed, since, according to the second equation (2), a large value of t_1 corresponds to a large radius. The curves of constant t_1 are again identical with the curves of constant t drawn across the envelope-curves—which are also shown in Figure 2, *b*. This figure indicates that large t_1 values, and hence large radii, are to be found only rather far to the left in the U–V plane.

The curves of constant M in Figure 2, *a*, and the curves of constant t_1 in Figure 2, *b*, together delineate a narrow section in the U–V plane in which the representative points are to be found which give models of the proper masses and radii for red giants. The construction of models thus selected is described in the following section.

IV. CONSTRUCTION OF THE MODELS

Two methods of construction of models were used to get the models whose characteristics are given in Table 1. For models *j*, *k*, *l*, and *m* the procedure was as follows:

Using the U–V plane shown in Figure 1, we start on a given envelope-curve (thus fixing the value of C and hence the mass-luminosity relation) and choose an arbitrary value of x_1. Thus U_{1c} and V_{1c} are determined. Next, choosing a value of l, we jump

radially outward from the origin, so as to satisfy condition (12), which fixes U_{1i} and V_{1i}. Finally, the appropriate core solution is found by interpolation at the point U_{1i}, V_{1i} between the available core solutions.

After the fitting is accomplished in the U–V plane, the mathematical characteristics of the models can be derived as follows: $\log p_1$, $\log t_1$, $\log q_1$, U_{1e}, and V_{1e} are read directly from the numerical integrations for the envelope in accordance with the C and x_1 values chosen. With the help of equation (12), U_{1i} and V_{1i} are obtained; ψ_0 is determined by the interpolation between the core integrations; and $F_{1/2}(\psi_0)$ and $F_{3/2}(\psi_0)$ are read from the available tables of the Fermi-Dirac integrals.[7] The value of $F_{1/2}(\psi_1)$ is found by

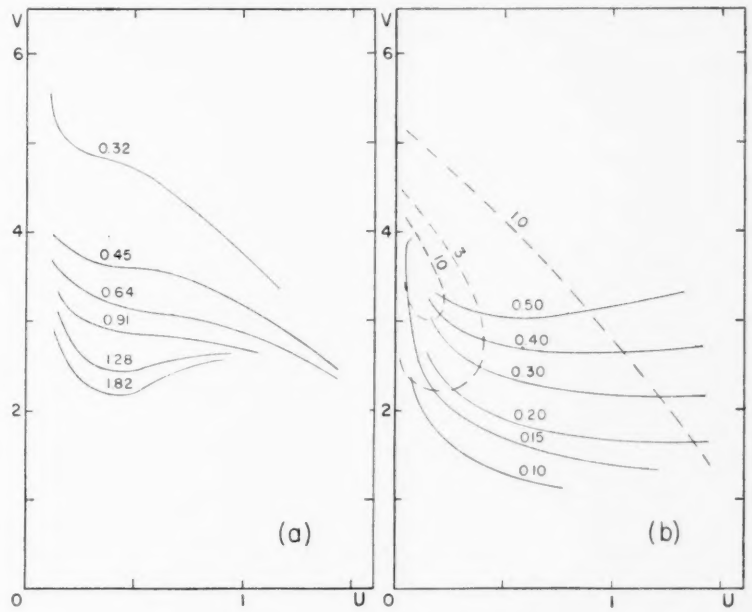

FIG. 2.—*a*, curves of constant mass for models with no jump in molecular weight. *b*, curves of constant q (*solid lines*) and of constant t (*dashed lines*), as determined from the envelope integrations.

interpolation between curves of constant $F_{1/2}(\psi_1)$ drawn across the core integrations in the U–V plane, and ψ_1 is determined from $F_{1/2}(\psi_1)$ by inverse interpolation in the above-mentioned tables.

The second method of fitting, which produced models *a*–*i*, was as follows: The models were assumed to have a core mass of 15 per cent. The curve $q_1 = 0.15$ was drawn by interpolation in the envelope-curves, and the jump-off point (U_{1e}, V_{1e}) was selected arbitrarily on it. Further, the point U_{1i}, V_{1i} was again obtained from equation (12). As before, it was necessary to interpolate between the core solutions in order to find ψ_0, ψ_1, $F_{1/2}(\psi_0)$, $F_{3/2}(\psi_0)$, and $F_{1/2}(\psi_1)$. However, since the jump-off point on the $q_1 = 0.15$ curve did not, in general, lie along one of the envelope-curves, it was here also necessary to interpolate between the envelope integrations to find $\log C$, x_1, p_1, and t_1.

[7] J. McDougall and E. C. Stoner, *Phil. Trans. R. Soc. London, A*, **237**, 67, 1938.

TABLE 1

MATHEMATICAL AND PHYSICAL CHARACTERISTICS OF MODELS

Characteristics	*a*	*b*	*c*	*d*	*e*	*f*	*g*	*h*	*i*	*j*	*k*	*l*	*m*
U_{1e}	+ 0.0608	+ 0.0608	+ 0.0608	+ 0.0471	+ 0.0471	+ 0.0471	+ 0.0512	+ 0.0512	+ 0.0512	+ 0.1304	+ 0.0986	+ 0.1304	+ 0.0986
V_{1e}	+ 3.223	+ 3.223	+ 3.223	+ 3.812	+ 3.812	+ 3.812	+ 3.936	+ 3.936	+ 3.936	+ 3.408	+ 3.704	+ 3.408	+ 3.704
U_{1i}	+ 0.0608	+ 0.0912	+ 0.1216	+ 0.0471	+ 0.0706	+ 0.0942	+ 0.0512	+ 0.0768	+ 0.1024	+ 0.1304	+ 0.0986	+ 0.2608	+ 0.1972
V_{1i}	+ 3.223	+ 4.834	+ 6.446	+ 3.812	+ 5.718	+ 7.624	+ 3.936	+ 5.904	+ 7.872	+ 3.408	+ 3.704	+ 6.816	+ 7.408
l	+ 1.0	+ 1.5	+ 2.0	+ 1.0	+ 1.5	+ 2.0	+ 1.0	+ 1.5	+ 2.0	+ 1.0	+ 1.0	+ 2.0	+ 2.0
log C	− 4.88	− 4.88	− 4.88	− 4.77	− 4.77	− 4.77	− 4.71	− 4.71	− 4.71	− 3.50	− 3.00	− 3.50	− 3.00
$1000x_1$	+ 4.9	+ 4.9	+ 4.9	+ 0.94	+ 0.94	+ 0.94	+ 0.32	+ 0.32	+ 0.32	+ 3.15	+ 0.282	+ 3.15	+ 0.282
log p_1	+ 5.84	+ 5.84	+ 5.84	+ 8.58	+ 8.58	+ 8.58	+10.78	+10.78	+10.78	+ 7.701	+11.729	+ 7.701	+11.729
log h_1	+ 0.98	+ 0.98	+ 0.98	+ 1.63	+ 1.63	+ 1.63	+ 2.12	+ 2.12	+ 2.12	+ 1.525	+ 2.533	+ 1.525	+ 2.533
q_1	+ 0.15	+ 0.15	+ 0.15	+ 0.15	+ 0.15	+ 0.15	+ 0.15	+ 0.15	+ 0.15	+ 0.360	+ 0.360	+ 0.360	+ 0.360
ψ_0	+ 8.70	+ 8.77	+ 9.83	+ 9.42	+10.15	+11.80	+ 9.35	+10.16	+12.25	+ 6.95	+ 7.90	+ 9.18	+10.50
log $F_{1/2}(\psi_0)$	+ 1.240	+ 1.245	+ 1.318	+ 1.291	+ 1.339	+ 1.436	+ 1.286	+ 1.339	+ 1.460	+ 1.098	+ 1.179	+ 1.275	+ 1.361
log $F_{3/2}(\psi_0)$	+ 1.985	+ 1.993	+ 2.110	+ 2.066	+ 2.143	+ 2.301	+ 2.059	+ 2.144	+ 2.340	+ 1.759	+ 1.887	+ 2.040	+ 2.179
ψ_1	− 5.25	− 3.70	− 2.54	− 5.04	− 3.52	− 2.48	− 4.85	− 3.40	− 2.04	− 4.12	− 4.21	− 1.35	− 1.52
log $F_{1/2}(\psi_1)$	− 2.333	− 1.663	− 1.167	− 2.242	− 1.585	− 1.130	− 2.160	− 1.534	− 0.957	− 1.844	− 1.883	− 0.675	− 0.744
X_e	0.0	+ 0.298	+ 0.596	0.0	+ 0.298	+ 0.596	0.0	+ 0.298	+ 0.596	0.0	0.0	+ 0.596	+ 0.596
μ_e	+ 1.342	+ 0.895	+ 0.671	+ 1.342	+ 0.895	+ 0.671	+ 1.342	+ 0.895	+ 0.671	+ 1.342	+ 1.342	+ 0.671	+ 0.671
log ρ_{1e}	+ 0.970	+ 1.46	+ 1.84	+ 1.07	+ 1.54	+ 1.87	+ 1.14	+ 1.59	+ 2.04	+ 1.46	+ 1.42	+ 2.33	+ 2.26
log ρ_c	+ 4.54	+ 4.55	+ 4.62	+ 4.59	+ 4.64	+ 4.74	+ 4.59	+ 4.64	+ 4.76	+ 4.40	+ 4.48	+ 4.58	+ 4.66
log P_c	+20.38	+20.39	+20.50	+20.46	+20.54	+20.69	+20.45	+20.54	+20.73	+20.15	+20.28	+20.43	+20.57
$M/M_\odot$	+ 1.9	+ 2.0	+ 2.0	+ 2.1	+ 2.2	+ 2.3	+ 2.5	+ 2.7	+ 2.5	+ 0.77	+ 0.80	+ 0.80	+ 0.86
$R/R_\odot$	+19	+13	+10	+91	+64	+51	+340	+250	+170	+27	+280	+14	+150
$L/L_\odot$	+14,000	+780	+87	+12,000	+680	+110	+19,000	+1,300	+92	+1,700	+2,100	+10	+15
log T_e	+ 4.15	+ 3.92	+ 3.74	+ 3.79	+ 3.56	+ 3.42	+ 3.56	+ 3.34	+ 3.13	+ 3.85	+ 3.36	+ 3.44	+ 2.96
M_{bol}	− 5.8	− 2.6	− 0.2	− 5.5	− 2.5	− 0.5	− 6.0	− 3.2	− 0.3	− 3.5	− 3.7	+ 2.1	+ 1.7

The remaining quantities in Table 1 relate to the physical characteristics of the models and were determined from the mathematical properties enumerated above as follows: Since we assume l and μ_i (l varying from model to model, μ_i the same for all models), we find μ_e from equation (12), and since we assume $Z_e = Z_i = 0.02$, we find X_e from μ_e. The central density and pressure, ρ_c and P_c, are obtained from equations (7) and (8). The mass is found from equation (13), and the radius from the second equation (2). The luminosity is derived from equation (4), and then the effective temperature and bolometric absolute magnitude follow at once. Finally, the density at the interface, ρ_{1e}, is obtained from the first two equations (2).

V. PHYSICAL CHARACTERISTICS OF MODELS

To judge how far the models here constructed are applicable to observed stars, the model stars have been plotted in a Hertzsprung-Russell diagram (Fig. 3) according to the

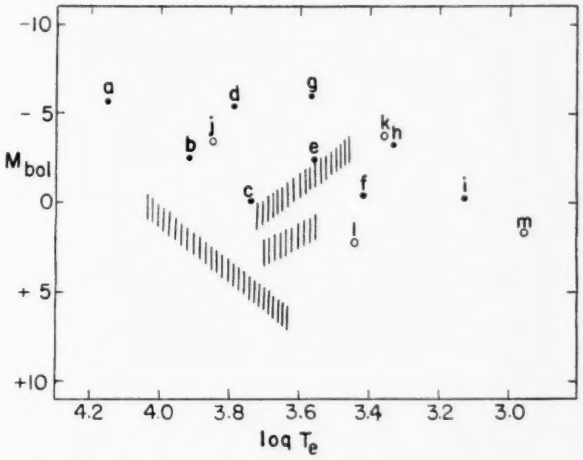

FIG. 3.—Hertzsprung-Russell diagram. The thirteen lettered symbols correspond to the models listed in Table 1. The dots represent cases in which the core contains 15 per cent of the mass (stellar masses from 1.9 to 2.7 solar masses), whereas the circles represent cases in which the core contains 36 per cent of the mass (stellar masses around 0.8 solar masses). The hatched regions indicate schematically the observed locations of the giants, subgiants, and main-sequence stars.

bolometric magnitudes and effective temperatures listed in Table 1. Figure 3 shows that the present models cover well the area occupied by the red giants. Hence the present detailed computations appear to substantiate the earlier tentative conclusions by Gamow and Keller[2] that models with partially degenerate isothermal cores may under certain circumstances have very large radii.

On the other hand, most of the models here considered—all but the four referring to relatively small stellar masses—have a rather small fraction of their mass in the isothermal core. Indeed, the mass of the core for all thirteen models lies between 28 and 40 per cent of a solar mass. Hence the masses of the isothermal cores—and even more the masses of the degenerate parts of the isothermal cores—lie well below the limit for a degenerate mass. This is in agreement with the general considerations pointed out by Chandrasekhar.[3]

After having compared the model stars with the observed red giants in terms of the

Hertzsprung-Russell diagram, i.e., in terms of luminosities and radii, it remains to compare the theoretical and real stars in terms of their masses, or rather their mass-luminosity relations. The large log C values listed in Table 1 (compared with log $C = -6.0$ for the Cowling model) show that the present models are, on the average, 20 times more luminous than main-sequence stars of the same mass or that their masses are, on the average, two times smaller than those of main-sequence stars of the same luminosity. In this regard the present models are similar to those discussed in the first paper of this series,[8] and correspondingly the discussion of the masses of red giants given there applies here too. Accordingly, one may conclude here again that the observational data on the masses of red giant stars are still insufficient either to corroborate or to contradict the mass-luminosity relation of the present models.

Even though there is no apparent discrepancy between the present models and red giants as far as luminosities, radii, and masses are concerned, the following consideration makes it seem somewhat unlikely that partially degenerate isothermal cores should be the main cause of the red giant phenomenon. The data represented in Figure 2 indicate that for a given stellar mass, M, and for a given jump in the molecular weight, l, the fraction of the mass contained in the exhausted core, q_1, must fall within very narrow limits if the star is to be comparable with observed red giants. For smaller values of q_1 the models will lie very close to the main sequence and thus not represent red giants. The cases of larger q_1 values have not been investigated here; it appears, however, rather likely that for larger q_1 values either no equilibrium configuration exists (for a given M and l), much as in the Schönberg-Chandrasekhar case of nondegenerate isothermal cores, or these cases show radii even larger than those of the observed red giants. In any case, the red giants can apparently be fitted only by models with partially degenerate isothermal cores if q_1—as a function of M and l—falls within fairly narrow limits, as has already been indicated by M. Hayashi. It does not appear too likely that such narrow conditions can actually be fulfilled by the entire red giant class of stars.

One may then conclude that the observable characteristics of red giants can be fitted with models with partially degenerate isothermal cores but that this fit can apparently be achieved only if the exhausted core fulfils rather narrow conditions. Hence it appears possible that partially degenerate cores are a contributing factor, but probably are not the main cause, for the large radii of red giants.

We wish to thank Dr. S. Chandrasekhar and Dr. G. W. Wares for their generously making available to us Dr. Wares's integrations for partially degenerate cores.

[8] J. B. Oke and M. Schwarzschild, *Ap. J.*, **116**, 317, 1952.

ASPHERIC FIELD CORRECTORS FOR LARGE TELESCOPES

A. B. MEINEL
Yerkes Observatory
Received May 26, 1953; revised June 10, 1953

ABSTRACT

The application of generalized aspheric aberration equations to the problem of providing aberration-free fields for large parabolic telescopes yields families of solutions that can substantially correct for third- and fifth-order coma and astigmatism.

The useful field of a large paraboloid is seriously limited by coma and to a lesser degree by astigmatism. In the case of the 200-inch Hale telescope, the useful field is only a few millimeters in diameter before the coma enlarges the stellar image by an amount equal to that caused by the general atmospheric turbulence. At 0°.05 off-axis, the linear coma is 1.9 seconds of arc, whereas the seeing disk is frequently 1 second of arc. The introduction of a corrector system by Ross[1] permitted the parabolic telescope to have a useful field many times larger. In the case of the 200-inch telescope, the correction is satisfactory over a field $\frac{1}{4}°$ in diameter; beyond that point, however, the residual aberrations rapidly become intolerable.

The typical Ross corrector obtains coma and astigmatism correction as the by-product of spherical lens elements, a typical corrector consisting of one negative and one positive element selected so that the spaced pair has approximately zero power but has negative coma and astigmatism. In later designs, a meniscus has been added to improve the performance, but the functional aspects remain the same. The chief limitation of the Ross corrector is that the variation of coma with field is only an approximation to the linear variation of coma for the paraboloid. As a consequence, the correction breaks sharply at a certain limiting field angle.

If we admit the use of aspheric elements, the problem of the coma and astigmatism correction appears to be relaxed. The aberrations in such systems are not by-products of the power terms of the individual elements but are the direct results of the asphericity. A preliminary ray-tracing study of one of the aspheric combinations which satisfies the general equations indicates that a field 1° in diameter can be achieved for the 200-inch telescope for monochromatic light. Further ray-tracing investigations are in progress to delineate the new limiting fields and will be completed in the near future; however, the trend of the results appears to warrant publication of the method at this time.

SPHERICAL ABERRATION

If we consider an optical system composed of one or more spherical elements, we can select an aperture stop in that system and ascribe to each point ρ in that aperture a deviation $\delta(\rho)$ equal to that required to correct the on-axis image. The form of $\delta(\rho)$ will be expressible as a power series in odd powers of the radius to the point ρ:

$$\delta(\rho) = \Sigma_i b_i \rho^{2i+1} \qquad (i = 0, 1, \ldots) . \tag{1}$$

Let us consider a typical optical system of astronomical interest utilizing a spherical concave mirror, as shown in Figure 1. If we place the aperture stop at the center of curvature, then $\delta(\rho)$ defines the conventional Schmidt plate. If we place the aperture stop at the mirror, then $\delta(\rho)$ defines the paraboloid. The ray passing through the point ρ and

[1] *Ap. J.*, **81**, 156, 1935.

being deviated an amount $\delta(\rho)$ will, after reflection, proceed to a common focal point on the axis. If we now find the piercing point r of this ray ρ in any other plane k in the converging beam, we will find it necessary to apply a transformation to $\rho = f(r)$ in order to have the r-field linear, since the ρ-field has become nonlinear:

$$\rho = \Sigma_j c_j r^{2j+1} \qquad (j = 0, 1, 2, \ldots) . \tag{2}$$

This nonlinearity for a Schmidt or a paraboloid is due to the dip of the curve on the spherical mirror. For a spherical mirror only, we have an additional term due to the spherical aberration. In all cases, however, we have $\rho \to r$ as $r \to 0$, which requires that $c_0 = 1$ and that $c_{j>0} < 1$. This means that, although the linear distance to the piercing point is a variable, ρ is constant for a given ray as it traverses the optical system.

If we place the deviation on a plane corrector at k rather than at C, we find, in terms of a linear radius measure r, that we have

$$\delta(r) = \Sigma_i a_i r^{2i+1} \qquad (i = 0, 1, 2, \ldots) , \tag{3}$$

where $a_i = f(b_i, c_j)$ and is defined by

$$\Sigma_i a_i r^{2i+1} = \Sigma_i b_i (\Sigma_j c_j r^{2j+1})^{2i+1} \qquad (i, j = 0, 1, 2, \ldots) . \tag{4}$$

For a system of aspheric plates, $\Sigma_k \delta_k(\rho) + \Delta = 0$, where Δ is the spherical aberration of the spherical mirror and $\delta_k(\rho)$ is the deviation at the point where the ray defined by ρ

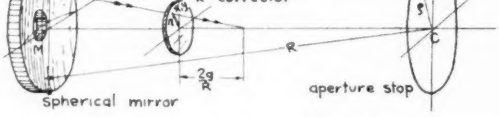

FIG. 1.—Diagrammatic orientation of a typical optical system

in the aperture stop pierces the kth corrector. This distinction is very important, since off-axis aberrations depend on $\delta_k(r)$ rather than on $\delta_k(\rho)$.

The coefficients $a_i(b_i, c_j)$ have been evaluated for $i \leqslant 5$ and are given in Table 1.

TABLE 1

TRANSFORMATION COEFFICIENTS $a_i(b_i, c_j)$

$$a_0 = c_0 + b_0$$

$$a_1 = c_1 b_0 + c_0^3 b_1$$

$$a_2 = c_2 b_0 + 3\, c_1 c_0^2 b_1 + c_0^5 b_2$$

$$a_3 = c_3 b_0 + 3\, c_2 c_0^2 b_1 + 3\, c_1^2 c_0 b_1 + 5\, c_1 c_0^4 b_2 + c_0^7 b_3$$

$$a_4 = c_4 b_0 + 3\, c_3 c_0^2 b_1 + 6\, c_2 c_1 c_0 b_1 + c_1^3 b_1 + 5\, c_2 c_0^4 b_2 + 10\, c_1^2 c_0^3 b_2 + 7\, c_1 c_0^6 b_3 + c_0^9 b_4$$

$$a_5 = c_5 b_0 + 3\, c_4 c_0^2 b_1 + 3\, c_2^2 c_0 b_1 + 6\, c_1 c_3 c_0 b_1 + 3\, c_2 c_1^2 b_1 + 5\, c_3 c_0^4 b_2 + 20\, c_2 c_1 c_0^3 b_2 + 10\, c_1^3 c_0^2 b_2 + 7\, c_2 c_0^6 b_3 + 21\, c_1^2 c_0^5 b_3 + 9\, c_1 c_0^8 b_4 + c_0^{11} b_5$$

OFF-AXIS ABERRATIONS

If we consider the path of a ray inclined at an angle φ to the optical axis through the point ρ, this ray will pass through the kth corrector at a new point, at which the deviation will be quite different. If $\delta(r)$ is the new deviation and $\delta(r)$ is the original deviation for the ray defined by ρ, then we can write a Taylor expansion in δ and r:

$$\delta'(r) = \delta(r) + \frac{\partial \delta}{\partial r}\Delta r + \frac{1}{2}\frac{\partial^2 \delta}{\partial r^2}\Delta r^2 + \ldots . \tag{5}$$

The aberration is, then,

$$\Delta\delta = \frac{\partial \delta}{\partial r}\Delta r + \frac{1}{2}\frac{\partial^2 \delta}{\partial r^2}\Delta r^2 + \ldots . \tag{6}$$

To facilitate the determination of Δr, we will refer to Figures 2 and 3. Two effects enter into Δr. If we consider the plane defined by the rays $\rho(\varphi = 0)$ and $\rho(\varphi)$ to be in

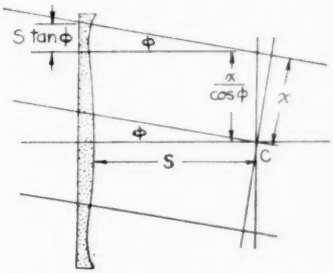

FIG. 2.—Diagram for the piercing point for an off-axis bundle and displaced corrector

the x-direction, σ the deviation in the x-direction, and τ the deviation in the y-direction, then

$$\Delta x = \left(\frac{x}{\cos\varphi} - x\right) + S\tan\varphi \cong x\frac{\sin^2\varphi}{2} + S\tan\varphi \qquad (\Delta y = 0). \tag{7}$$

In addition to the change in σ, τ due to the geometrical factors, there will be an additional term in refracting-type correcting elements due to the increased deviation produced by the plate upon the inclined ray. When the ray for $\varphi = 0$ is normal to the plane of the corrector, the new deviation becomes

$$\sigma'' = \sigma\left(1 + \frac{n+1}{2n}\sin^2\varphi\right), \qquad \tau'' = \tau\left(1 + \frac{1}{2n}\sin^2\varphi\right). \tag{8}$$

In the cases that we are about to consider, $S > x$, and φ is small, $<4°$. As a consequence, we will not explicitly carry the $(x\sin^2\varphi)/2$ and index-of-refraction terms. In specific cases, for the refinement of the design, these terms can be considered.

In the case in which the kth corrector is located in the converging beam of the system as illustrated in Figure 1, it is necessary to determine what S-value should be used. Referring to Figure 3, we see that, for the case of paraxial rays,

$$u'' - u = R\tan\varphi,$$

$$h'' - h = (h'' - h') + (h' - h) = \tan\varphi(1 - g) + gR\tan\varphi,$$

$$\frac{h'' - h}{u'' - u}\frac{u}{h} = \frac{\tan\varphi(1-g) + Rg\tan\varphi}{R\tan\varphi}\frac{1}{g} = \frac{1}{R}\left(\frac{1-g}{g} + 1\right);$$

but $(1 - g)/g = L$, the distance behind the mirror M that the image of the kth corrector is located. Since the factor u/h changes the size of the kth corrector to that of M for the ray ρ, then

$$\frac{\Delta h}{\Delta u}\frac{u}{h} = \frac{L+R}{R} = \frac{S}{R}, \tag{9}$$

where $S = L + R$ is the distance of the image of the kth corrector from the center of curvature of the mirror. With this interpretation of S, we can proceed to evaluate the aberration equations.

The deviation of the corrector in the σ- and τ-directions, in terms of the depth of the aspheric curve t, can be written in the form

$$\sigma = C\frac{dt}{dx}, \qquad \tau = C\frac{dt}{dy}. \tag{10}$$

To facilitate this operation, let us write the depth of the curve first explicitly in x and then explicitly in y:

$$\begin{aligned} t &= C\{M_0(y) + M_1(y)\,x^2 + M_2(y)\,x^4 + \ldots\}, \\ t &= C\{N_0(x) + N_1(x)\,y^2 + N_2(x)\,y^4 + \ldots\}, \end{aligned} \tag{11}$$

where $r^2 = x^2 + y^2$.

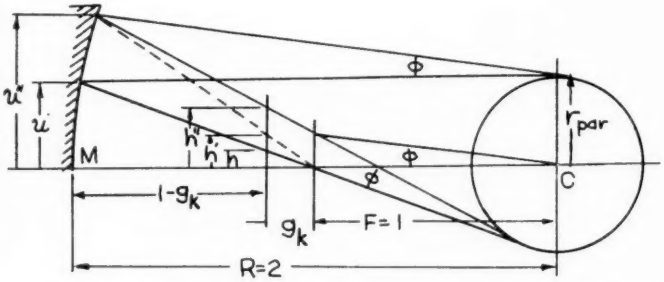

FIG. 3.—Diagram for the determination of S for the kth corrector. All values refer to paraxial bundles, although shown as finite for clarity.

In terms of the coefficients a_i defined in equation (3), the exact expressions for $N_i(x)$ and $M_i(y)$ are

$$\begin{aligned} N_i(x) &= \frac{1}{i!}\sum_n \frac{(n+1)!}{(n-i+1)!}\frac{a_n}{2n+2}\,x^{2n-2(i-1)} \qquad (n \geqslant i-1), \\ M_i(y) &= \frac{1}{i!}\sum_n \frac{a_n}{2n+2}\frac{(n+1)!}{(n-i+1)!}\,y^{2n-2(i-1)}. \end{aligned} \tag{12}$$

Then

$$\sigma(r) = \Sigma_i 2iM_i(y)x^{2i-1}, \qquad \tau(r) = \Sigma_i 2iN_i(x)y^{2i-1} \qquad (i = 0, 1, 2, \ldots). \tag{13}$$

The corresponding partial derivatives with respect to x can be formed from these defining equations.

The preceding evaluation is necessary when it is desirable to have the combination of the aspherics produce a given (say, zero) aberration in either the x- or the y-direction.

In general, an exact solution cannot be had for zero aberration in both directions. As a consequence, it may prove more advantageous for general application to consider the solution in terms of the x-direction, since the aberrations are largest in this direction. When $y = 0$, then $N_i(x) \to N_0(x)$, $\Sigma^1 M_i(y) x^{2i-1} \to N_0(x) \to \delta(r)$. Thus we can consider $\delta(r)$ and r, when r is measured in the direction of φ:

$$\begin{aligned}
\delta(r) &= \Sigma_i a_i r^{2i+1} && (i = 0, 1, 2, \ldots), \\
\frac{d\delta(r)}{dr} &= \Sigma_i a_i (2i+1) r^{2i}, \\
\frac{d^2\delta(r)}{dr^2} &= \Sigma_i a_i (2i+1) 2i r^{2i-1}, \\
\frac{d^m\delta(r)}{dr^m} &= \Sigma_i a_i (2i+1) \ldots (2i-m+2) r^{2i-m+1}.
\end{aligned} \tag{14}$$

Then, evaluating these equations for $i = 0, 1, \ldots$, we have

$$\begin{aligned}
\Delta\delta = S \tan \varphi \Sigma_i a_i (2i+1) r^{2i} + \tfrac{1}{2} S^i \tan^2 \varphi \Sigma_i a_i (2i+1) 2i r^{2i-1} + \ldots \\
+ \frac{1}{m!} S^m \tan^m \varphi \Sigma_i a_i (2i+1) 2i \ldots (2i-m+2) r^{2i-m+1}.
\end{aligned} \tag{15}$$

To classify the various terms of this series into one of the standard aberration types, let us define coma $C(\delta)$ as the aberration arising from odd values of m, while defining astigmatism $A(\delta)$ as that arising from even values of m. Then

$$\left.\begin{matrix} C(\delta),\ m \text{ odd} \\ A(\delta),\ m \text{ even}, >0 \end{matrix}\right\} = S^m \tan^m \varphi \Sigma_i a_i (2i+1)(2i) \ldots (2i-m+2) r^{2i-m+1}. \tag{16}$$

And, for a system of k aspherics,

$$\Sigma_k C_k(\delta) = 0, \qquad \Sigma_k A_k(\delta) = 0. \tag{17}$$

APPLICATION

The application of the foregoing theory at once points the way to the design of a set of aspheric elements to provide field correction for parabolic telescopes. The paraboloid is a special case of a sphere and an aspheric in which the two coincide. In this case, $S = R$. The system of a paraboloid plus aspherics can therefore be treated exactly as shown above. We have three basic equations governing the ensemble:

$$\begin{aligned}
\Sigma_k \delta(\rho) + \Delta &= 0, && \text{spherical aberration } H(\delta); \\
\Sigma_k S_k \tan \varphi \frac{d\delta}{dr} + \ldots &= 0, && \text{coma } C(\delta); \\
\Sigma_k \frac{S_k^2}{2} \tan^2 \varphi \frac{d^2\delta}{dr^2} + \ldots &= 0, && \text{astigmatism } A(\delta).
\end{aligned} \tag{18}$$

Under special conditions, these equations can be reduced to the "optical see-saw" conditions discovered by Burch[2] but seldom used because of the ambiguity of the original

[2] *M.N.*, **102**, 159, 1942.

description. It is hoped that these exact expressions will clarify the situation and bring these methods into fuller use.

The control that each element exerts on these aberrations can roughly be divided into terms of S. The value of S is largest for the element nearest the focal plane, becoming infinite at the focal plane. As a consequence, a weak aspheric near the focal plane will have a large effect on the astigmatism but a small effect on the coma or spherical aberration. In general, the corrector with smallest S controls the spherical aberration; the intermediate corrector, the coma; and the last corrector, the astigmatism.

In the case of the simplest aspheric,

$$\begin{aligned} &\delta(r) = a_0 r + a_1 r^3, \qquad t(r) = \frac{a_0 r^2}{2} + \frac{a_1}{4} r^4; \\ &C(\delta) = \Sigma S (a_0 + 3a_1 r^2) \tan\varphi + S^3 \tan^3\varphi^{(a_1)}; \\ &A(\delta) = \Sigma S^2 3a_1 r \tan^2\varphi. \end{aligned} \tag{19}$$

The constant terms in $C(\delta)$ are not strictly comatic; they only describe a total displacement of the comatic image. The appearance of constant terms in the aberration equations can consequently be considered as affecting the scale and distortion of the system:

$$\begin{aligned} &C(\delta) = \Sigma S\, 3a_1 r^2 \tan\varphi, \\ &D(\delta) = \underset{\text{change in scale}}{\Sigma S a_0 \tan\varphi} + \underset{\text{distortion}}{\Sigma S^3 \tan^3\varphi a_1}. \end{aligned} \tag{20}$$

If an aspheric system of three elements is employed, we can find the aspheric coefficients a_1 required for an arbitrary distribution of the elements when $\delta(r)$ can be expressed exactly by $a_0 r + a_1 r^3$ terms for each element other than the primary mirror. In order to achieve this condition, the physical shape of each succeeding corrector must have higher-order terms in which the a_{2j} . . . terms cancel as well as possible the effect of the modified array of piercing points produced by the preceding corrector on the succeeding aspheric. To be exact, one should apply a transformation, as was previously done, in order to have r_{k+1} linear; however, since the nonlinearity is small and since it also operates on the paraxial off-axis rays, the net effect can be considered as contributing to higher-order a_i terms.

While this simple form is inadequate for the accuracy required for large telescopes (1 part in 10^7), we can make use of it to map out a preliminary design. Although the equations are written for $y = 0$, $x = r$, it is relatively easy to prove that the zonal distributions of the third-order aberrations in the σ- and τ-directions are the same as for the paraboloid. As a consequence, we have assurance that, although we explicitly balance the aberrations in the σ-direction, they will automatically be balanced in the τ-direction.

If we evaluate the expressions for $N_i(x)$ and $M_i(y)$ given in equation (12), we find that

$$\begin{aligned} &C(\tau) = \Sigma S \tan\varphi 8a_1 xy, \qquad C(\sigma) = \Sigma S \tan\varphi(12a_1 x^2 + 4a_1 y^2); \\ &A(\tau) = \Sigma S^2 \tan^2\varphi 8a_1 y, \qquad A(\sigma) = \Sigma S^2 \tan^2\varphi 24a_1 x. \end{aligned} \tag{21}$$

That this is pure coma is seen from the relationship of $C(\sigma)$ and $C(\tau)$ to x and y. When

$$\begin{aligned} &x = \pm 1 \text{ and } y = 0, && C(\sigma) \propto 12a_1 \text{ and } C(\tau) = 0; \\ &x = 0 \text{ and } y = \pm 1, && C(\sigma) \propto 4a_1 \text{ and } C(\tau) = 0; \\ &x = \pm\frac{1}{\sqrt{2}} \text{ and } y = \pm\frac{1}{\sqrt{2}}, && C(\sigma) = 0 \text{ and } C(\tau) \propto \pm 4a_1. \end{aligned}$$

Likewise, for astigmatism, when

$$x = \pm 1 \text{ and } y = 0\,, \quad A(\sigma) \propto \pm 24a_1 \text{ and } A(\tau) = 0\,;$$
$$x = 0 \text{ and } y = \pm 1\,, \quad A(\sigma) = 0 \text{ and } A(\tau) \propto \pm 8a_1\,;$$

and the ratio of axes is 3:1 in the Petzval plane. Both patterns are shown in Figure 4. Since the aberrations of the primary paraboloid are very nearly third order under the range of F-ratios encountered, the corrector ensemble should provide excellent correction for all rays, although the solution is explicit for the σ-direction aberrations. The only remaining question is how well the fifth-order aberrations that arise in the corrector ensemble can be balanced for all rays. If there were no distortion of the piercing-point array in successive correctors, we could equally well demonstrate that they can be exactly balanced as far as the zonal distribution is concerned. It is believed, however, that the residual arising from the array distortion can be kept small enough to justify a solution

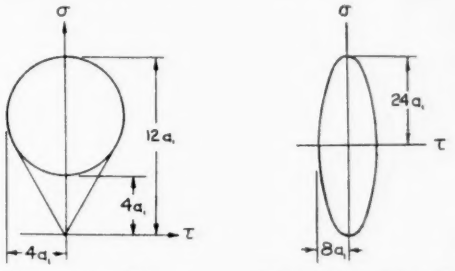

FIG. 4.—Diagram of resultant coma and astigmatism patterns for a_1 terms, showing that the aberration zonal distribution is typical third-order aberration.

in the σ-direction only. Knowledge of how the higher-order terms affect the aberrations is then imperative in refining preliminary designs. For a paraboloid with three aspherics each having only a_0- and a_1-coefficients, we have the expressions

$$\begin{aligned} 0 &= a_{1,1} + a_{1,2} + a_{1,3} \qquad \text{(subscripts refer to } i, k)\,, \\ S_0 a_{10} &= S_1 a_{1,1} + S_2 a_{1,2} + S_3 a_{1,3}\,, \\ S_0^2 a_{10} &= S_1^2 a_{1,1} + S_2^2 a_{1,2} + S_3^2 a_{1,3}\,, \end{aligned} \tag{22}$$

where S_0 and a_{10} refer to the appropriate values to represent the paraboloid. Solutions for $a_{1,k}$ can be ready-made for positions S_k. The solutions of interest are those for which all aspheric elements are within 15 per cent of the focal length in front of the focal plane. This places a severe restriction on the solution, since S is of one sign and of limited value unless reimaging is introduced.

Since r is closely related to ρ, and ρ is defined by the ray (ρ), one must multiply r by g to get the linear value of r. The total depth for a corrector of the same linear diameter but different g is approximately $a_{1,k}(g/g_k)^4$. As a consequence, a corrector near the focal plane may have a small numerical value of $a_{1,k}$, whereas the actual aspheric may be deeper than one of larger $a_{1,k}$ and larger g in order to provide an unvignetted field. Figure 5*a* shows the relative values of $a_{1,k}$ with $\Delta S_{k,k+1} = \Delta S_{k+1,k+2}$, which closely represents the condition for minimum $a_{1,k}$-values for a given $\Delta S_{k,k+2}$-value. Figure 5*b* shows

the relative depths of the aspheric, taking g into account and normalized to the g-values for $\Delta S_{k,k+1} = 5$. It is apparent that the optimum ΔS-value is approximately 6 for both $S_1 = 10$ and $S_1 = 8$, with the absolute asphericity being substantially less for $S_1 = 8$. The corresponding values for $a_{2,k}$ are approximately 20–50 per cent of $a_{2,0}$, and consequently rather small.

Because of the nonlinear distortion of the r-grid on element $k + 1$ by the preceding elements, the succeeding elements will effectively have coefficients $a_i\ (i > 1)$. Since this simple case will not hold because of this distortion and since we must attempt to balance the higher-order aberrations, the practical case is more nearly represented by

$$\delta(r) = a_0 r + a_1 r^3 + a_2 r^5 , \tag{23}$$

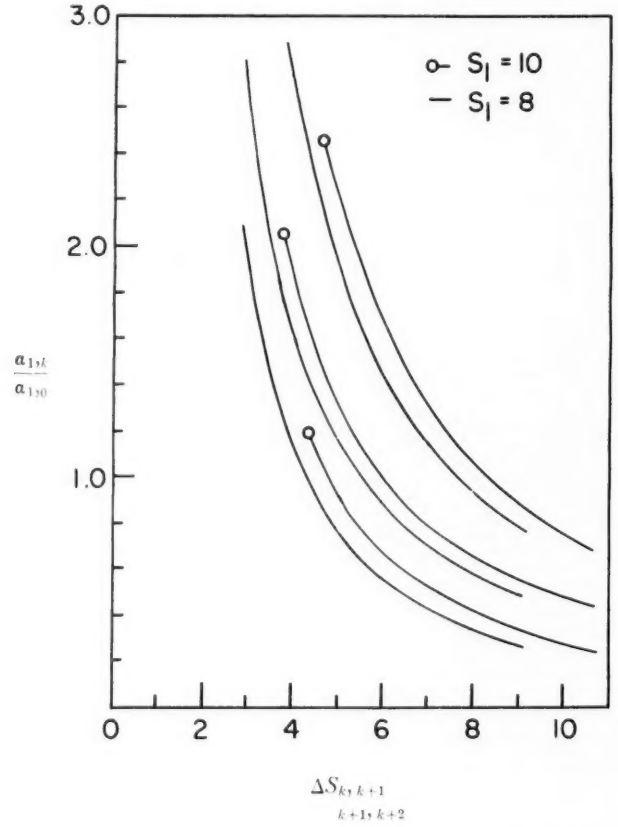

FIG. 5a.—Diagram showing the asphericity of the kth corrector in terms of the asphericity of the paraboloid in terms of a common ρ-value; the three pairs of curves refer to $k = 3$, 1, 2 reading down.

where the aberration equations become

$$\begin{aligned} C(\delta) &= \Sigma S \tan\varphi(3a_1r^2 + 5a_2r^4) + \Sigma S^3 \tan^3\varphi 10a_2r^2 , \\ A(\delta) &= \Sigma S^2 \tan^2\varphi(3a_1r + 10a_2r^3) + \Sigma S^4 \tan^4\varphi 5a_2r , \\ D(\delta) &= \Sigma S \tan\varphi a_0 + \Sigma S^3 \tan^3\varphi a_1 + \Sigma S^5 \tan^5\varphi a_2 . \end{aligned} \tag{24}$$

change in scale — distortion

For an exact solution we must have a set of simultaneous equations that are independent of r and φ. If r appears in the equation, a solution can be made for only one par-

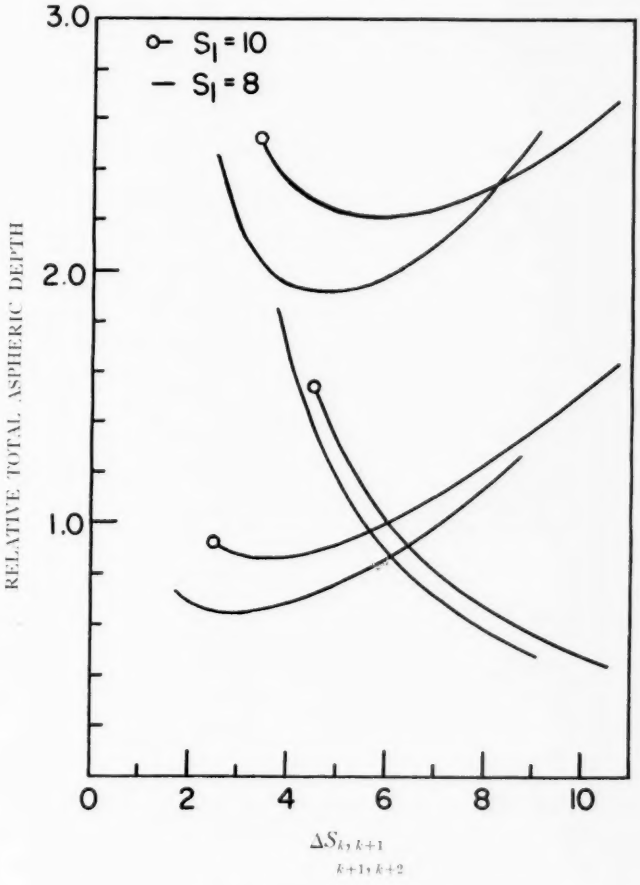

FIG. 5b.—Diagram showing the total asphericity of the corrector for constant corrector diameter; the three pairs of curves refer to $k=3$, 1, 2 reading down at $\Delta S=4$.

ticular selected r; likewise, if φ appears, a solution can be made for only one particular selected field angle. The condition for an exact solution for $C(\delta)$ and $A(\delta)$ occurs, therefore, only when each term in the summation is equal to zero. We must then satisfy

$$\text{Coeff. } a_{1,k}\begin{cases}\Sigma_k a_{1,k} + \Delta \cong \Sigma_k b_{1,k} + \Delta = 0\,, & \text{spherical aberration}\\ \Sigma_k S_k a_{1,k} = 0\,, & \text{third-order coma}\\ \Sigma_k S_k^2 a_{1,k} = 0\,, & \text{third-order astigmatism}\end{cases}, \tag{25}$$

and

$$\text{Coeff. } a_{a,k}\begin{cases}\Sigma_k S_k a_{2,k} = 0\,, & \text{fifth-order coma}\\ \Sigma_k S_k^2 a_{2,k} = 0\,, & \text{fifth-order astigmatism}\\ \Sigma_k S_k^3 a_{2,k} = 0\,, & \text{fifth-order coma}\end{cases}. \tag{26}$$

Solve for $a_{1,k}$, $a_{2,k}$ for positions S_k.

In general, we can neglect $\Sigma_k a_{2,k} \neq 0$, since the residual has negligible effect on the on-axis bundle.

With the values of S_k limited to one sign and to a rather small range, it is not possible to achieve an exact solution using three elements. The residual aberrations that cannot be eliminated are the $\Sigma S^4 a_2$ astigmatism term and the two $D(\delta)$-terms. Only for a four-element corrector can the $\Sigma S^4 a_2$- and $\Sigma S^3 a_1$-terms be eliminated. For survey and other nonastrometric programs, the elimination of $D(\delta)$-terms is not essential.

When the factor $f(n, \varphi)$ is included in the general equations to take into account the effect of the index of refraction for inclined rays, we find that it enters each term of the summation in the same manner, except for terms involving $a_{1,0}$ . . . arising from the paraboloid. As a consequence, we can satisfactorily correct for $f(n, \varphi)$ by modifying $S^m a_{i,0}$ and solving the determinants for $a_{i,k}$ in the usual manner. Final refinement of the designs must be done by ray-tracing the actual system. The preceding discussion should be of value, however, in obtaining an approximate solution.

As a final correction, it is possible to add an $a_{0,3}$-term to make the Petzval sum $\Sigma(1/nf_{\text{psr}}) = 0$, in order to place the aberration-free images on a flat field. This term is small and has a negligible effect on the other aberrations.

NOTES

BLUE GIANTS IN THE DIRECTION OF THE GALACTIC CENTER

The great concentrations of blue giants (OB stars) between galactic longitudes $l = 320°$ and $l = 20°$ lie in the rather narrow range $l = 333°$–$345°$. On passing from the region of Messier 8 toward the direction of the galactic center, there is a marked decrease in the number of early-type stars of high luminosity.

Three objective-prism plates covering most of the area $326° < l < 330°$, $+2° > b > -6°$, were obtained with the Tonantzintla objective-prism camera. On these plates, a total of thirty-eight OB stars have been classified; the latter are listed in Table 1

TABLE 1

BLUE GIANTS

No.	HD	m_{vis}	Sp. (HD)	Notes	No.	HD	m_{vis}	Sp. (HD)	Notes
1	161061	8.7	B8		21	316436	.....	B5	
2	161103	7.9	B0	1	22	316464	.....	F5	
3	161291	8.5	B0	2	23	316520	.....	B0	6
4	163065	8.3	B3		24	316568	.....	B3	
5	164032	7.28	B2	3	25	316569	.....	B3	
6	163453	10.4	B0	4	26	316587	.....	B3	7
7	163454	7.9	Oe5	5	27	316589	.....	B5	
8	163667	8.9	B0		28	316729	.....	B3	
9	164019	9.0	B0		29	316786	.....	G0	
10	316204	.....	B5		30	Anon.	.....	.....	8
11	316232	.....	F8		31	Anon.	.....	.....	9
12	316274	.....	(B)		32	Anon.	.....	.....	10
13	316311	.....	B		33	Anon.	.....	.....	11
14	316325	.....	B		34	Anon.	.....	.....	12
15	316326	.....	B2		35	Anon.	.....	.....	13
16	316332	.....	B		36	Anon.	.....	.....	14
17	316341	.....	B3		37	Anon.	.....	.....	15
18	316393	.....	B5		38	Anon.	.....	.....	16
19	316406	.....	B2						
20	316409	.....	G0						

NOTES TO TABLE 1

1. MWC 268 (B0ne); strongly reddened.
2. Probably strongly reddened.
3. Uncertain; overexposed.
4. Strongly reddened.
5. MWC 276 (B1ne).
6. MB 248 (see Merrill and Burwell, *Ap. J.*, **112**, 72, 1950).
7. MB 249 (see *ibid.*).
8. 1′.5 N., 1′.5 W., of HD 161647.
9. 4′ N., 3′ W., of HD 163895.
10. 5′ N., 2′.5 E., of HDE 316078; strongly reddened.
11. 6′ W., 2′ S., of HDE 316219.
12. 2′.5 S., 4′ E., of HDE 316245.
13. 6′ E., 1′.5 S., of HDE 316328.
14. 4′.5 S., of HDE 316435.
15. 3′ N., 2′ E., of HDE 316441.
16. 1′ W., 2′.5 N., of HDE 316498.

and may be of especial interest. The thirty-four stars fainter than visual magnitude 8.4 are plotted in Figure 1, which is a negative reproduction of a Ross 3-inch plate.

These new OB stars lie in a direction very near that of the galactic center; their distances are unknown. It seems likely, however, that at least some of them are located at distances greater than that of the inner spiral arm recently announced by Morgan, Whitford, and Code.[1] Nos. 9 and 31, for example, are projected against a fairly bright region of the Milky Way—that is, the interstellar absorption is probably not very great; the faintness of the two stars suggests that they may be considerably more distant than the clusterings around Messier 8 and Messier 20. It seems quite possible that the majority of the thirty-eight stars lie at distances of the order of 3 kiloparsecs or more. Slit spectrograms and accurate color excesses and magnitudes will be necessary, however, to settle the question.

Several of the stars appear to be heavily reddened; they are located in regions where strong absorption can be seen in Figure 1.

The three objective-prism plates were taken by L. Münch, L. Terrazas, and E. Chavira, respectively.

W. W. Morgan
Guillermina González
Graciela González

Observatorio de Tonantzintla
Tonantzintla, Puebla, Mexico
and
Yerkes Observatory
Williams Bay, Wisconsin
April 6, 1953

[1] *Ap. J.* (in press).

NOTE ON THE CEPHEID VARIABLE ZETA GEMINORUM*

Zeta Geminorum is a 10-day Cepheid whose period is decreasing at the rate of nearly 3.6 seconds a year.[1] At the request of W. N. Abbott, the star was put on the photometric program to determine the correction to the elements. Twenty-eight three-color observations were obtained at the McDonald Observatory, and, through the co-operation of V. M. Slipher and H. L. Johnson, observations were continued five more nights at the Lowell Observatory with completely different equipment.

The comparison star HDE 268518 is only 96 seconds north of the variable, so that extinction difficulties were minimized. The magnitude and color of the comparison star, as determined from ten comparisons with standards on the U, B, V system,[2] are $V = 7^{m}578$, $B - V = 0^{m}618$, and $U - B = 0^{m}086$. The constancy of the comparison star during the interval of observations was checked by comparisons with 48 Geminorum.

The observations are given in Table 1 arranged in order of phase as computed from Nielsen's elements:

$$\text{Max.} = \text{JD } 2410639.801 + 10^{d}.153527E - 0^{d}.000000575E^{2}.$$

Each observation consists of two or more intercomparisons, with the exception of the three of half-weight, in which only one intercomparison was made. The internal accuracy of the observations is ± 0.003 mag.

* *Contributions from the McDonald Observatory, University of Texas*, No. 228.

[1] Nielsen, *Ole Rømer-Observatoriet*, No. 5, 1930.

[2] Johnson and Morgan, *Ap. J.*, **117**, 313, 1953.

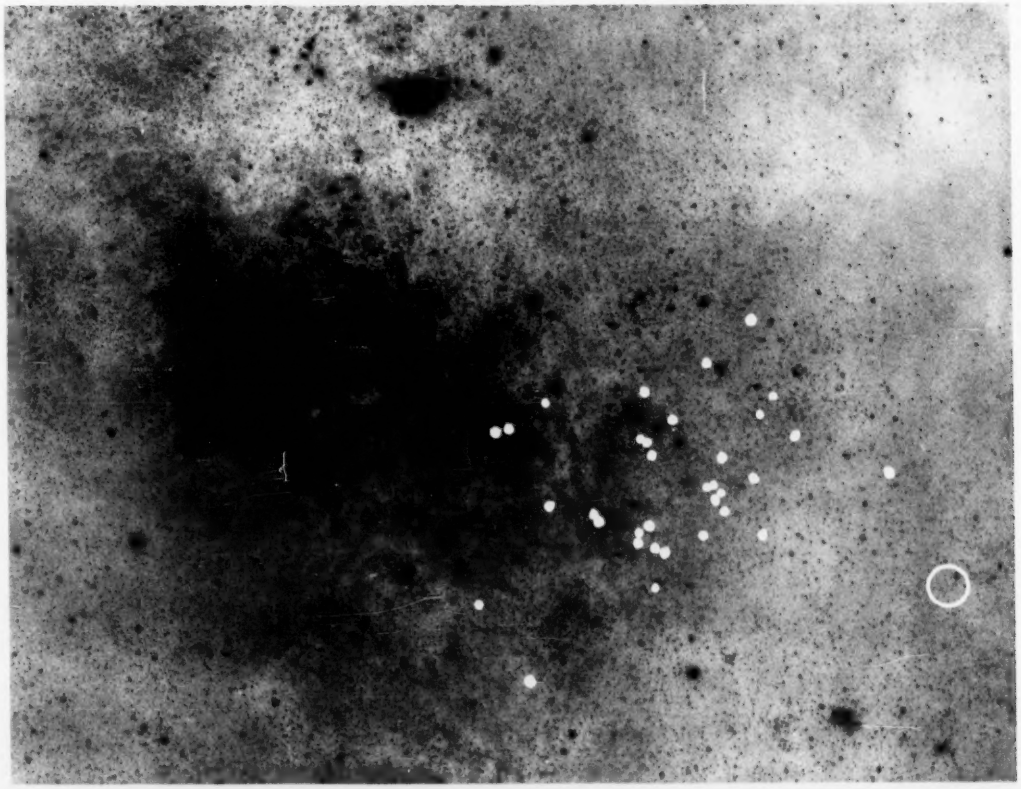

FIG. 1.—Negative reproduction of Ross 3-inch plate, showing location of faint OB stars in direction of galactic center. Stars listed in Table 1 having apparent visual magnitudes 8.5 and fainter are plotted. Circle at lower right marks the position $l = 325°$, $b = 0°$. Messier 8 is at top left center; the great Sagittarius cloud is at left center. Original negative on Eastman 103*a*-O emulsion.

The light- and color-curves plotted in Figure 1 are very nearly cosine curves. In order to demonstrate the deviations from simple cosine curves, the differences determined from the relations

$$\Delta V = V - 3^{m}902 + 0^{m}236 \cos (2\pi P - 10^{\circ}61),$$

$$\Delta(B - V) = B - V - 0^{m}829 + 0^{m}143 \cos (2\pi P + 11^{\circ}05),$$

are plotted in Figure 2; the radius of the circles is equal to 0.003 mag. The Lowell observations are indicated by crossed circles. The deviations, ΔV, are very similar to those shown by Hall's observations in the near infrared[3] and indicate that the form of the light-curve has not changed during this interval. No curve is given for $\Delta(U - B)$, as the deviations from a cosine curve at phases 0.6–0.9 are obvious from Figure 1.

Nielsen's procedure for the determination of the epoch of maximum gives O − C = $+0^{p}029$ at $E = +2343$. In visual light, the dispersion resulting from errors of observa-

TABLE 1

OBSERVATIONS OF ζ GEMINORUM

Heliocentric JD 2434400+	Phase (Period)	V	$B-V$	$U-B$	Remarks
26.570	0.0209	3.665	0.694	0.457	
16.778	.0562	3.679	.700	.482	
27.566	.1190	3.706	.749	.523	
27.643	.1266	3.709	.752	.534	
27.758	.1379	3.719	.757	.538	
7.773	.1691	3.746	.785	.566	Weight ½
18.662	.2379	3.824	.850	.614	
28.807	.2413	3.825	.856	.620	
39.742	.3185	3.946	.902	.....	Lowell
19.609	.3351	3.977	.917	.714	
19.688	.3429	3.985	.921	.727	
9.801	.3689	4.028	.926	.753	
40.658	.4088	4.077	.955	.....	Lowell
20.585	.4313	4.101	.965	.775	
20.690	.4416	4.110	.975	.780	
10.650	.4525	4.113	.978	.788	
10.773	.4647	4.123	.976	.796	
41.619	.5034	4.147	.976	.....	Lowell
21.567	.5280	4.158	.971	.778	
21.744	.5455	4.156	.965	.772	
11.809	.5667	4.155	.950	.752	
1.696	.5705	4.150	.960	.737	Weight ½
42.615	.6015	4.127	.926	.....	Lowell
12.667	.6512	4.065	.871	.652	
12.773	.6617	4.044	.862	.638	
2.704	.6698	4.021	.860	.617	
43.622	.7008	3.976	.841	.....	Lowell
23.747	.7428	3.945	.805	.552	
13.633	.7464	3.928	.814	.554	
3.838	.7815	3.890	.772	.530	Weight ½
4.686	.8650	3.786	.720	.519	
15.663	.9464	3.730	.700	.500	
15.779	0.9578	3.715	0.693	0.495	

[3] *Ap. J.*, **79**, 145, 1934.

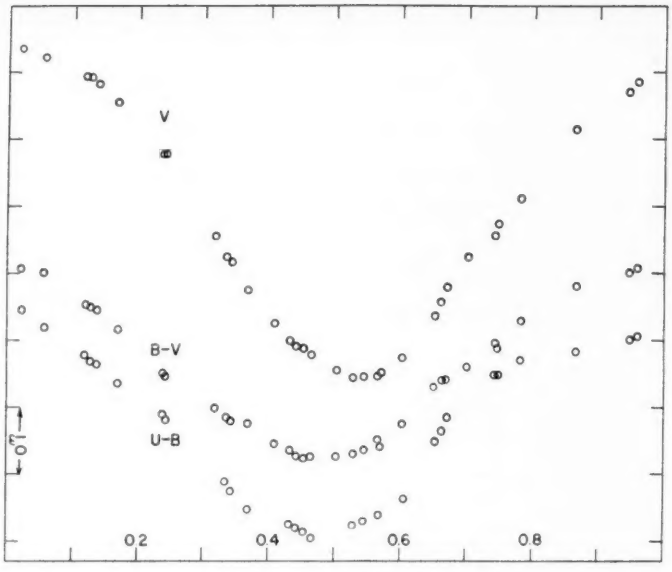

FIG. 1.—Observed light- and color-curves

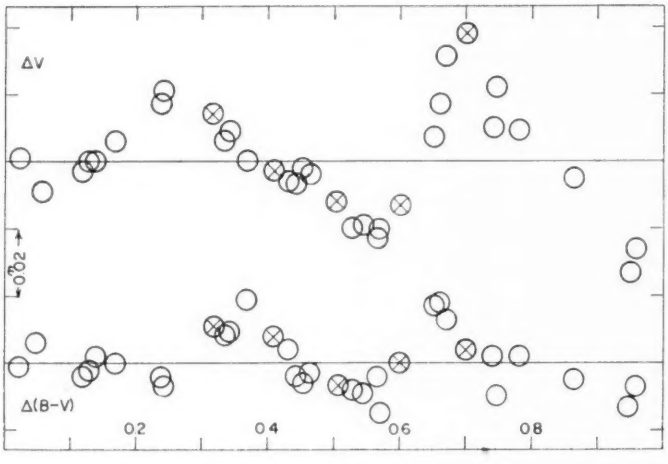

FIG. 2.—Deviations of V and $B-V$ from cosine curves

tions and neglect of real deviations from a cosine curve is ± 0.017 mag. The maximum occurs 0.022 period earlier for our B-magnitude and 0.036 period earlier for our U-magnitude.

The discussion of Loreta's visual observations by Nielsen[4] gave a correction to the epoch of maximum light of $O - C = +0^{d}009$ at $E = +1631$. It appears that the period predicted by the elements is slightly too short. A preliminary examination shows that the residuals from Nielsen's ephemeris can be represented by

$$O - C = -0^{d}115 + 0^{d}000064E + 0^{d}000000044E^{2},$$

if the early observations by Schmidt are not considered. The formula gives $O - C = +0^{d}010$ at $E = +1631$ and $O - C = +0^{d}027$ at $E = +2343$. Before discussing all the photometric data available since Nielsen's paper, to determine improved elements, it would be desirable to obtain further photoelectric observations.

The analysis of our observations with regard to the theory of pulsating stars is the subject of a later paper.

D. L. HARRIS

YERKES AND MCDONALD OBSERVATORIES
April 5, 1953

[4] *Ole Rømer-Observatoriet*, No. 16, 1941.

EM CYG, A POSSIBLE EX-NOVA*

EM Cyg[1] was discovered by Hoffmeister[2] on Sonneberg plates to be a variable with the range 12.5–14.5 mag. He first thought the light-variation to be of the Algol type, but later (unpublished) observations by Gaposchkin ruled out this possibility. In the variable star catalogue[3] the star is listed as a semiregular variable, with the note that the light-fluctuations resemble those of a cepheid but that the period varies from 23.6 to 27.1 days.

The spectrum of this star was observed with the Cassegrain spectrograph of the 82-inch telescope at the McDonald Observatory. The camera and glass prisms used give a dispersion of 113 A/mm at $H\gamma$; the spectrum extends from $H\beta$ to λ 3900, and the definition is good from about λ 4500 to the K line. The date and time of mid-exposure was May $19^{d}10^{d}5^{m}$, 1953, U.T., and the star was estimated to have a photographic magnitude slightly fainter than 13.

The spectrum shows the hydrogen lines $H\beta$, $H\gamma$, $H\delta$, and $H\epsilon$ to be rather broad emission bands, with no absorption present. *He* II 4686 appears as a weak emission band, considerably fainter than the hydrogen lines. No absorption lines are visible. The distribution of light in the continuous spectrum is that of an early-type star.

The spectrum itself resembles that of V Sge, which was described by Joy[4] and by Elvey and Babcock[5] and which is probably a former nova. However, the 4686 band is much stronger relative to the hydrogen lines in V Sge than it is in EM Cyg. Also the

* *Contributions from the McDonald Observatory, University of Texas*, No. 229.

[1] $\alpha_{1900} = 19^{h}34^{m}44^{s}$; $\delta_{1900} = 30^{\circ}\ 16'.9$; $l = 32^{\circ}.8$; $b = +3^{\circ}.2$.

[2] *A.N.*, **233**, 5571, 1928.

[3] Kukarkin and Parenago, *General Catalogue of Variable Stars* (Moscow, 1948).

[4] *Pub. A.S.P.*, **44**, 387, 1932.

[5] *Ap. J.*, **97**, 412, 1943.

interstellar lines of *Ca* II are described by Joy as being of moderate strength in V Sge and are clearly visible on a spectrogram of that star which was obtained by Dr. W. P. Bidelman at the McDonald Observatory (with a dispersion of 150 A/mm at $H\alpha$), but they are not visible at all in our spectrogram of EM Cyg.

The focus of our spectrogram begins to deteriorate at the position of the K line, and this makes it difficult to assign an accurate distance to EM Cyg on the basis of the absence of interstellar K. However, a rough estimate by Dr. W. W. Morgan indicates that the star is less than 1200 parsecs distant, and it may well be much nearer than this. Thus the absolute magnitude must be fainter than about +2.5, while the estimated absolute magnitudes of known postnovae range from +3.2 to +4.9.[6]

We conclude that EM Cyg is probably a former nova. Ryves[7] deduced from the light-curve of V Sge, before its spectrum had been observed, that it might be an old nova. It would be interesting to know whether the light of EM Cyg undergoes long-term variations such as those with apparent periods of 530 days[7] and 230 days[8] which have been observed in V Sge.

E. MARGARET BURBIDGE
G. R. BURBIDGE

YERKES AND MCDONALD OBSERVATORIES
June 9, 1953

[6] D. B. McLaughlin, *Ap. J.*, **117**, 279, 1953.

[7] *M.N.*, **92**, 715, 1932.

[8] L. Campbell, *Pop. Astr.*, **46**, 112, 1938.

ROTATIONAL TEMPERATURES OF AURORAL N_2^+ BANDS*

There has been for some time a discrepancy between the temperature of certain regions of the upper atmosphere derived from the intensity distribution of the rotational fine structure of the N_2^+ bands of the aurora and temperatures measured in other ways.[1]

We have recently obtained photographs of the spectra of the 3914 A N_2^+ band from the aurora with a new spectrograph having a dispersion of 7 A/mm. The rotational fine structure of the *R* branch is completely resolved, and a good estimate of the relative intensities of the rotational lines may be made from the microphotometer tracing of the band (Fig. 1). If the population of the rotational levels of the upper state follows a Boltzmann distribution corresponding to the local kinetic temperature, this temperature may be calculated from the intensity distribution of the rotational lines.

The best method[2, 3] is to consider the intensities of all the lines by measuring the slope of the straight line obtained by plotting $\log I/K'$, for each line against $K'(K'+1)$. This method gives a rotational temperature of $330° \pm 40°$ K. A simpler method is to utilize the connection between temperature and the K number of the line of maximum intensity of the *R* branch. The strongest line appears to be either $R(7)$ or $R(6)$, cor-

* The research reported in this paper has been sponsored by the Geophysics Research Directorate of the Air Force Cambridge Research Centre, Air Research and Development Command, under Contract AF (19(122)-152.

[1] See, e.g., L. Spitzer, *The Atmospheres of the Earth and Planets* (1st ed.; Chicago: University of Chicago Press, 1947), p. 218.

[2] Vegard and Tonsberg, *Geofys. Pub.*, Vol. **11**, No. 2, 1935; Vol. **13**, Nos. 1 and 5, 1941.

[3] W. Petrie, *Defense Research Board Telecommunications Establishment, Project Report No. 20-1.*

responding to temperatures of 390° or 300° K. [The possibility that $R(8)$ is the most intense line corresponding to $T = 490°$ K is not entirely ruled out.]

The spectrum was obtained from arc and band features during a strong auroral display on the night of April 3, 1953; the height of typical features during this display was found to be 100–120 km by two-station photography.

The estimated temperature of 330° K is in agreement with other estimates of the temperature at 100–120 km. Recent measurements with rockets give temperatures of 214°–330° K for these heights.[4] It does not agree with the later results of Vegard,[2] who used the same methods of analysis with unresolved spectra. The present result is lower than recent estimates by Petrie[3] based on spectra obtained earlier at Saskatoon with a spectrograph having a dispersion of 28 A/mm. Petrie's spectra are very much superior

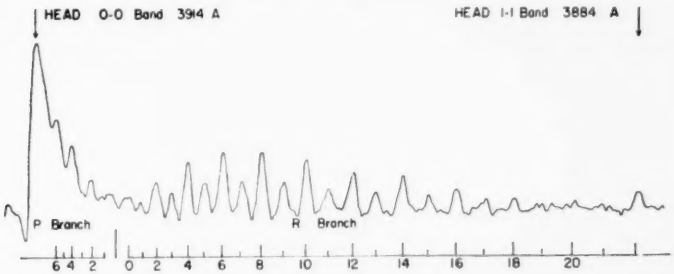

FIG. 1.—Microphotometer tracing of 0–0 N_2^+ band at 3914 A

to those obtained by Vegard, and the strong and weak lines are clearly resolved toward the short-wave-length edge of the R branch, but the lines are nowhere completely separated. The complete resolution of the R branch reported here has eliminated a number of serious uncertainties from the method.

A. VALLANCE JONES
D. M. HUNTEN
G. G. SHEPHERD

DEPARTMENT OF PHYSICS, UNIVERSITY OF SASKATCHEWAN
April 15, 1953; revised May 27, 1953

[4] "The Rocket Panel," *Phys. Rev.*, **88**, 1027, 1952.

NOTE ON THE PAPER "STUDIES OF VARIABLES IN THE MAGELLANIC CLOUDS. I. TWENTY NEW FAINT VARIABLES IN A REGION IN THE SMALL CLOUD"[1]

Dr. Shapley has called our attention to the fact that some variables announced as new ones under the above title have previously been announced by the Harvard College Observatory though the periods have not been given. The publications containing these

[1] *Ap. J.*, **115**, 279, 1952.

announcements had not reached us; we, therefore, considered them as having been discovered by us. The objects in question are:

C.V. 158 = H.V. 12093	C.V. 92 = H.V. 12097
C.V. 109 = H.V. 12107	C.V. 70 = H.V. 11287
C.V. 95 = H.V. 12092	C.V. 229 = H.V. 12102
C.V. 127 = H.V. 12090	

The period for C.V. 18 = H.V. 11174 given in *Harvard Circular* No. 444 differs from the one announced by us, which our observations suggest to be correct.

MARTIN DARTAYET
JORGE LANDI DESSY

OBSERVATORIO ASTRONÓMICO
CÓRDOBA, ARGENTINA
March 31, 1953

THE ASTROPHYSICAL JOURNAL

announces the publication of

A GENERAL INDEX, Volumes 76–100

Price: $5.00*

ORDERS NOW ACCEPTED

Also available:

GENERAL INDEX, Volumes 1–25 .....$2.50
GENERAL INDEX, Volumes 26–50 .....$2.50
GENERAL INDEX, Volumes 51–75 .....$2.50

* Postage $0.15 per copy extra to foreign addresses.

THE UNIVERSITY OF CHICAGO PRESS
5750 ELLIS AVENUE CHICAGO 37 · ILLINOIS

A Completely Revised Edition

THE ATMOSPHERES OF THE EARTH AND PLANETS

By GERARD P. KUIPER

Important new material has been added to make this edition the most modern and complete monograph on planetary atmospheres.

Additions include:

—Information recently obtained in V-2 flights about our upper air and the x-ray spectrum of the sun.

—Identification of the strong red and infra-red emissions of the night sky.

—A new determination of the cosmic abundances of the chemical elements.

—A derivation of the ozone temperature in the upper stratosphere.

—A determination of the age of meteorites.

—A discussion of the presence of nitrous oxide in the lower atmosphere and its connection with the life-cycle.

—A reconstruction of the conditions leading to the escape of the "proto-atmosphere."

—A new section on Jovian planets.

—A development of the atmospheric conditions on Mars.

Paperbound $5.50 *Clothbound $8.50*

THE UNIVERSITY OF CHICAGO PRESS
5750 ELLIS AVENUE CHICAGO 37, ILLINOIS

IMPORTANT BOOKS IN THE HISTORY OF ASTRONOMY

THE ARYABHATIYA OF ARYABHATA

An Ancient Indian Work on Mathematics and Astronomy

Translated with Notes by WALTER EUGENE CLARK

Aryabhata's work, which was composed in A.D. 499, is probably the earliest preserved Indian mathematical and astronomical text bearing the name of an individual author; the earliest Indian text to deal specifically with mathematics; and the earliest preserved astronomical text from the third or scientific period of Indian astronomy. This is the first complete translation from the Sanskrit of this historical document.

120 pages 7¼ × 5¼ $2.50

LATIN TREATISES ON COMETS BETWEEN 1238 and 1368 A.D.

By LYNN THORNDIKE

This volume publishes for the first time the Latin texts of important tracts on comets observed between 1238 and 1368 A.D. Among the treatises are works by Aegidius of Lessines, Gerardus de Silteo, Peter of Limoges, Geoffrey of Meaux, and John of Legnano. As a summary of the Aristotelian doctrine of comets, the commentaries of Thomas Aquinas and of Albertus Magnus on Aristotle's *Meteorology* are included in English translation.

286 pages 6 × 9 *Index* $5.00

THE SPHERE OF SACROBOSCO AND ITS COMMENTATORS

By LYNN THORNDIKE

A critical edition of the Latin text, together with an English translation, of the SPHERE of John of Sacrobosco—for centuries the best and best known manual of astronomy by a Western author. Also included is the hitherto unpublished commentary by Robert of England, with an English translation. In addition, the commentary of Cecco d'Ascoli and the commentary ascribed to Michael Scot are made available for the first time outside of rare books printed in abbreviated Latin.

506 pages 6 × 9 *Index* $10.00

THE UNIVERSITY OF CHICAGO PRESS